(12) LEVEL II

DNA 4631Z

DYNAMIC STRUCTURAL ANALYSIS OF MAP SHELTERS

Weidlinger Associates
3000 Sand Hill Road
Menlo Park, California 94025

June 1978

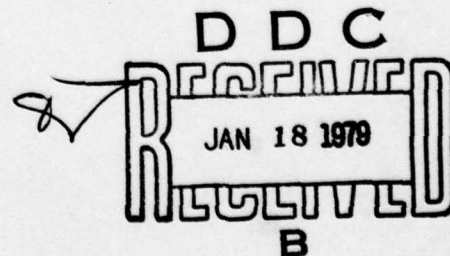Interim Report for Period February 1977—April 1978

CONTRACT No. DNA 001-77-C-0104

APPROVED FOR PUBLIC RELEASE;
DISTRIBUTION UNLIMITED.

DDC
RECEIVED
JAN 18 1979
B

Prepared for
Director
DEFENSE NUCLEAR AGENCY
Washington, D. C. 20305

Destroy this report when it is no longer
needed. Do not return to sender.

PLEASE NOTIFY THE DEFENSE NUCLEAR AGENCY,
ATTN: TISI, WASHINGTON, D.C. 20305, IF
YOUR ADDRESS IS INCORRECT, IF YOU WISH TO
BE DELETED FROM THE DISTRIBUTION LIST, OR
IF THE ADDRESSEE IS NO LONGER EMPLOYED BY
YOUR ORGANIZATION.

SECURITY CLASSIFICATION OF THIS PAGE (When Data Entered)

REPORT DOCUMENTATION PAGE		READ INSTRUCTIONS BEFORE COMPLETING FORM
1. REPORT NUMBER DNA 4631Z	2. GOVT ACCESSION NO.	3. RECIPIENT'S CATALOG NUMBER
4. TITLE (and Subtitle) DYNAMIC STRUCTURAL ANALYSIS OF MAP SHELTERS.		5. TYPE OF REPORT & PERIOD COVERED Interim Report, for Period February 1977—Apr 78
		6. PERFORMING ORG. REPORT NUMBER R-7834
7. AUTHOR(s) Felix S. Wong Jeremy Isenberg		8. CONTRACT OR GRANT NUMBER(s) DNA 001-77-C-0104
9. PERFORMING ORGANIZATION NAME AND ADDRESS Weidlinger Associates 3000 Sand Hill Road Menlo Park, California 94025		10. PROGRAM ELEMENT, PROJECT, TASK AREA & WORK UNIT NUMBERS NWED Subtask Y99QAXSG655-10
11. CONTROLLING OFFICE NAME AND ADDRESS Director Defense Nuclear Agency Washington, D.C. 20305		12. REPORT DATE June 78
		13. NUMBER OF PAGES 210
14. MONITORING AGENCY NAME & ADDRESS(if different from Controlling Office) G655		15. SECURITY CLASS (of this report) UNCLASSIFIED
		15a. DECLASSIFICATION/DOWNGRADING SCHEDULE

16. DISTRIBUTION STATEMENT (of this Report)

6270411

Approved for public release; distribution unlimited.

17. DISTRIBUTION STATEMENT (of the abstract entered in Block 20, if different from Report)

19. KEY WORDS (Continue on reverse side if necessary and identify by block number)

MAP Shelters
Structural Dynamics
Finite Element Methods

20. ABSTRACT (Continue on reverse side if necessary and identify by block number)

The study is part of the DNA C-6 Program to investigate the feasibility of one of the multiple aim point (MAP) basing concepts for the advanced M-X missile systems; namely, the shelter concept. Its objective is to identify requirements in the finite element analysis of the shelter response when the structure is subjected to nuclear environments, and to define an analysis methodology which can be followed in performing dynamic analyses of a shelter-like structure.

DD FORM 1473 1 JAN 73   EDITION OF 1 NOV 65 IS OBSOLETE

UNCLASSIFIED
SECURITY CLASSIFICATION OF THIS PAGE (When Data Entered)

392 150

SUMMARY AND RECOMMENDATIONS

This study examines the application of dynamic finite element methods to shelter-like structures in a nuclear environment. In particular, the study investigates the deformation modes of the shelter under different loading conditions, their sensitivity to variations in the overpressure wave form, important features of the shelter which affect the response, the effect of inelastic material properties and the role of elastic analyses and ground motions in a shelter analysis of this kind.

Based on results of case studies obtained using implicit elastic (GENSAP) and explicit inelastic (TRANAL) finite element codes an analysis methodology is refined and a procedure for performing dynamic analysis of the shelter is developed. The procedure involves modeling the shelter-like structure and its medium according to the guidelines established in the study, factoring in those characteristics of the air overpressure which have been found significant and separating the analysis into two distinct but complementary components: short-term analysis and long-term analysis.

In the short-term analysis the response of the front-end of the shelter which is exposed to direct airblast load is examined using a refined model which includes detailed subcomponents of the front end such as the closure, gap, bearing ring, etc. The portion of the shelter aft of the transition section may be replaced by a simpler model which approximates its impedance and energy radiation characteristics. This analysis yields peak stresses in the headworks, frame and closure and peak deformation of the closure.

In the long-term analysis, a coarse model of the front end is used to approximate the front load distribution and its transfer to the tubular section. The long-term analysis which yields the gross motion of the headworks and the tubular section is best carried out using the soil island approach to minimize boundary effects.

This methodology is a natural consequence of the shelter concept wherein the structure is subjected both to direct airblast which dominates short-term response of the front end and indirect ground motion which is responsible for the long-term gross motion of the shelter. The distinction between short and long-term response is also dictated by computational expediancy; this combination makes comprehensive three-dimensional analyses of the shelter structure possible and economically acceptable.

The present study contributes to the definition of the methodology and substantiates the recommended approach with results from case studies. Its emphasis, however, has been on the short-term response of the structure. Even there the scope of the work is limited by the airblast data available. Limited attention has been devoted to the other facet of the methodology, i.e., the long-term response and especially the role of the soil

1

island approach. Observations made in this study regarding the long-term response should be confirmed by additional studies at least as extensively as the conclusions on short-term response have been substantiated.

PREFACE

The work reported herein is sponsored by the Defense Nuclear Agency under Contract No. DNA 001-77-C-0104, and covers the period from February 1977 to April 1978. T. Kennedy is the project monitor.

The study is part of the DNA C-6 Program to investigate the feasibility of one of the multiple aim point (MAP) basing concepts for the advanced M-X missile system, namely, the shelter concept. Its objective is to identify requirements in the finite element analysis of the shelter response when the structure is subjected to nuclear environments and to define an analysis methodology which can be followed in performing dynamic analyses of a shelter-like structure.

The authors wish to thank T. Kennedy for helpful comments throughout the course of the study and his thorough review of the draft. Thanks are also due to D. Hulse for typing the manuscript.

ACCESSION for		
NTIS	White Section	
DOC	Buff Section	☐
UNANNOUNCED		☐
JUSTIFICATION		
BY		
DISTRIBUTION/AVAILABILITY CODES		
Dist.	AVAIL. and/or	SPECIAL
A		

3

CONVERSION FACTORS
FOR U.S. CUSTOMARY TO METRIC (SI)
UNITS OF MEASUREMENT

To Convert From	To	Multiply By
degree (angle)	radian (rad)	1.745 329 X E −2
foot	meter (m)	3.048 000 X E −1
foot-pound-force	joule (J)	1.355 818
inch	meter (m)	2.540 000 X E −2
pound-force (lbf avoirdupois)	newton (N)	4.448 222
pound-force inch	newton-meter (N·m)	1.129 848 X E −1
pound-force/inch	newton/meter (N/m)	1.751 268 X E +2
pound-force/foot^2	kilo pascal (kPa)	4.788 026 X E −2
pound-force/inch^2 (psi)	kilo pascal (kPa)	6.894 757
pound-mass (lbm avoirdupois)	kilogram (kg)	4.535 924 X E −1
pound-mass-foot^2 (moment of inertia)	kilogram-meter^2 (kg·m^2)	4.214 011 X E −2

TABLE OF CONTENTS

TABLE OF CONTENTS (CONTINUED)

LIST OF FIGURES

LIST OF FIGURES (CONTINUED)

LIST OF FIGURES (CONTINUED)

LIST OF FIGURES (CONTINUED)

LIST OF FIGURES (CONTINUED)

11

LIST OF FIGURES (CONTINUED)

12

LIST OF TABLES

SECTION I

INTRODUCTION

The shelter concept is one of the many multiple aim point (MAP) basing mode concepts under consideration for deployment of the M-X advanced ballistic missile system. In the shelter based mode, missiles are moved by transporter/launcher vehicles among widely dispersed shelters as compared to the current Minuteman ballistic missile force which is based in hardened silos arranged in clusters or wings. Random shifting of the M-X missiles in the MAP shelters would increase their survivability by complicating the targeting options of an enemy attack.

Although many different shelter configurations are under consideration at this time, there are some structural characteristics which are common to all configurations and a structure is said to be shelter-like if it displays these characteristics: if it is buried, it is buried with the tube horizontal and the front face vertical or near vertical. The shelter may house the transporter/carrier in addition to the missile and in that case some portion of it must be large enough to accommodate the vehicle. This larger portion is joined to the tube portion through a transition section. Access to the shelter is through one end (the front end) which is normally guarded by a door or closure, while the other end is closed. To enable the transporter/carrier to move in and out of the shelter with some speed and efficiency, a key to the shelter basing concept, a driveway leading to the door and front end is necessary. The driveway is below grade if the shelter is below grade.

The large front-end portion of the shelter (called the headworks) is usually rectangular in shape and has a rectangular cavity to house the carrier/vehicle. Hence, the closure is also rectangular. When the missile alone is to be accommodated, the rectangular front end is no longer a requirement. However, some form of a front end, more massive than the shelter tube proper is still necessary to house the closure envisioned. In this case, the front end (and the closure) can also be circular in order to mesh in more naturally with the tubular section. The transition between front end and tube may be less abrupt as in the rectangular headworks case. This study deals with the more complex analysis problem of the rectangular headworks and closure but the results may also be applied to a circular headworks and closure configuration.

Whereas the shelter is protected on its top, flanks and aft-end from the hostile environment by the soil medium in which it is buried, its front is necessarily exposed to nuclear airblasts because of the open accessway. What compounds this situation is the fact that the front end is vertical or near vertical. When the airblast impinges on it head-on,

the overpressure is greatly magnified due to the reflection phenomenon. A central problem in the design of a shelter-like structure is the design of the closure and frame (front face) which must withstand this tremendous load. Dynamic analyses of the structure are dominated by the analysis of the front-end response and its effects on the remainder of the structure.

The present study is conducted mainly to seek answers to the following questions:

• What are the deformation modes of the shelter under different loading conditions (side-on, head-on, oblique front-on), and how sensitive are these deformation modes to variations in the overpressure wave forms?

• What are the important features of the shelter which must be included in the analysis model, and how should these features be modeled?

• What is the correct use of an elastic analysis of the shelter structure? What pertinent information can be and cannot be obtained from such an elastic analysis?

• What are the main effects of inelasticity and how important is an inelastic analysis in the analysis of the shelter?

• What is the role of ground motion in the shelter analysis? Is the soil island technique necessary for a complete analysis of the shelter structural response?

Through answers to these questions certain guidelines emerge, culminating in a methodology that can be followed in performing future dynamic analyses of a shelter-like structure in a nuclear attack environment. This methodology constitutes the main result of the present study.

A byproduct of this effort is the wealth of quantitative results computed for certain prototype shelters which have served as case studies. The data may be used to aid in the evaluation and validation of these shelter configurations (S1 and S4). Whereas numerical data tend to become obsolete as the design is changed, it is believed that the methodology applicable to a class of shelter-like structures may have longer lasting value to the study of protective structures.

SECTION II

SCOPE

The scope of this effort as originally outlined in Reference 1 has undergone several modifications during the course of the study in response to different project requirements. Due to the lack of overpressure data and the need to support SAMSO's closure design validation effort, the study has deviated from a research type to include limited applications; in particular it includes some detailed analyses of the S4 test configuration.

The scope presented herein reflects these changes, and can be divided into three phases: Phase 1 which identifies the elastic structural deformation modes and their sensitivity to variations in the applied airblast wave forms, Phase 2 which provides response definitions for a particular shelter configuration subjected to a particular airblast load in order to show the effect of inelasticity and modeling techniques, and Phase 3 which comprises the work performed in support of the S4 test and closure design evaluation. Phases 1 and 2 will be described herein, and because of its somewhat different purpose Phase 3 will be described in a subsequent report (Reference 2).

The shelter-like structure is assumed to be located at a generic site, at the 600 psi range from a 1 MT nuclear explosion, or about 1,850 feet from ground zero. The airblast wave front can impinge the shelter/berm configuration head-on, at an oblique angle, side-on or rear-on. This study addresses only the head-on, oblique (30°) and side-on cases with emphasis on head-on incidence.

2.1. PHASE ONE

As a first step, elastic calculations were performed to identify basic structural response modes of the MAP shelter. These calculations are both two-dimensional, in which the cylindrical portions of the shelter are modeled as a ring, and three-dimensional in which the shelter is modeled in its entirety. In the head-on configuration, where the airblast impinges on the front face head-on, there is a vertical symmetry plane containing the longitudinal axis; consequently, only half of the shelter/berm ensemble needs to be modeled. When the airblast approaches the front face at an oblique angle (other than head-on), this symmetry is lost and the entire shelter/berm ensemble is modeled. All shelter structures studied in Phase 1 correspond to the HAVE HOST S1 configuration (Reference 3).

The calculations were performed using GENSAP, an implicit elastic three-dimensional finite element code. The major shelter/loading configurations studied are as follows:

Calculation 1A has a side-on loading of the cylindrical portion of the shelter from an air overpressure which passes over the berm, with subsequent modification in both pressure and time characteristics due to reflections and rarefactions by the berm. This calculation is two dimensional.

Calculation 1B has a front-on loading in which the air overpressure directly loads the front-face of the shelter and then progresses over the berm in a direction parallel to the longitudinal axis of the structure. Because of the symmetry in structure and overpressure with respect to the center plane, only half of the physical configuration is included in the three-dimensional calculation.

Calculation 1C is similar to Calculation 1B with one exception. The monolithic front face used in 1B is modified to reflect the existence of a gap between the closure and frame. Air overpressure which acts on the front face is allowed to penetrate into this gap. By comparing the results of Calculations 1B and 1C, the effect of the gap on structural response is identified.

Calculation 1D has a front-on loading in which the direction of airblast propagation is inclined at 30° to the normal to the front face which is modeled as a monolithic structure (i.e., no gap). By comparing the results of Calculations 1B and 1D, the effect of oblique incidence is ascertained.

In addition to identifying the basic response modes to loading conditions, it was the intention of the study to investigate the sensitivity of these response modes to variations in the overpressure wave forms. In particular, the following three types of wave forms were considered for use in the study:

    a. Free-air wave form from a 1 MT surface burst.

    b. Precursed wave form from a 1 MT surface burst with thermal layer.

    c. Precursed wave form from a 1 MT surface burst in dusty air.

However, since airblast data available from the Air Force Weapons Laboratory (AFWL) were limited, all Phase 1 calculations used basically the free air wave form from a 1 MT surface burst (References 4 and 5). Consequently, the question of how sensitive the structural response is to variations in overpressure wave forms remains unanswered. To gain some insight into this sensitivity, however, results of Calculations 1A to 1C have been compared with results obtained in some checkout calculations, which use the Brode overpressure wave form for flat ground, modified in some cases to account for reflections at the shelter front face.

All Phase 1 calculations are made using airblast loadings only and only the short-term response (e.g., somewhat greater times than two transit times of the shock wave across the cylindrical section of the shelter in the two-dimensional, side-on case and somewhat greater times than the times of peak stress in the headworks and transition section in the three-dimensional cases) is obtained.

2.2. PHASE TWO

In this phase of the study, the inelastic structural response is analyzed. The behavior of the structure under airblast loading identified in the first phase is quantified, and deformation modes due to inelastic material behavior are defined. These inelastic calculations are three-dimensional. Where symmetry exists, as in the head-on loading case, only half of the shelter/berm ensemble is modeled. All shelter structures studied in this phase correspond to the HAVE HOST S4 configuration, or its replacement the HEST S4 configuration (Reference 6). Phase 2 study consists of the following three-dimensional calculations:

Calculation 2A has a front-on loading condition. The concrete in the structure is modeled as an elastic perfectly plastic material and the back and side plates in the closure are assigned a yield strength corresponding to that of A36 steel. The steel plates are modeled by two elements across the plate thickness. The backfill model corresponds to the medium backfill of HAVE HOST (Reference 7).

Calculation 2B is similar to Calculation 2A except that the concrete is the only inelastic material assumed. The elastic back and side plates are modeled by only one element across its thickness. The backfill has the elastic unloading properties.

Calculation 2C is similar to Calculation 2B, but with all materials (concrete, steel, backfill, soil) elastic.

Whereas the shelter structure analyzed in Phase 1 corresponds to the S1 configuration, the structure analyzed in Phase 2 corresponds to the S4 configuration. This change in configuration is made to support the closure design validation program; it tends to make correlation of the results obtained in Phases 1 and 2 more difficult.

The air overpressure used as input to the Phase 2 calculations is provided by the AFWL (Reference 8), based partly on test data, partly on design handbooks and partly on two-dimensional numerical calculations.

All Phase 2 calculations are made using Weidlinger Associates' TRANAL code, an explicit inelastic three-dimensional dynamic finite element program (Reference 10). To accommodate the rather complicated geometry and applied load distribution of the S4 configuration, extensive modifications are made to the code and numerous subroutines written with most of the changes occurring in the input module, element table processing, coordinate and applied load processing. A brief summary of these changes and a description of the added code capability are given in Appendix A.

Results of Phases 1 and 2 calculations are described in Sections III and V, respectively. Although it is not the purpose of this study to examine structural response of the shelter in detail, some description of the structural response is necessary in order to lead into the main discussion of the study results. Accordingly, the description in Sections III and V will be brief and is presented on a calculation basis, as if each calculation is performed alone.

These results are compared and contrasted in Section IV for Phase 1 and in Section VI for Phase 2. Through such comparisons it is possible to (a) identify the shelter deformation modes and their relationship to loading conditions and airblast characteristics; (b) isolate vulnerable shelter elements and their modeling requirements; and (c) clarify the effect of inelasticity on shelter response and hence the importance of an inelastic analysis. The conclusions presented in Section VII lead naturally to a procedure for the dynamic analysis of the shelter structure, the major goal of the present study.

SECTION III

PHASE 1 RESULTS

Results of calculations performed in Phase 1 will be described in this section. Data presented consist of time histories of stress/strain in the elements and velocity/ displacement of the nodes. A brief description of the finite element model, the air over-pressure and ground motion input will be given where appropriate.

All Phase 1 calculations are based on a prototype shelter corresponding to the HAVE HOST S1 test structure as shown in Figure 3-1 (Reference 3). The headworks is symmetric on two planes and the tube axis is coincident with the headworks axis. The closure, a thick concrete slab, is simply bolted to the bearing area. In this configuration the front face and part of the sides and top portion of the headworks are exposed to direct air-blast load. There are no headwalls.

3.1. CALCULATION 1A--TWO-DIMENSIONAL ELASTIC CALCULATION WITH SIDE-ON INCIDENCE

The two-dimensional calculation considers deformation in a plane perpendicular to the shelter longitudinal axis and the shelter is represented by a circular cross section of the cylindrical portion, i.e., a ring. No displacement is allowed in the direction of the shelter longitudinal axis.

Model and Airblast Load--the plane strain model is shown in Figure 3-2. It consists of plane strain quadrilateral finite elements (approximately 1,700 in soil and 70 in the structure). The refinement in the structure is determined from a preliminary finite element calculation of natural mode shapes and frequencies of the structure in vacuo which are compared with its analytical solutions, such as shown in Table 3-1. Improved agreement for higher modes could be obtained by refining the grid further, but this is deemed unnecessary for the purpose of the present study.

The elastic material properties for the native soil, berm and backfill are given in Table 3-2. The grid sizes of the individual finite elements are selected so as to provide undistorted components of airblast-induced ground motion up to frequencies of 40 Hz in the native soil and 20 to 25 Hz for the berm and backfill. The overall size of the model is selected to give approximately 80 msec. of useful structural response time, or about two cycles of the ovaling (n = 2) mode.

The airblast used in this calculation is generated by the AFWL HULL code, designated HULL 19.8042 (Reference 5). It is generated for free-air, but takes into account reflections due to the existence of the berm. Later on in the discussion reference will be made to the Brode description which is the classical nuclear wave form for a flat rigid ground.

3-1

Because of the limited data on air overpressure which are available a direct investigation of the effect of variations in overpressure wave form is not feasible. By comparing response results obtained using the HULL 19.8042 and the Brode wave forms, even though the latter is not compatible with the berm, some insight into the wave form effect can be obtained.

A comparison of the peak overpressure profile over the berm surface for the two airblast descriptions is given in Figure 3-3. To obtain an understanding of the differences in temporal characteristics between the two airblast descriptions, the overpressure time histories at selected points on the berm surface are scaled to a constant peak of unit magnitude and the scaled histories compared in Figure 3-4. Note that the temporal characteristics of the two airblast wave forms are quite similar for all points on the berm with possibly the exception of the side away from GZ which is considered to have very minor effect on structural response. Hence, it is fair to say that any sensitivity of structural response to wave form is probably induced by differences in peak overpressures as illustrated in Figure 3-3, the more significant of which occurs along the blast side and also at the top of the berm.

Deformation Mode--the deformation pattern of the structure is mainly that of the breathing and ovaling ($n = 2$) mode. This is illustrated in Figure 3-5 which shows the radial displacement (not to same scale as the ring radius) as a function of the circumferential distance along the ring at different action times. The dotted line corresponds to the breathing mode contribution. It can be seen that aside from the breathing mode the deformation is dominated by the $n = 2$ mode; the finding is also confirmed by a Fourier analysis of the deformation pattern, shown in Figure 3-6.

Stresses--the stress/time histories for elements in the structure are consistent with the deformation pattern just described. The circumferential stresses for the three elements which make up the thickness of the ring can be used to estimate the amount of bending and hoop compression which exist in the structure. Figure 3-7 shows the circumferential stresses at the crown (12 o'clock position) for the innermost and outermost elements; these can be averaged to yield the hoop compression assuming plane sections remain plane. The difference between the circumferential stresses and hoop compression is proportional to the bending moment. Similar time histories are obtained for points at the bottom of the structure (6 o'clock position) and at the springlines (9 o'clock position and 3 o'clock position).

The maximum bending moment thus obtained is approximately 2.4×10^6 in.-lb./in., and the maximum membrane stresses due to bending, i.e., bending stress at the extreme fibre, is 11,000 psi.

Soil-Structure Interaction--the first wave to reach the structure is from the top of the berm which is about 10 feet of overburden. The structure then senses the airblast load coming from the windward side of the berm and finally that from the leeward side of the berm. There is some evidence of outrunning ground motion in the native soil underlying the backfill but its effect does not appear significant.

The initial airblast induced ground motion wave front is reflected at the crown of the shelter and again reflected at the free-air boundary. Consequently, significant ringing (vibration) is observed in the soil motion time histories (as Figure 3-8 shows). This effect which is prominent in an elastic calculation is expected to diminish greatly when more realistic nonlinear soil properties are used to model hysteresis and other dissipative mechanisms inherent in the backfill.

Another soil-structure interaction phenomenon manifests itself at depths lower than the crown, where the first loading of the soil is induced by waves propagated through the shelter and out into the soil (an outrunning effect). The structure is flattened by the ground shock at the crown and pushes out at the soil at the springline. This effect can be observed before the arrival of the direct airblast-induced ground motion. Figure 3-9 shows the stress-time histories for a soil element left on the springline; the horizontal stress (σ_x) induced by motion of the structure precedes the main airblast load which is almost all vertical (σ_y). Similarly, Figure 3-10 illustrates this phenomenon for a soil element to the right of the springline. Note the synchronization of the σ_x pulse with that of Figure 3-9 and the main pulse from the overpressure load acting at the top and sides of the beam arriving later in time.

3.2. CALCULATION 1B--THREE-DIMENSIONAL ELASTIC CALCULATION WITH HEAD-ON INCIDENCE

This three-dimensional calculation considers deformation symmetric to the center plane of symmetry of the structure/berm configuration. Hence, only one half of the configuration needs to be modeled. The airblast-load impinges on the front face, progresses over the top and then travels down the berm in the direction of the longitudinal axis of the shelter.

Model and Airblast Load--a view of the three-dimensional finite element model which consists of eight node (brick) elements is shown in Figure 3-11. The model consists of approximately 1,000 elements in soil and 600 elements in the structure and covers the full length of the structure with approximately 40 feet of soil in front of, 20 feet below and to the side of the structure. A cross-sectional view of the model is shown in Figure 3-12 and Figure 3-13 gives another view of the structure, with soil elements removed. Note that special attention has been given to the transition region, where the main headworks change from a rectangular box to a circular cylinder.

In this calculation the front face is modeled simply as a monolithic plate, i.e., no distinction is made between the closure and its frame, and the gap between them is ignored. The gap though small, allows the high reflected overpressure which exists on the front face a passage inside the frame and is shown in Section 3.3 to have a significant effect on the behavior of the frame when included in the model. Henceforth, the term no-gap refers to the situation where the front face is modeled as monolithic and gap denotes the presence of the gap in the model.

The elastic material properties for the native soil, berm, backfill and structure are the same as those used in Calculation 1A, the elastic side-on two-dimensional calculation. The grid sizes on the individual finite elements are not as refined as would be desirable. For instance, the cylindrical portion of the structure is modeled by two elements across the thickness of the ring in contrast to three in Calculation 1A and some of the soil elements below and to the side of the structure are rather large. However, the element sizes can still provide undistorted components of motion up to frequencies of 160 Hz in the structure and 14 Hz in the overburden.

The AFWL HULL 19.8041 airblast (Reference 4) for free air is used in this calculation. Some model checkout results obtained using a modified Brode airblast for flat, rigid ground will be referred to in a later section. This corresponds to using the Brode description unchanged everywhere in the configuration with the exception of the front face where the nominal peak overpressure of 600 psi is scaled to 5,400 psi, the peak value in the AFWL data. A comparison of the peak overpressure profiles over the shelter/berm surface for the two airblast descriptions is given in Figure 3-14. Scaled time histories at selected points on the structure/berm surface are compared in Figure 3-15. Differences in wave form are apparent, especially for points in front of the shelter which encounter the incoming airblast and then the reflected wave from the front face. A more important difference, however, is in the impulse or the area under the curves. Referring to Figure 3-15a for a point on the front face, the Brode curve has about two times the impulse as the HULL 19.8041 in the first 20 msec. alone. Its significance will be apparent when the response results are described.

Both airblast descriptions are obtained assuming cylindrical symmetry, i.e., the axis of symmetry being a line at the burst point (ground zero) and perpendicular to the ground. Hence, modifications would be necessary for use on a three-dimensional structure. In the HULL 19.8041 description the side of the front face is assumed to have the same airblast load distribution as the top of the front face. In the modified Brode description, all points on the front face are assumed loaded uniformly. When the gap is modeled (Section 3.3), the same pressure is assumed to apply within the gap. Loads at the

exposed side and top surfaces of the headworks are obtained using magnification factors measured in the HAVE HOST S1 test (Reference 11).

A comparison of the peak overpressure distributions on the front face for these two descriptions is given in Figure 3-16. A portion of the front face is shielded by soil and hence is not subjected to direct airblast loading. On the portion which is exposed is plotted the peak overpressure distributions. The dotted line represents the HULL 19.8041 pressure and the dashed line represents the modified Brode pressure which of course is constant over the front face. The volume under each spatial surface is the total axial load acting on the front face in each case. The resultant force acts at a point in the front face which is offset from the geometric center of the face. The product of the resultant force and the offset gives a measure of the bending moment acting on the headwork in each case.

Deformation Mode--the deformation pattern of the loaded structure is similar to that of a beam-column on an elastic foundation. The tremendous airblast load acting directly at the front face dictates the deformation pattern that the structure follows. The shelter is compressed as a column and because of the load/resistance imbalance acting at the front, i.e., offset between resultant force and geometric (stiffness) centroid, a certain amount of bending (rotation) of the headworks in the plane of symmetry occurs; the extent of this bending deformation depends on the magnitude of the resultant axial load and the degree of load imbalance or offset. The airblast overpressure acting on the overburden tends to push the shelter down and in so doing contributes somewhat to the aforementioned longitudinal bending. These two actions, however, are not synchronous since one is effected by direct airblast load whereas the other indirectly by induced ground motion at the overburden. The deformation mode is illustrated in Figure 3-17 where the displacements are exaggerated for illustration purpose.

Some breathing and ovaling deformation in planes perpendicular to the longitudinal axis are observed, although at this early time, they have not been fully developed compared to the axial load induced deformations (both axial compression and longitudinal bending).

Stresses--the direct load on the front face produces high axial stresses in the front portion of the structure which become even higher as the stress wave propagates into the transition region and finally into the tubular region (see Figures 3-18 and 3-19). This follows immediately from the fact that the load-bearing cross-sectional area of the shelter decreases as one moves along the structure.

For a particular cross-section of the tube the bending moments and stresses in that plane can be estimated in exactly the same manner as in Calculation 1A.

Similarly, the bending moment responsible for longitudinal bending can be estimated using axial stress time histories (Figures 3-20 and 3-21) at the top and bottom of the shelter.

Maximum average axial compression is found to be 7,300 psi. The longitudinal bending moment is estimated to be 3.4×10^9 in.-lb., and the corresponding extreme fibre bending stress is 2,800 psi. The maximum bending and compressive stresses occur at different times.

The peak pressure exerted by the closure on the bearing surface has a distribution as shown in Figure 3-22. The pressure is highest at the top bearing ring and is in general higher at midspan. The average peak pressure of 9,000 psi is slightly less than twice the peak applied load whereas the ratio of the closure loaded area to bearing area is 2.5. Since the front face of the headworks is monolithic in this calculation not all of the closure load is supported by the bearing area. Some support is afforded by the surrounding frame in this model.

Soil-Structure Interaction--at early times the berm overburden effectively isolates the structure (tubular section) from most of the top airblast overpressure. For instance it takes a little more than 10 msec. for an airblast induced ground motion to transverse the overburden and reach the crown of the tubular section of the shelter.

The soil shielding the lower portion of the shelter front causes the center of pressure to become offset from the center of stiffness. This offset, multiplied by the applied load generates a bending moment and is the imbalance referred to in earlier paragraphs.

3.3. CALCULATION 1C--THREE-DIMENSIONAL ELASTIC CALCULATION WITH HEAD-ON INCIDENCE AND FRONT-FACE GAP

The gap refers to the opening between sides of the closure and the headworks frame surrounding the closure. Despite its diminutive dimension, if it is assumed that the high reflection pressure which acts on the front face penetrates into the gap cavity as well, its effect on stress distribution in the headworks becomes significant as shown by results of this calculation.

Model and Airblast Load--the finite element model used in Calcuation 1B is modified to include the presence of a gap between closure and headworks. This is achieved by eliminating the connectivity between elements on the two sides of the closure/frame interface. All other aspects of the model remained basically unchanged.

The airblast description used in Calculation 1B, namely AFWL HULL 19.8041, is again employed in order to assess the effect of the gap alone. Additional results have also been obtained using the modified Brode airblast and important comparison results will be presented later. The airblast loading which impinges on the front face is assumed to act in the gap cavity as well and its action is one that tends to compress the closure, but push the frame outward.

Deformation Mode--Figure 3-23 shows the deformation mode of the longitudinal cross-section of the structure with gap when subjected to the AFWL airblast and should be compared with Figure 3-17, the deformed shape of the structure without gap under the same loading conditions. The snapshots are taken at 10 msec. after airblast arrival with front-on incidence and for clarity the displacements are exaggerated by the same magnification factor for both cases.

Definite and significant opening of the gap, as compared to deformation of the other portions of the structure, can be readily observed. It is noted that the opening is larger at the bottom edge of the closure than at the upper edge.

Another view of the response of the gap under loading is given in Figure 3-24 which shows the deformation portion of the front face at 10 msec. Again, it is clear that the lower lip opens up much more than the upper lip and that significant shear stress is induced in the headworks especially around the corners.

Stresses--to illustrate this point further, the stress time history at a point in the lower corner of the headworks is monitored and the result shown in Figure 3-25 in the form of generalized shear stress ($\sqrt{J'_2}$, where J'_2 is the second invariant of the deviatoric stress tensor) versus mean normal stress ($J_1/3$, where J_1 is the first invariant of the stress tensor) plots. Comparing the responses with gap and without gap and referring to the approximate failure criterion for plain concrete included in the figure, it can be concluded that the presence of the gap increases the possibility of failure, at least locally, in the frame.

Similar results have been obtained for other locations on the headworks front face. It appears that the four corner locations are susceptible to shear failure due to the presence of air pressure in the gap, with the lower corners the more vulnerable. This finding is consistent with the S-1 post-test observation that "all four sides of the head-works (frame) exhibited gross shear deformation and the top and bottom edges sheared completely off" (Reference 11).

Introducing the gap in the model also uncouples the sides of the closure from the frame and the total load applied to the closure face is now supported by the bearing

ring. As shown in Figure 3-26 the peak bearing pressures on the upper and side bearing ring are increased as expected. However, the bearing pressure on the lower bearing ring shows a decrease which is rather surprising. In any event the average peak bearing pressure to peak applied load ratio is below the area ratio of 2.5. It should be emphasized that the pressure quoted here is actually the axial stress which exists in the elements which make up the bearing ring and hence is only an approximate measure of the contact pressure in the closure/bearing interface.

Soil-Structure Interaction--the fact that the lower lip opens up more than the upper lip can be due to one or both of the following two reasons. The applied pressure is slightly higher in the lower lip than the upper lip and hence results in a slightly greater opening force. Also, the passive resistance to opening of the lower lip due to soil is less than the resistance applied to the upper lip due to direct airblast load. The fact that the same phenomenon is observed in the modified Brode case where the upper and lower lip (and front face) are loaded by the same overpressure load suggests that the latter is more important.

3.4. CALCULATION 1D--THREE-DIMENSIONAL ELASTIC CALCULATION WITH 30° OBLIQUE FRONT-ON INCIDENCE

This calculation is performed to investigate the effect of the angle of incidence (sometimes referred to as quartering attack) on structural response. The airblast approaches the front face at an angle of 30° to the longitudinal plane, wherein it impinges the edge of the front face on the blast side before sweeping across the face and the exposed headworks surface and acting on the back side.

Model and Airblast Load--this is a full three-dimensional calculation in which no plane of symmetry exists and the complete shelter/berm configuration needs to be modeled. The head-on elastic model used in Calculation 1B is expanded to include both sides of the soil-structure about the geometric plane of symmetry and the resulting model is illustrated in Figure 3-27.

For lack of full three-dimensional airblast data, an estimate of the loadings based on HAVE HOST test data (Reference 11) and AFWL HULL calculation data (Reference 4) is used. The longitudinal component corresponds to that used in the head-on calculations so that any change in shelter response observed in this calculation can be attributed to the change in angle-of-incidence from zero to 30°.

In addition to the front face, the blast side of the headworks is subjected to high overpressure loading due to reflection of the wave front by the headworks and berm and the magnitude assumed for this loading is obtained from S1 test data with an approximate

3-8

magnification factor of four. On the back side as well as on top of the headworks the overpressure drops drastically and the nominal free-field pressure is assumed to act on these surfaces.

Deformation Mode--the deformation pattern of the structure 20 msec. after first arrival of the wave front is given in Figure 3-28 for a cross-section in the vertical plane of symmetry (pitch plane) and in Figure 3-29 for a cross section in the horizontal plane of symmetry (yaw plane). The pitch plane deformation is similar to that observed in the head-on calculation. The yaw deformation consists of compression in the longitudinal direction and lateral displacement of the headworks in the direction of wave propagation. Again, the displacements are magnified to illustrate the deformation mode.

Stresses--axial stress-time histories (Figures 3-30 and 3-31 for the pitch plane) are similar to those obtained in the head-on calculation. The effect of quartering shows up mainly in stresses and bending moments in the yaw plane. As shown in Figures 3-32 and 3-33, in addition to exhibiting the expected amplification as it progresses along the structure, the axial stress-time history in the yaw plane also shows the effect of arrival time since the wave front impinges first on the blast edge then progressively sweeps across the closure and front face before the back edge experiences the loading. This imbalance in axial stress in the yaw plane due to wave front arrival times generates a yaw bending moment in such a way that the headworks is initially torqued toward the blast. Later on the lateral load from over-pressure acting on the blast side of the headworks tend to counter balance this torque and turns the headworks with the wind. This behavior is shown in Figure 3-34, the bending moment being measured by the difference between the axial stresses on the blast and back sides. The maximum yaw bending moment obtained is about 1.7×10^9 in.-lbs., approximately half of that observed in the pitch plane.

The effect of quartering on shear stress distribution as measured by $\sqrt{J_2'}$ in the headworks and shelter is also investigated and found not to be significant in general. A typical comparison of the head-on calculation and quartering calculation with respect to shear is shown in Figure 3-35. Each data point in the figure corresponds to the maximum shear stress measured relative to the reference failure criterion at a location along the structure. In both the head-on and the quartering cases shear stress is amplified as one moves along the longitudinal direction of the shelter in much the same way that axial stress is amplified due to the decrease in load bearing area. The quartering calculation gives slightly higher shear stresses than those obtained from the head-on calculation; the magnitude of the difference is however not significant.
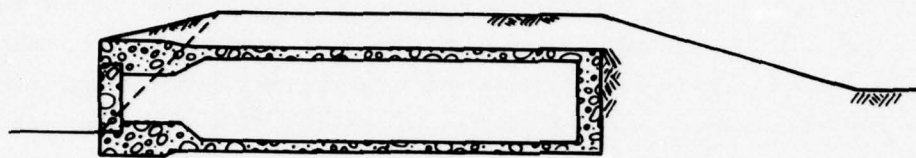
a. Elevation View

Full Scale (FT)
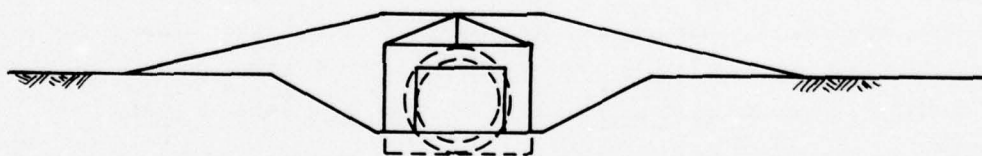
0. 20. 40.

b. Front View

Full Scale (FT)

0. 20. 40.

Figure 3-1. S1 shelter configuration
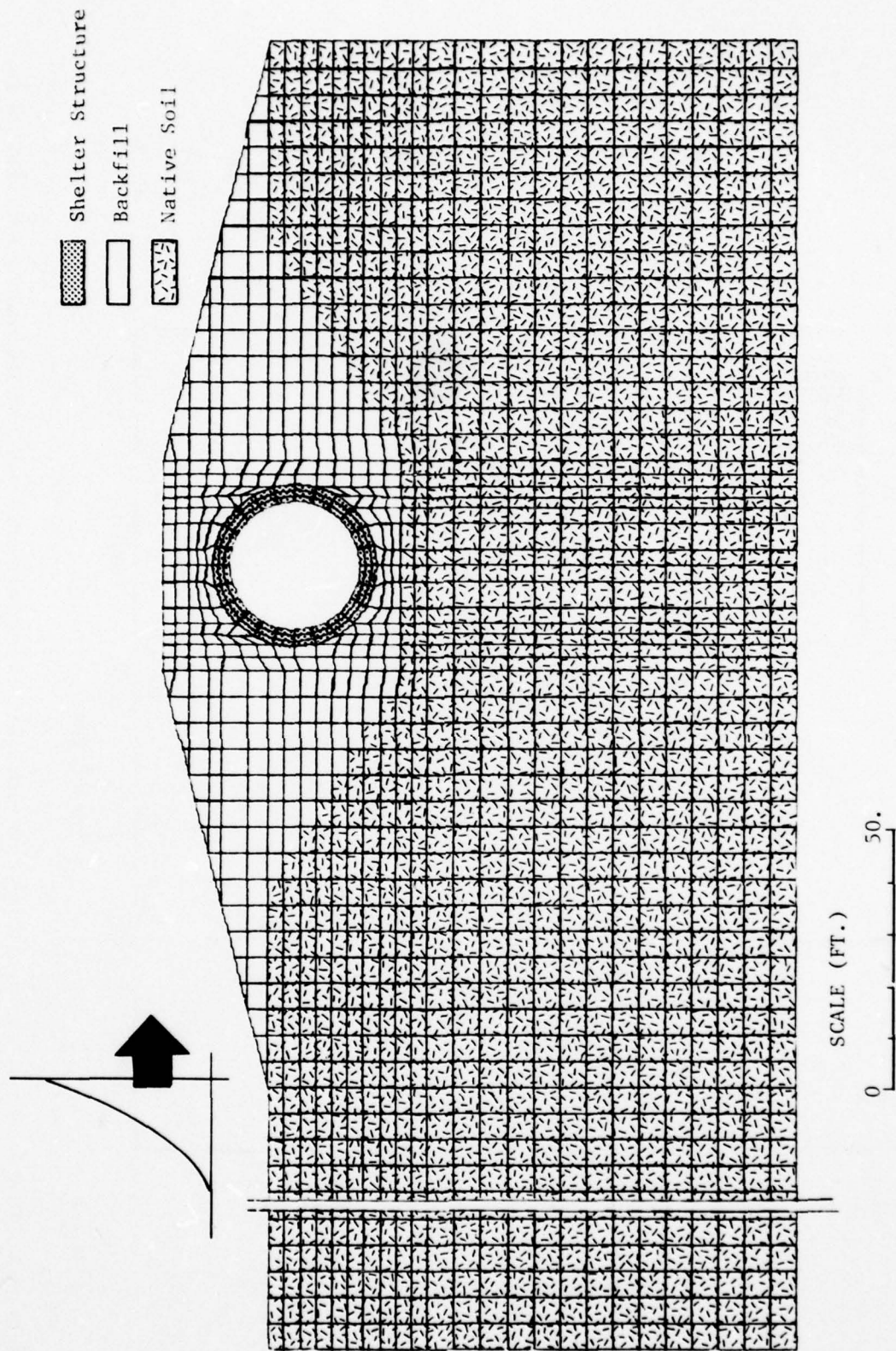
Figure 3-2. Two-dimensional (plane strain) finite element model of shelter and media, side-on incidence, Calculation 1A
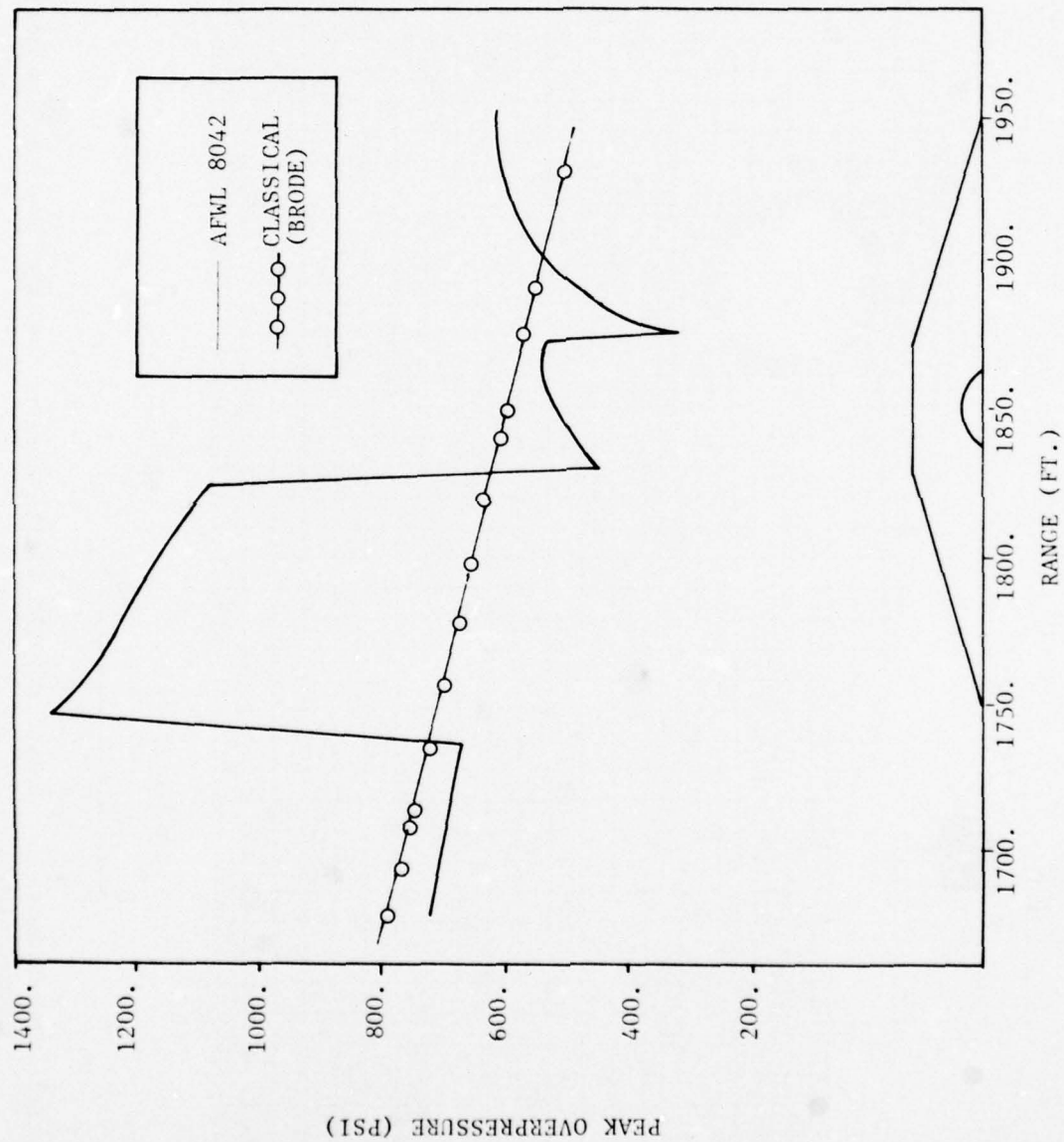
Figure 3-3. Comparison of peak overpressure profiles, two-dimensional side-on incidence, Calculation 1A
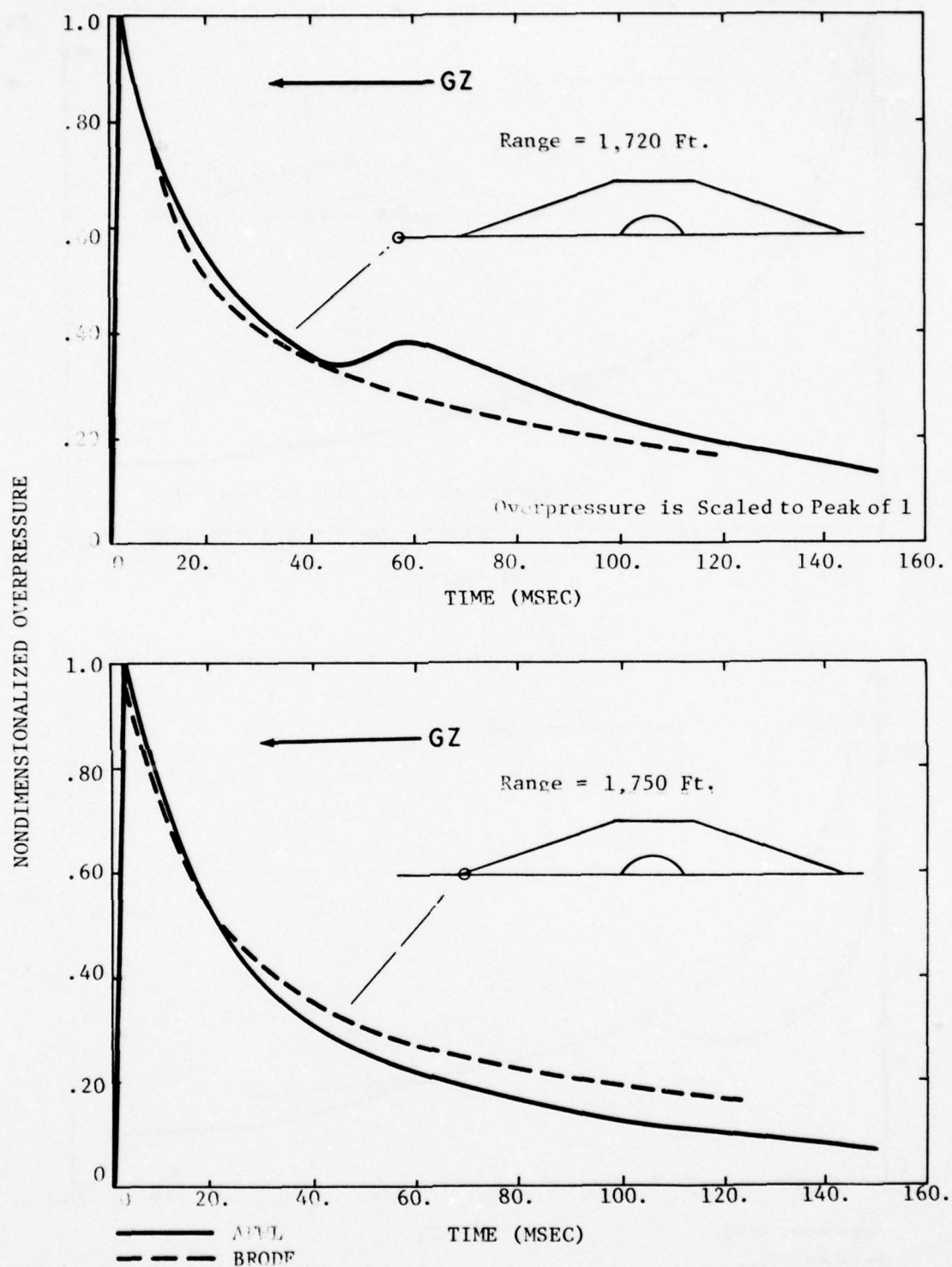
Figure 3-4a. Comparison of pressure/time histories, free-field, side-on incidence, Calculation 1A
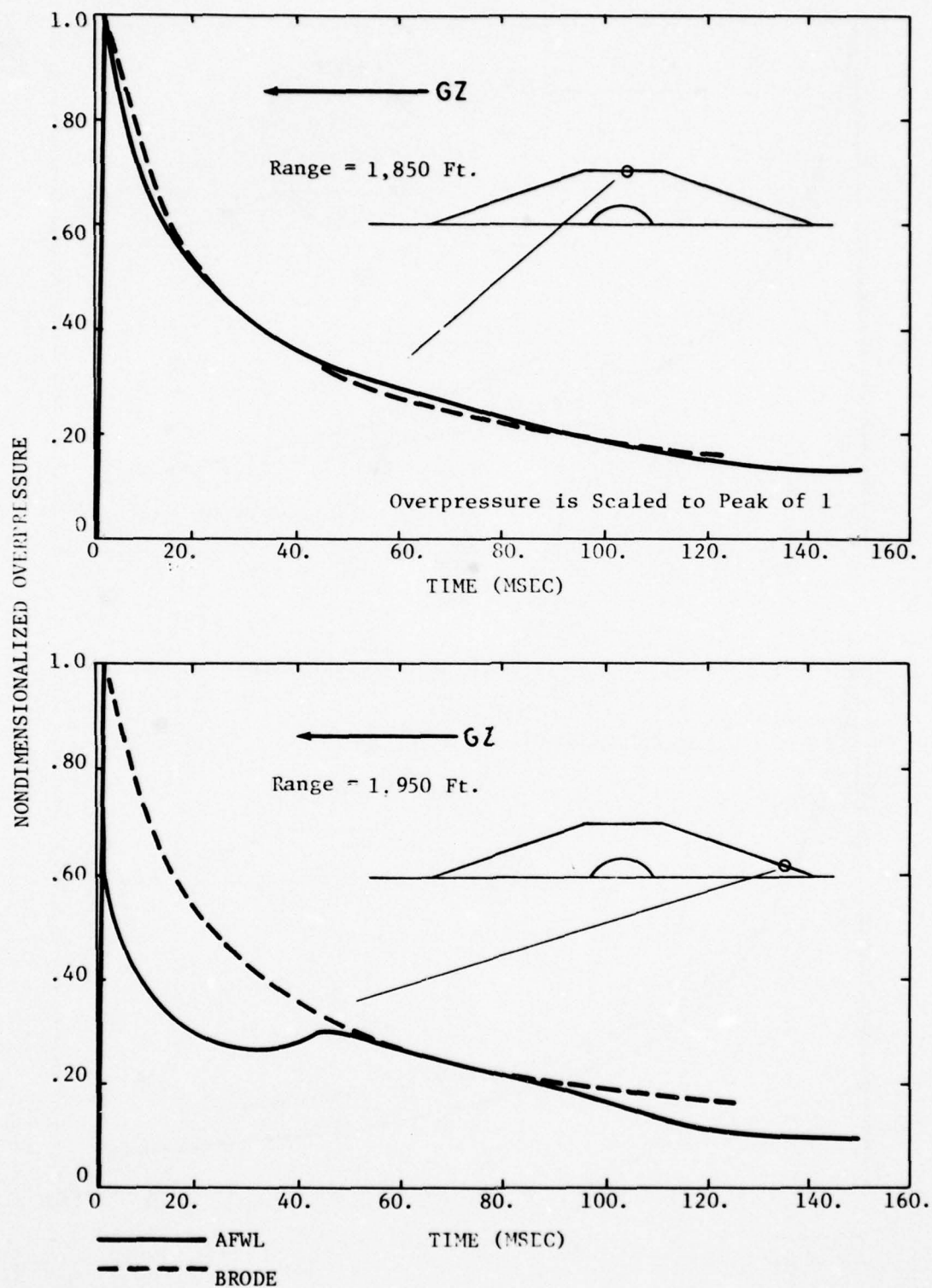
Figure 3-4b. Comparison of pressure/time histories, berm, side-on incidence Calculation 1A
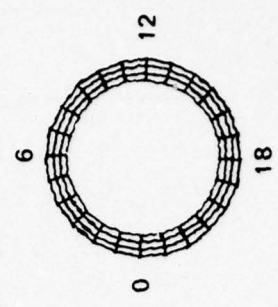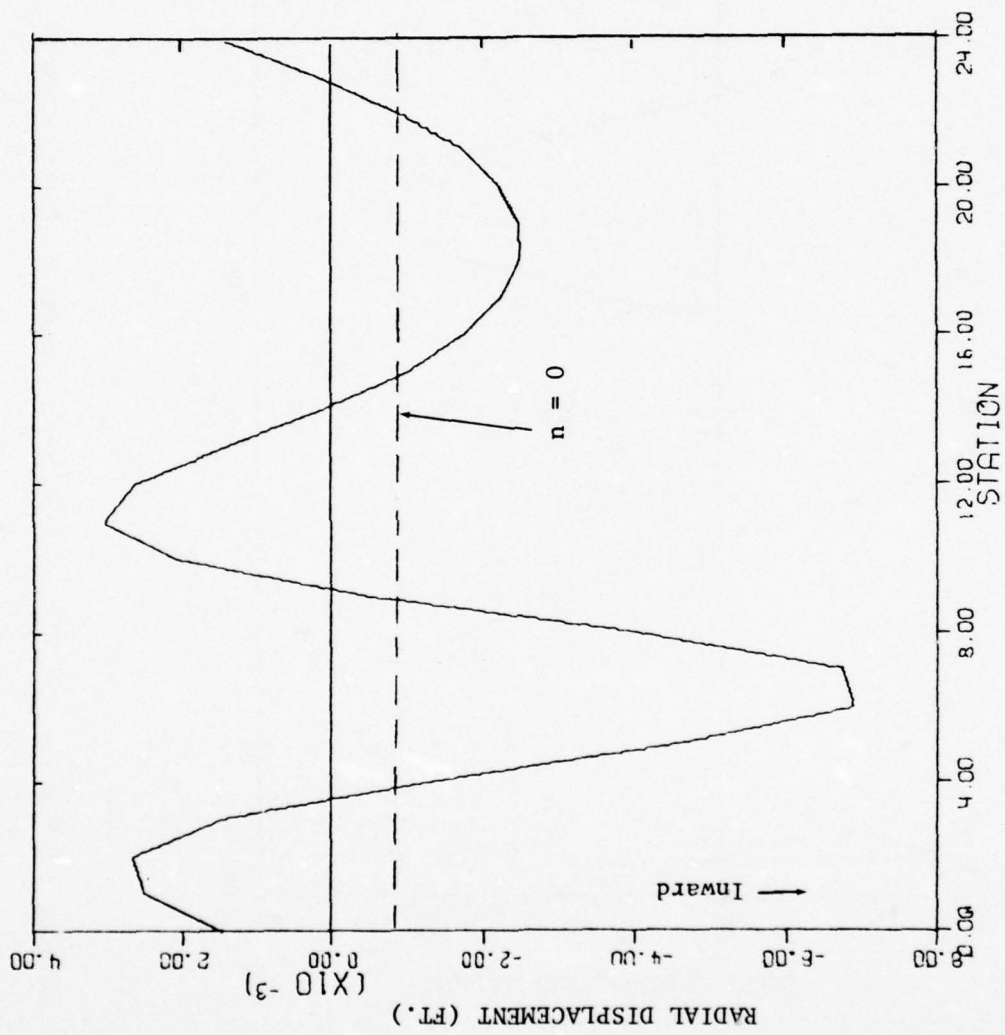
Figure 3-5a. Deformation mode T = 40 msec., side-on incidence, Calculation 1A
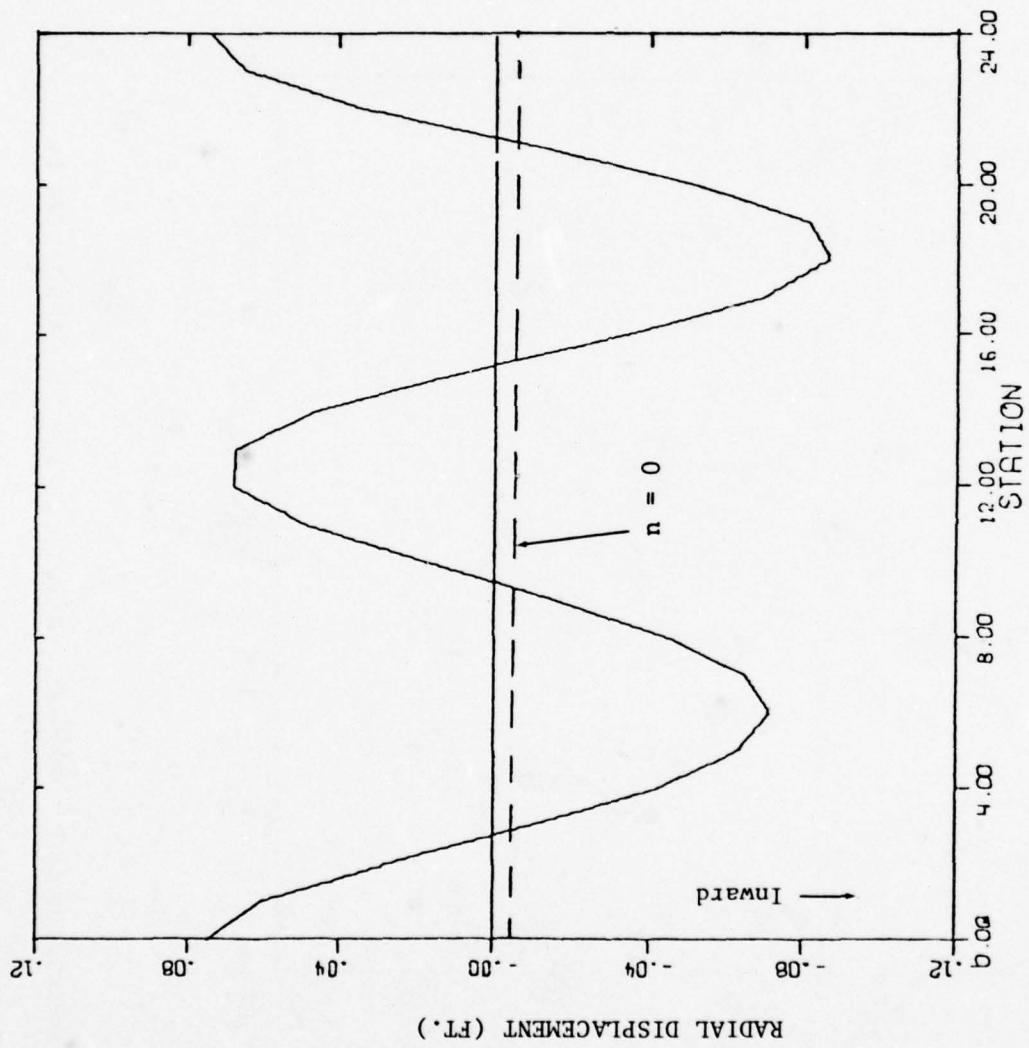
Figure 3-5b. Deformation mode at T = 60 msec., side-on incidence, Calculation 1A
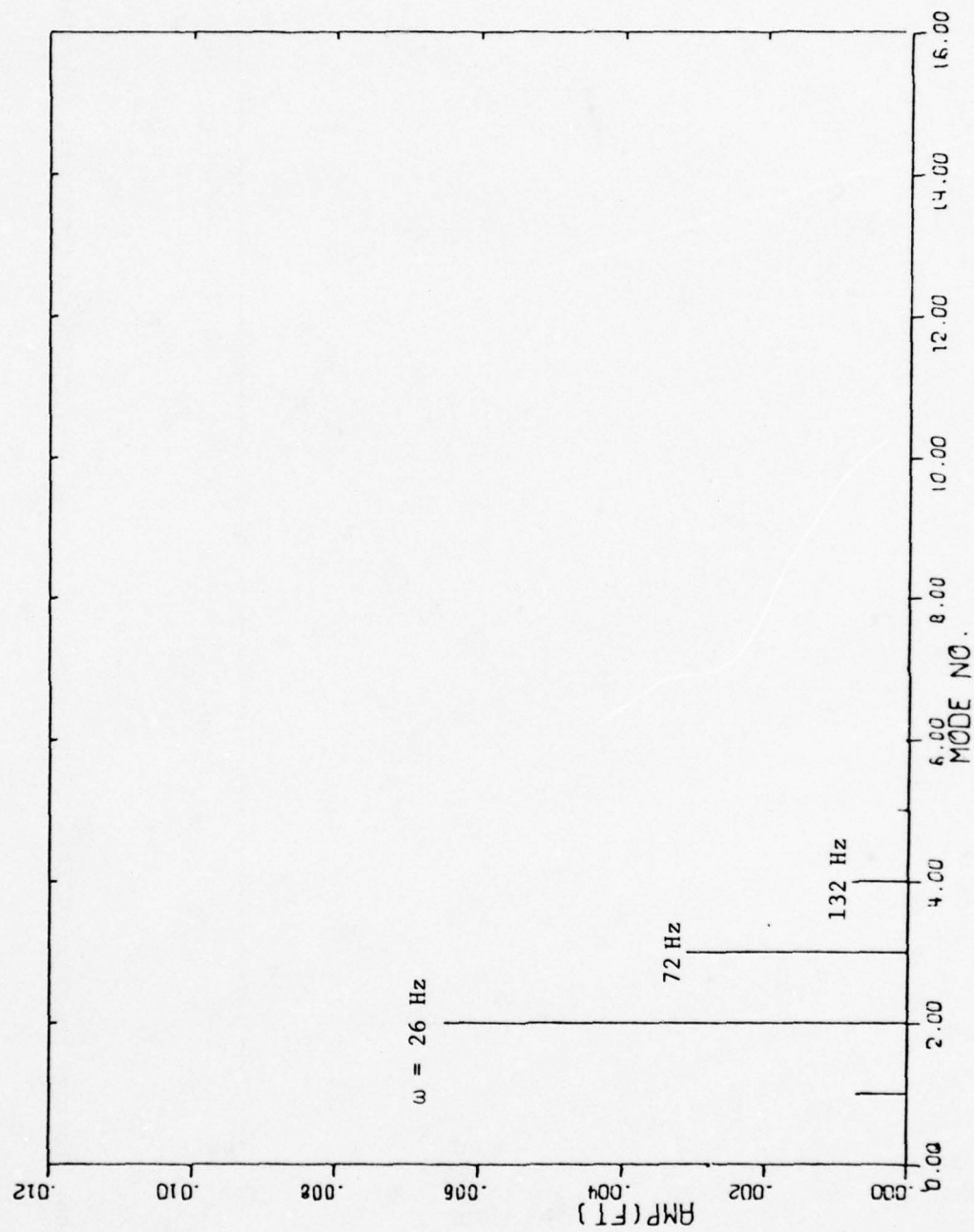
Figure 3-6a. Fourier spectrum of deformational mode at T = 40 msec., side-on incidence, Calculation 1A

3-17
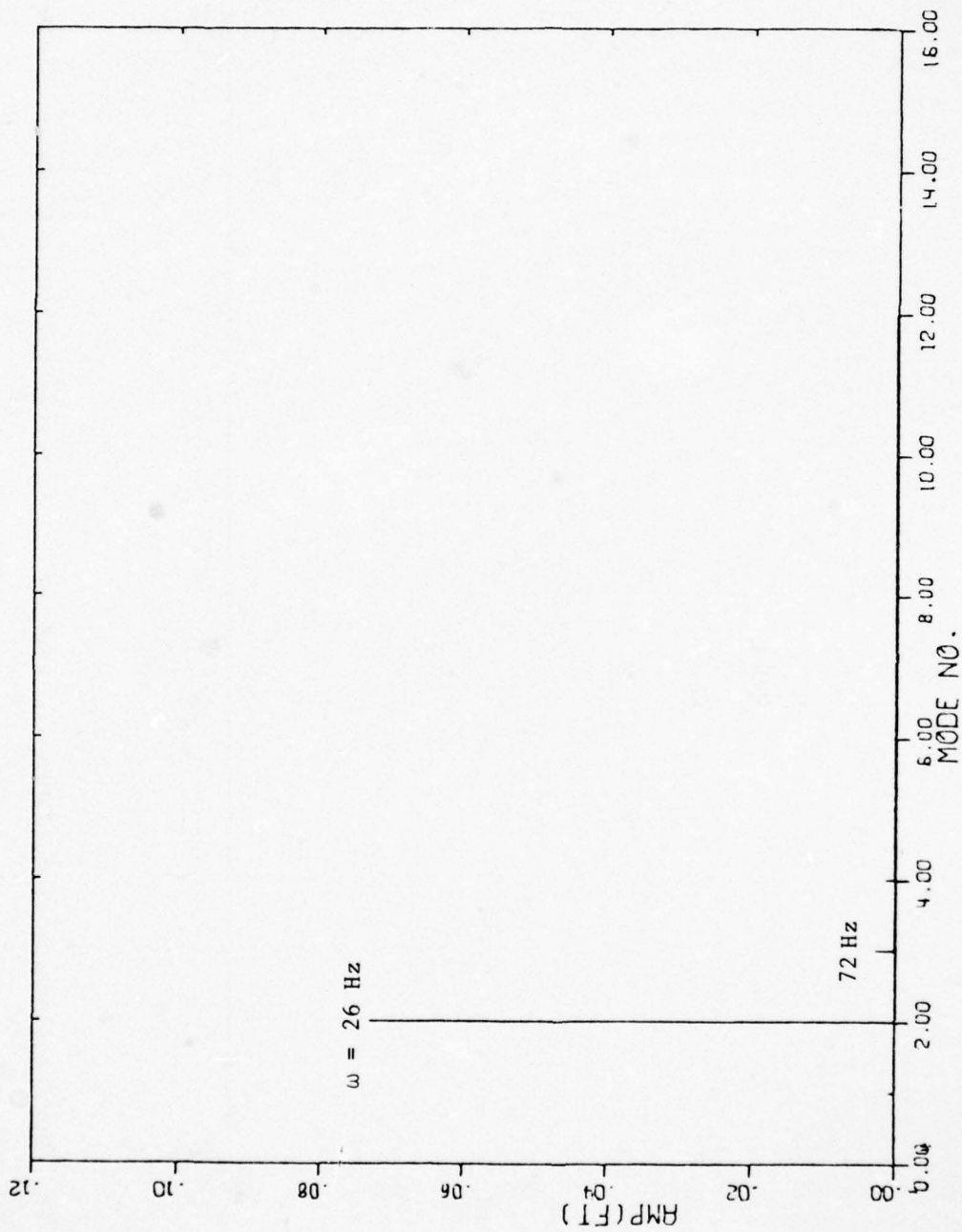
Figure 3-6b. Fourier spectrum of deformational mode at T = 60 msec., side-on incidence, Calculation 1A
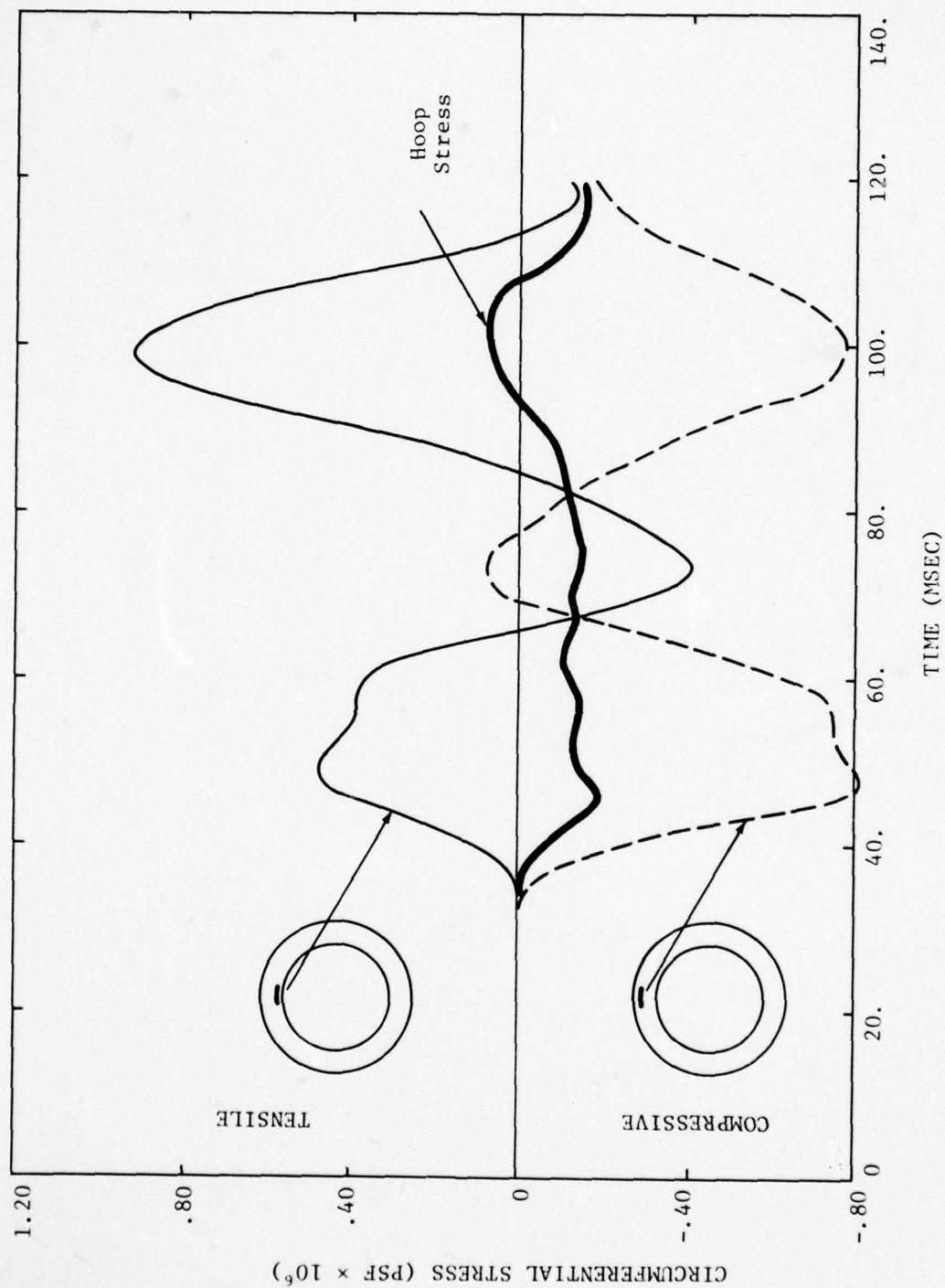
Figure 3-7. Hoop compression and bending stress time histories (AFWL 8042), crown, side-on incidence, Calculation 1A
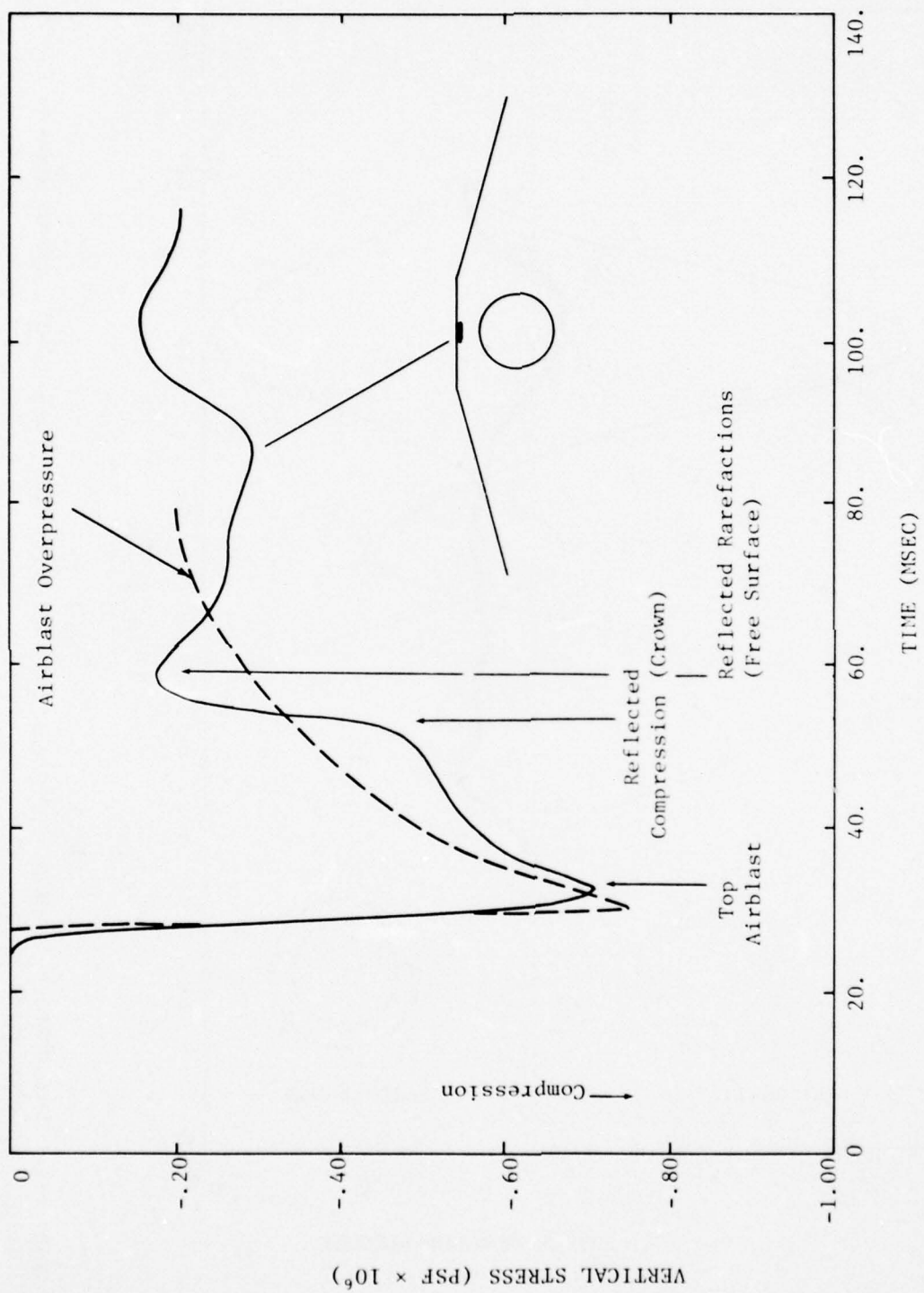
Figure 3-8. Soil response, top of berm, side-on incidence, Calculation 1A
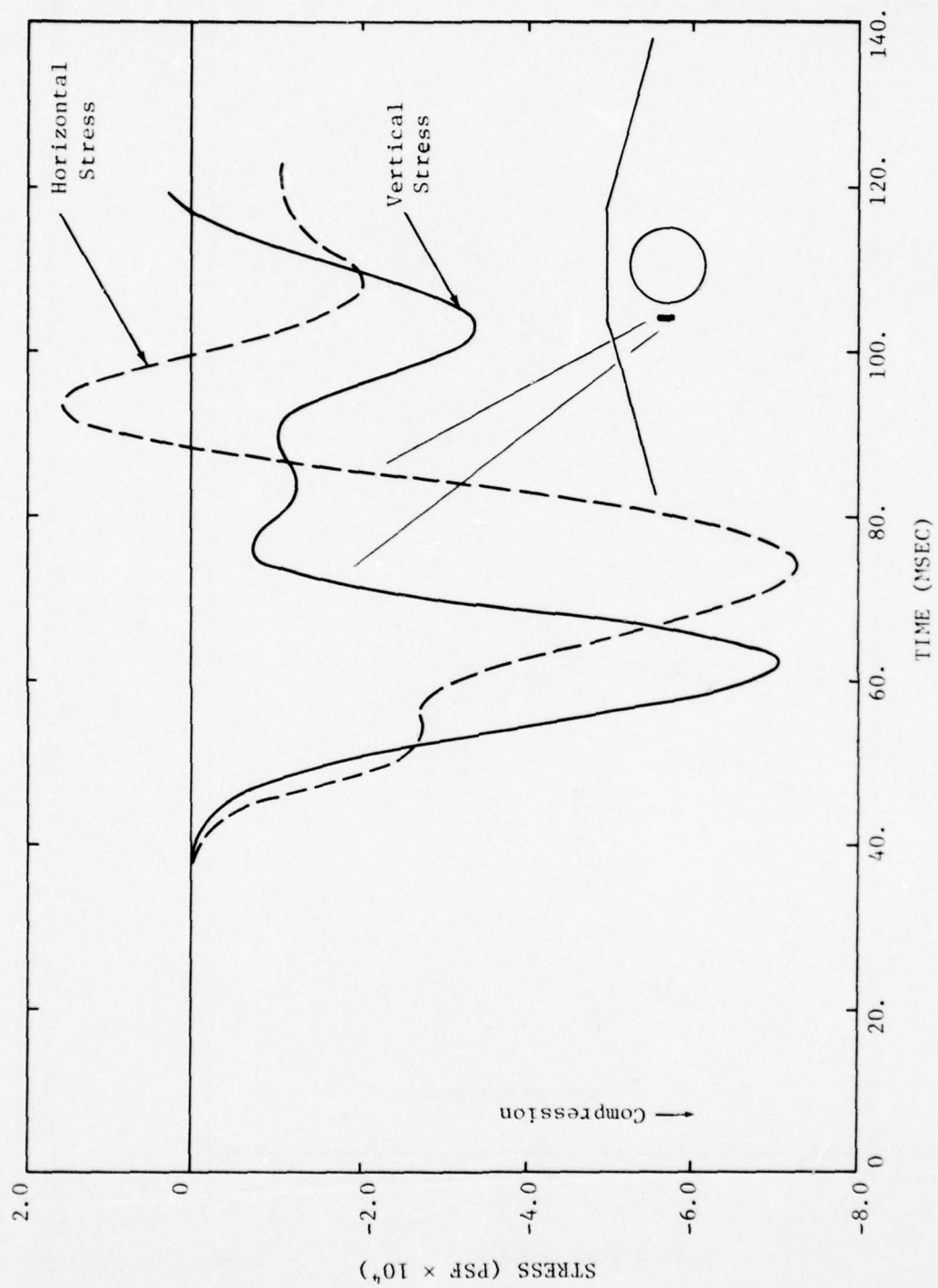
Figure 3-9. Horizontal and vertical stress/time histories in soil, GZ springline, side-on incidence, Calculation 1A
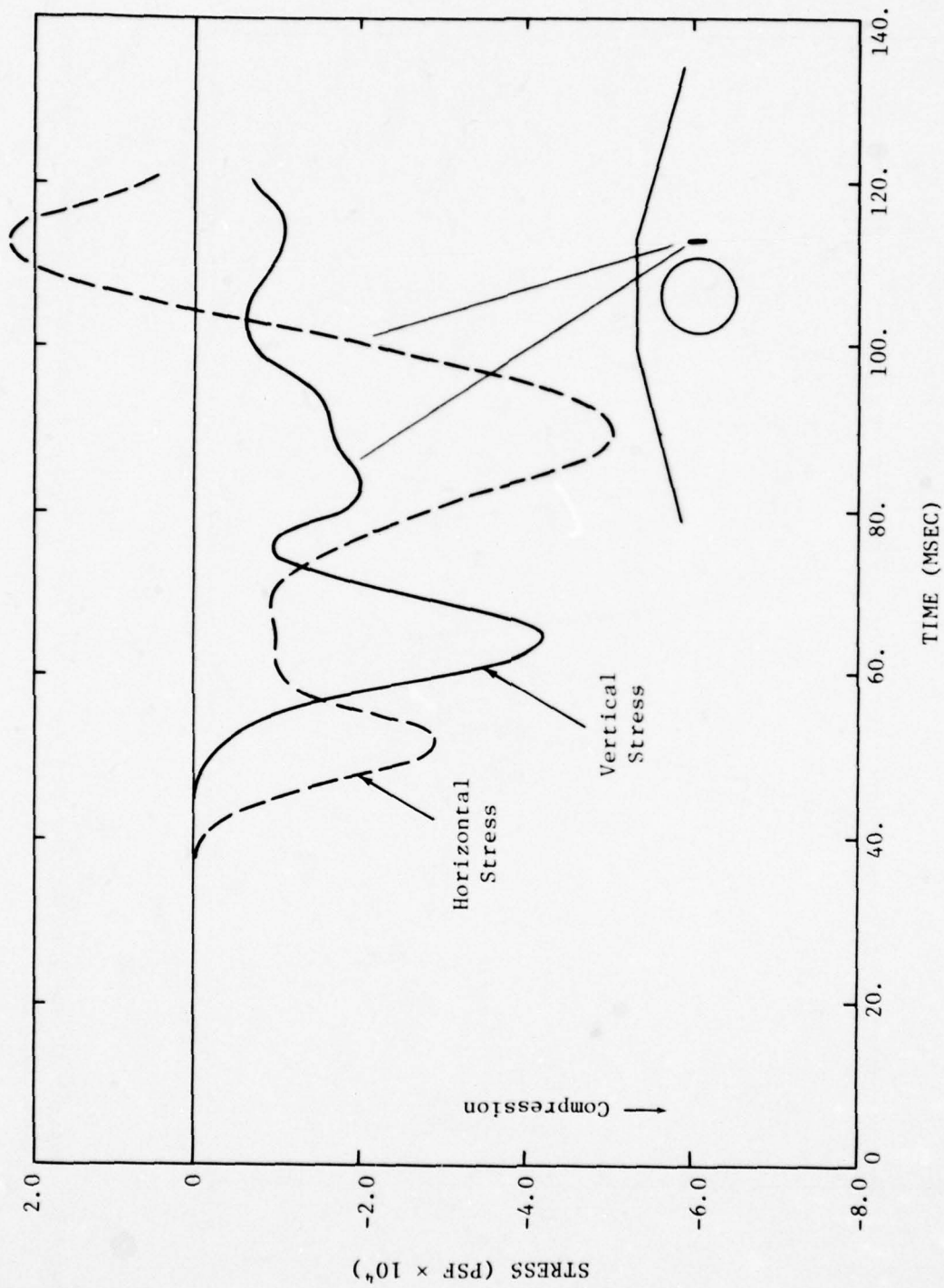
Figure 3-10. Horizontal and vertical stress/time histories in soil, rear springline, side-on incidence, Calculation 1A
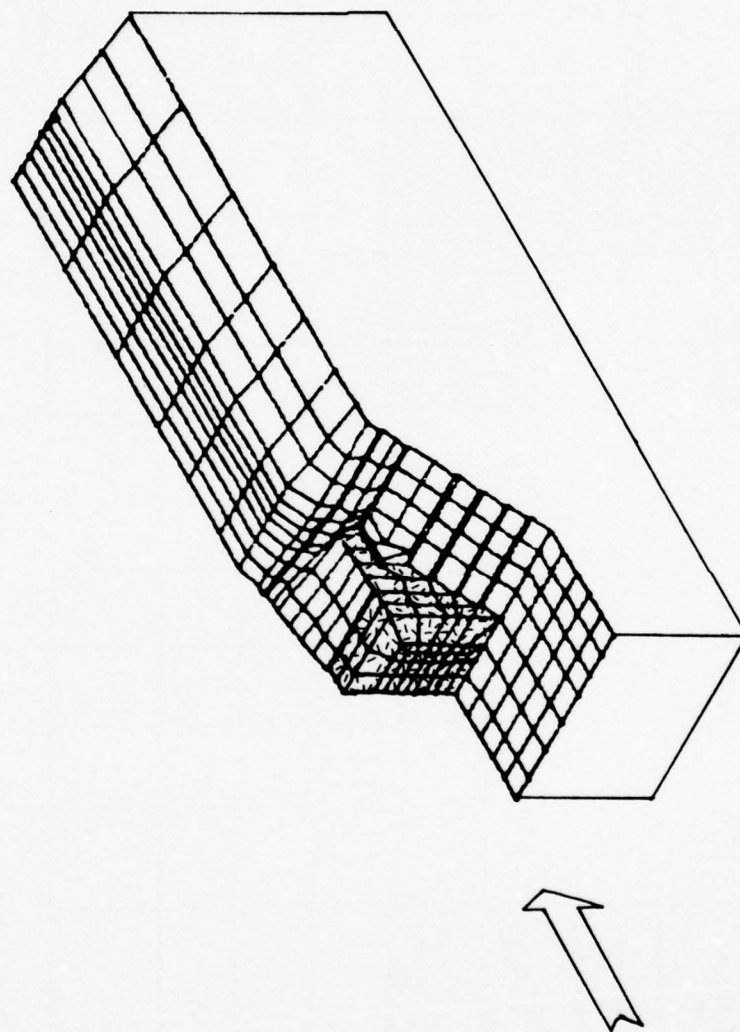
Figure 3-11. Three-dimensional finite element model of shelter and media, front-on incidence, Calculations 1B and 1C

CROSS SECTION BB

CROSS SECTION AA

SCALE (FT.)

0   10.   20.
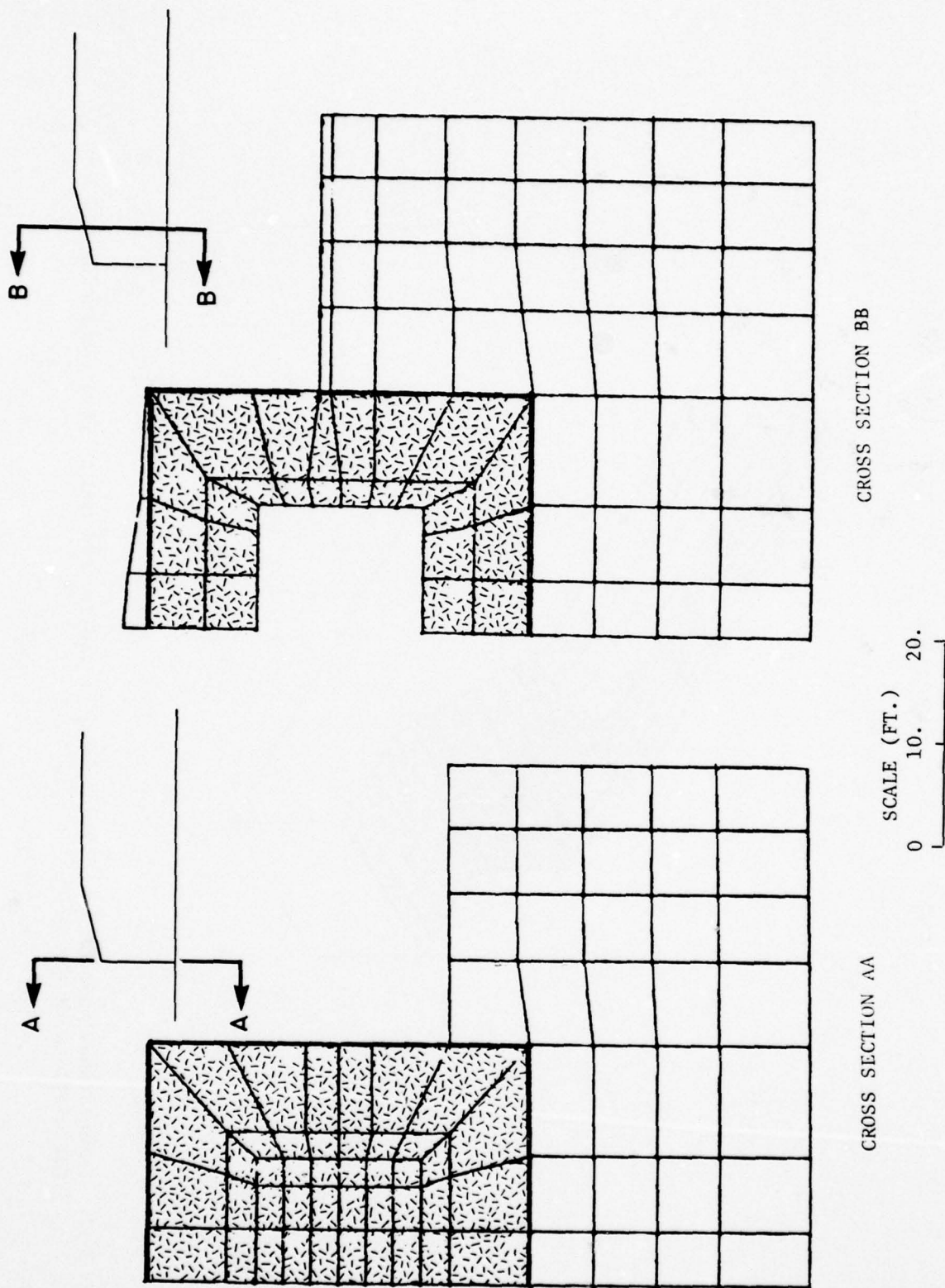
Figure 3-12a. Cross-sectional view of three-dimensional model, front face and headworks

3-24

CROSS SECTION DD

CROSS SECTION CC

SCALE (FT.)

0   10.   20.
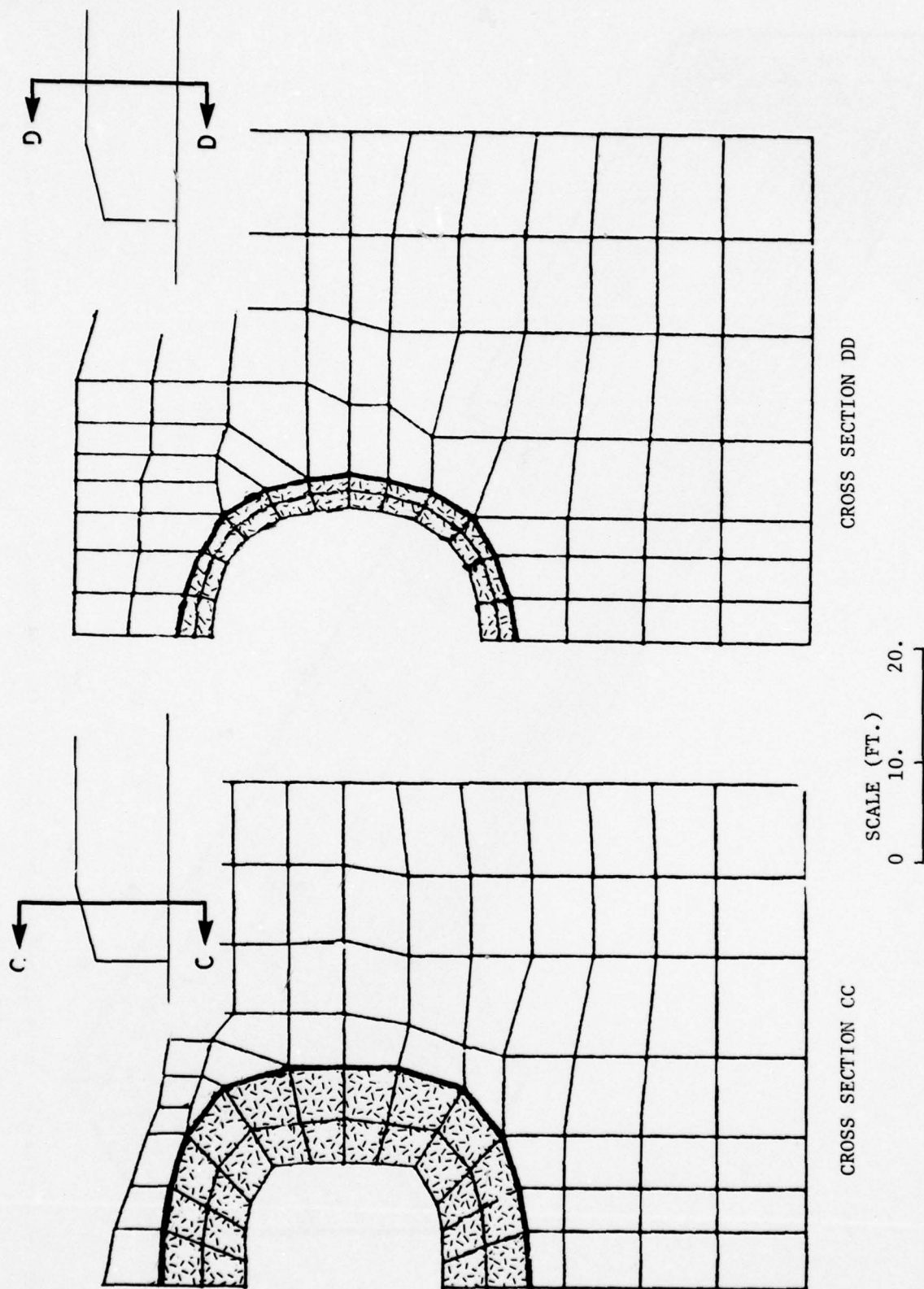
Figure 3-12b. Cross-sectional view of three-dimensional model, transition section and tube
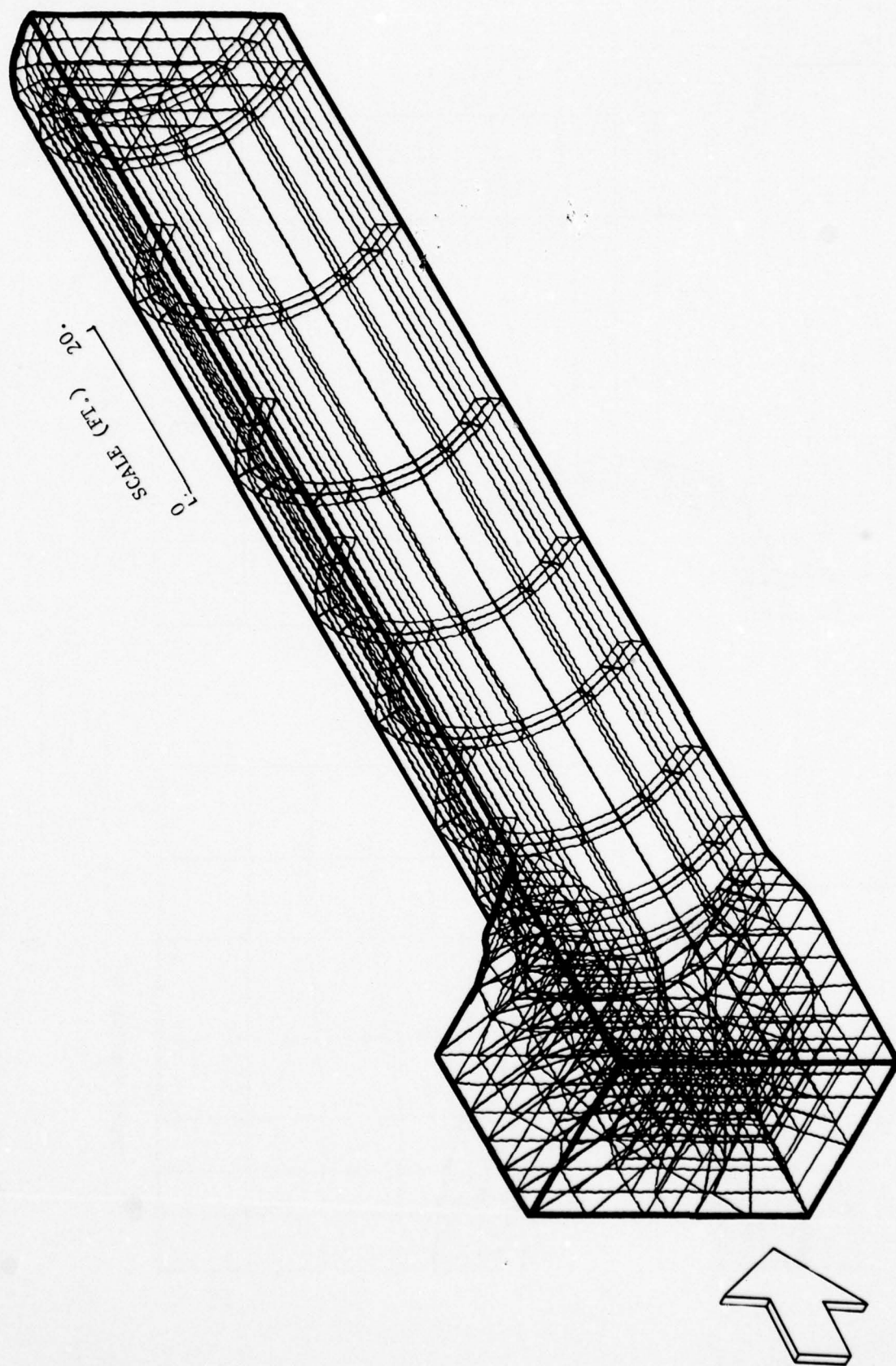
Figure 3-13. View of the three-dimensional model of the bare shelter structure, soil elements not shown

SCALE (FT.)

20.

0.
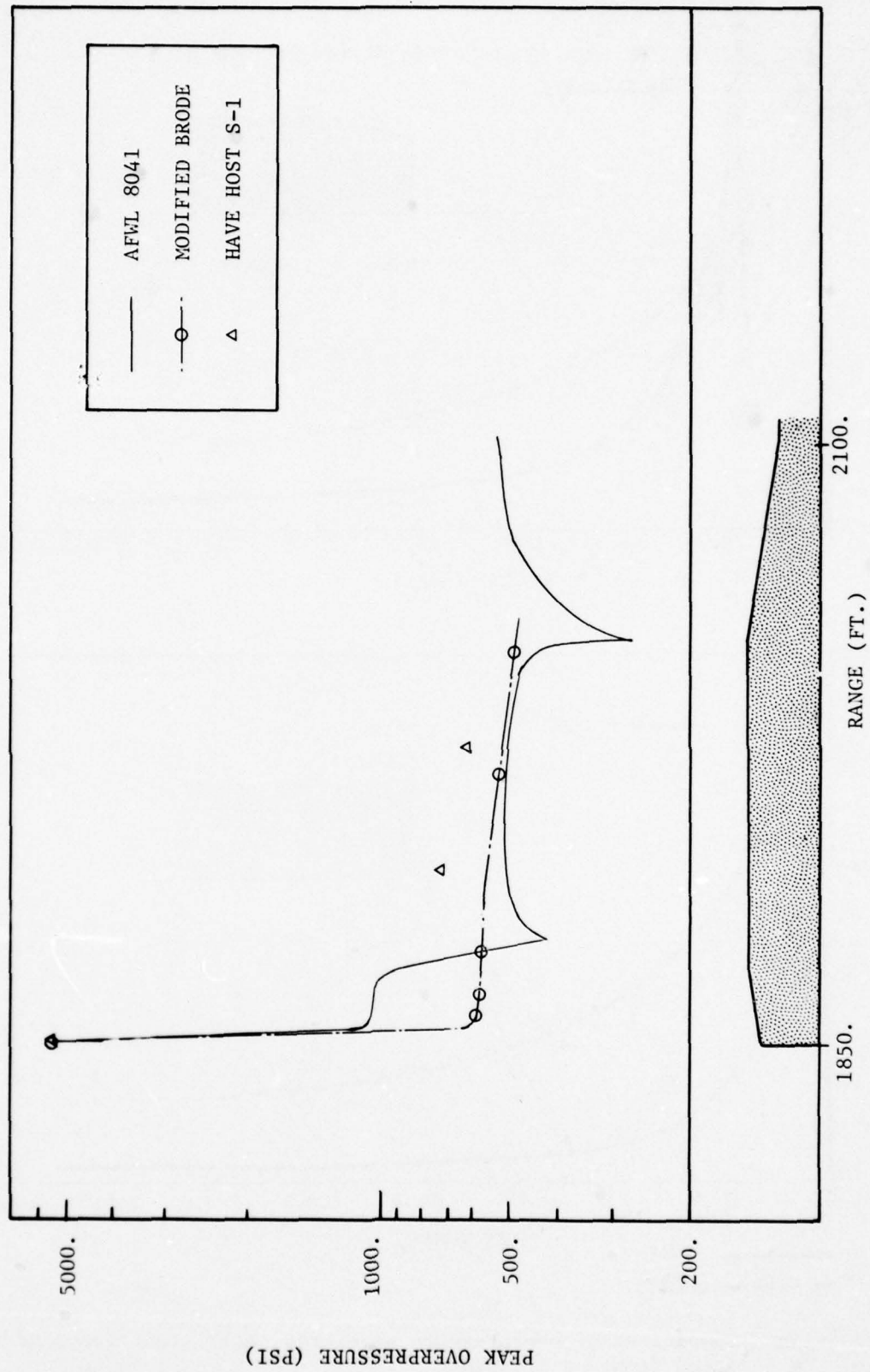
Figure 3-14. Comparison of peak overpressure profiles, front-on incidence, Calculations 1B and 1C

3-27
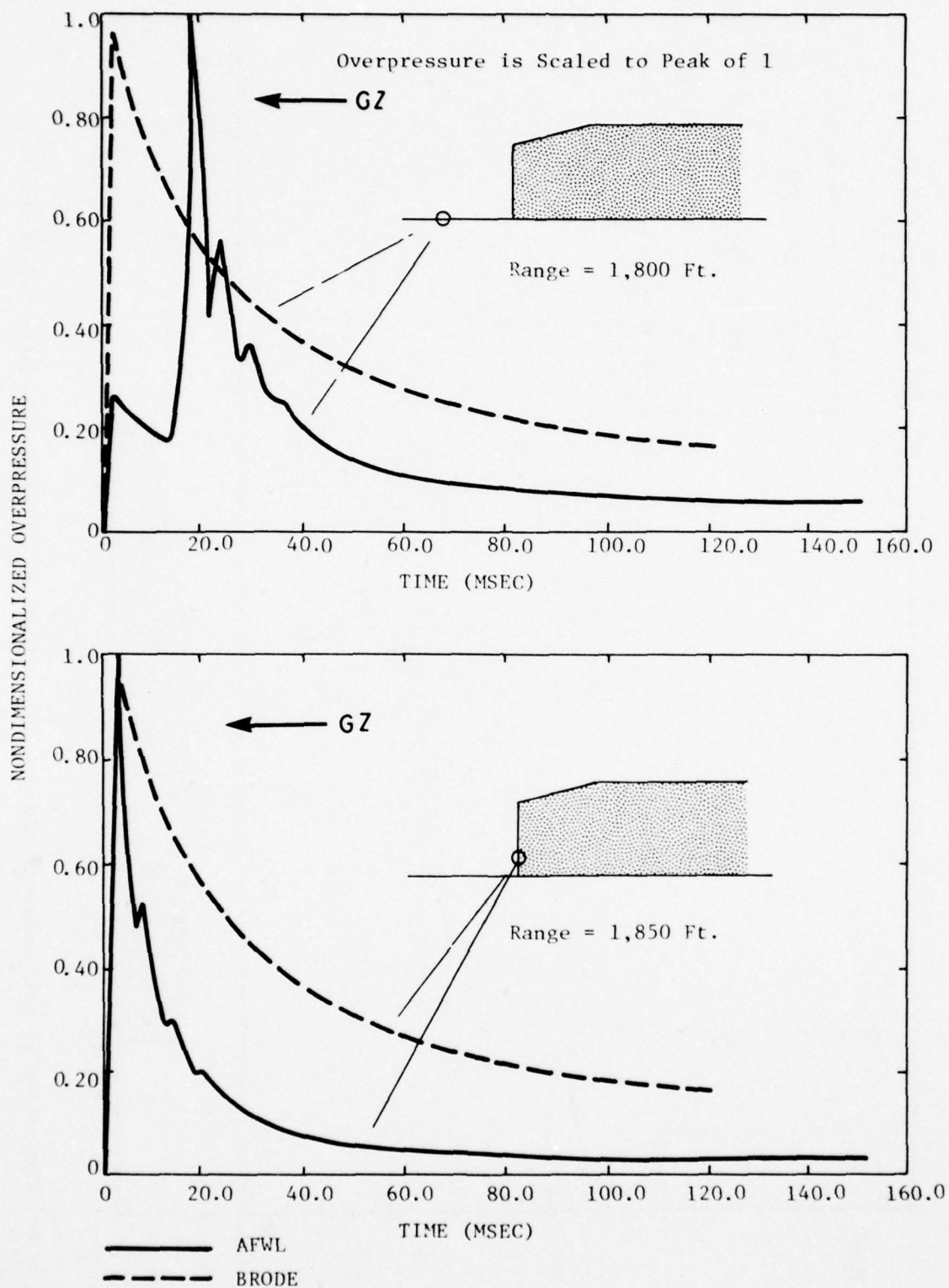
Figure 3-15a. Comparison of overpressure waveforms, near front face, at front face, front-on incidence
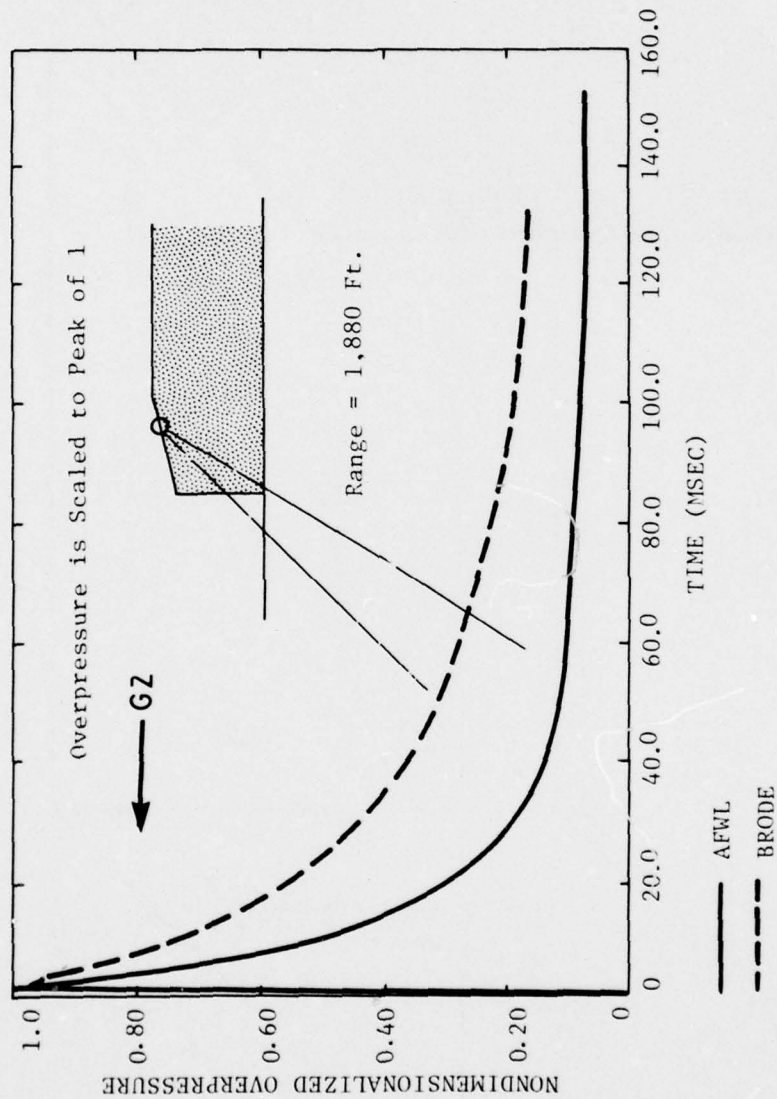
Figure 3-15b. Comparison of overpressure waveforms, top, front-on incidence
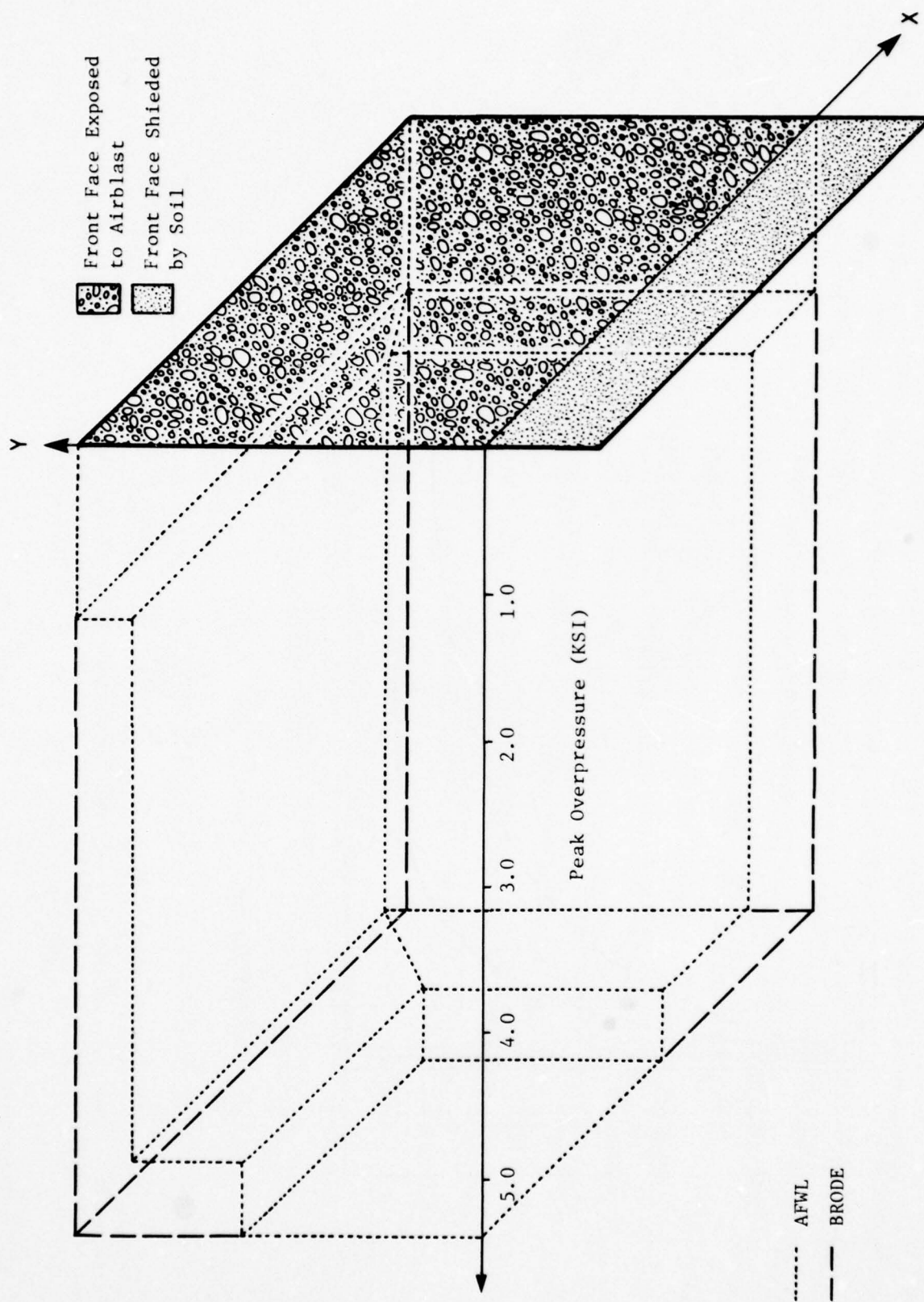
Figure 3-16. Comparison of peak overpressure distribution on front face
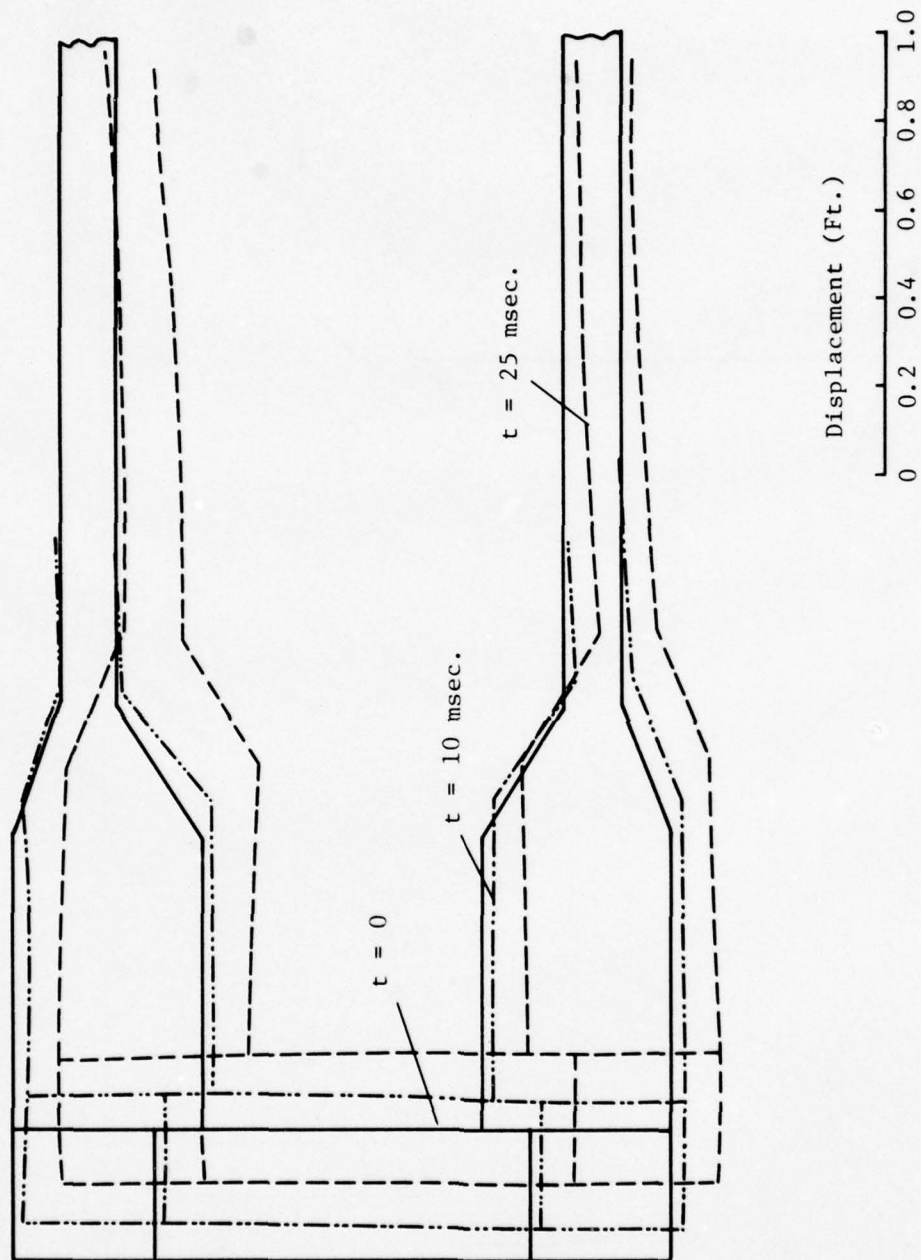
Figure 3-17. Deformation modes, exaggerated, AFWL 8041 load, front-on incidence, Calculation 1B

t = 25 msec.

t = 10 msec.

t = 0

Displacement (Ft.)

0   0.2   0.4   0.6   0.8   1.0
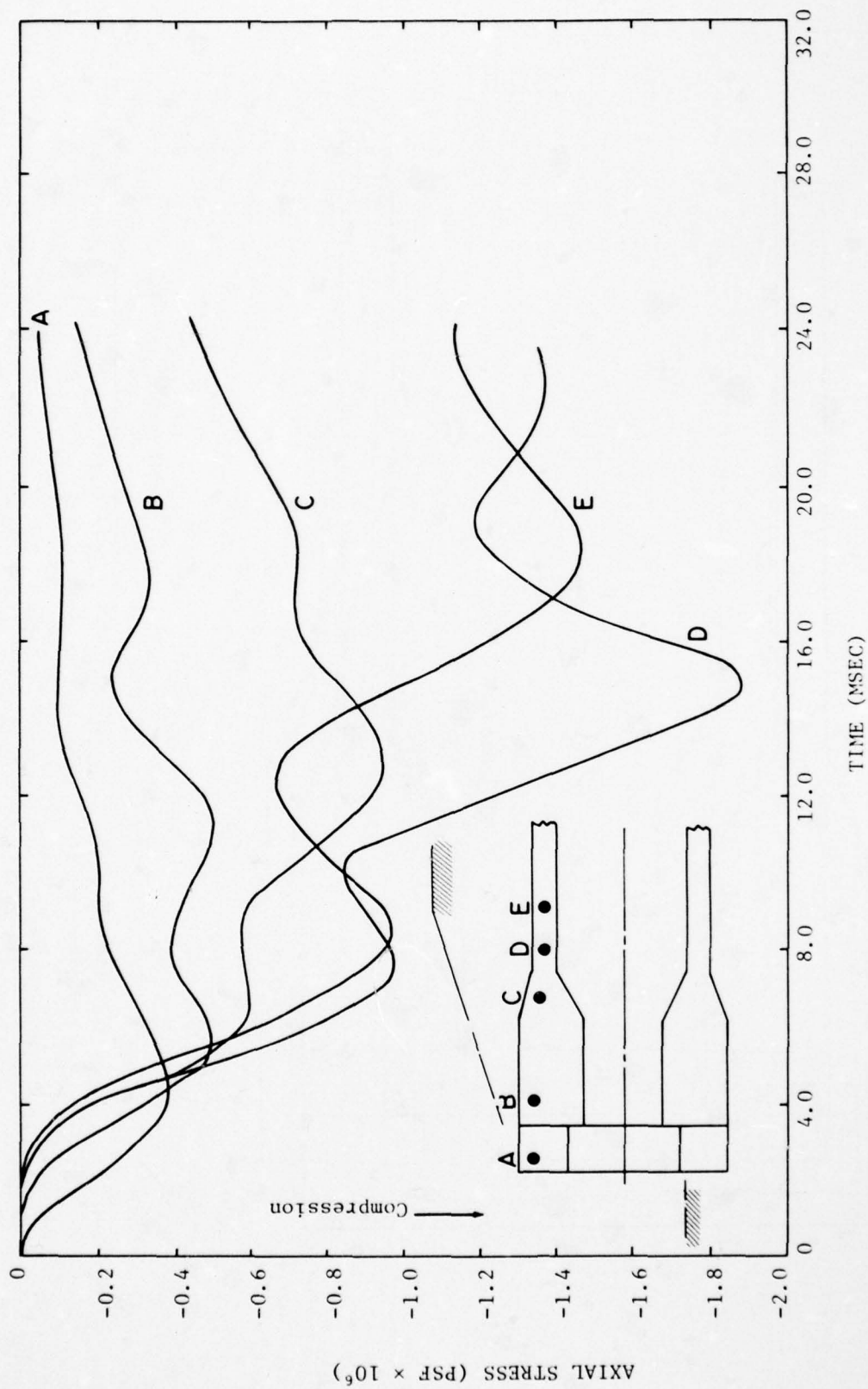
Figure 3-18. Axial stress-time histories along shelter length, upper headworks, front-on incidence, Calculation 1B
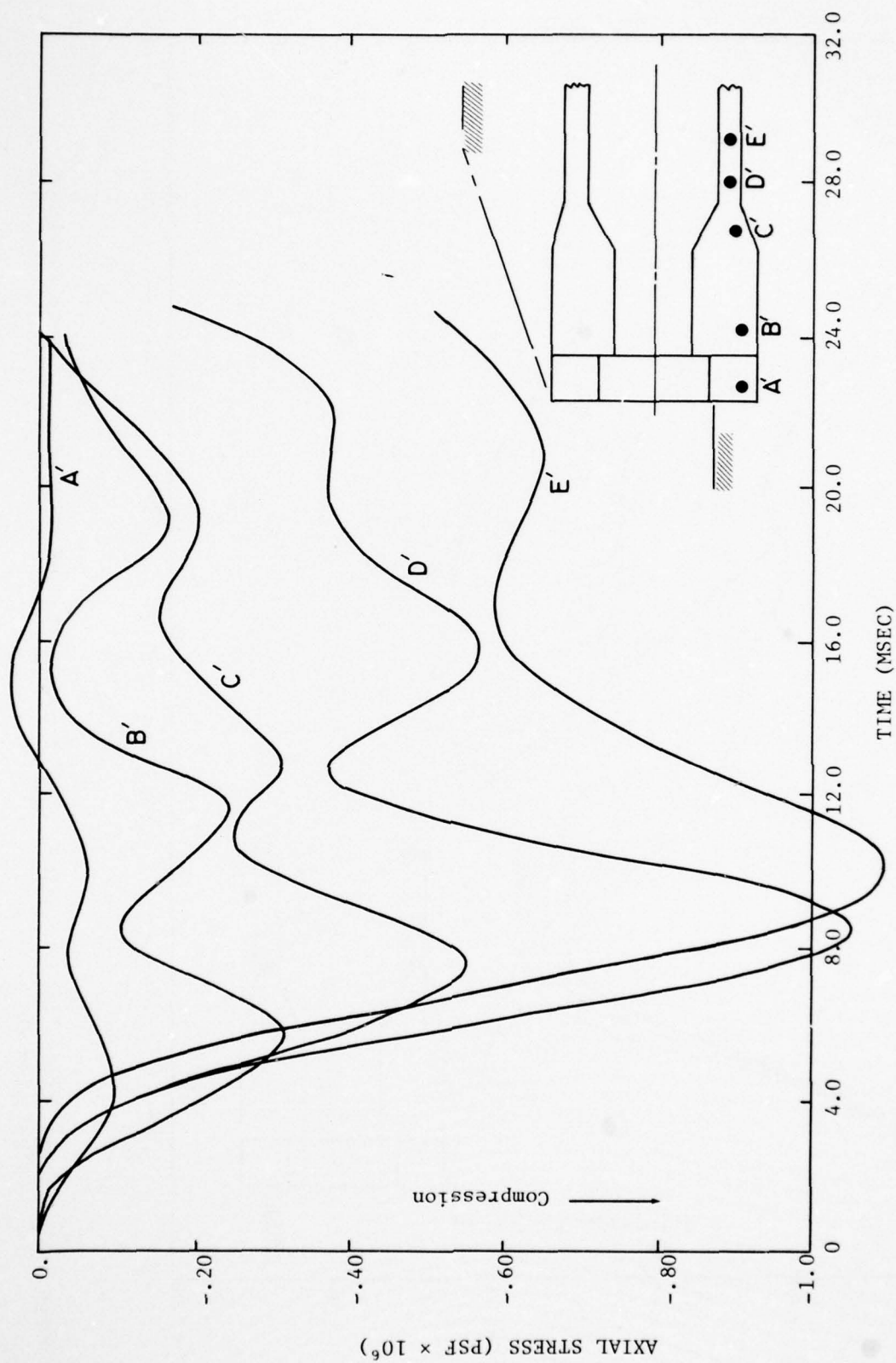
Figure 3-19. Axial stress/time histories along shelter length, lower headworks, front-on incidence, Calculation 1B
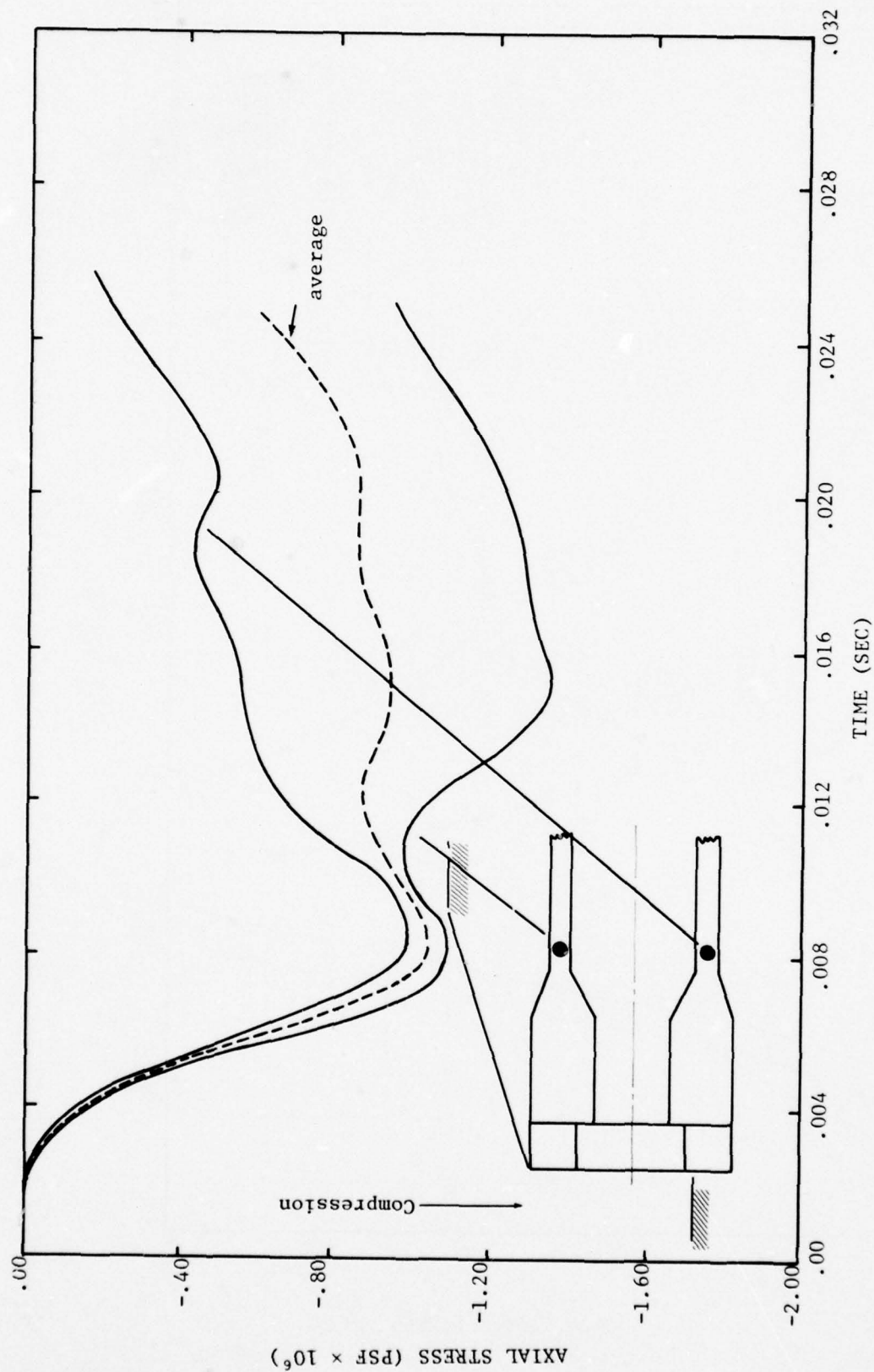
Figure 3-20. Axial stress time histories, tubular portion behind headworks, front-on incidence, Calculation 1B
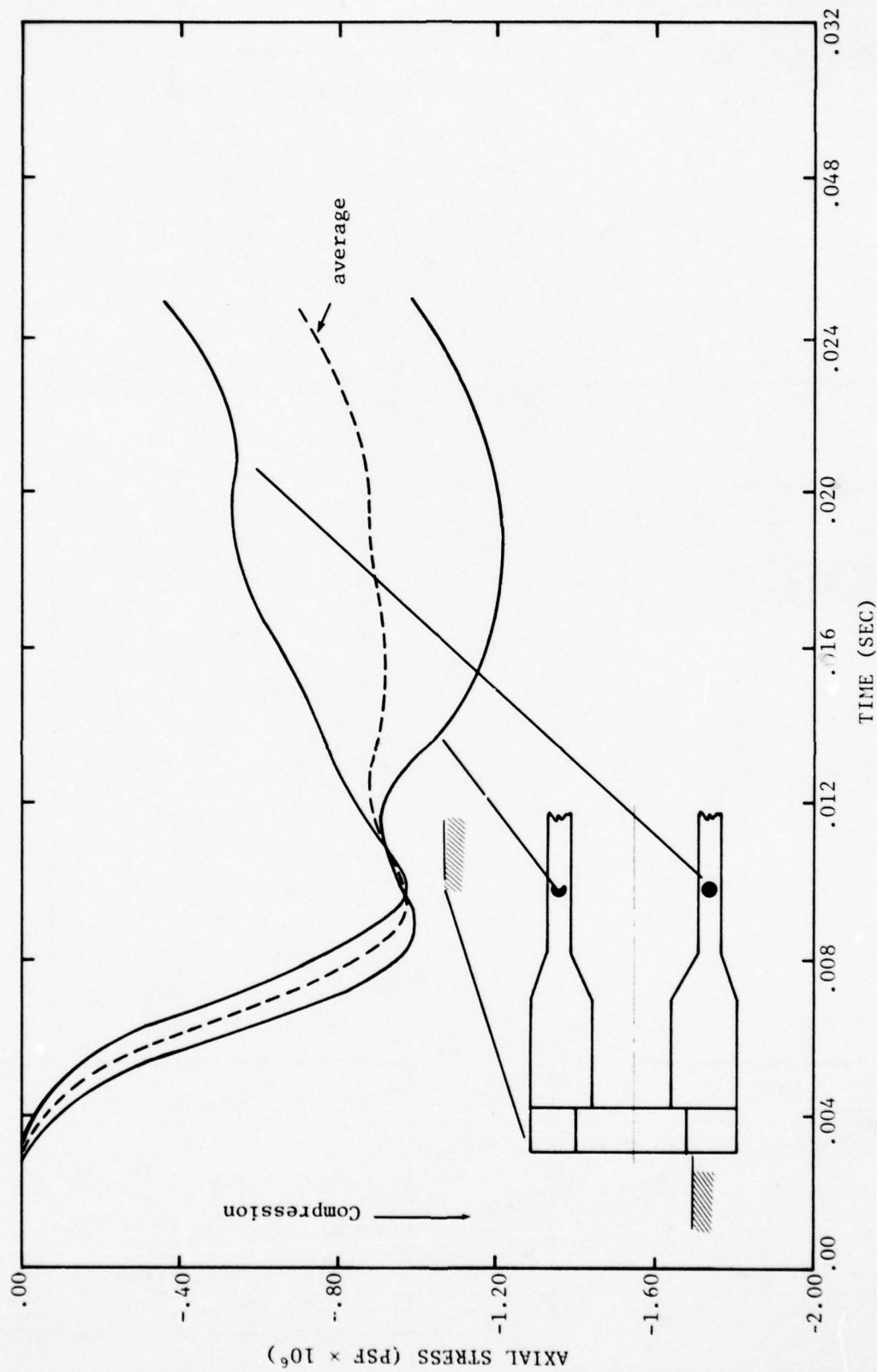
Figure 3-21. Axial stress time histories, tubular portion half tube diameter behind headworks, front-on incidence, Calculation 1B
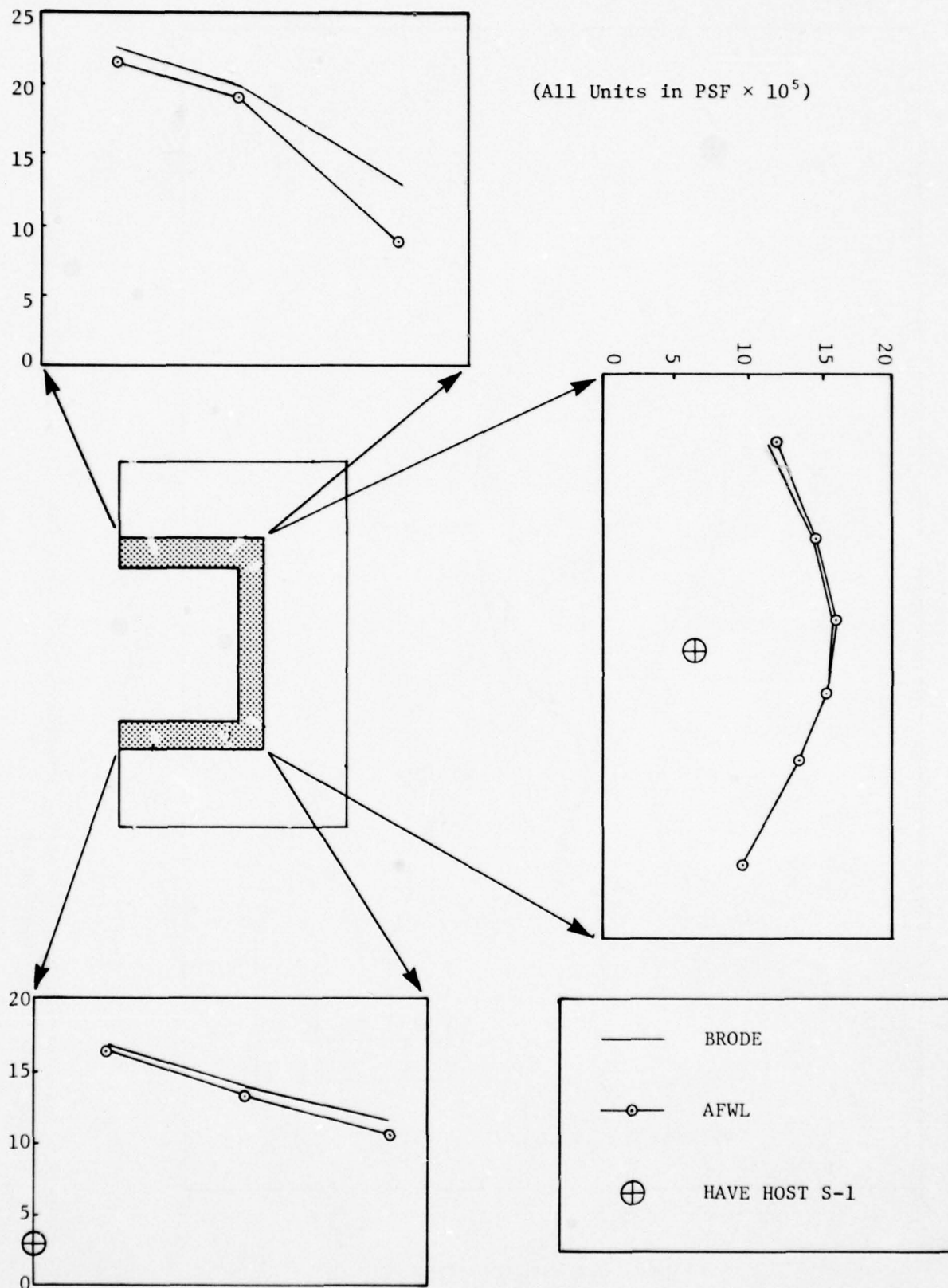
Figure 3-22. Distribution of peak bearing load exerted by closure on headworks,
front-on incidence, Calculation 1B
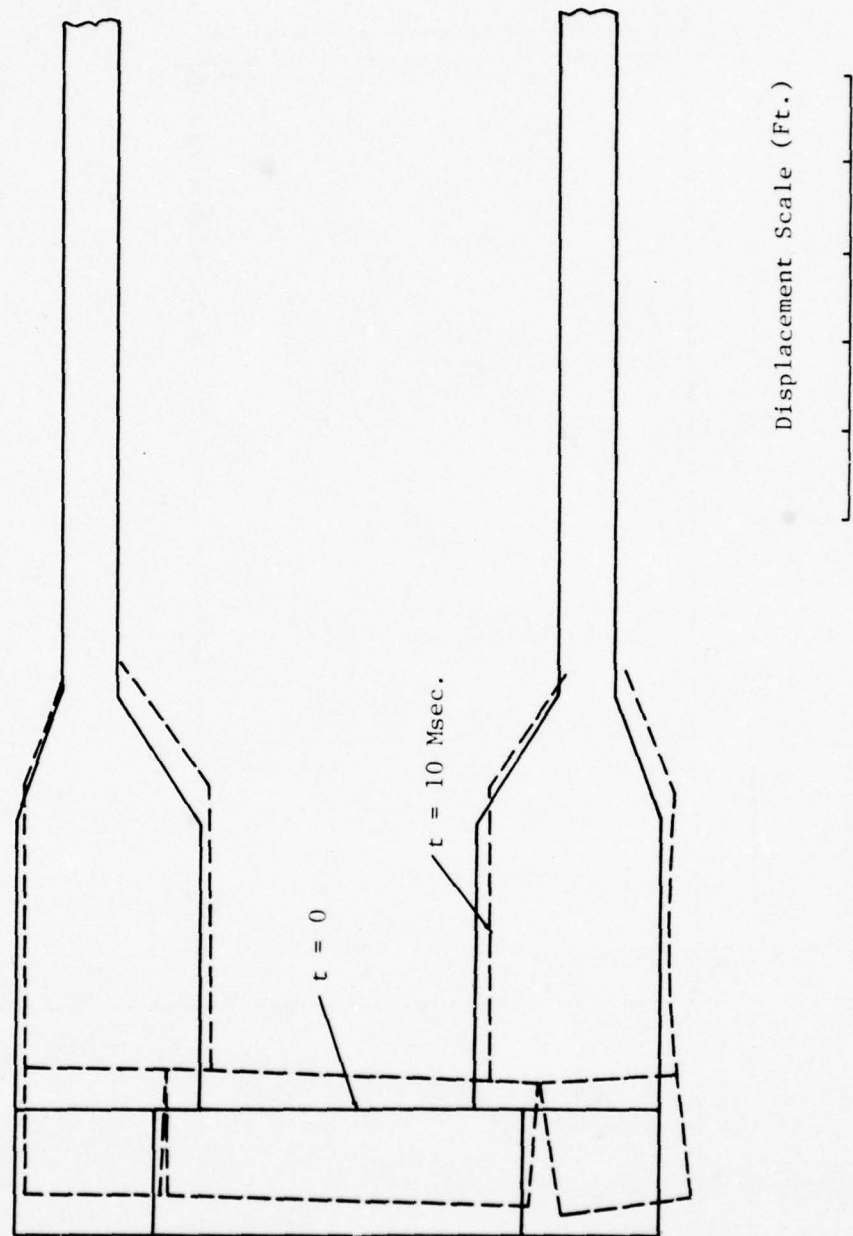
Figure 3-23. Deformation mode, exaggerated, gap, front-on incidence, Calculation 1C

DISPLACEMENT SCALE
(FT.)

0   0.1
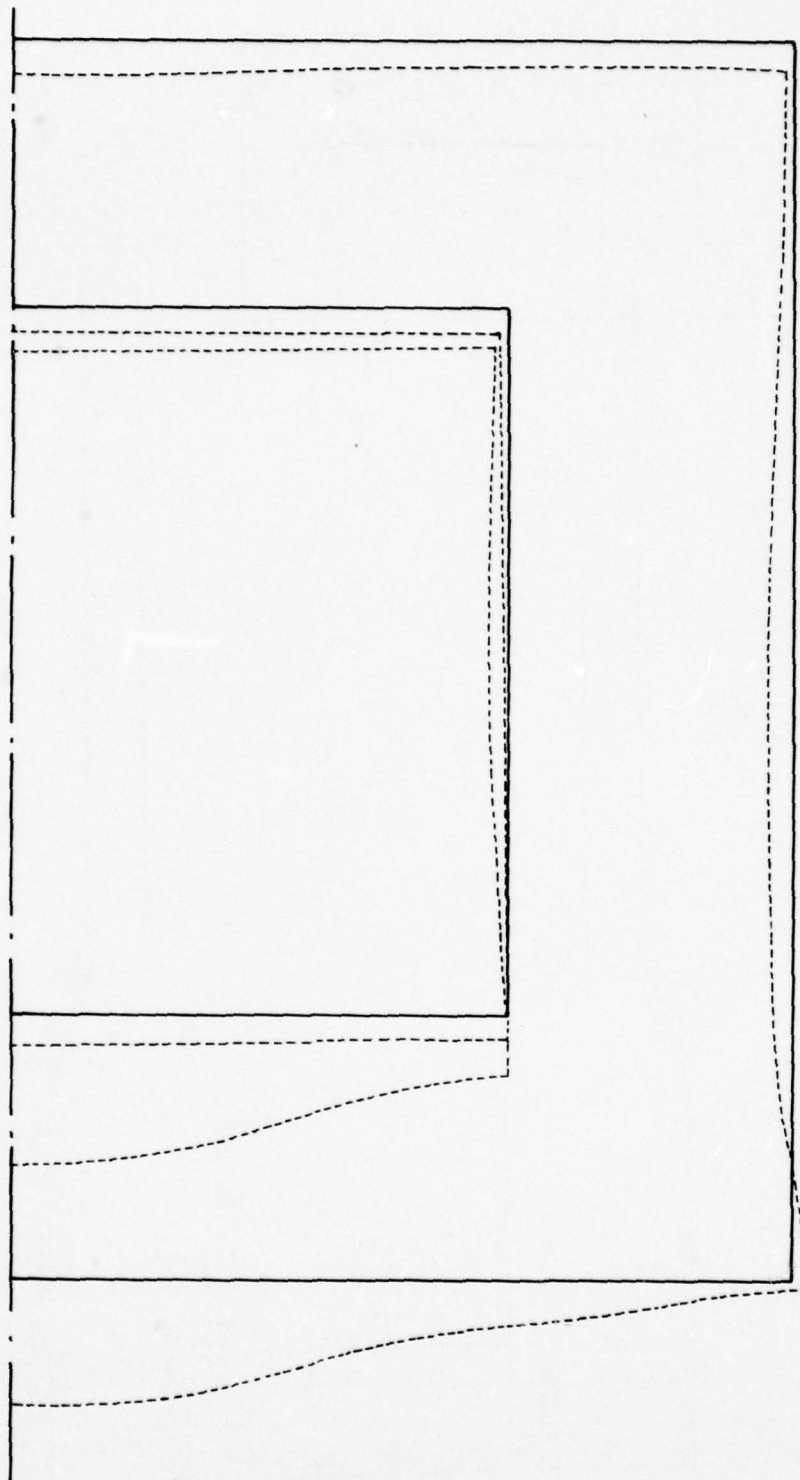
Figure 3-24.   Deformation pattern of closure and front face at t = 10 msec.,
exaggerated, front-on incidence, Calculation 1C
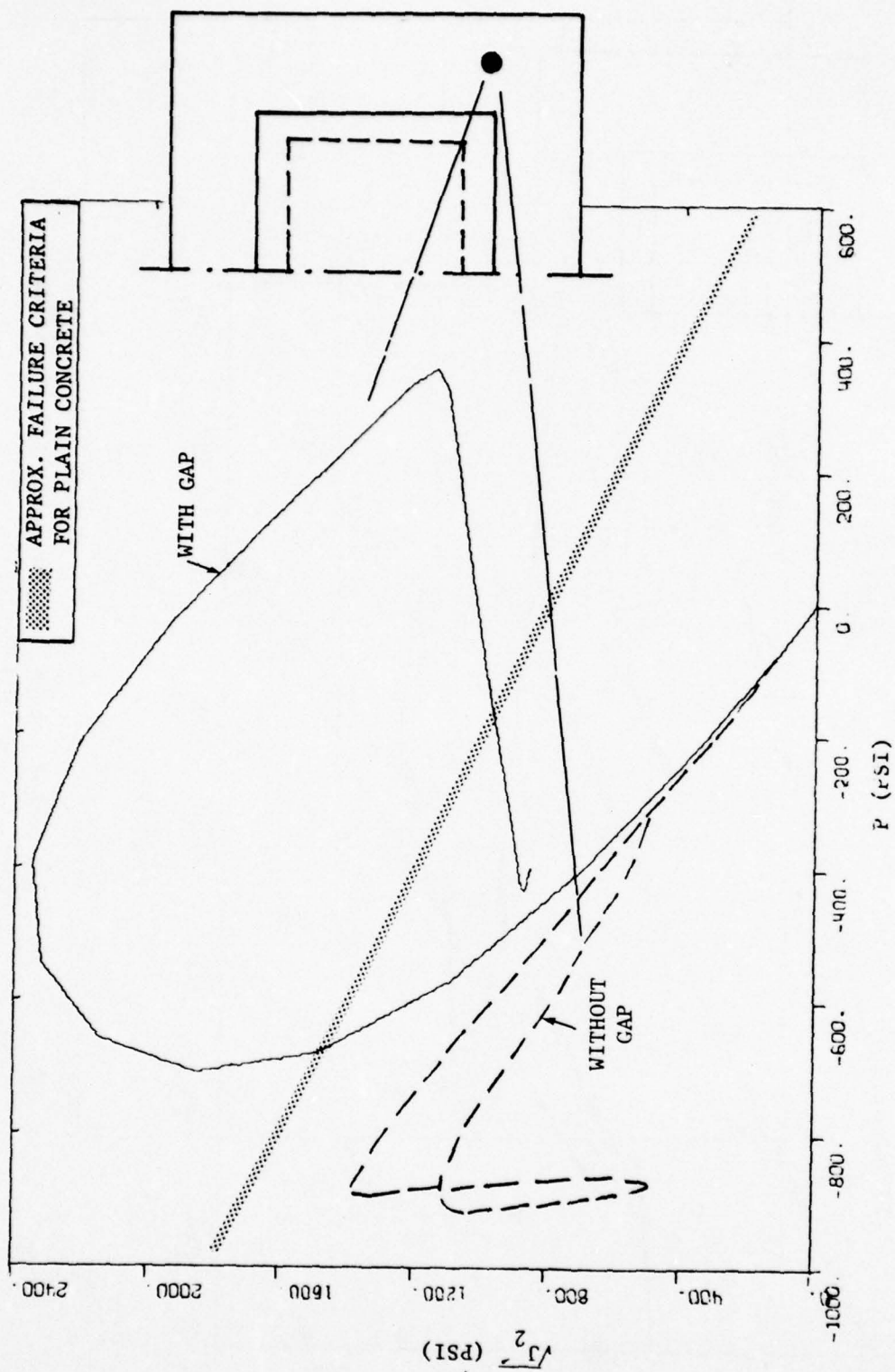
Figure 3-25a. Plot of first and second stress invariants at front face, gap, front-on incidence, Calculation 1C
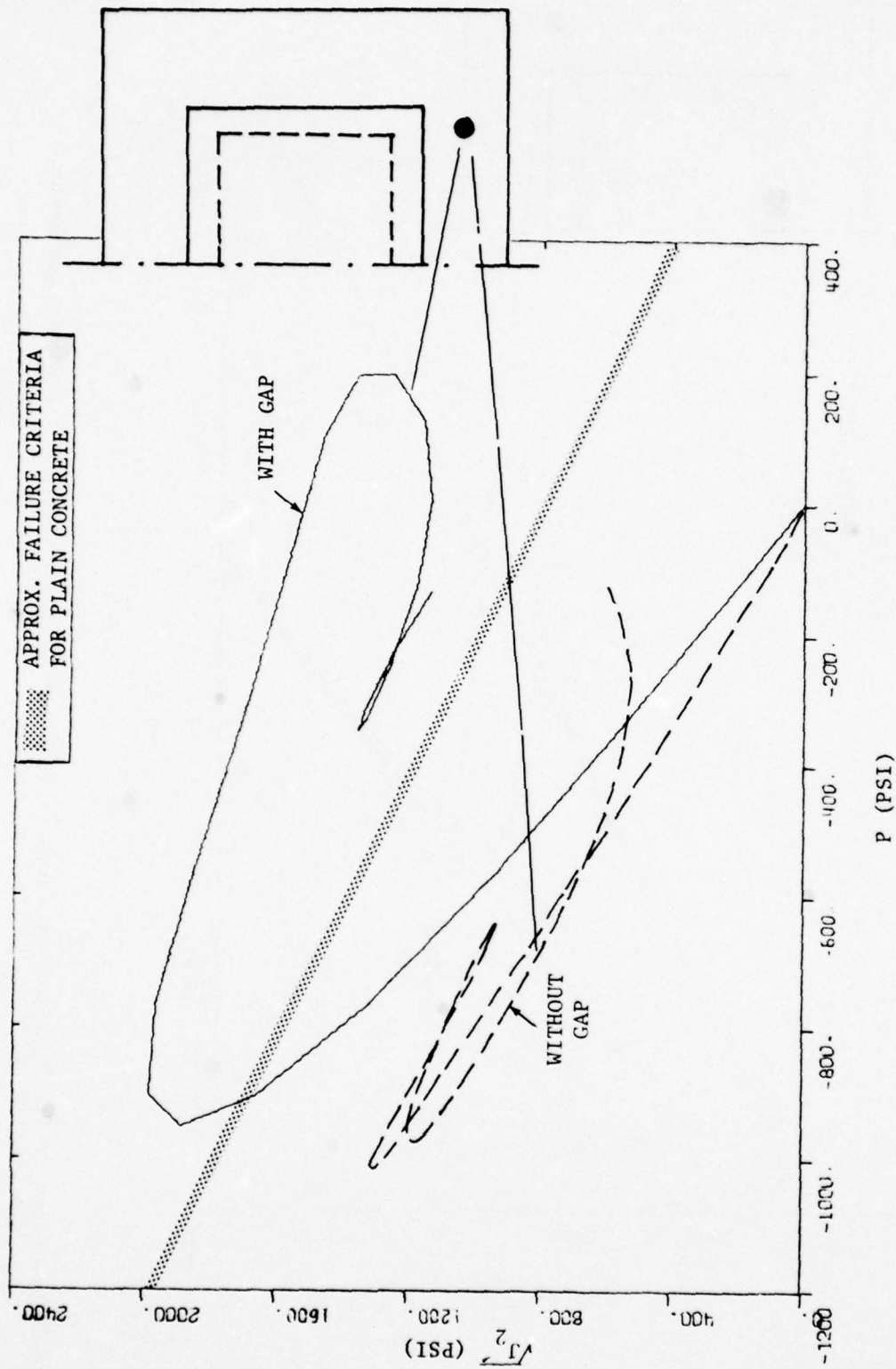
Figure 3-25b. Plot of first and second stress invariants at front face, gap, front-on incidence, Calculation 1C

(All Units in PSF × 10^5)
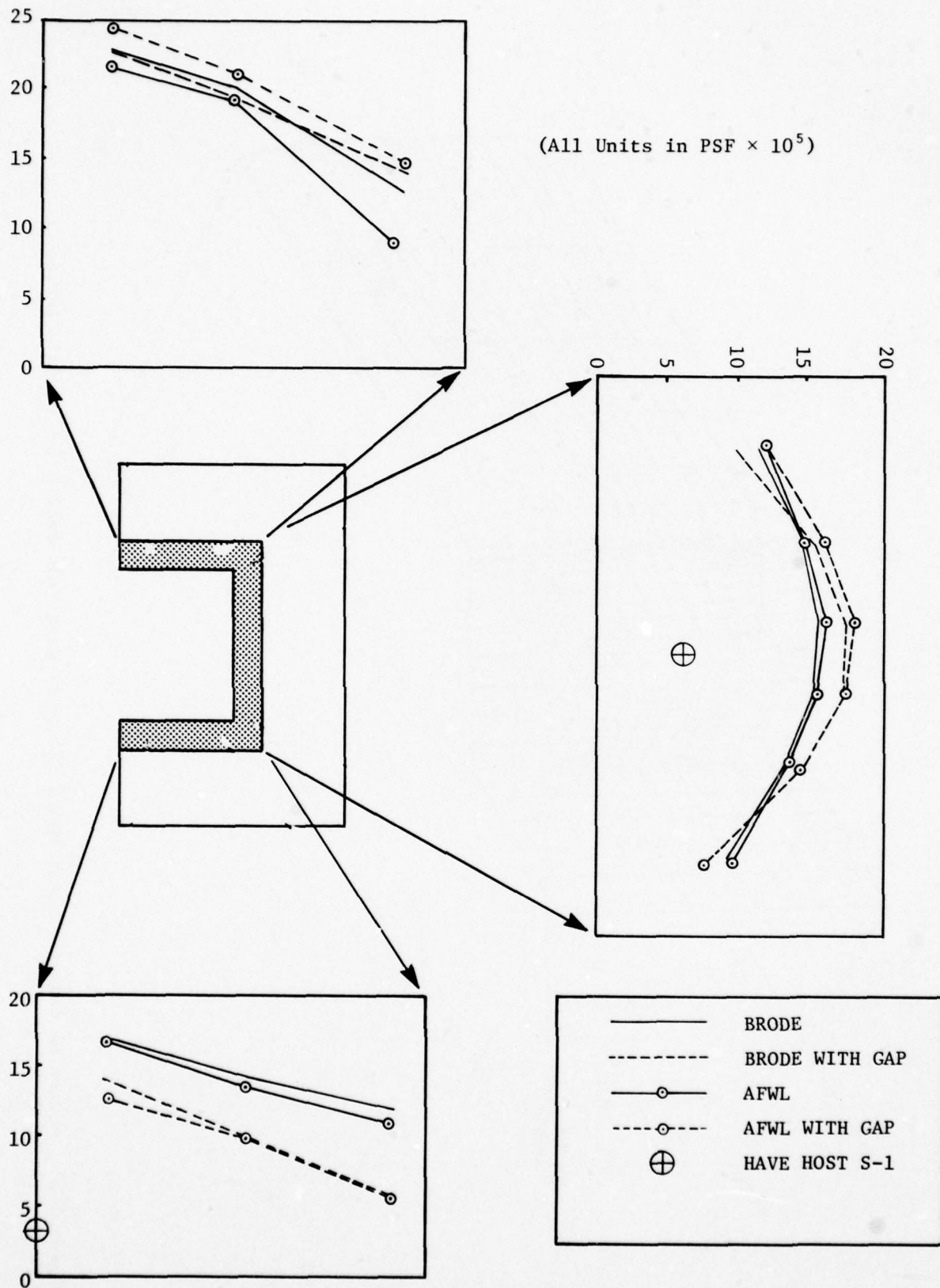
Figure 3-26. Effect of gap on peak bearing load exerted by closure on headworks

3-41
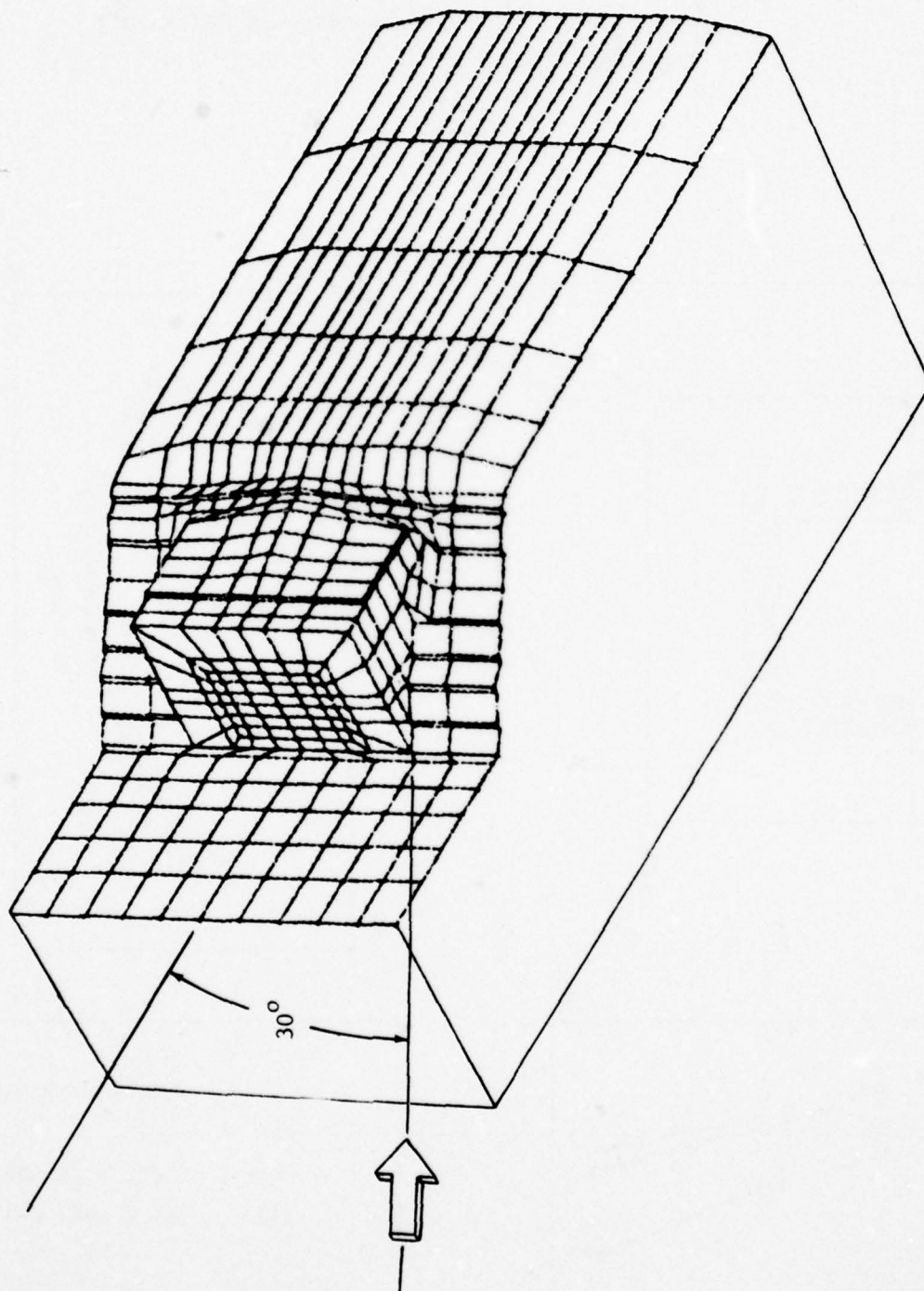
Figure 3-27. A view of finite element model for quartering calculation (30°), Calculation 1D
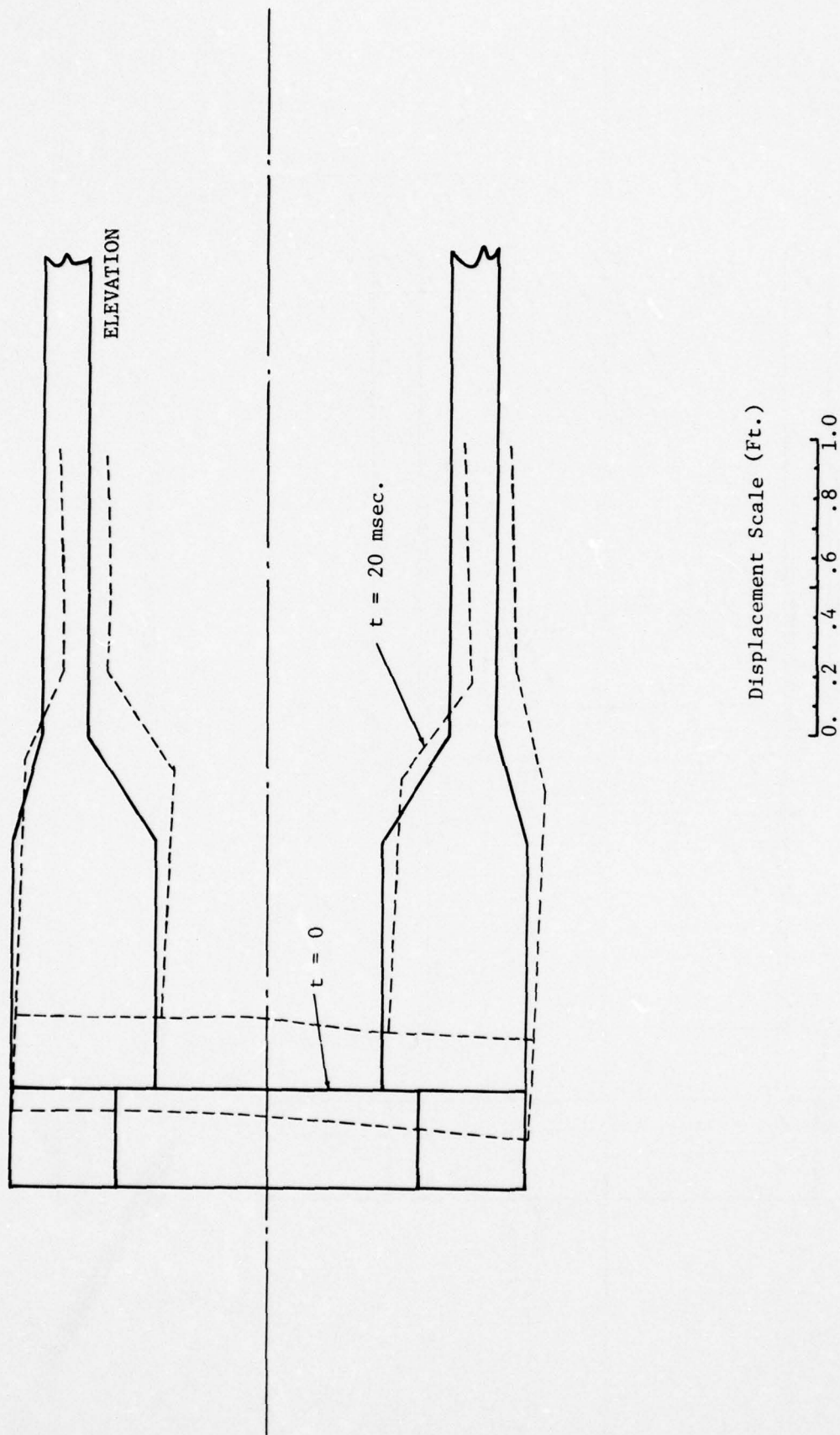
Figure 3-28. Deformation mode, vertical plane of symmetry, 30° oblique front-on incidence, Calculation 1D
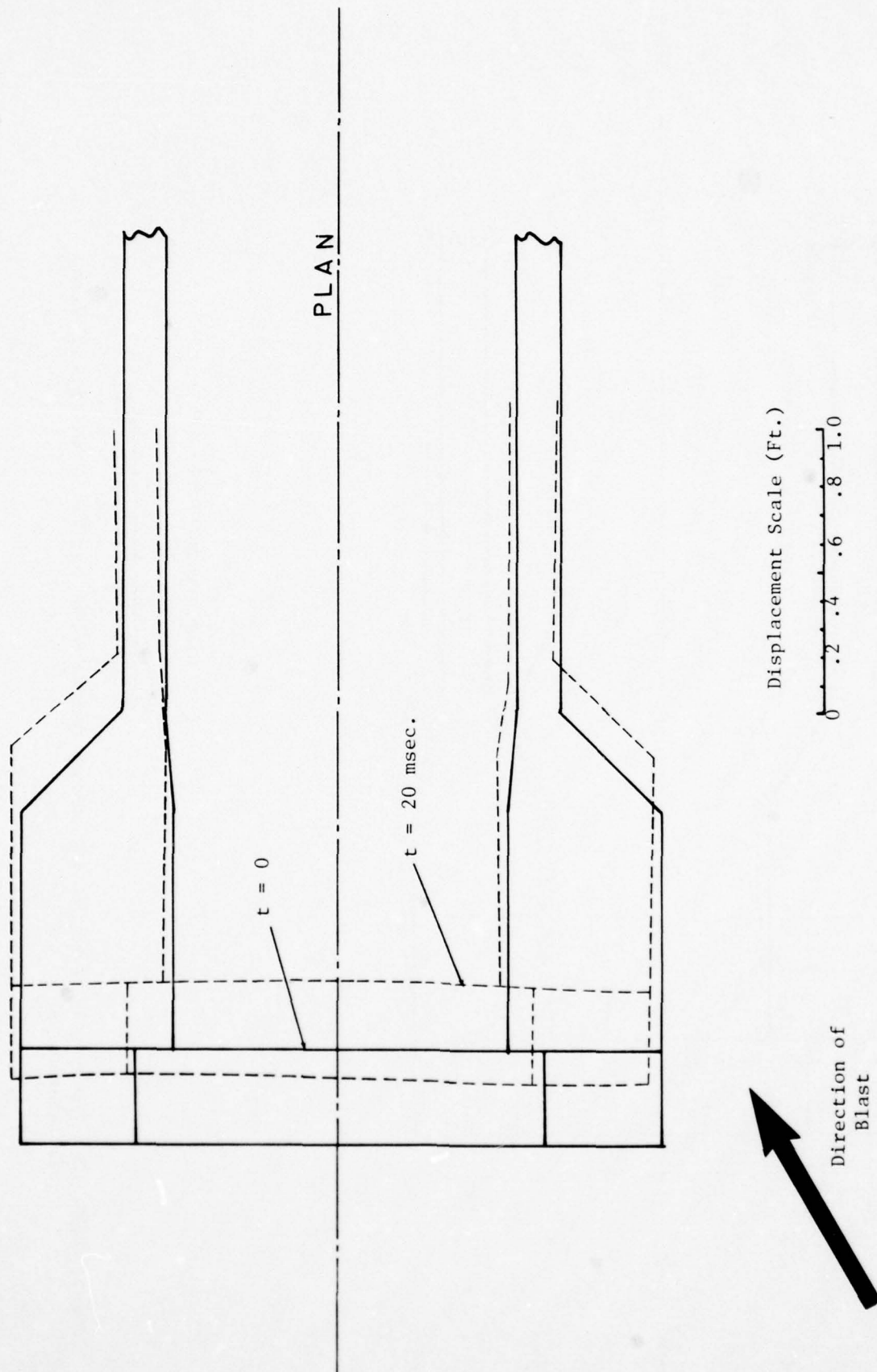
Figure 3-29. Deformation mode, horizontal plane of symmetry, 30° oblique front-on incidence, Calculation 1D
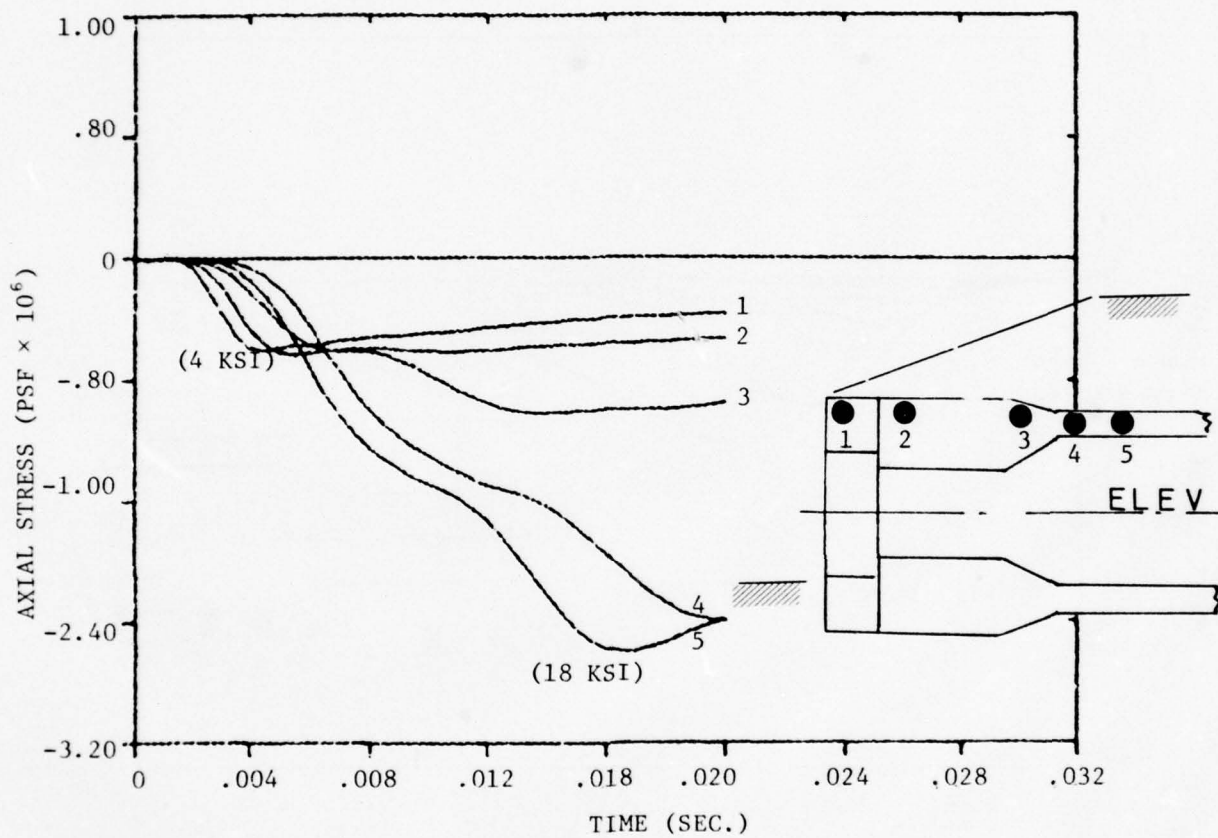
Figure 3-30. Variation in axial stress along top of structure, 30° oblique front-on incidence, Calculation 1D
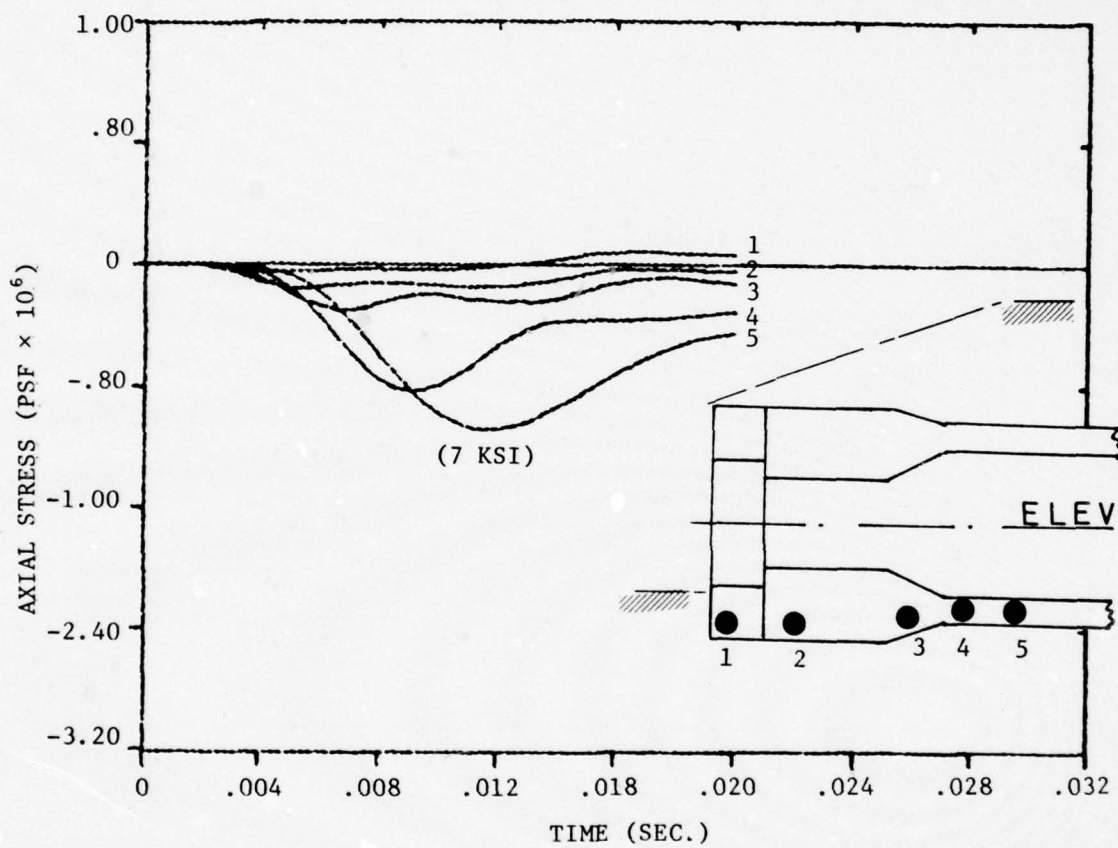
Figure 3-31. Variation in axial stress along bottom of structure, 30° oblique front-on incidence, Calculation 1D
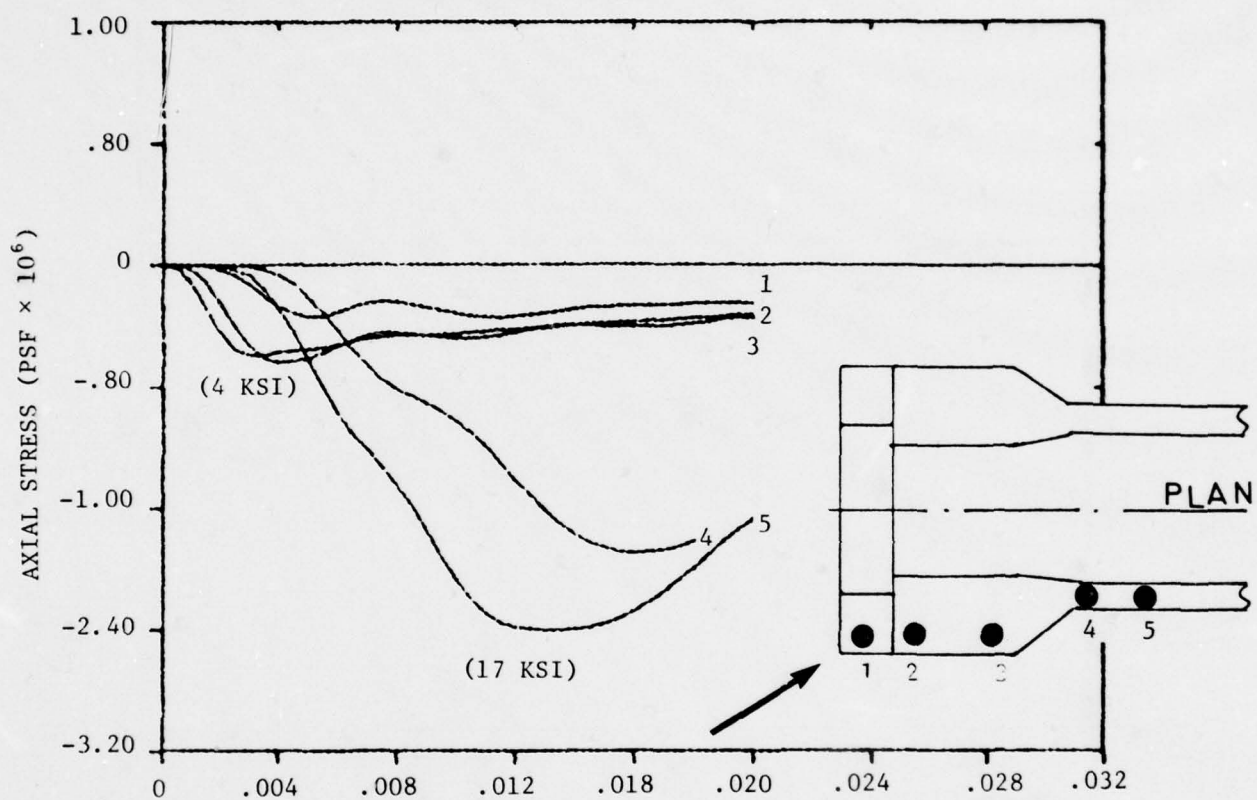
Figure 3-32. Variation in axial stress along springline, blast side of struc-
ture, 30° oblique front-on incidence, Calculation 1D
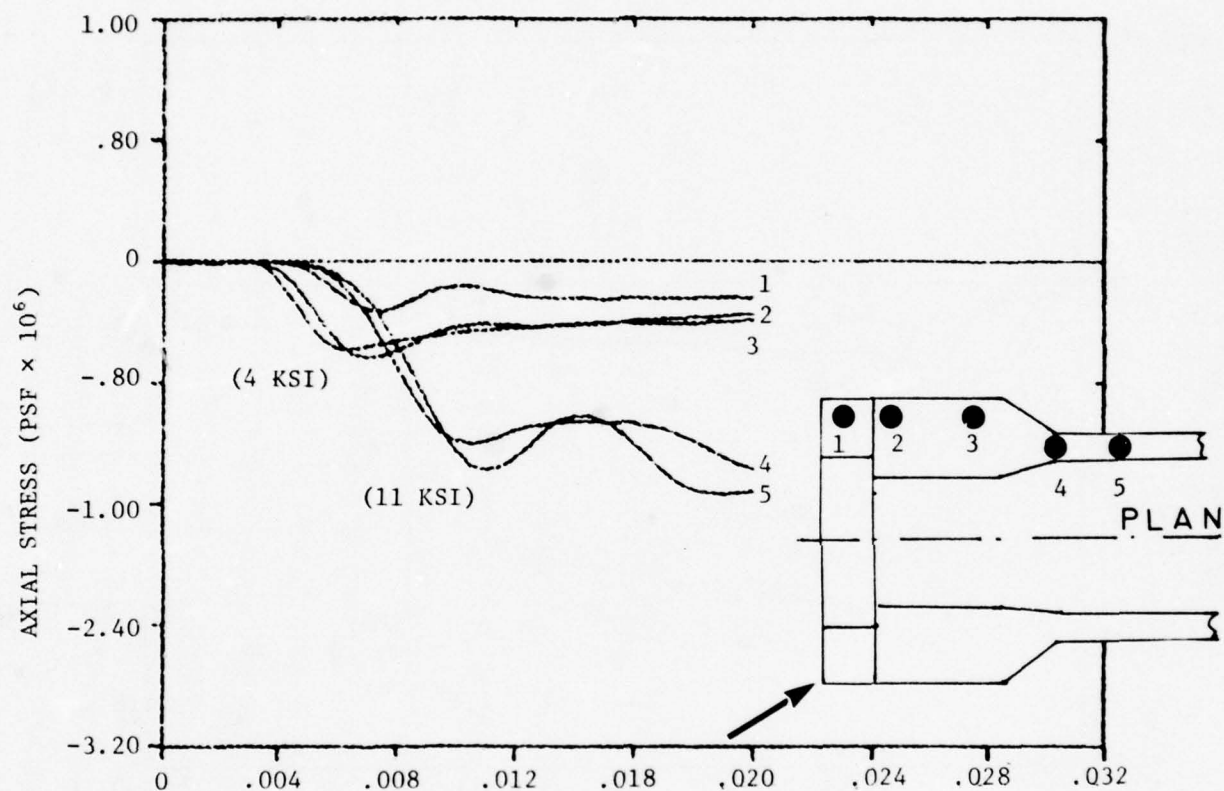
Figure 3-33. Variation in axial stress along springline, back side of structure, 30° oblique front-on incidence, Calculation 1A
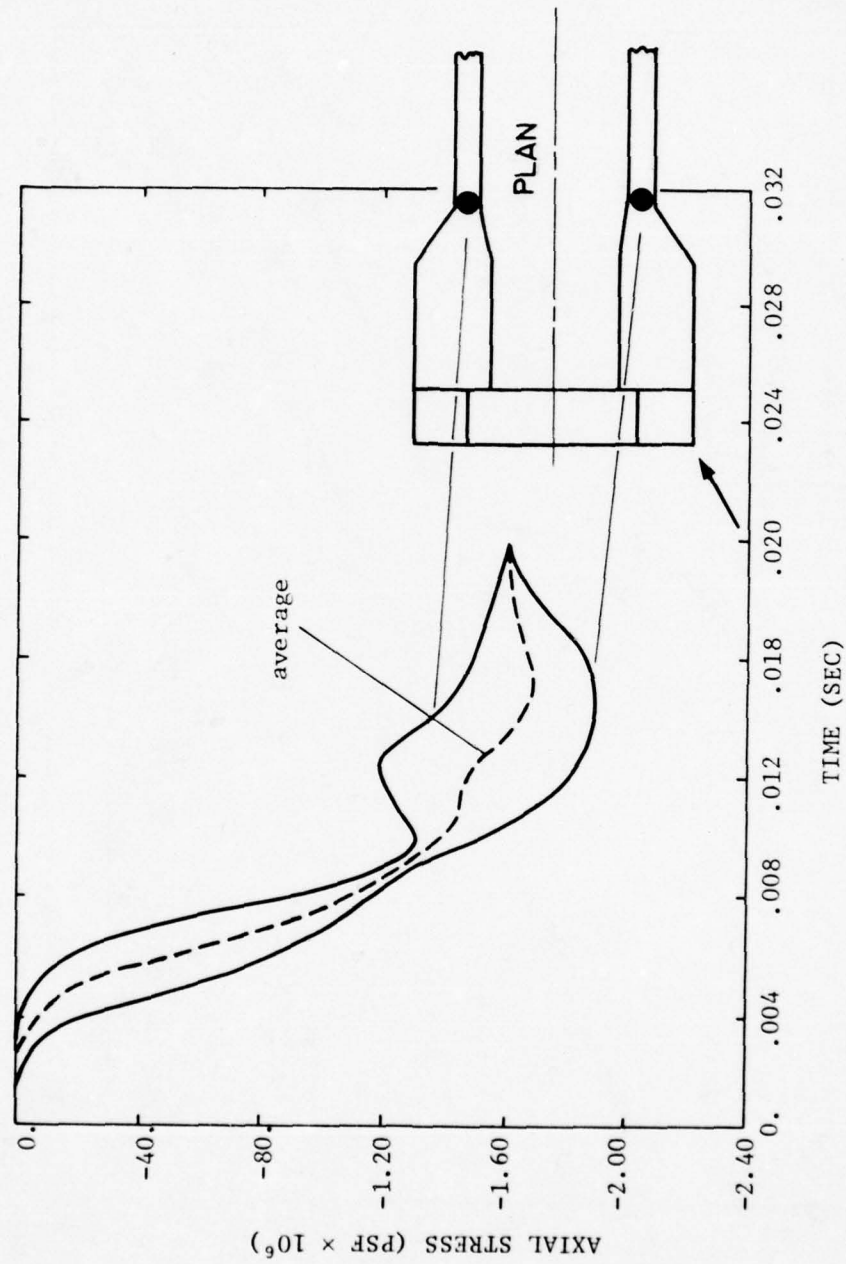
Figure 3-34. Axial stresses at transition, difference in axial forces reflects bending, 30° oblique front-on incidence, Calculation 1D
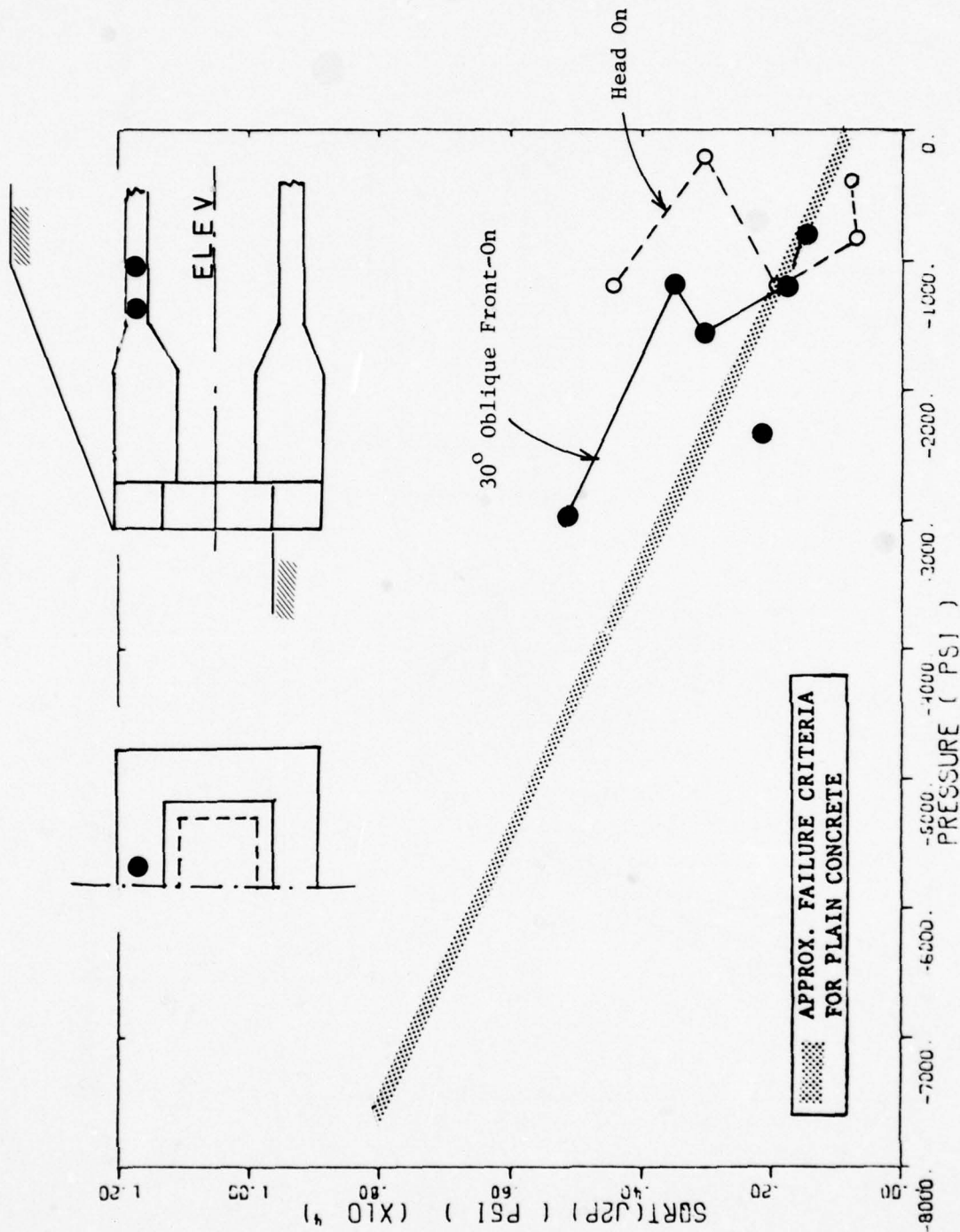
Figure 3-35. Comparison of shear stress distribution in longitudinal direction, upper shelter, 30° oblique front-on incidence, Calculation 1D

TABLE 3-1

SHELTER "RING" IN VACUO FREQUENCIES (HZ)

Flexural Mode	Finite Element Model	Thin Shell Theory
$n = 2$	25-27.	26
$n = 3$	72.	73.
$n = 4$	131-133.	141.
$n = 5$	202.	227.
$n = 6$	280.	333.
$n = 7$	359.	459.

Breathing Mode		
$n = 0$	138.	134.

TABLE 3-2

ELASTIC PROPERTIES OF SOIL AND STRUCTURE

Material	E (psf)	ν	C_p (fps)
Native Soil	1.016E7	.3	2,000
Berm	2.46E6	.1	900
Backfill	2.46E6	.1	900
Concrete	6.48E8	.2	10,000

SECTION IV

INTERPRETATION OF PHASE 1 RESULTS

Major results of Calculations 1A through 1D all based on the S1 configuration are discussed herein. The discussion begins with a brief summary of the structural response mode in order to lead into the conclusions which follow. The response of the S1 configuration is used only to illustrate certain observations on the methods of the dynamic analysis of a shelter-like structure. Note also that the Phase 1 results are obtained through elastic calculations and the conclusions are drawn based on the elastic assumption. Some conclusions are modified as inelastic calculation results from Phase 2 become available.

4.1. DEFORMATION MODE

The main deformation mode of the shelter under head-on loading is similar to that of a beam column in an elastic medium (see for example Figure 3-17). The tremendous load acting on the front face dominates the response of the structure at early times and produces two major effects: high axial stresses in the headworks and particularly the tube (Figures 3-18 and 3-19) and bending of the headworks as a result of the offset between the center of pressure and the center of stiffness (Figure 3-20). The airblast on the top of the berm tends to push the headworks downward and contributes to the bending effect. The effect of the overburden load lags the effect of the front load because of the necessary transmission time through the backfill.

When the airblast incidence is oblique, there exists in addition to the deformation described above a yaw deformation consisting of compression in the longitudinal direction and lateral displacement (Figure 3-29) and bending of the headworks in the direction of wave propagation. The effect of the oblique incidence is first manifested as the effect of airblast arrival time at the front face, torquing the headworks initially into the blast. Later on the lateral load acting on the blast side of the headworks tends to counterbalance this torque and turns the headworks with the blast (Figure 3-34).

The longitudinal and lateral bendings of the headworks are transmitted to the tubular section. Consequently the tube section closest to the headworks is under severe distress especially at the crown. In addition, although only substantiated by a two-dimensional calculation the tube undergoes in-plane deformations due to the overburden load. This in-plane deformation is dominated by the breathing and ovaling modes (Figure 3-5).

Other possible areas of distress have been identified as the inside corners of the frame; the distress is local and is caused exclusively by the air pressure in the gap, i.e., the space between the closure and the frame (see Figure 3-25).

The bending moment at the center of the closure is compared to the values given by plate theory in Figure 4-1. It can be summarized that the closure in its elastic state behaves like a thick plate in flexure with fixed edges when the gap is not present and is simply-supported otherwise.

The velocity-time histories for a point at the center of the closure in the monolithic front face (i.e., no gap) are shown in Figure 4-2 and contain a strong component with a period of about 8 msec. The maximum midspan deflection relative to the support is less than an inch. Corresponding time histories for the case with gap are not available since that particular calculation is terminated at 10 msec. after airblast first arrival.

4.2. COMPUTER MODELING CONSIDERATIONS

It follows from the foregoing discussions that several regions of the shelter need to be modeled in considerable detail. These are: the transition region between the headworks and the tube including the front portion of the tube, the gap between the closure and frame, the inside corners in the frame and the front face and closure itself.

Details in the transition region and tube should be sufficient to model the longitudinal stress transfer/amplification and the severe distress induced by bending of the headworks. The gap between the closure and frame should be included if air pressure is allowed to get into this cavity, i.e., no gap seal is anticipated. The mesh in upper and lower corners on the inner surface of the frame should be sufficiently fine to reflect the high stress gradient which exists. Finally the front face details should adequately represent the spatial variations of the overpressure distribution.

It has also been found during the course of the study that the soil region immediately in front of the shelter plays an important role in the shelter response. The airblast load acting on this surface changes very rapidly with distance from the front face as the reflected overpressure decays rapidly from its full value at the front face. This distribution can only be reproduced with a fine mesh for the soil surface in question. Of course a fine mesh is also necessary to allow accurate transmission of the load into the buried portion of the headworks.

A fine surface subdivision may be necessary for another reason. It is common practice in most codes to distribute the load acting on a surface equally to nodes which define that surface. Consider the discretized soil surface adjacent to the front face which has nodes on the structure and nodes on the soil; it this surface is coarse (large) part of the high soil surface load will act (erroneously) on the structure, trying to bring it downward together with the soil. This pitfall is to be avoided, particularly in an elastic calculation where the strength of the soil material is not limited.

Another important aspect of the model is the modeling of the material properties. For example, in an elastic analysis, material modeling involves choosing the elastic material constants (bulk and shear moduli) which best approximate the real material behavior in particular situations. Although it is not considered as part of the scope of the present study, the success of the methodology established here for the dynamic analysis of shelter-like structures depends strongly on adequate material modeling for the reinforced concrete, steel and the soil medium as is true for any analysis of this kind. In particular as will be shown in Section VI, the effectiveness of the methodology in predicting closure response depends on an accurate dynamic model representation of the closure materials.

4.3. AIRBLAST CHARACTERISTICS AND SHELTER RESPONSE

As far as their effects on shelter response is concerned, the characteristics of the overpressure wave form can be discussed under two separate groups: spatial and temporal. Spatial characteristics refer to the distribution of peak overpressures acting on the structure and ground surface. Temporal characteristics refer to the details of the time history and include parameters such as arrival time, rise time, dominant frequency and overpressure impulse. These two sets of characteristics are interrelated and it is often difficult to isolate the effects of one from the other. The temporal parameter found to be significant is the arrival time of the peak overpressure at a point and equivalently the relative timing of the various peak load arrival times. Spatial characteristics are found to be important in some situations and not so in others.

Before going into a discussion of these characteristics, however, it is emphasized that the results obtained in this respect are limited because of the lack of authentic air-blast data. What little comparison has been done is between the AFWL 19.8041 (Reference 4), 19.8042 (Reference 5) loads obtained under two-dimensional conditions and the modified Brode. Accordingly, this aspect of the study is limited in scope and the conclusions tentative. Furthermore, the conclusions are based on elastic results which tend to exaggerate the response sensitivity.

The elastic response of the shelter depends a great deal on the peak applied load and its distribution on the loaded surface area. This is so because of the peculiar geometry of the shelter, with its exposed front face and sides, top, gap, berm, overburden, etc., and the sensitivity of the peak overpressure to this geometry, the amplification factor being such a nonlinear and sensitive function of the reflection and diffraction angles. This sensitivity is best illustrated by comparing the peak overpressure distributions used in the two-dimensional studies (Figure 3-3) and three-dimensional studies (Figure 3-14). In the three-dimensional studies, the peak overpressure suffers a big jump in value as the

airblast encounters the door; the factor of reflection ranges from 7 to 9. This peak then decreases rapidly as the airblast rounds the top and side edges of the structure and finally regains the free air profile some distance down the berm. Meanwhile, the reflected airblast acts on the soil medium in front of the shelter as well with peak value decaying rapidly with distance from the front face.

To the structure the front load collected at the front face must be supported by the headworks and the medium surrounding it. High axial stresses result and the situation is made more acute as the stress wave propagates along the structure due to a drop in load bearing area in going from the headworks to the tube. This effect is, without doubt, the single-most dominant effect of airblast characteristics. Hence, the front-face reflection coefficient of the surface overpressure is an important airblast parameter.

The front-face reflection coefficient is not the only important parameter related to the front face. Its distribution about the front face is another significant factor. To illustrate this point, the modified Brode distribution (see Figure 3-16) which has the same high peak overpressure (5,400 psi) as the AFWL 8041 load, but is uniformly applied over the entire front face is used to generate results for comparison. This distribution is different enough from the AFWL 19.8041 distribution to yield some interesting response sensitivity observations. Figure 3-16 shows a portion of the front face shielded by soil and hence not subjected to direct airblast loading. On that portion which is exposed is plotted the peak overpressure distributions. The dotted line represents the AFWL 19.8041 pressure and the dashed line represents the modified Brode pressure constant over the front face. The volume under each surface is the total axial load acting on the front face in each case and the moment about the center of the front face can be measured accordingly.

Due to the presence of the layer of soil in the lower front-face area the center of pressure is offset from the shelter center line. This offset in the modified Brode description is larger than that in the AFWL description because of the uniform assumption. So is the resultant load. This offset of about 4 feet in combination with the higher air-blast load (4.7×10^8 lbs. for uniform distribution) generates a moment of 2.4×10^{10} in.-lbs., which turns the headworks clockwise. Hence it is not surprising that the deformation mode of the structure (illustrated in Figure 4-3) due to the modified Brode load shows both a greater axial compression and higher bending of the headworks. In fact, the bending action is so severe that there is a lift-off of the headworks at the toe, a phenomenon also observed in the S1 test (Reference 11). The deformation mode of the same structure and at the same time for the AFWL load is also included for comparison. It also follows that compared to the AFWL load the modified Brode load should also produce higher mean axial compression (14 ksi versus 7 ksi) and higher bending moment in the tube (1.3×10^{10} in.-lbs. versus 0.36×10^{10} in.-lbs.) as shown in Figure 4-4. This load/response sensitivity

is the most evident because the load is not only directly applied to the structure, but also the most dominant.

A similar conclusion can be drawn regarding the load distribution on the exposed side of the headworks in the side-on incidence case, although the actual calculation has not been made. An indication that this should follow the trend of the axial load in the head-on incidence is given by results of the oblique front-on calculation. The relevant parameters are now the lateral bending and shear in planes perpendicular to the longitudinal axis.

When the loading is not direct, however, this sensitivity is greatly diminished. Such are the effects of the overburden load on the headworks and tube. First of all the overburden load effect is delayed somewhat because of the berm. For instance, for the material assumed, it takes a little more than 10 msec. for the airblast-induced ground motion to traverse the overburden and reach the tubular section of the shelter. Accordingly, the magnitude of this loading, small to begin with when compared to the front load, is further attenuated due to propagation through the backfill material. An indication of this decrease in sensitivity can be obtained by looking at the results of the elastic two-dimensional calculation.

As shown in Figure 3-3, the peak overpressure at the blast side of the berm experiences amplification of a factor of two above the pressure for flat ground (Brode). This load, however, must travel through about 80 feet of backfill material in order to reach the structure and hence, as one would expect, the effect of this amplification of two on structural response is small. For instance, the tube response shows slightly higher hoop compressions in the structure, but not in the same proportion as the amplification (see Figure 4-5). The bending stress due to the ovaling mode is also quite insensitive to the details of the overpressure distribution also (3,800 psi and 2.5×10^6 in.-lbs./in. for the AFWL load and 3,200 psi and 2.6×10^6 in.-lbs./in. for the Brode load). In particular, when more realistic soil properties are used to include hysteresis and damping, any sensitivity shown in the elastic calculations will diminish even further.

With regard to temporal characteristics, there are at least two important parameters which need to be addressed: the rise/decay time associated with the overpressure peak and the impulse associated with the load. From a frequency viewpoint, the former is considered a high frequency effect and the latter belongs to the medium/low frequency regime.

The importance of these parameters and the sensitivity of the structural response to them again depends on the loading configuration. In the front-on case, the direct application of the load to the exposed surface of the structure affords the best conditions for

the transfer of the high frequency vibration to the structure. Potential problems are resonance of the closure, if it remains elastic, and shock isolation of missile/equipment inside the headworks. Farther down the shelter, the pulse wave form is dispersed and distorted due to the geometry of the structure and the medium; the frequency content is modified. When loading is not direct, the backfill and soil mass surrounding the structure will filter out high frequency contents of the overpressure and structural response is expected to be much less sensitive than in the direct loading case.

The overpressure impulse appears to be the most difficult parameter to be isolated and studied. It is usually a long time effect with influence on the maximum displacement, permanent set and ductility ratio, etc. An analysis of this parameter is made more difficult because the results obtained from such a calculation are usually masked by different loads originating from different stations. It is probably more pertinent to address this parameter in an inelastic calculation, as is done in Phase 2 in discussing the inelastic response of the closure.
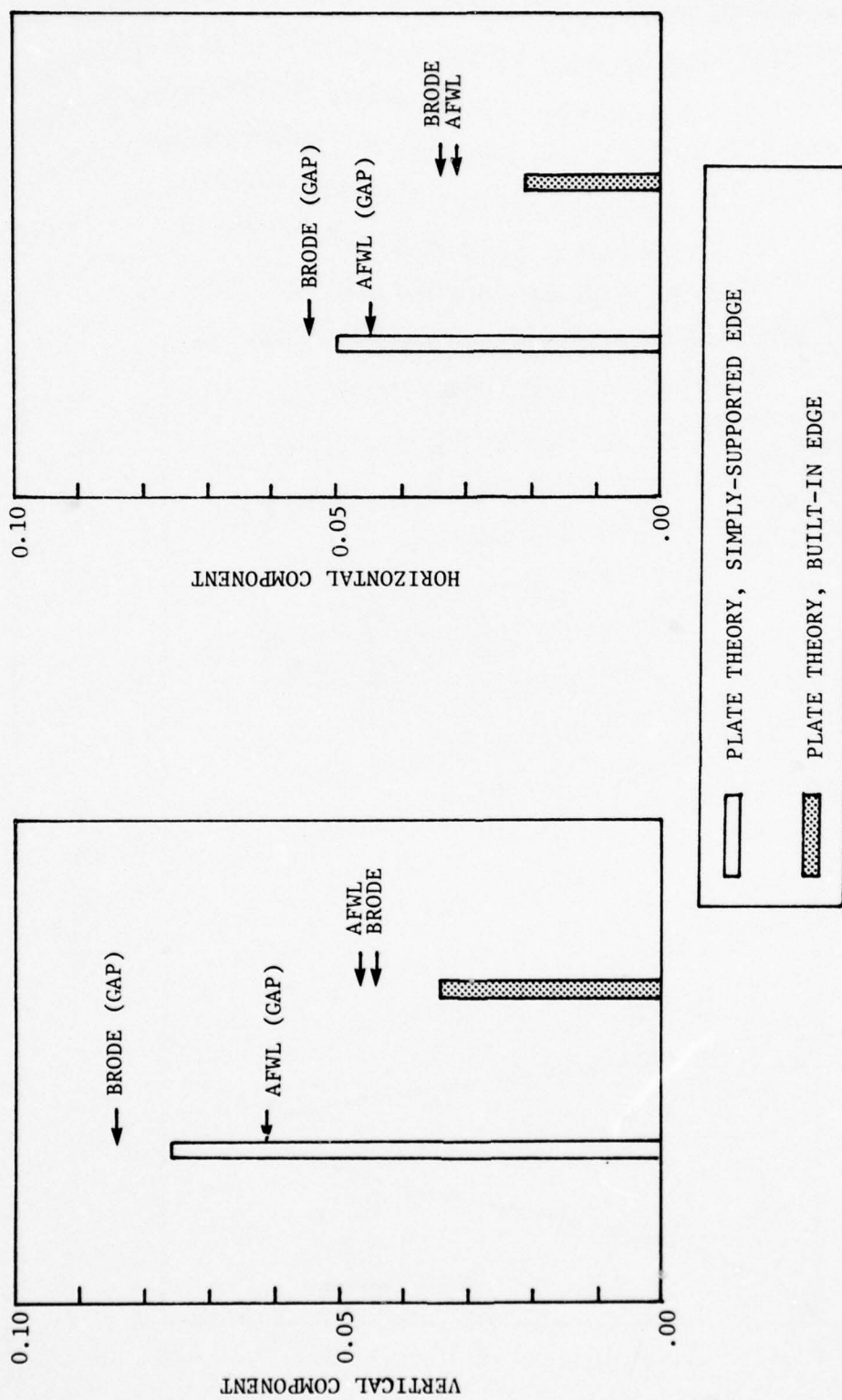
Figure 4-1. Bending moment coefficients at center of closure, front-on incidence, comparison of finite element and plate theory results
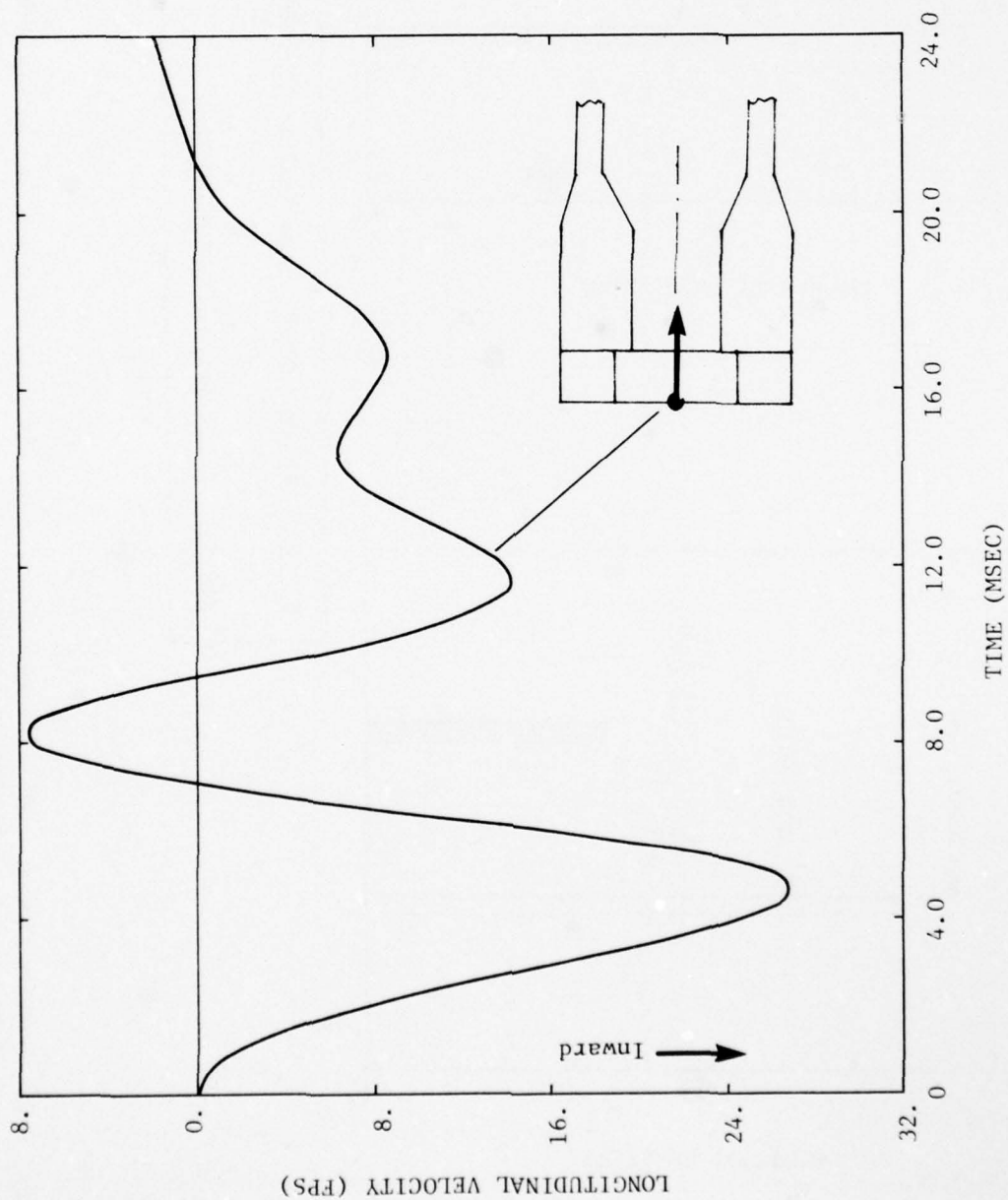
Figure 4-2a. Velocity/time history for a point at center of closure, longitudinal component, front-on incidence, Calculation 1B
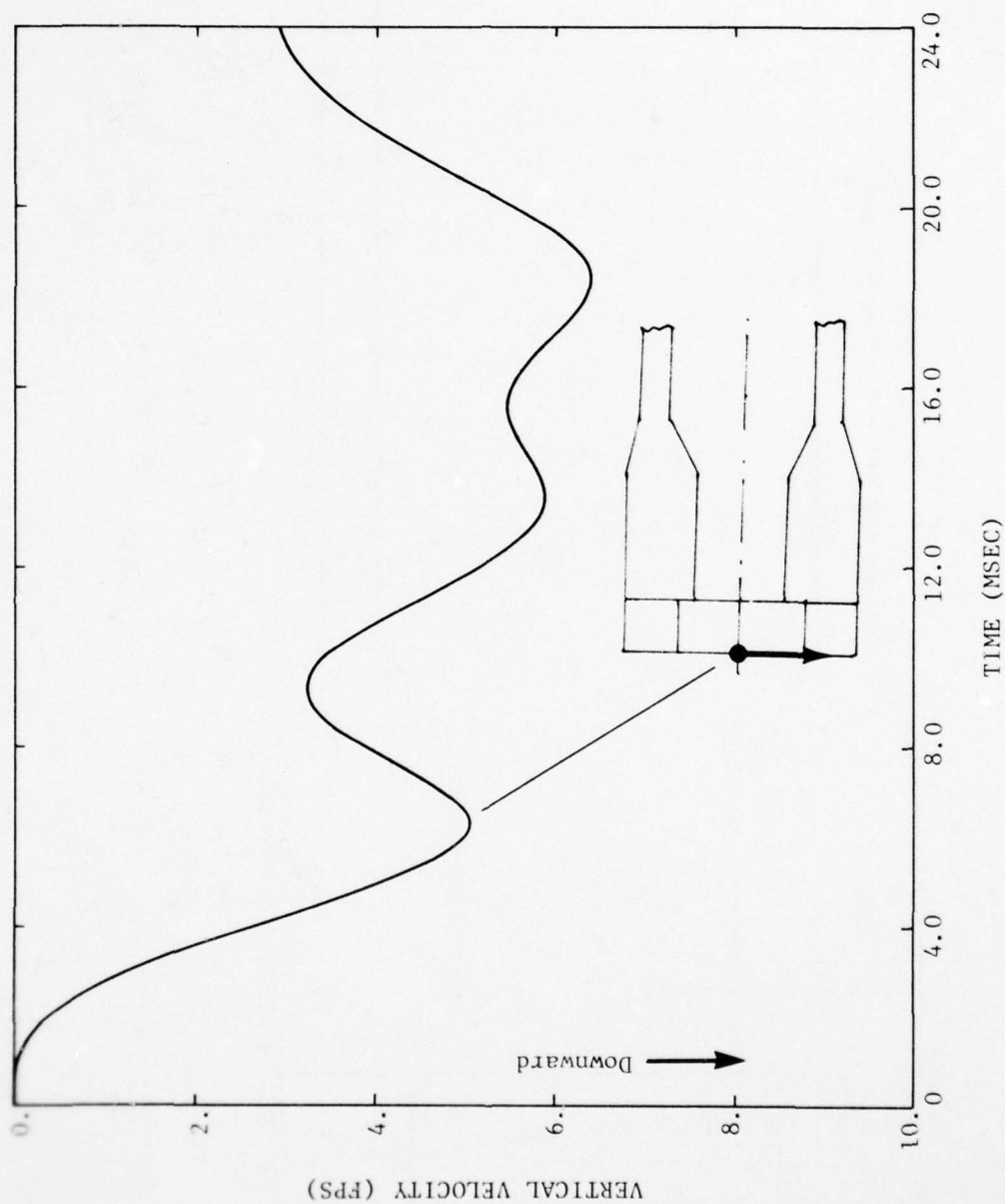
Figure 4-2b. Velocity/time history for a point at center of closure, vertical component, front-on incidence, Calculation 1B
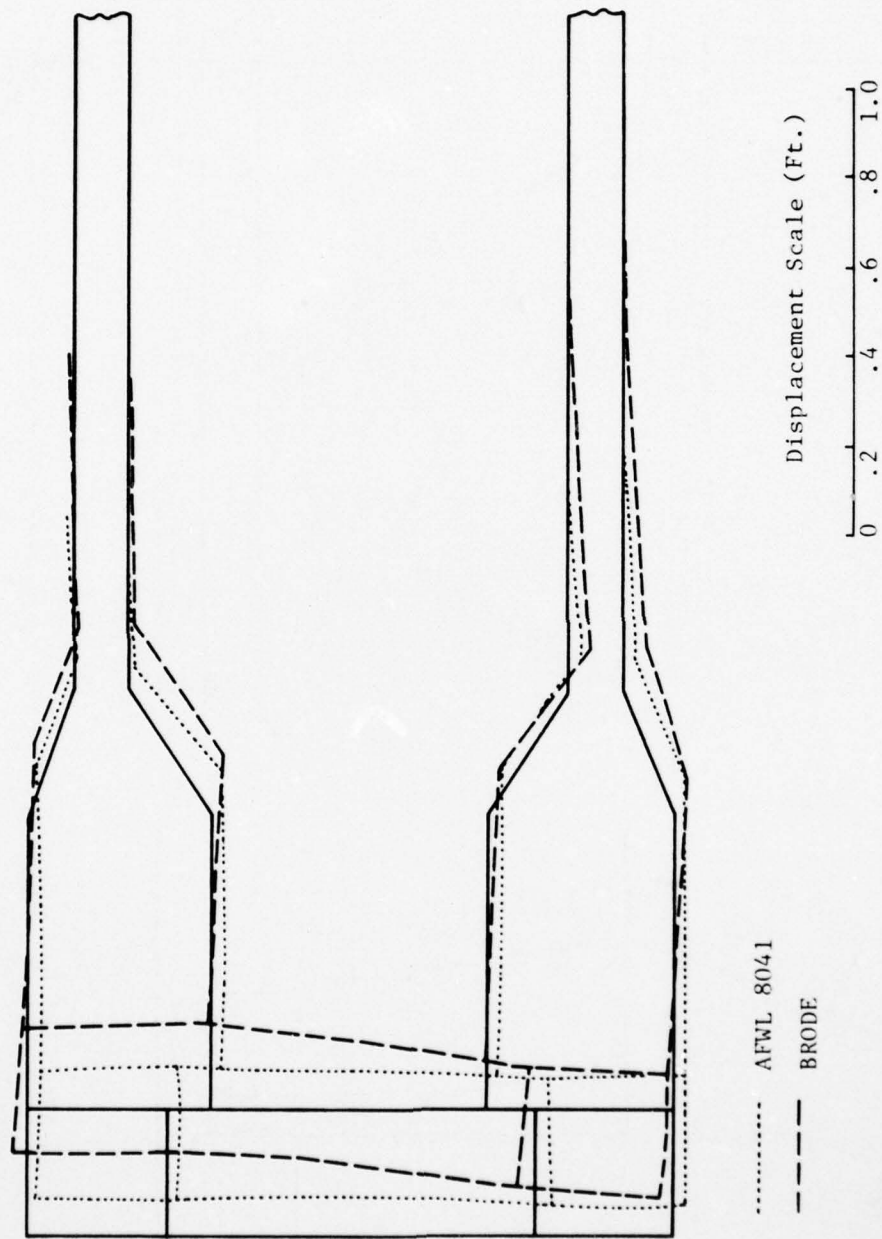
Figure 4-3a. Comparison of deformation patterns at t = 10 msec., exaggerated, front-on incidence

Displacement Scale (Ft.)

.... AFWL 8041
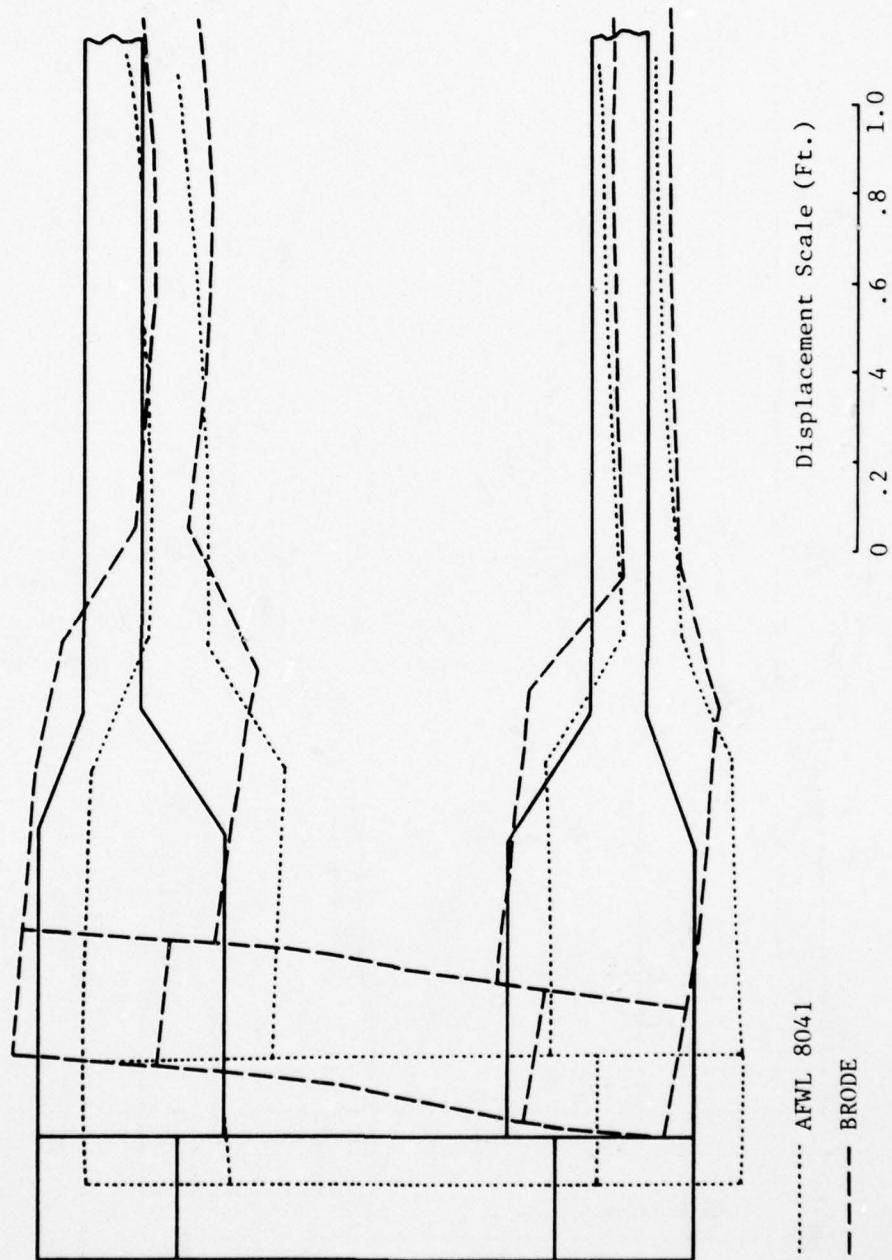
— — — BRODE

Figure 4-3b. Comparison of deformation patterns at t = 25 msec., exaggerated, front-on incidence

Displacement Scale (Ft.)

0   .2   .4   .6   .8   1.0

.... AFWL 8041
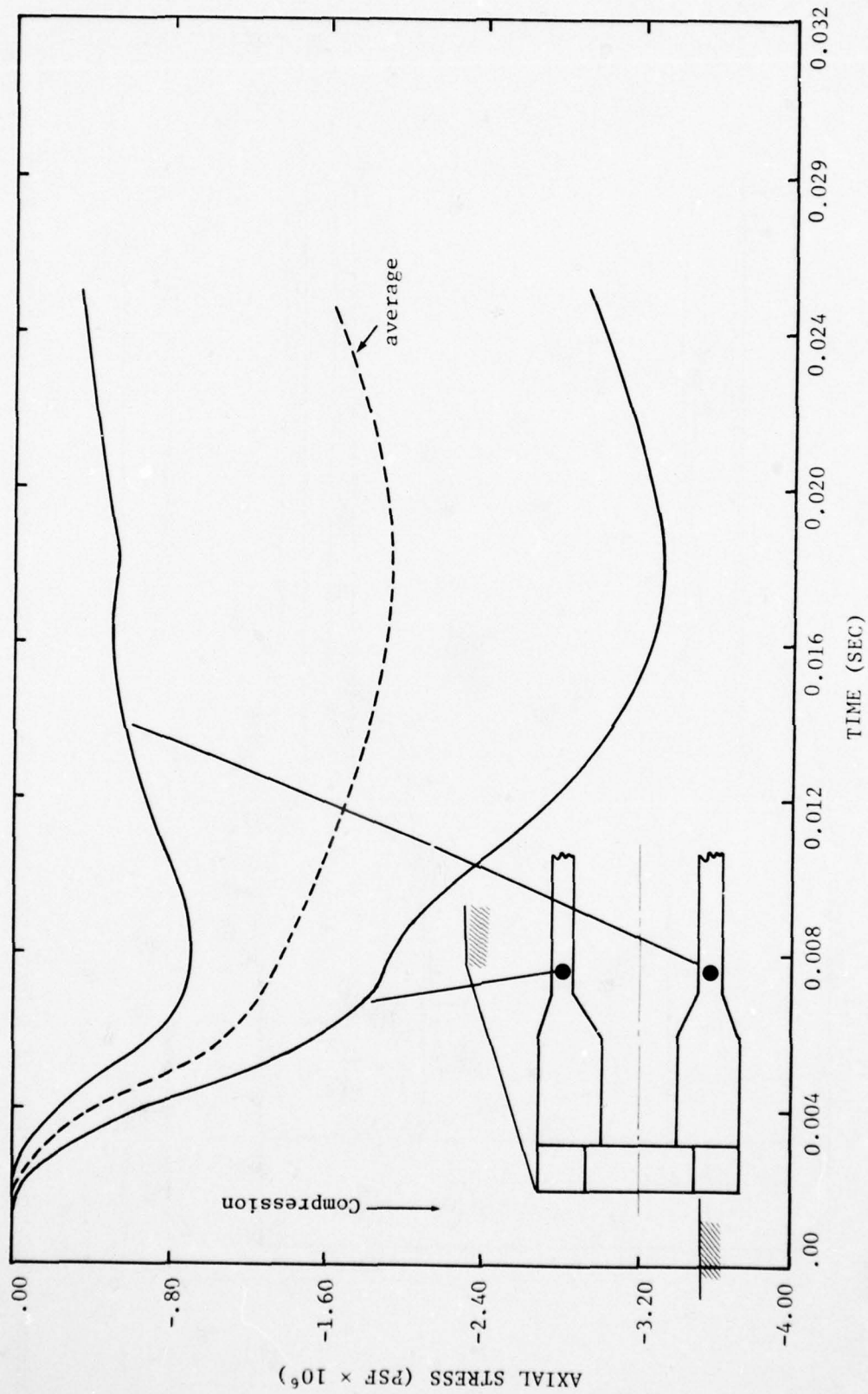
– – – BRODE

Figure 4-4a. Axial stress time histories, tubular portion behind headworks, modified Brode, front-on incidence
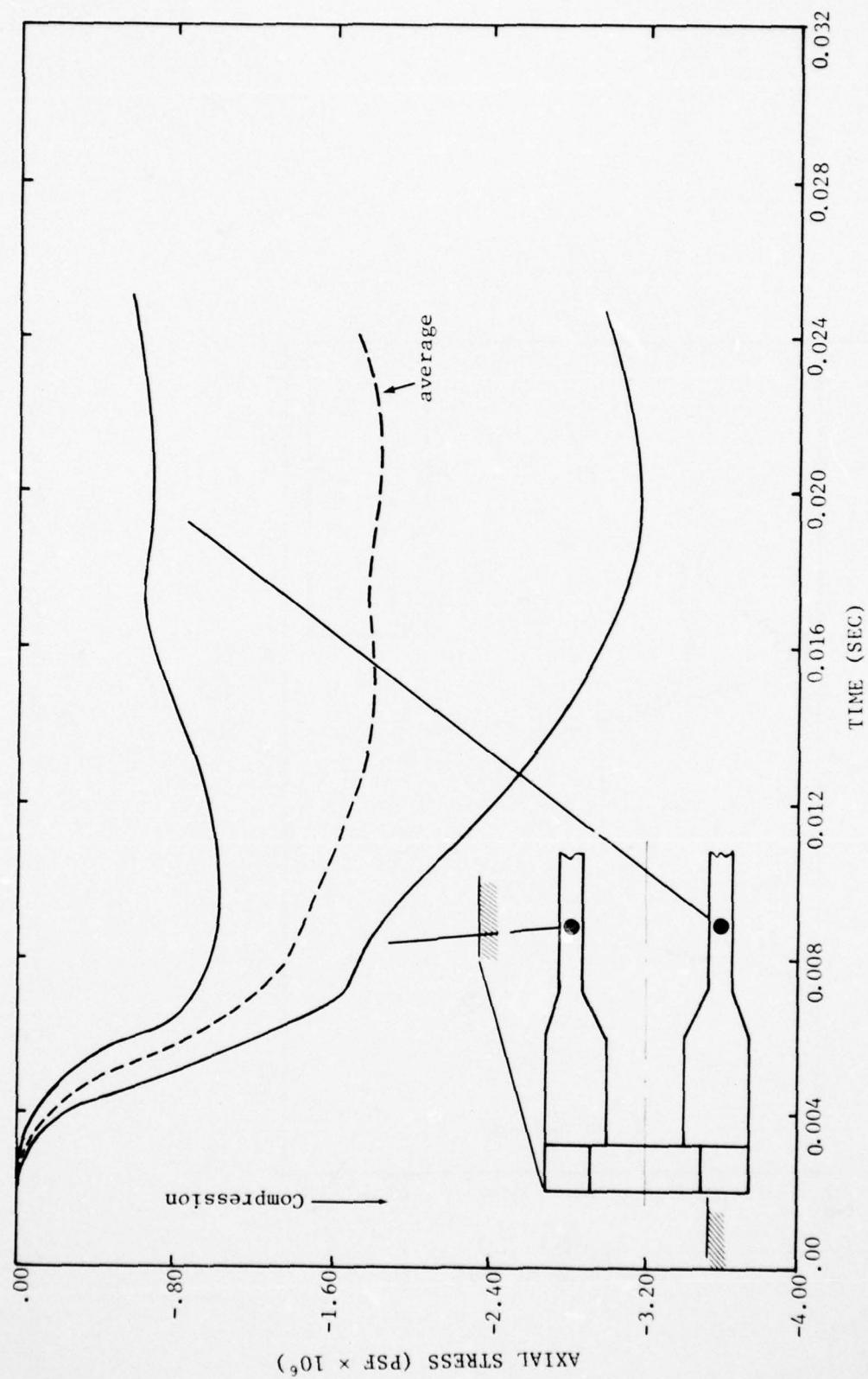
Figure 4-4b. Axial stress time histories, tubular portion half tube diameter behind headworks, modified Brode, front-on incidence
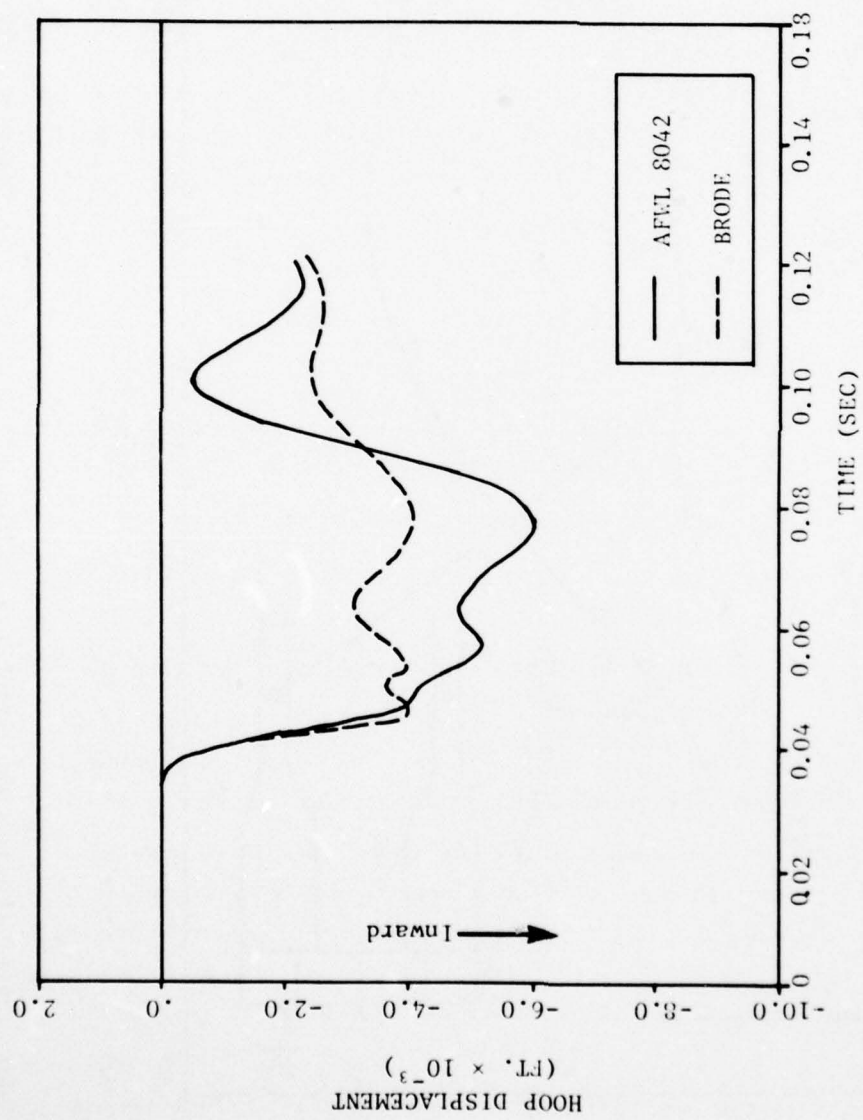
Figure 4-5. Comparison of breathing mode (n = 0) time histories, side-on incidence

SECTION V

PHASE 2 RESULTS

Since the initiation of this study, the design of the MAP shelter prototype has undergone several major changes; it was decided that the Phase 2 studies should parallel the concurrent design of the shelter, designated the S4. Furthermore, the scope of the Phase 2 studies was modified in order to provide analytic support to the testing of a one-half size shelter in the HAVE HOST DABS (Reference 12) series. This test was eventually cancelled and replaced by the HEST S4 test (Reference 13). The structure, however, is basically the same one and will be referred to simply as the S4 structure hereinafter. The full size S4 structure is studied in Phase 2.

Some of the major changes in the design from S1 to S4 are (see Figures 5-1 and 5-2):

• A smaller front face which slants at 10° to the vertical.

• A smaller shelter diameter and a thinner wall.

• A different closure/frame design; the closure is a thick composite slab (concrete supported by steel side and back plates) with bevelled edges.

• The bearing ring (closure support) area is smaller.

• The headworks remains basically rectangular, but has a thicker wall on the hinge side to accommodate the power actuator.

• The center line of the rectangular headwork cavity is offset from the center line of the tubular portion of the shelter.

• Only the front face and a very small portion of the top of the headworks are exposed. The top is covered by overburden and the sides by two wing walls and fill.

These changes and the requirement to include as much detail as possible of the closure/headworks resulted in a formidable finite element model. The advantage of such a model is that detailed response of the structure, especially the closure/headworks section can be obtained; the disadvantage is that small integration time steps must be used. Even with the subcycling capability of TRANAL, this requirement still results in long computation/run time.

All Phase 2 calculations use basically the same model which includes the gap between closure and frame. They are all made in the head-on loading condition with the same overpressure description. Major results of these calculations will be described in this section; a detailed interpretation of the Phase 2 findings is given in Section VI.

5.1. CALCULATION 2A--THREE-DIMENSIONAL INELASTIC CALCULATION WITH HEAD-ON INCIDENCE

Model and Airblast Load--symmetry is assumed about the center vertical plane of the tube and the model includes only half (hinge side) of the shelter/berm configuration. The finite element model which consists of about 18,000 hexahedrons is shown in Figure 5-3. As can be seen from this figure special attention has been given to details in the closure, headworks and transition region. In addition to the gap, the steel side and back plates encasing the concrete closure are modeled using two elements across the plate thickness. The steel bearing ring and the steel plates in the frame are modeled likewise. The closure is assumed rigidly bonded to the bearing ring where contact is made. Two elements are used across the thickness of the shelter cylindrical wall.

The in situ soil and backfill are modeled as "CAP" materials; the corresponding CAP parameters are given in Table 5-1. The in situ soil model as presented is identical to that designated as DRY SAND-1 in Weidlinger Associates' ground motion study DNA 001-77-C-0036 (Reference 9). DRY SAND-1 has a density of 110 pcf and an uniaxial loading modulus corresponding to a wave speed of 1,500 fps and an unloading wave speed of 3,600 fps. Its uniaxial behavior is illustrated in Figure 5-4.

The backfill model is based on data obtained from the AFWL (Reference 7) and corresponds to the so-called medium backfill of the AFWL data. The uniaxial behavior of the model is compared in Figure 5-4b with the AFWL data; the loading wave speed is 800 fps and the unloading wave speed 3,600 fps.

The concrete and steel are modeled as elastic perfectly plastic materials, the concrete having an exponential yield surface based on a compressive strength of 6,000 psi and the steel a von Mises' yield surface corresponding to A36 steel. The model parameters are listed in Table 5-1. In the concrete model the tension cut-off point is varied based approximately on the amount of reinforcing steel that exists in different parts of the prototype structure (i.e., headworks, frame, closure and tube) and the basic yield surface is kept unchanged.

Since detailed airblast loading on the S4 shelter configuration does not exist, a combination of test and handbook data is used for this calculation based on recommendations from AFWL (Reference 8). A sample of these data are given in Figure 5-5 where they are compared with the axisymmetric AFWL HULL results. The loading at the front face is found identical to the HULL values and close to that measured in the HAVE HOST S1 test.

The integration time step used in TRANAL can be different for different groups of elements called zones. Within each zone, however, the time step is constrained by the

5-2

minimum transit time across an element in that zone. In Calculation 2A the time step for the zone containing the closure details is necessarily small due to the small size (2.5 inches) of the elements used to model the steel side and back plates. Consequently the computation time per major cycle is long: about 50 CDC 7600 CPU seconds for 0.1 msec. of real time and approximately 18,000 elements. (This figure, of course, would be higher if not for the subcycling capability of the code.) Because of the formidable run time only about 10 msec. of structural response time has been obtained for Calculation 2A. Although not long enough to fully examine the behavior of the tube portion of the structure this response time is sufficient to yield results for an analysis of the headworks and closure.

Deformation Mode--an illustration of the deformation pattern of the headworks is given in Figure 5-6 with magnified displacements for points on the longitudinal plane. It is seen that the early time response of the structure is basically longitudinal compression. Front loading acting at the closure tends also to push it downward in addition to backward due to the 10° incline and the bearing support is forced to move with it since perfect bond is assumed in the model. The overall downward movement elsewhere in the headworks, however, is not significant. This is because at early times the soft overburden effectively isolates the structure from top airblast loads.

In Figure 5-7 are shown the displaced profiles of the backplate vertical center line at different times. Profiles for the horizontal center line are given in Figure 5-8. The deformation pattern is one of punching, or shear, where the plate yields along the support edges, but retains a relatively uniform (flat plate) displacement elsewhere.

The development of this deformation mode is illustrated in Figure 5-9 which shows the growth of inelastic regions with time in the back plate. It is apparent that the area near the bottom support yields first, followed by areas near the side support and finally those near the top support.

The deformation pattern in the concrete portion of the composite closure is shown in Figure 5-10 where three patterns are given for each action time corresponding to (from left to right) the top, mid and bottom layers which make up the concrete slab model. The bottom layer undergoes inelastic deformation first which is then seen to propagate to the mid and top layers at later times. It is also clear that inelastic deformation is initiated in the concrete before it is initiated in the back plate, giving some evidence to the theory that shear deformation propagates from back to front of the concrete slab; it is only after the completion of the so-called shear crack that the load is transferred to the backplate causing it to yield also. Results obtained appear to be consistent with this theory although the deformation pattern is more complex due to dynamic and wave propagation effects.

5-3

Velocity-time history for the closure center of gravity (cg) is shown in Figure 5-11. It is a predominantly longitudinal motion with some downward component, due to the 10° incline of the closure.

Stresses--the stress invariant plot of Figure 5-12 is typical of result obtained for points in the concrete portion of the closure where it becomes inelastic. Notice that the mean pressure ($J_1/3$) remains compressive and the inelastic deformation is due to shear. For regions in the closure which remain elastic the stress invariant plot looks like Figure 5-13.

Stress pattern in the backplate falls into two categories, supported or unsupported. The supported or edge region behavior is shown in Figure 5-14; the unsupported regions is dominated by the membrane tension and the resulting stress invariant plot has the characteristics of Figure 5-15. The maximum shear allowed ($\sqrt{J_2}$) is 20,800 psi and corresponds to a uniaxial yield stress of 36,000 psi for A36 steel.

Experience from Phase 1 results indicates that other vulnerable areas in the structure are the inner corners of the frame. Figures 5-16 and 5-17 are the stress invariant curves for the upper and lower corners, respectively, of the steel ring lining the frame. Two elements are used to model the ring thickness, and in both the upper and lower corners, the inner ring element (which is in direct contact with the gap pressure) sustains hoop tension while the outer ring element (which is adjacent to the frame concrete) sustains compressive stresses as the ring is bent and the corner "rounded." Yielding is observed in both cases.

Minor inelastic deformation is also observed in the concrete portion of the frame near the corners and center gussets as Figures 5-18 through 5-20 indicate.

The stress invariant plot of Figure 5-21 is typical of the results obtained in the transition section which remains elastic, due to the beneficial confining effect of the neighboring soil. As the stress wave travels onward to the tubular section, the decrease in load bearing area results in an increase in the longitudinal stress. This axial compression is sufficient to cause inelastic deformation in the tubular section behind the transition section. Figure 5-22 is typical of the results obtained at the crown and springline. The invert portion remains elastic at this early time.

This amplification of the longitudinal stress as shown in Figures 5-23 and 5-24 has been mentioned in previous discussions (Sections 3.2 and 3.4). In the case of the inelastic calculation, the amplification factor measured is less than 2 which is much less than the ratio of the load bearing areas (about 6 for the S4 configuration). There are two possible explanations: the axial stress which can be sustained in the tubular

section is limited for an inelastic material depending on its yield strength and the lateral confinement. Secondly, the front load which acts on the closure is not completely transmitted to the transition section due to the shear or punching deformation at the support edges. More insight into the former can be gained by looking at results of Calculations 2B and 2C to be presented later (Sections 5.1 and 5.2). The matter of the bearing load is examined in the next paragraph.

The ratio of the closure area versus bearing area is approximately 12. Hence, it follows that in static uniform loading of the closure, the average bearing pressure is 12 times that of the loading, or a peak of 64,000 psi in this case. The bearing pressure obtained in Calculation 2A is shown in Figure 5-25 for points located on the top, bottom and side of the bearing ring. The peak pressure is higher at the top and bottom mainly because the bearing area is less there than on the side. In any event, its value of 30,000 psi is only half of the corresponding static value. One element length away from the edge of the bearing ring, about 5 inches, the peak bearing pressure drops to 14,000 psi as Figure 5-26 shows. A similar though less drastic drop is also observed in the bearing load one element length back of the contact surface. These results indicate that the bearing load is highly localized. The fact that the bearing ring extends into and forms an integral part of the base of the frame makes interpretation of this kind even more difficult.

Analysis of the response of the tubular section of the shelter is somewhat limited because of the early cut-off time. However, some quantitative design values can still be obtained for the fore portion of tubular section, i.e., the region behind the transition section.

From the axial stress plots of Figures 5-27 for sections behind the headworks the peak mean axial compression is estimated to be 9,000 psi. Similarly, the peak hoop stress and the peak in-plane bending can be obtained from Figure 5-28 for the tube cross-section immediately behind the headworks and from Figure 5-29 for the cross-section half tube diameter behind. Note that whereas the crown immediately behind the headworks is flattened (the outer fibre stress is higher than the inner fibre stress at the crown, Figure 5-28) the crown half tube diameter behind the headworks shows the opposite response (the outer fibre stress is lower than the inner fibre stress at the crown, Figure 5-29). The difference in the response pattern is depicted in Figure 5-30. It should be noted that at this early time all tubular section response is induced by loading up front and ground motion induced by airblast at the berm has yet to come into play.

Strains--as might be expected from the description of the closure deformation mode, the shear strains in the closure, especially for points near the support are significant. A maximum of 14 percent in the steel backplate is found near the bottom edge and shear strains of 2 to 6 percent are not uncommon. A typical strain invariant plot ($\sqrt{I_2'}$ versus I_1) for a point in the backplate is given in Figure 5-31.

Shear strains in the closure concrete are in general of the order of 1 to 3 percent, with the highest strain (8 percent) occurring in the vicinity of the top and bottom shear crack. A typical strain invariant plot is given in Figure 5-32 which is based on the strain/time histories of Figure 5-33 for a point near the upper support. Comparing Figure 5-33 to Figure 5-34 which is for a point at the center of the closure clearly indicates that much deformation occurs near the support while the center part of the closure is relatively unstrained.

5.2. CALCULATION 2B--THREE-DIMENSIONAL CALCULATION WITH HEAD-ON INCIDENCE; INELASTIC MODEL FOR CONCRETE ONLY

Model and Airblast Load--the basic model and airblast loading are identical to those of Calculation 2A. The only changes in the model are: the steel side and backplates are assumed elastic and only one element is used across the plate thickness. This is done for two reasons. Dropping the number of elements across the plate thickness from two to one relaxes the constraint on the integration time step somewhat and computation time per major cycle is decreased. Secondly, the change is made to investigate what effect details in modeling of the backplate have on the overall response of the closure and the main shelter structure. Using an elastic material for steel will also show up the effect of steel properties (A36 versus A415, for instance) on closure response. As a final change, the overburden is given a rather high stiffness (wave speed of 3,500 fps) in order to illustrate the effect of this parameter on structural response.

Deformation Mode--the deformation pattern of the headworks at about 15 msec. after airblast arrival is illustrated in Figure 5-35. The displacements are magnified as in Calculation 2A. The early time response is seen to have the headworks pushed back and down; the latter is no doubt due to the stiff overburden assumed. In Figure 5-36 are shown the displaced profiles of the backplate vertical center line at several action times. Profiles for the horizontal center line is given in Figure 5-37. The deformation pattern of the closure, that of punching, is relatively unaffected by the elastic backplate assumption.

A spot comparison of the deformation in the concrete closure indicates that the closure response is also similar to that in Calculation 2A.

5-6

A comparison of Figure 5-38 which shows the closure cg velocity time history with its counterpart from Calculation 2A (Figure 5-11) also confirms this view. Minor differences are observed in the downward velocity.

Stresses--a typical stress invariant plot for points in the concrete closure is given in Figure 5-39 which is similar to the results obtained in Calculation 2A. Figure 5-40 consists of stress invariant plots for points in the backplate. Because of the elastic assumption there is no yielding. However, two trends are evident. Had the steel been replaced by a A36 material with octahedral shear stress limit of 20,800 psi, inelastic deformation would certainly occur near the edges, an observation which is confirmed in Calculation 2A. Secondly, for the plate to remain elastic a steel with grades much higher than A36 is necessary. However, this upgrading does not seem to have significant effect on the behavior of the closure as was pointed out earlier.

Behavior of the two corners of the frame is also examined. While the concrete response is similar to that of Calculation 2A, as is exemplified in Figures 5-41 and 5-42, the elastic assumption for steel brings out an interesting observation. Referring to Figures 5-43 and 5-44 for points in the upper and lower steel frame corners, respectively, one sees now that the lower corner sustains a higher shear stress whereas the upper corner is lightly stressed by comparison. Limiting the shear load in the steel transfers part of the bottom load to the top as observed in Calculation 2A and pushes both the upper and lower corner beyond the elastic range.

From invariant plots obtained for points in the headworks and tubular section, it is observed that the response is quite similar to that of Calculation 2A.

Loads exerted by the closure on the bearing ring are shown in Figure 5-45. Since the direct bearing (contact) area is modeled by one element width the contact stress given in the figure lies roughly between the upper and lower bound values given by Figures 5-25 and 52-6 for Calculation 2A. Again the bearing load transfer does not seem to be significantly effected by the lack of details in modeling of the backplate in this case.

Similar remarks can be made about the propagation of the longitudinal stress along the shelter. One significant difference is noted, however: referring to Figure 5-46 which shows the longitudinal stress/time histories for points in the tubular sections behind the headworks the differential between the longitudinal stresses at the crown and invert (a measure of the bending moment acting in the tubular section) is larger than that shown in Figure 5-27 for Calculation 2A; furthermore, it does not seem to diminish with time or distance along the tube. This bending moment can be attributed to the effect of the downslap force acting on the headworks. The stiff backfill properties assumed make the effect far more significant than it is in Calculation 2A.

5-7

The in-plane bending moment indicates an ovaling deformation of the circular cross-section immediately behind the transition section and of higher mode deformation for the section about 6 feet back (see Figure 5-47), not unlike the results obtained in Calculation 2A.

5.3.   CALCULATION 2C--THREE-DIMENSIONAL ELASTIC CALCULATION WITH HEAD-ON INCIDENCE

Model and Airblast Load--the model and airblast load of Calculation 2B are used with all material properties assumed elastic. Consequently, the response of the closure so obtained corresponds to one which is designed to remain elastic under the prescribed load.

Deformation Mode--the deformation patterns of the headworks at 15 msec. and 22 msec., after airblast arrival are illustrated in Figure 5-48, the displacements having been magnified. Aside from the expected backward and downward movement, there is an almost rigid-body like appearance about the deformation pattern which is typical of an elastic solution (see Phase 1 results, for instance). Note that the closure support point is no longer pushed straight backward as is observed in Calculations 2A and 2B. Instead the support point moves as part of the rigid body which is the headworks.

In Figure 5-49 are shown the displaced profiles of the backplate vertical center line at several action times. Profiles for the horizontal center line are given in Figure 5-50. Maximum deflection at mid-span relative to the support is about two inches.

The velocity-time history of the closure cg is shown in Figure 5-51 and is oscillatory as typical of an elastic system. The dominant period of the longitudinal component is between 7 and 8 msec., giving the closure a natural frequency of 125 to 140 Hz. The downward velocity on the other hand contains a 250 Hz component superimposed on the overall headworks motion.

Stresses--typical stress invariant plots for points in the concrete closure are given in Figure 5-52. The concrete near the support edges would have yielded if the yield criterion as shown also on the figures had been imposed. The concrete at the center of the closure, on the other hand, remains elastic; it would appear to remain so even when the yield criterion is imposed.

The behavior of the backplate is illustrated in the invariant plots of Figure 5-53 for points near the support edges and for a point at the center of the backplate. As expected the plate center sustains high tensile stresses as the closure deforms as a plate under uniform load.

5-8
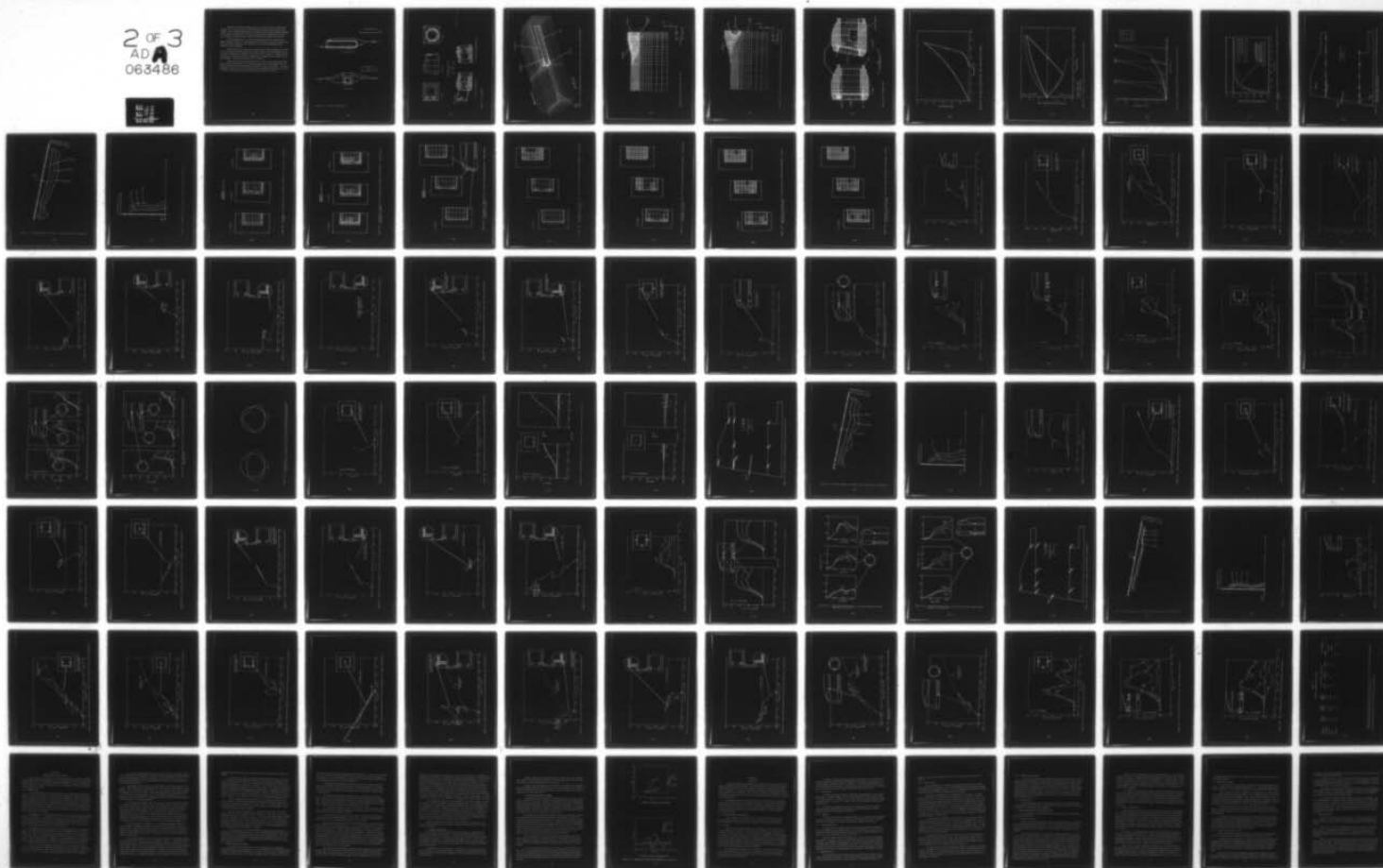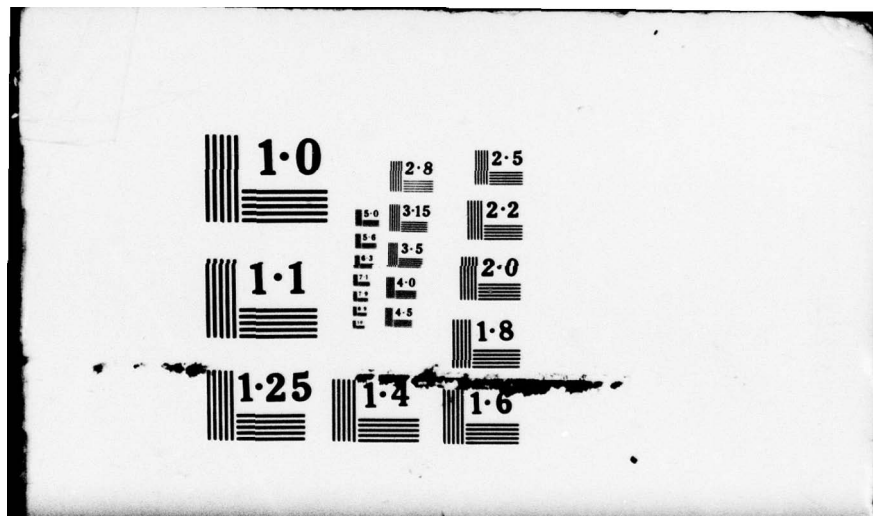
Behavior at the upper and lower corners of the frame is shown in Figures 5-54 through 5-57. It is seen that both steel and concrete (being elastic) sustain tensile stresses. One can readily surmise that if the shear and tensile stress bearing capability of the concrete is limited most of the tensile stress will be transferred to the steel liner and this is indeed the case as shown in Calculation 2B (Figures 5-43 and 5-44).

Stress invariant plots for a point in the tubular section of the shelter are shown in Figures 5-58 and 5-59. When compared with the yield criterion for concrete they show that inelastic deformation will take place at the crown and springline and to a nominal extent at the invert.

Loads exerted by the closure on the bearing ring are shown in Figure 5-60. Note that the top and side bearing pressures are almost identical and are higher than that at the bottom, a behavior also observed in the elastic results of Phase 1. Further the time histories have a dominant oscillatory component with a frequency close to that of the closure vibration. The peak bearing load is about 32,000 psi.

Longitudinal transfer from headworks into the tubular section follows the usual pattern with an amplification factor of slightly higher than two (see Figure 5-61). The axial stresses at the crown and springline are higher than that at the invert. It is also worthwhile to point out that the pulse behaves like an exponential pulse with a rise time of 5 msec. (the airblast load rise time) and main pulse duration of 20 msec.

FULL SCALE (FT.)

0   50.

a.   Elevation View

FULL SCALE (FT.)

0   20.   40.
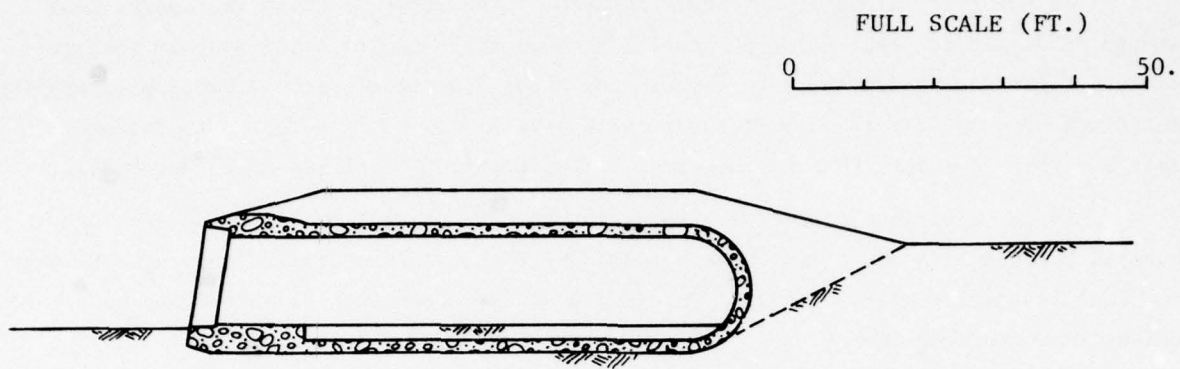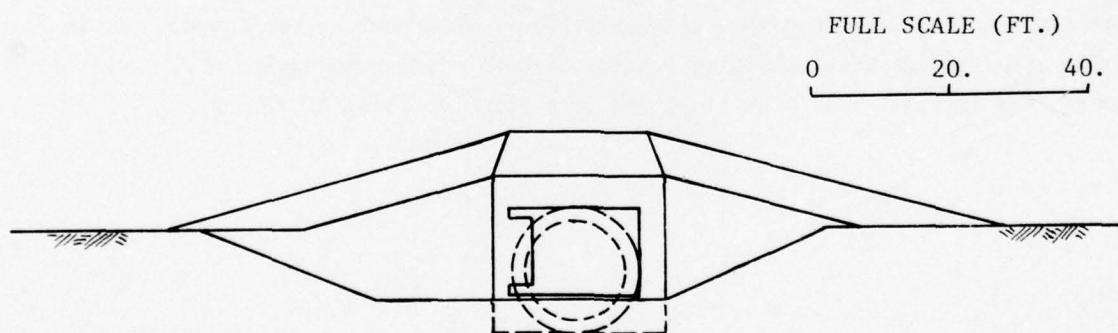
b.   Front View

Figure 5-1.   S4 shelter configuration
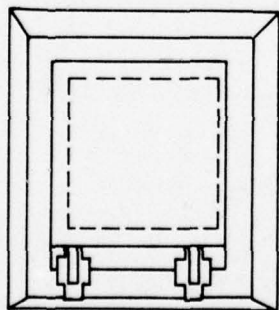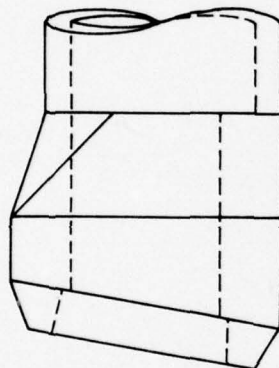
c. Back

b. Side
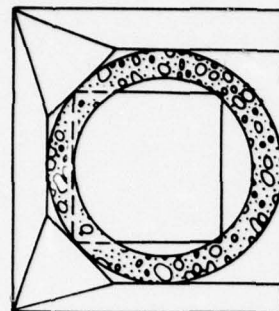
Full Scale (Ft.) for
all Figures

0.   10.   20.

a. Front

door (open)
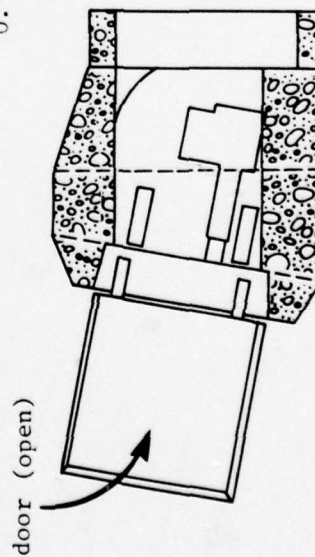
d. Elevation (Hinge Side)
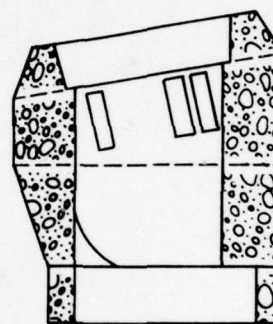
e. Elevation (Non-Hinge Side)

Figure 5-2.   S4 Headworks
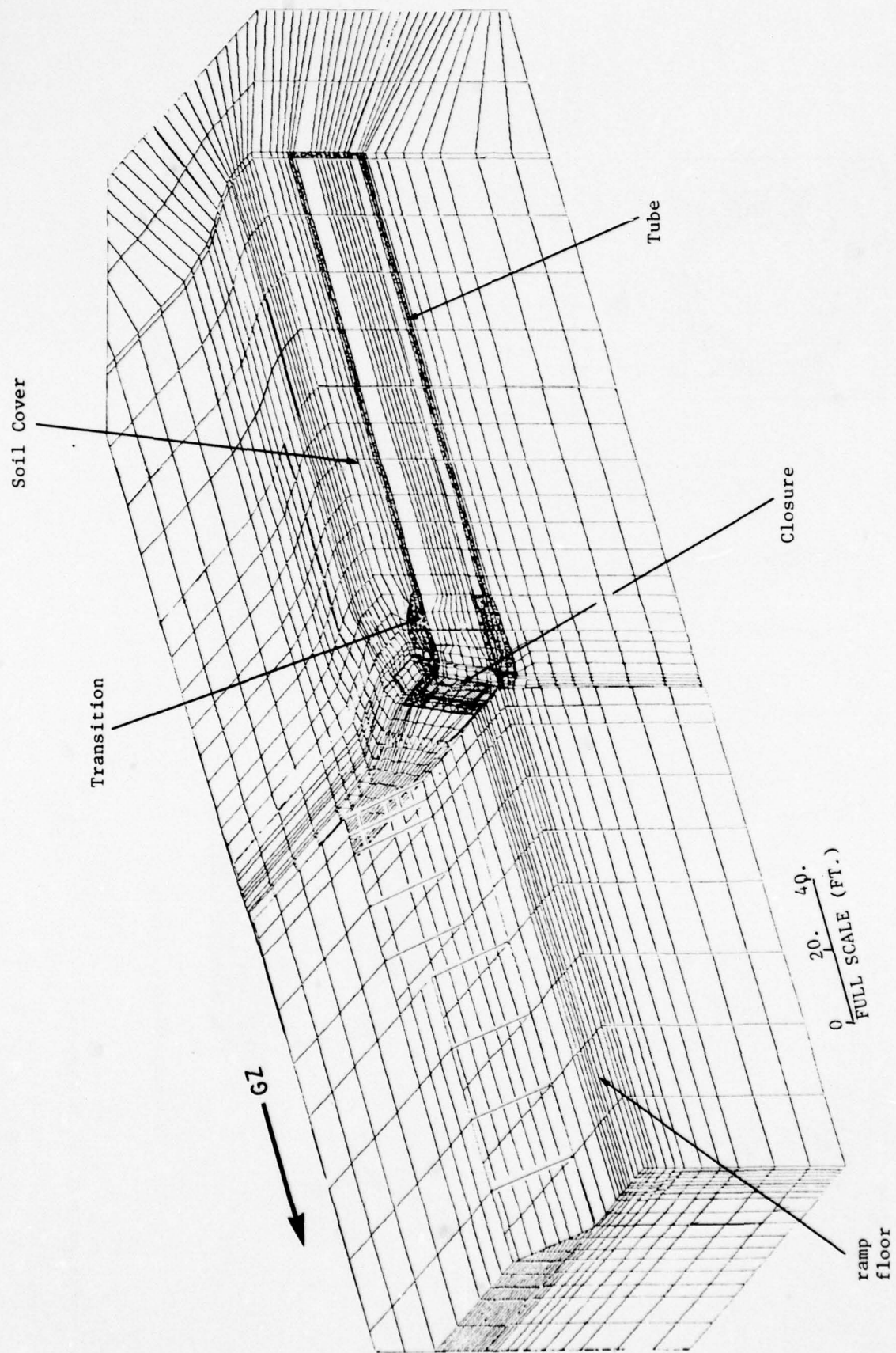
Figure 5-3a. Three-dimensional FE model of S4 used in Phase 2 analysis, plane of symmetry assumed
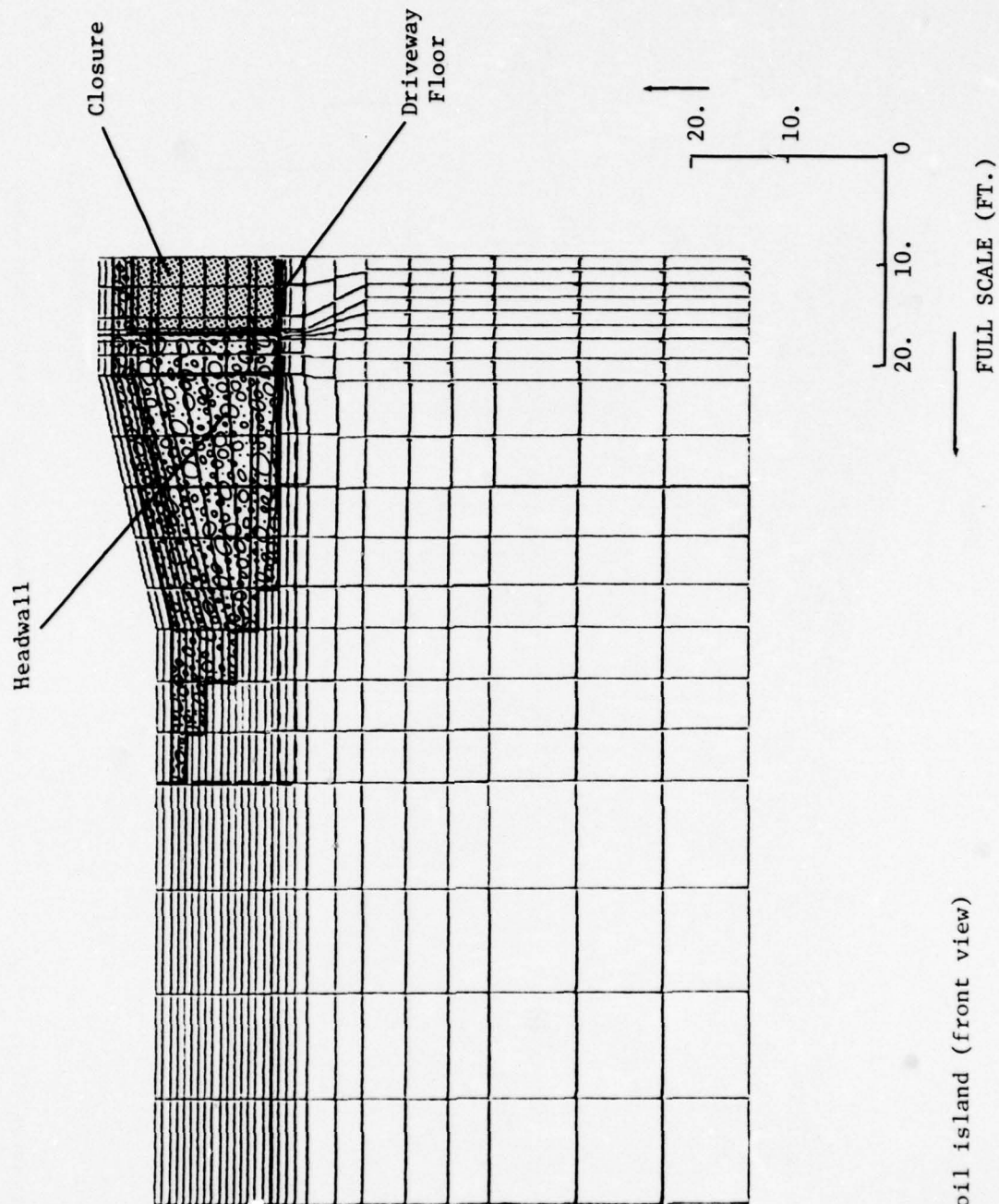
Figure 5-3b. S4 soil island (front view)
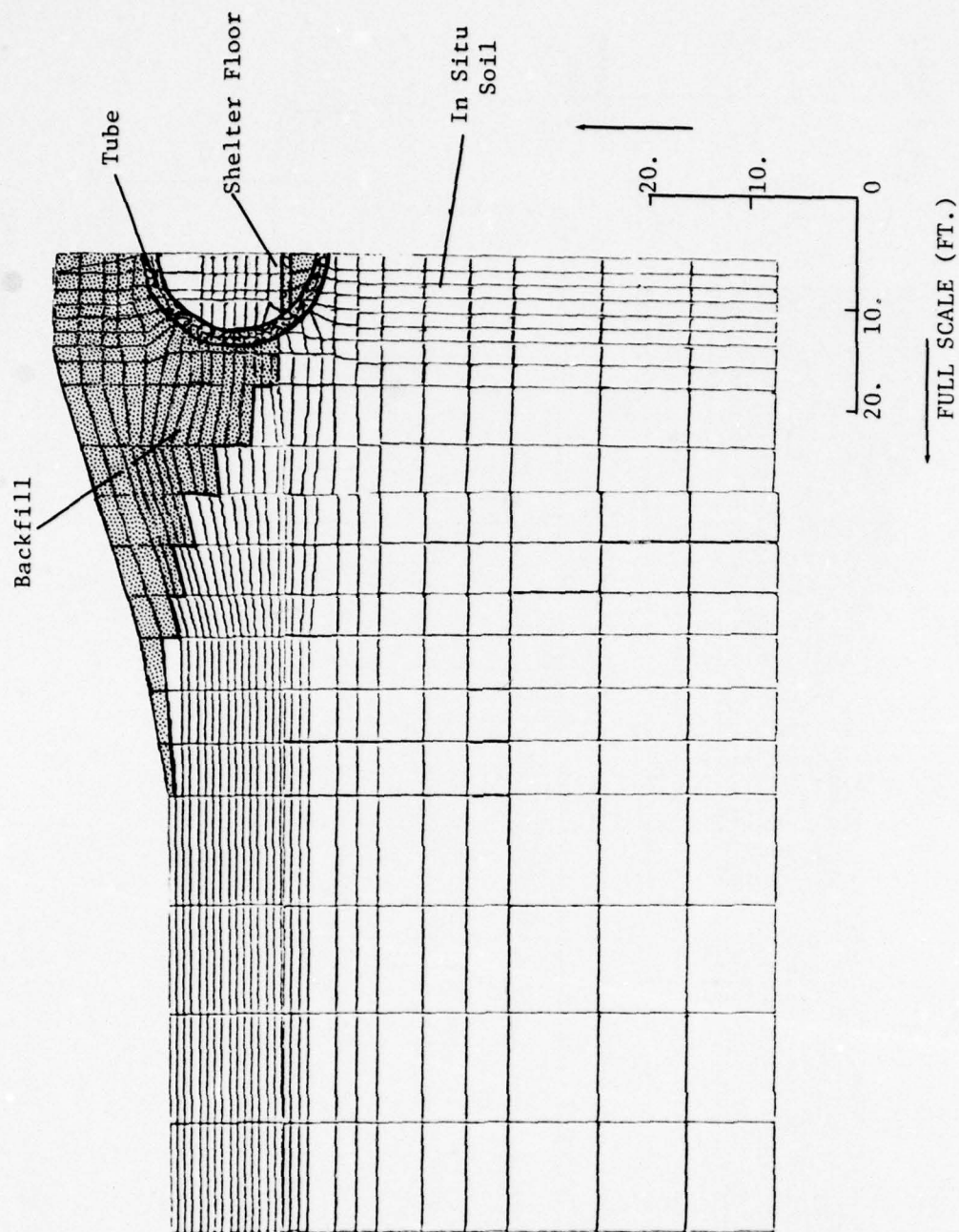
Figure 5-3c. Cross-section of S4 soil island and shelter perpendicular to axis of the tube

Transition Section

Cap

Closure

Actuator Housing

b. Elevation

Tube

Hinge

Closure

Gap

a. Plan

FULL SCALE (FT.)

0   10.   20.
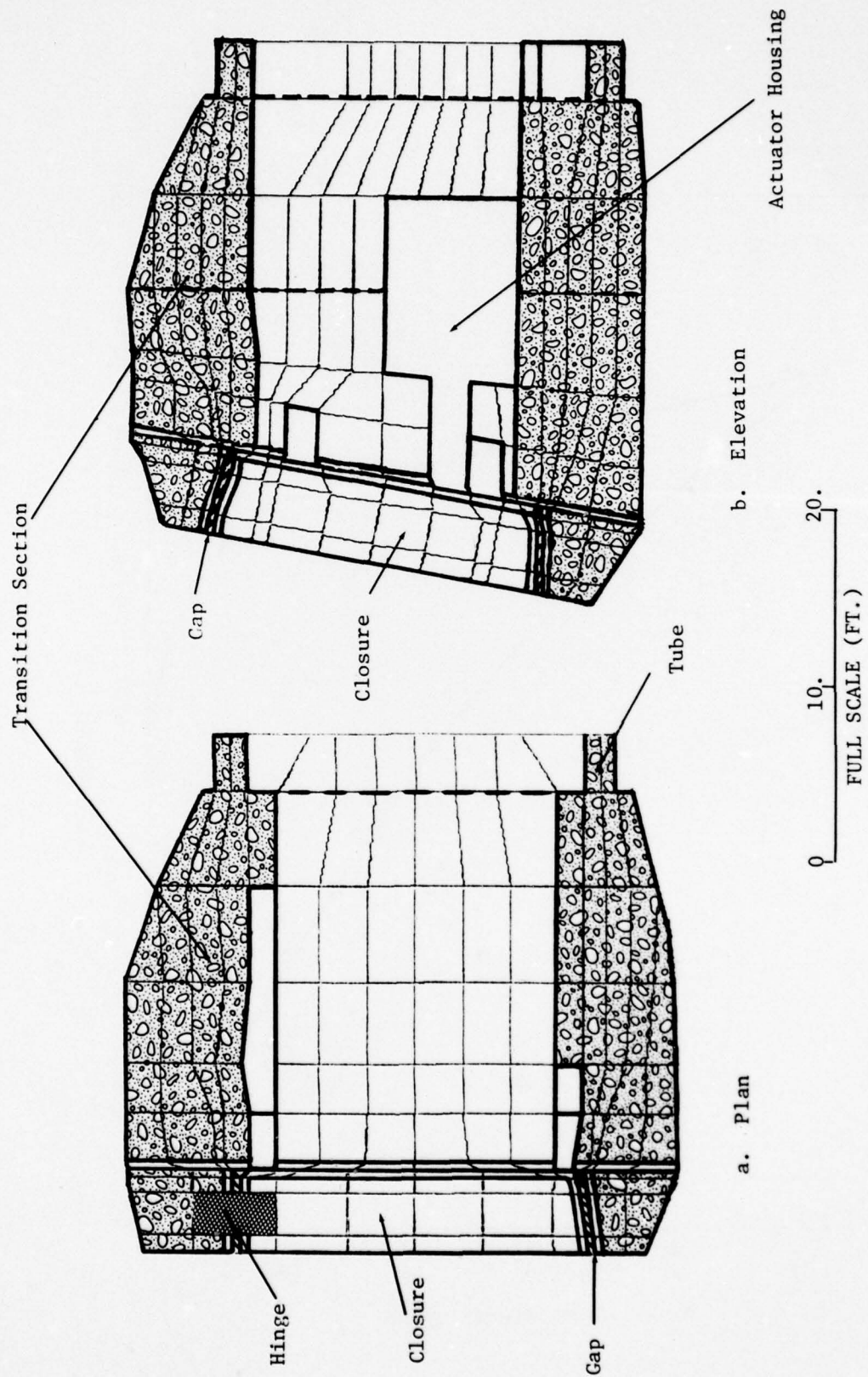
Figure 5-3d. S4 headwork model
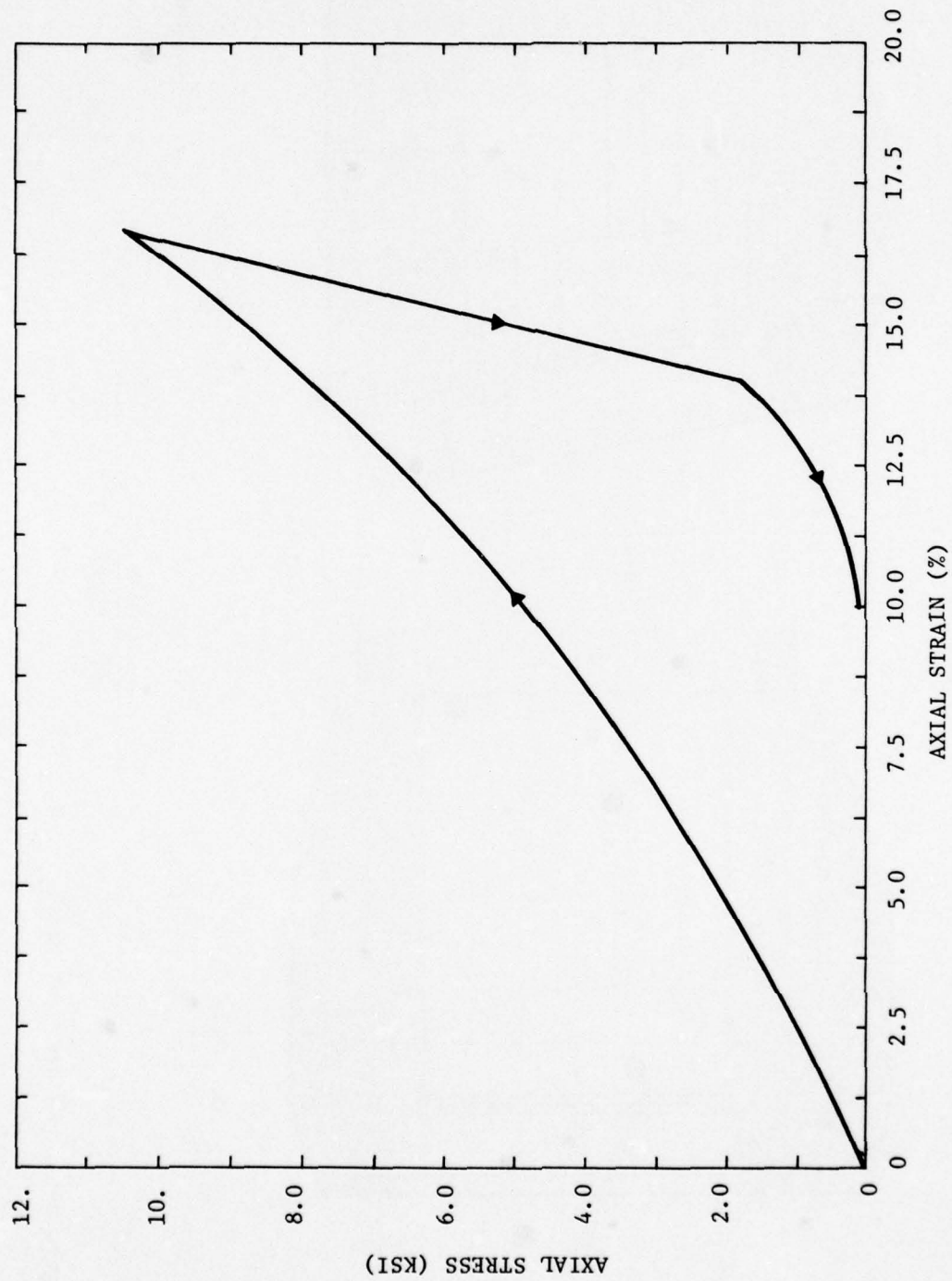
Figure 5-4a. Soil model in uniaxial strain, axial stress versus axial strain
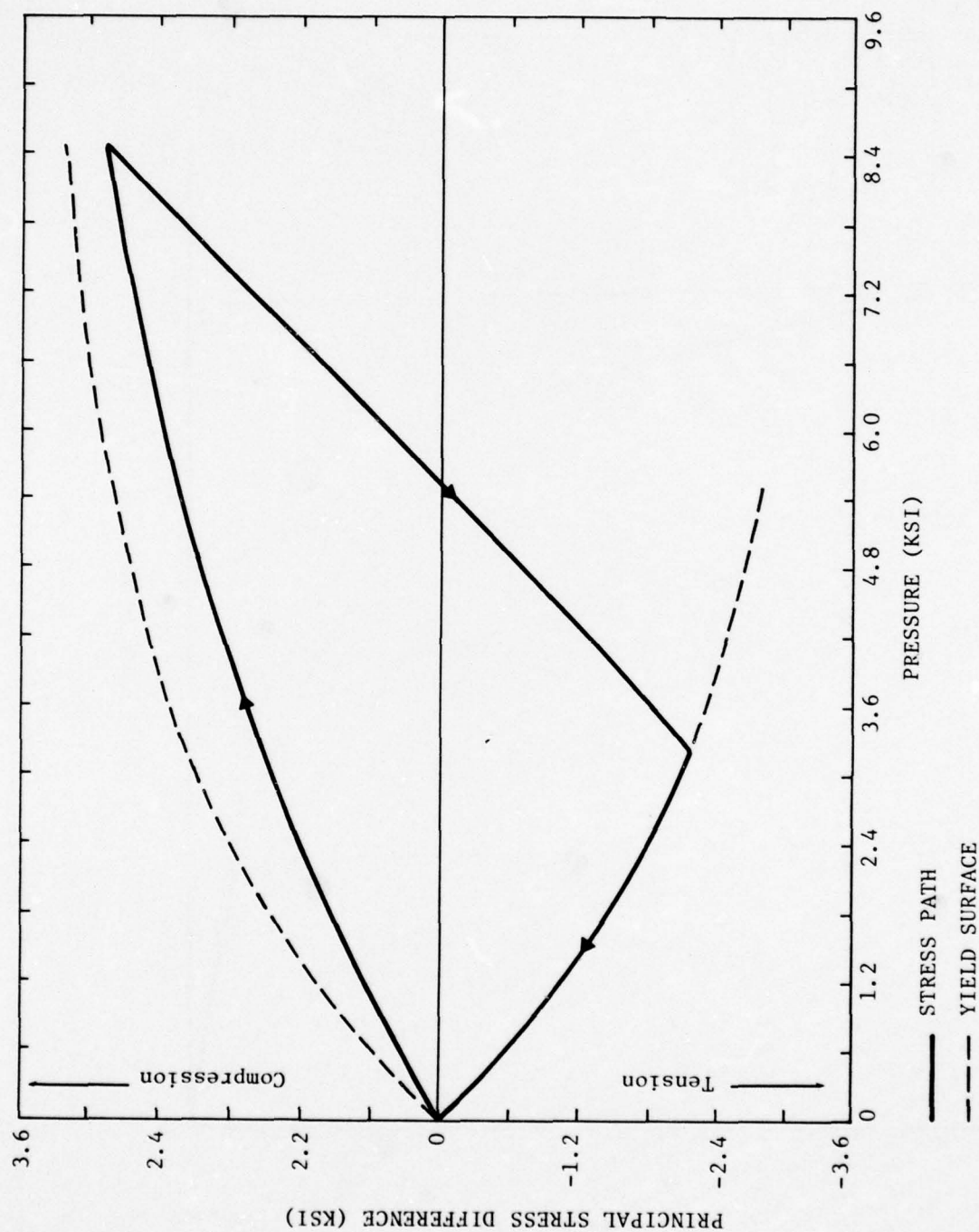
Figure 5-4b. Soil model in uniaxial strain, stress difference versus pressure

STRESS PATH

YIELD SURFACE
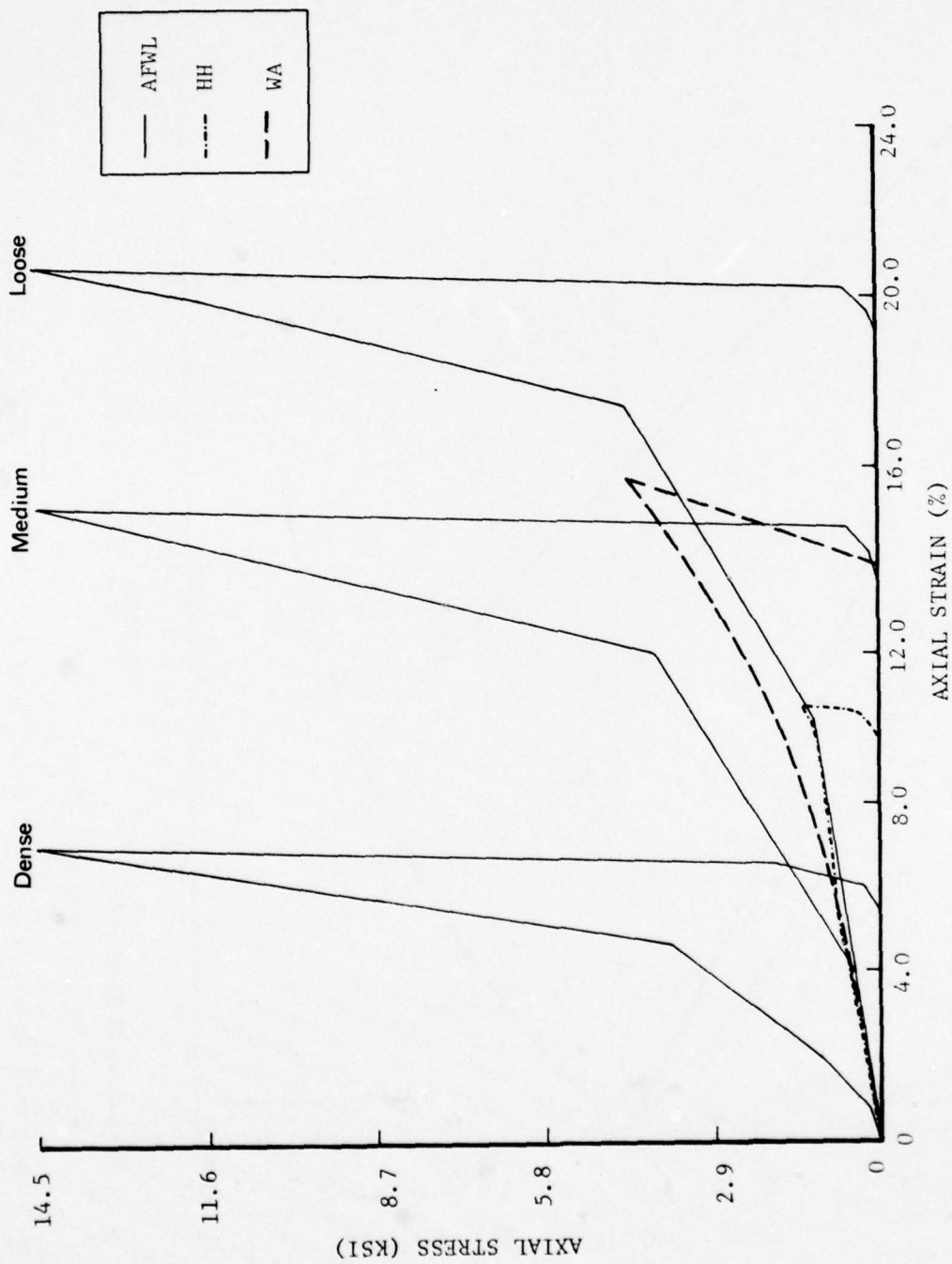
Figure 5-4c. Comparison of backfill models, uniaxial stress/strain curves
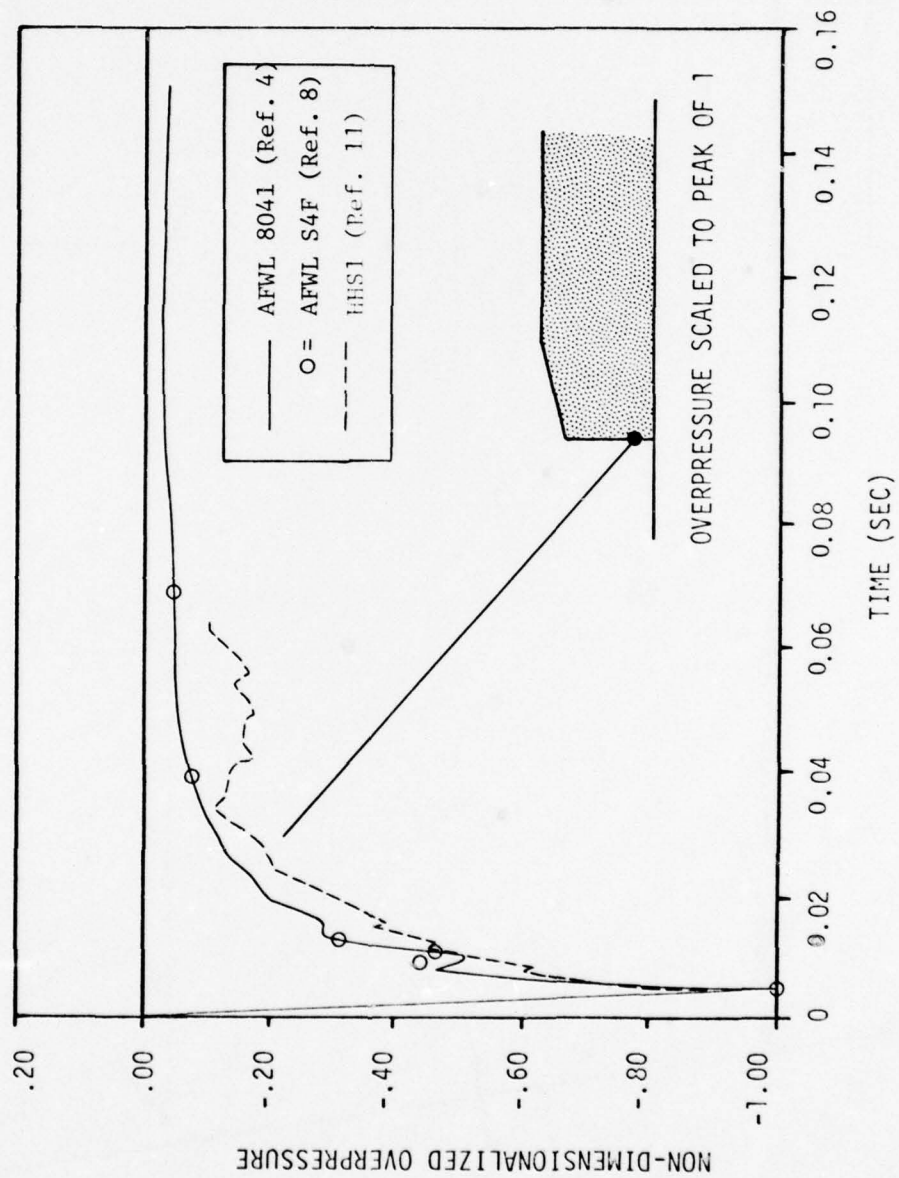
Figure 5-5. Comparison of overpressure waveforms at front face, front-on incidence, Calculations 2A, 2B and 2C
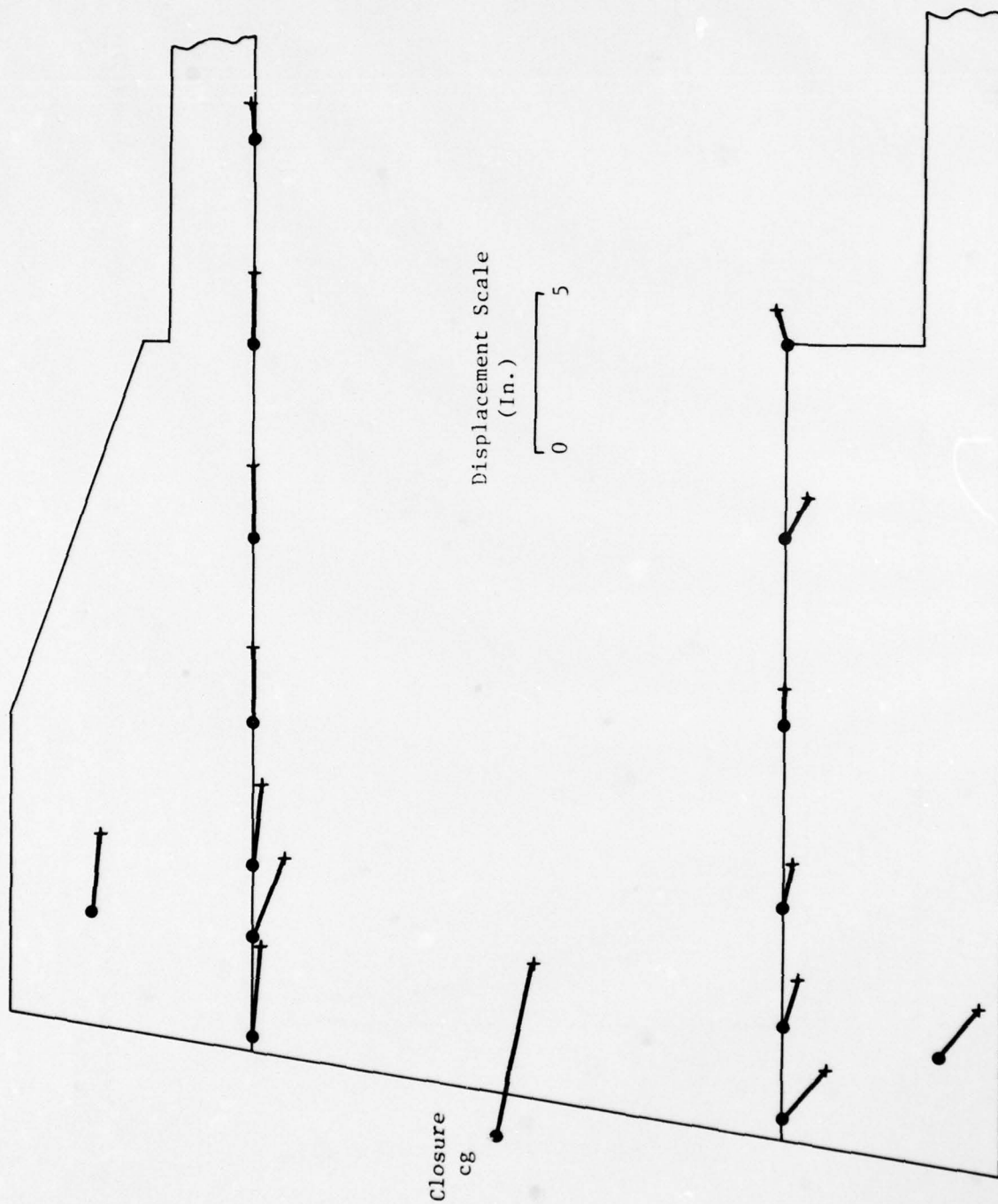
Figure 5-6. Deformation mode of headworks at 123 msec, 10 msec after airblast first arrival (113 msec), head-on incidence, Calculation 2A
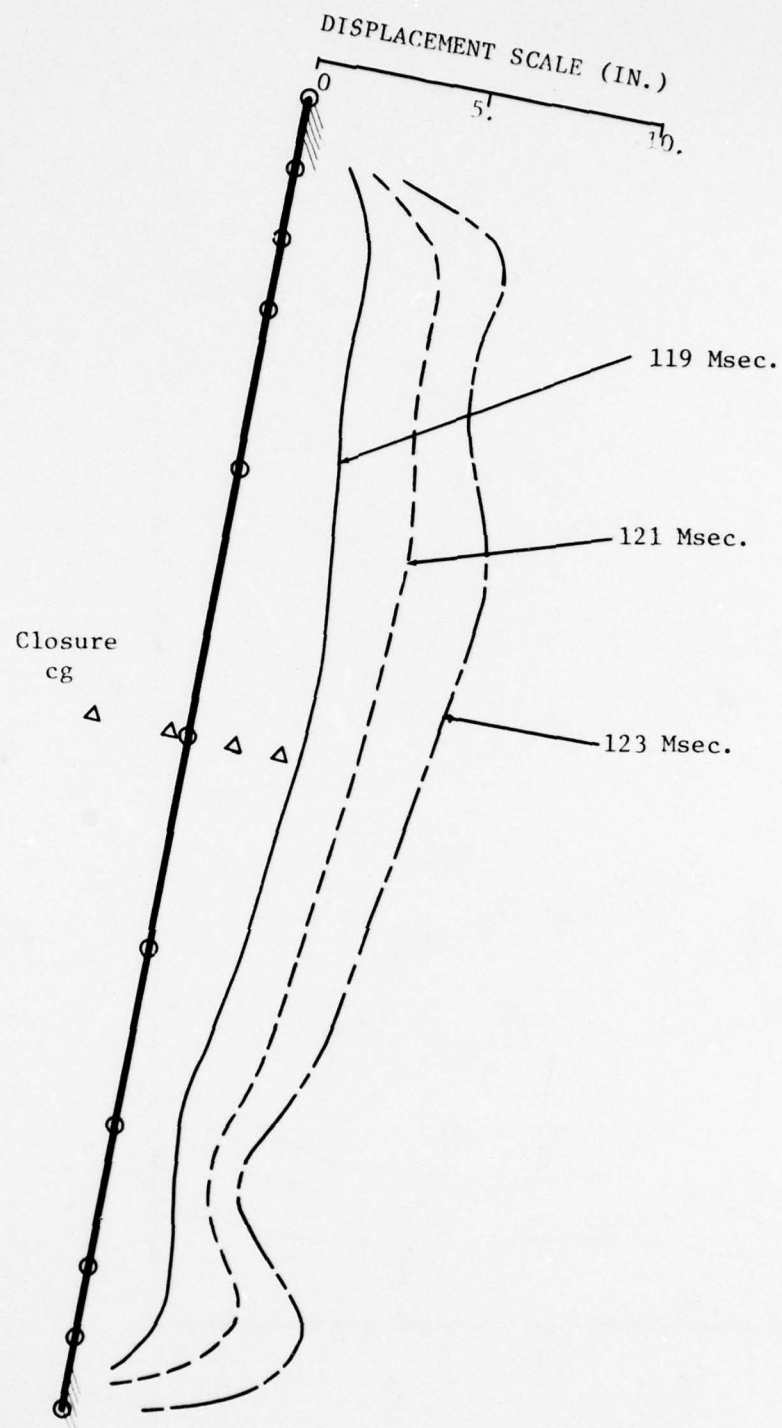
Figure 5-7. Deformation mode of backplate, vertical centerline, Calculation 2A
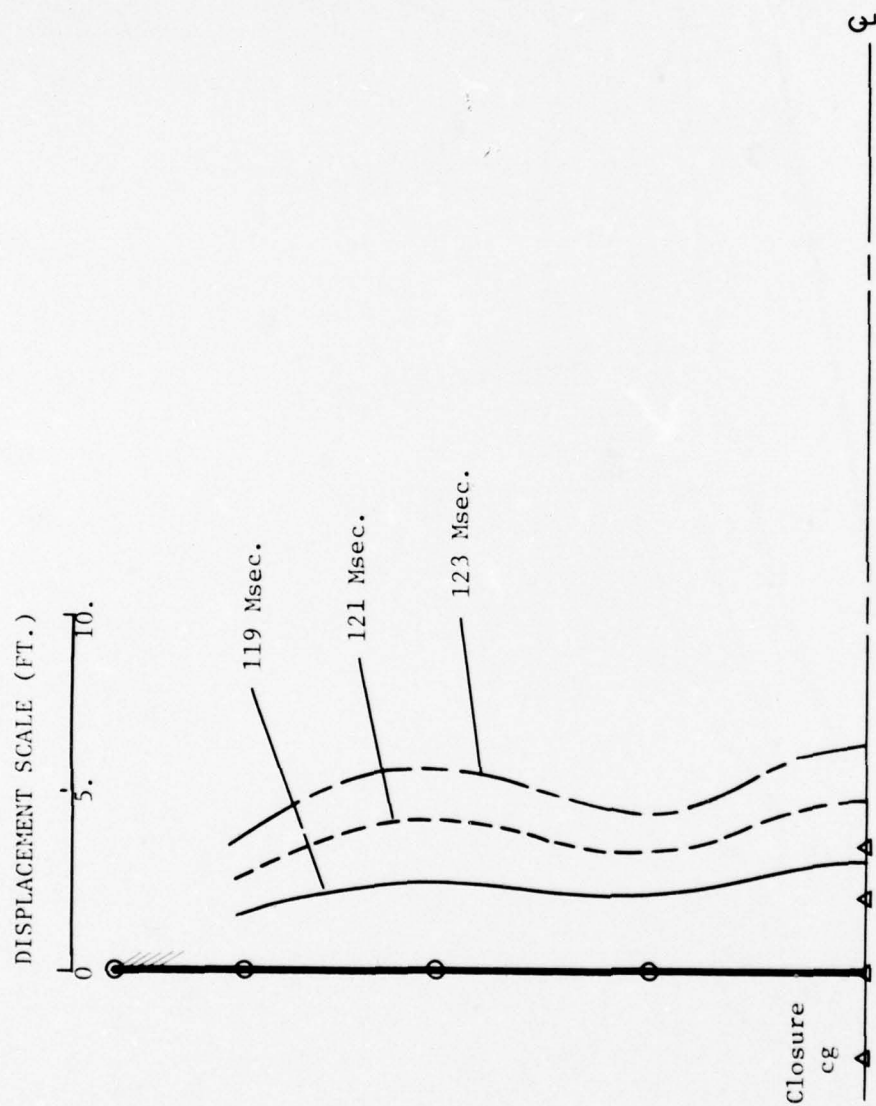
Figure 5-8. Deformation mode of backplate, horizontal centerline, Calculation 2A

Inelastic Zone

t = 117 Msec.
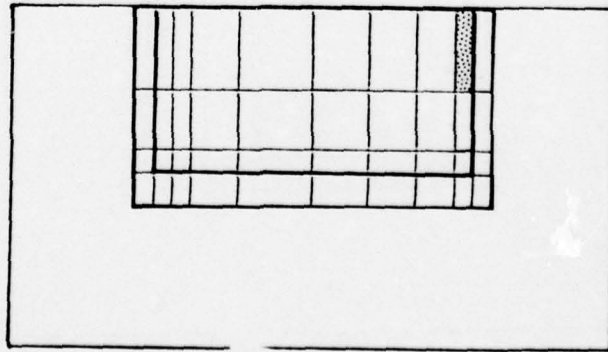
t = 118 Msec.
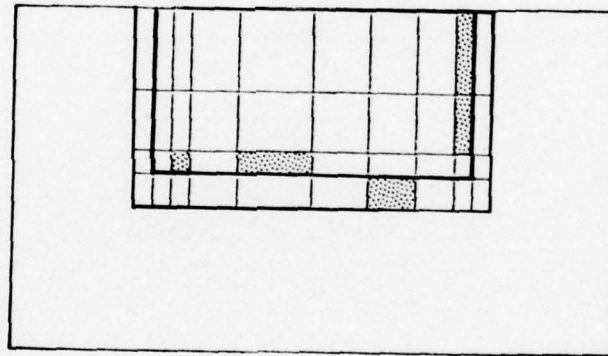
t = 119 Msec.
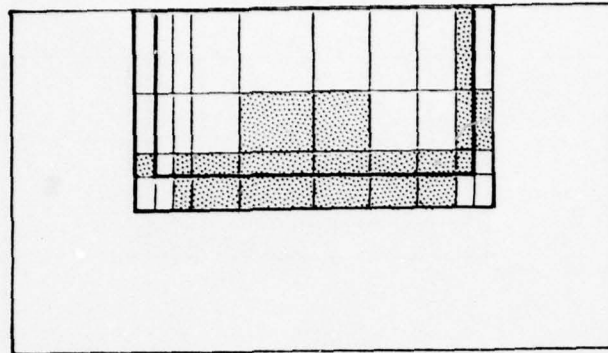
Figure 5-9a. Development of inelastic zones in backplate, Calculation 2A. Arival time of airblast is 113 msec.

Inelastic Zone

t = 120 Msec.
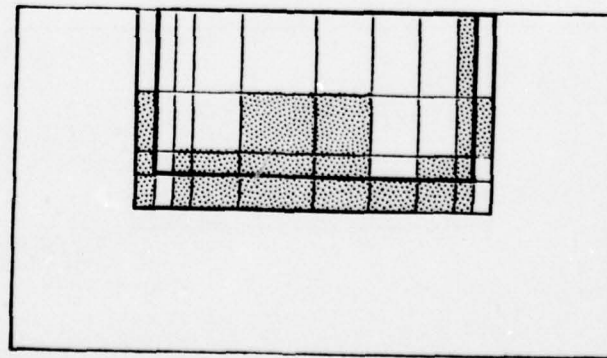
t = 121 Msec.
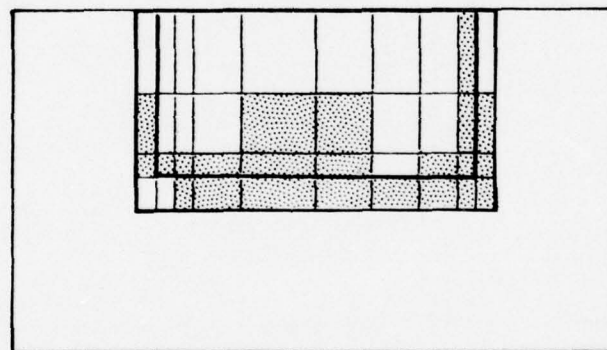
t = 122 Msec.
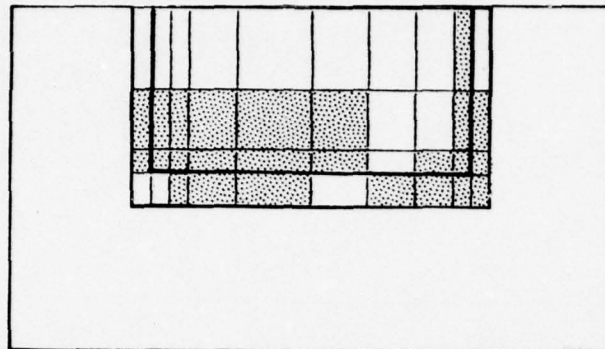
Figure 5-9b. Development of inelastic zone in backplate, Calculation 2A (continued). Arrival time of airblast is 113 msec.

Inelastic Zone

t = 115 Msec.
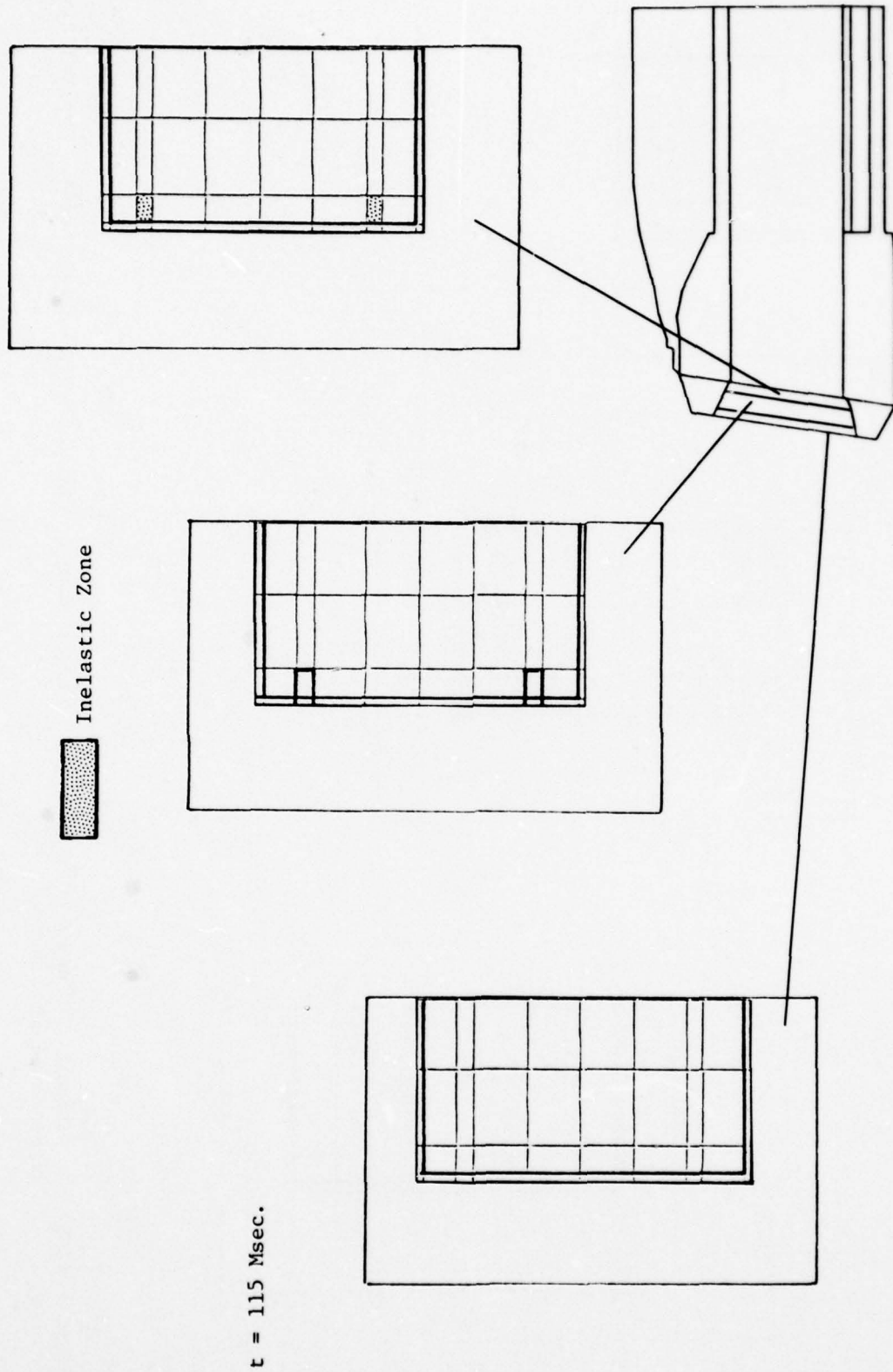
Figure 5-10a. Development of inelastic zone, in closure concrete, Calculation 2A. Arrival time of airblast is 113 msec.

5-25

t = 116 Msec.
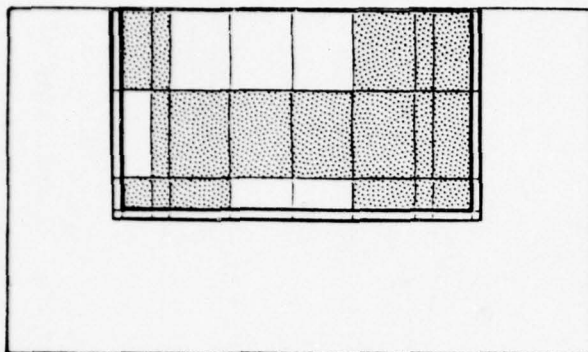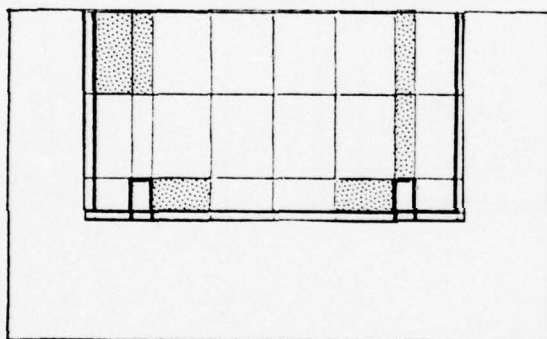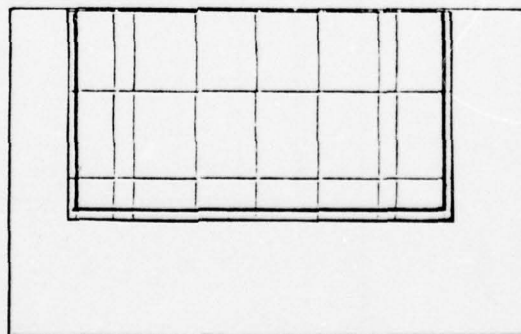
Figure 5-10b. Development of inelastic zone, in closure concrete, Calculation 2A (continued). Arrival time of airblast is 113 msec.
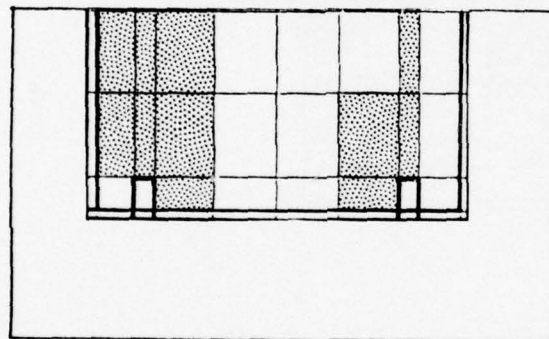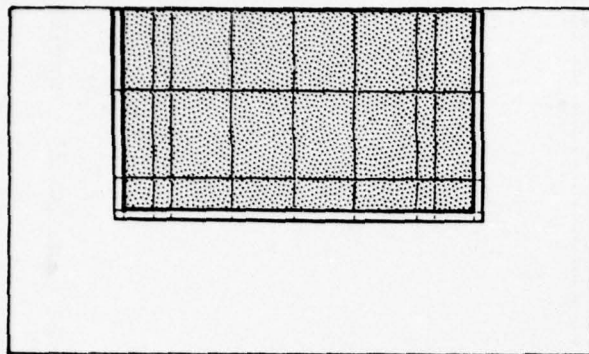
t = 117 Msec.
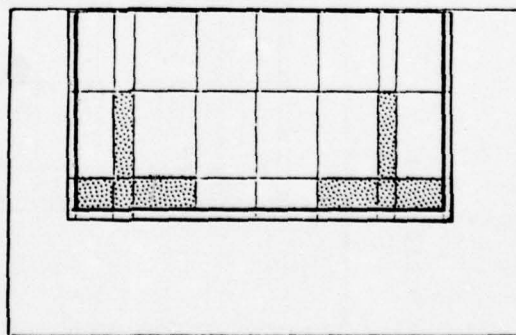
Figure 5-10c. Development of inelastic zone, in closure concrete, Calculation 2A (continued). Arrival time of airblast is 113 msec.
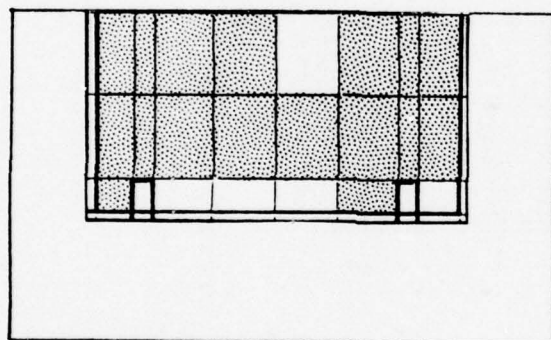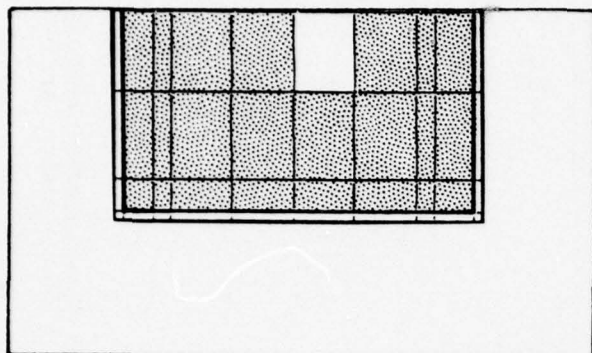
t = 118 Msec.
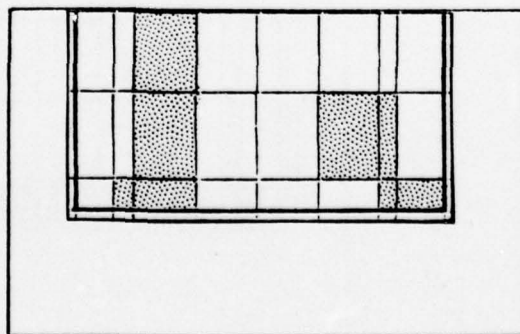
Figure 5-10d. Development of inelastic zone, in closure concrete, Calculation 2A (continued). Arrival time of airblast is 113 msec.
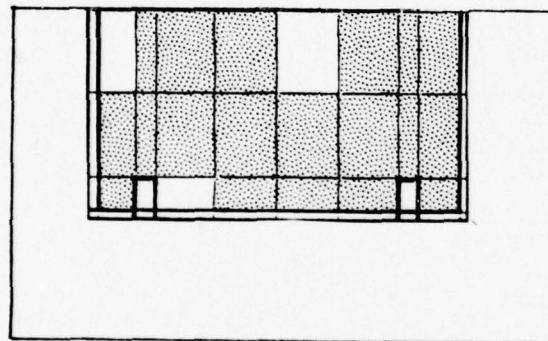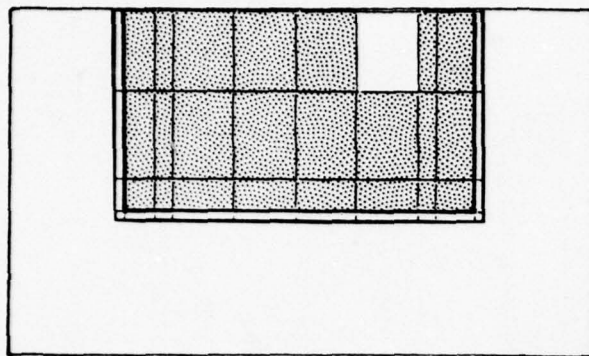
t = 123 Msec.
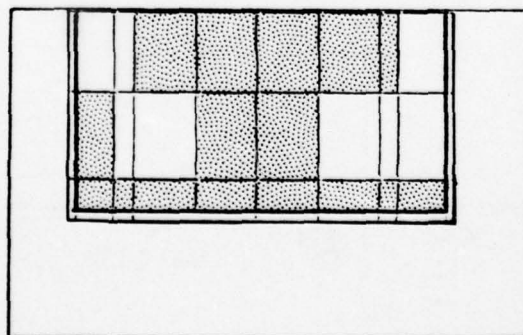
Figure 5-10e. Development of inelastic zone, in closure concrete, Calculation 2A (continued). Arrival time of airblast is 113 msec.
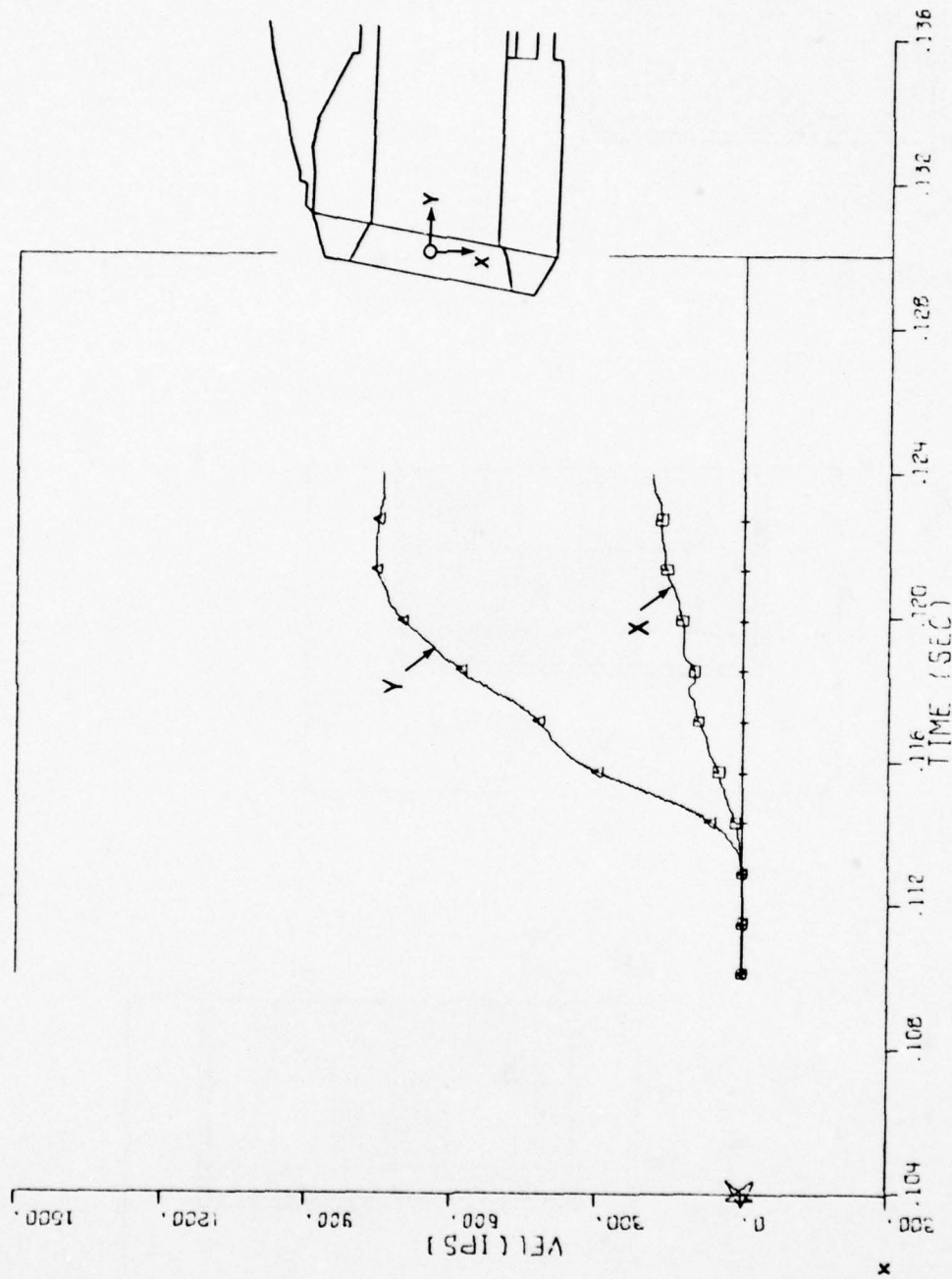
Figure 5-11. Velocity/time histories of closure cg, Calculation 2A

Figure 5-12. Typical stress invariant plot for points in closure concrete near support, Calculation 2A

All points shown have similar response
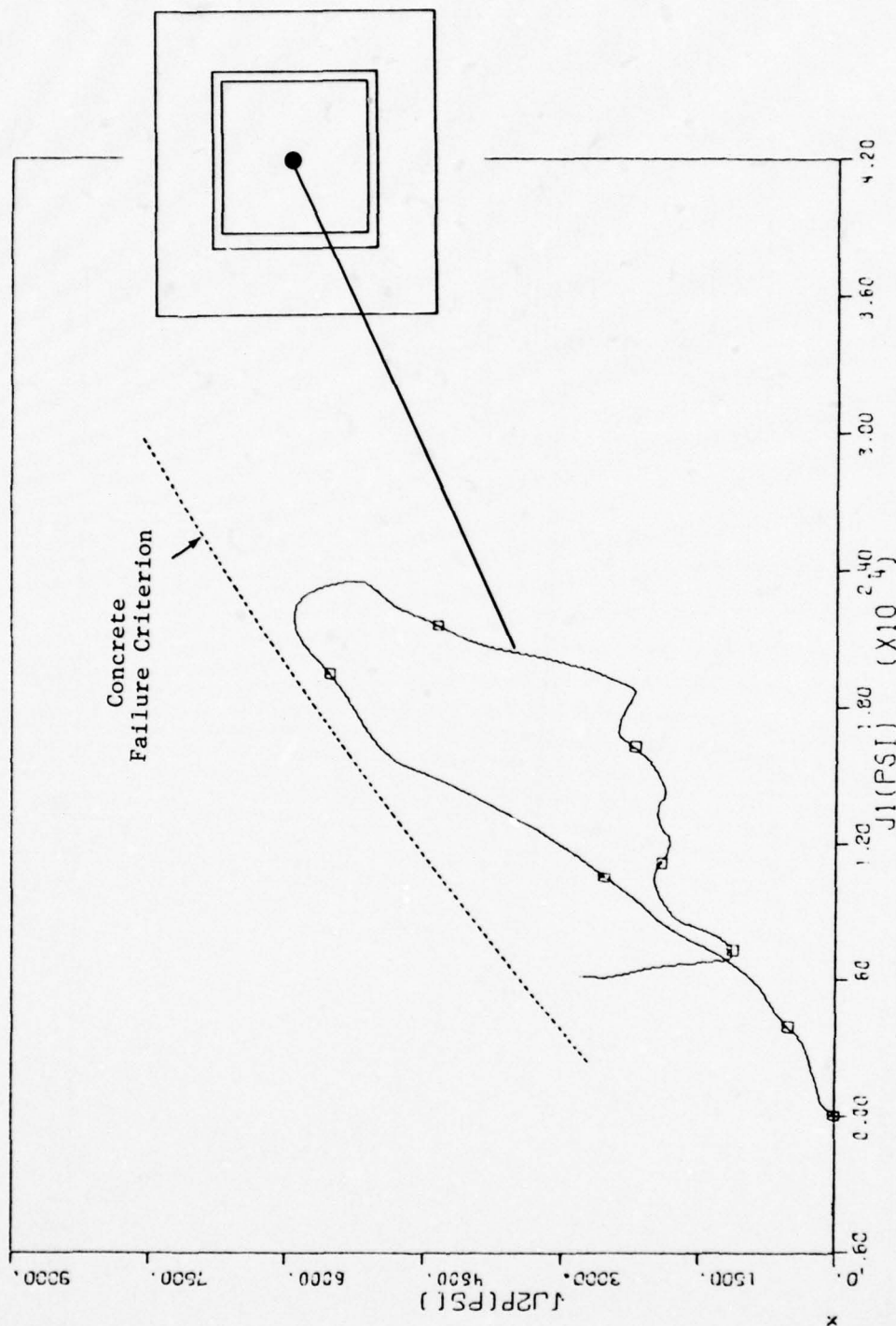
Figure 5-13. Typical stress invariant plot for points in center of closure concrete, Calculation 2A
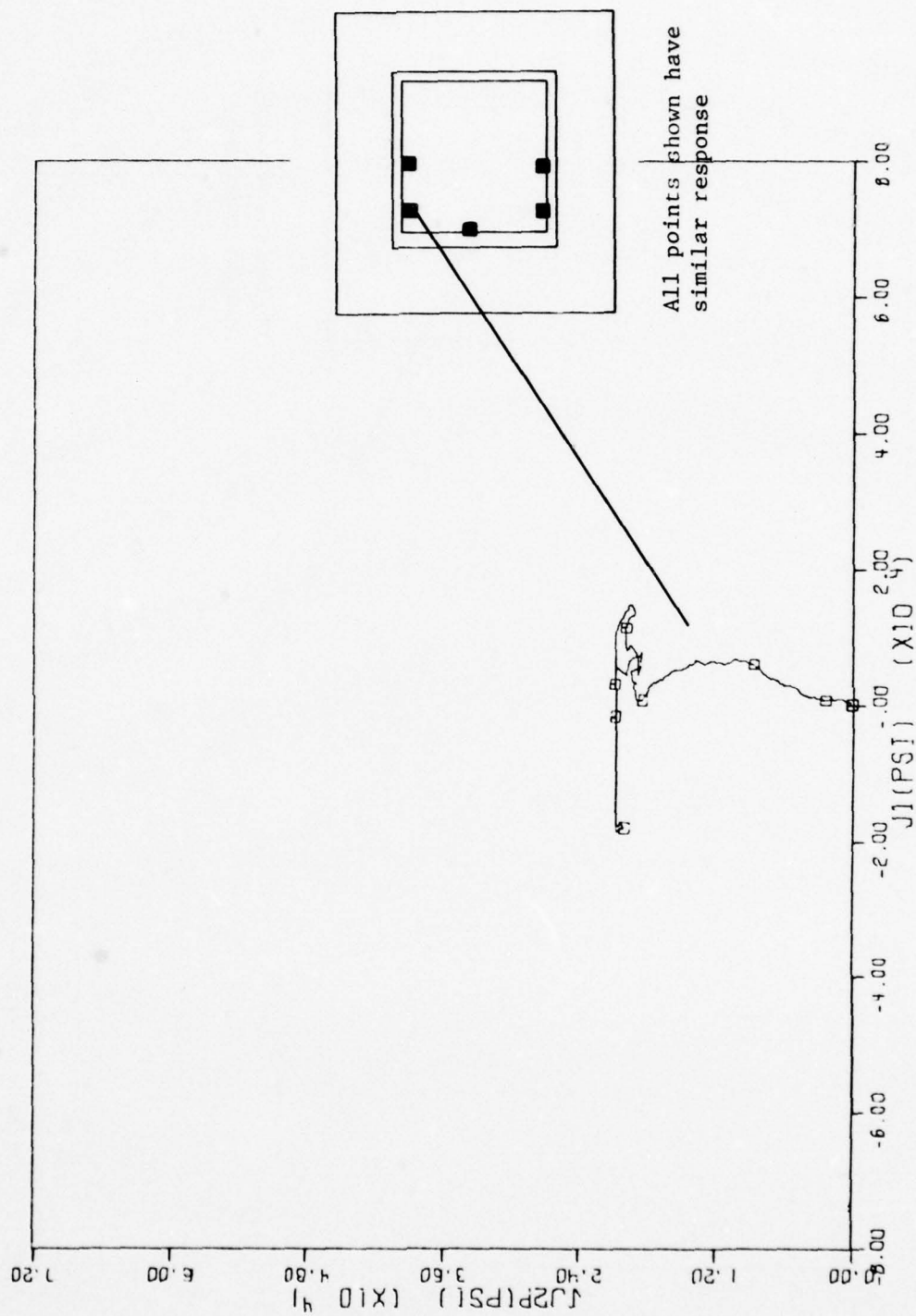
Figure 5-14. Typical stress invariant plot for points in backplate near support, Calculation 2A
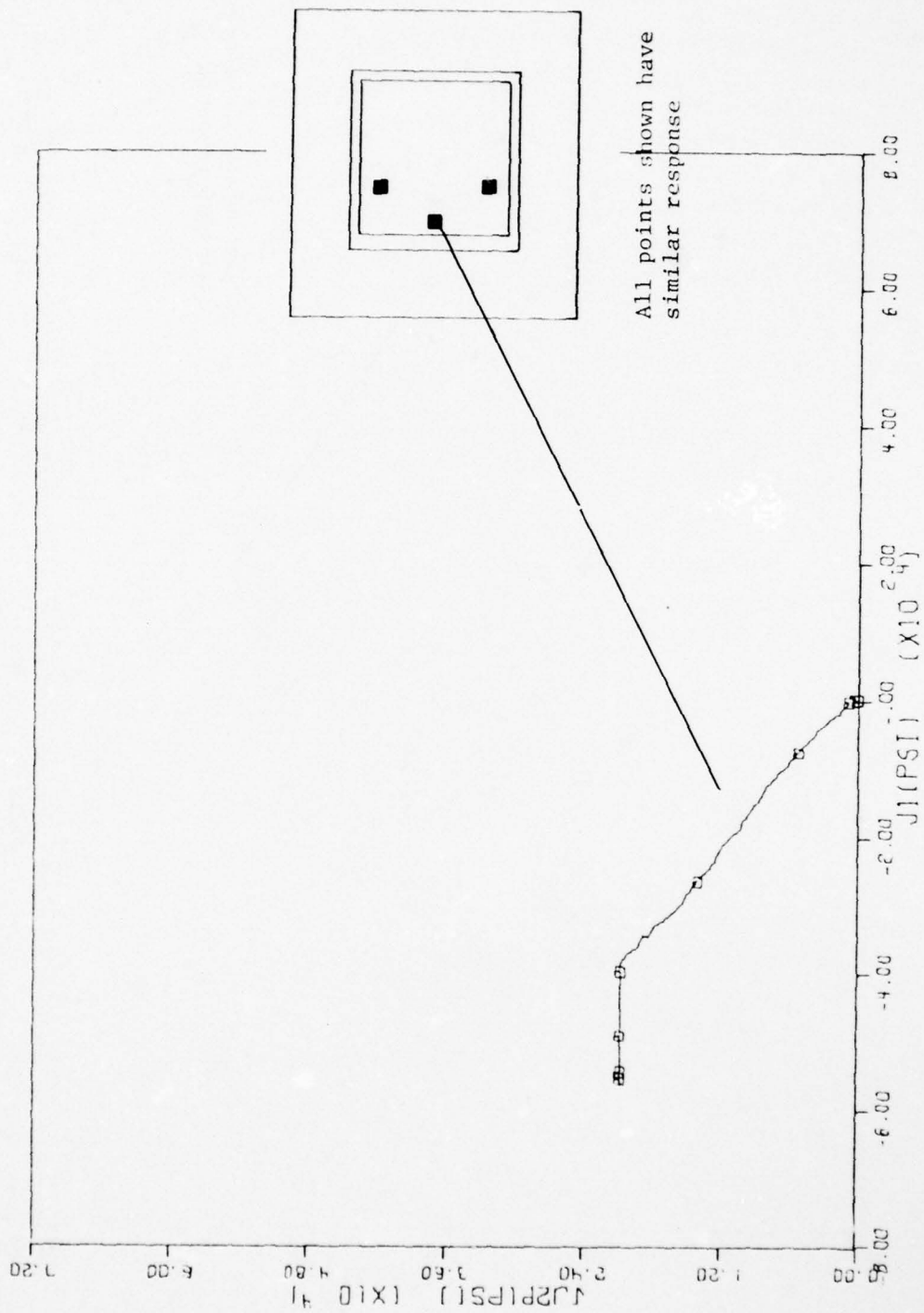
All points shown have
similar response

Figure 5-15. Typical stress invariant plot for points in backplate unsupported, Calculation 2A
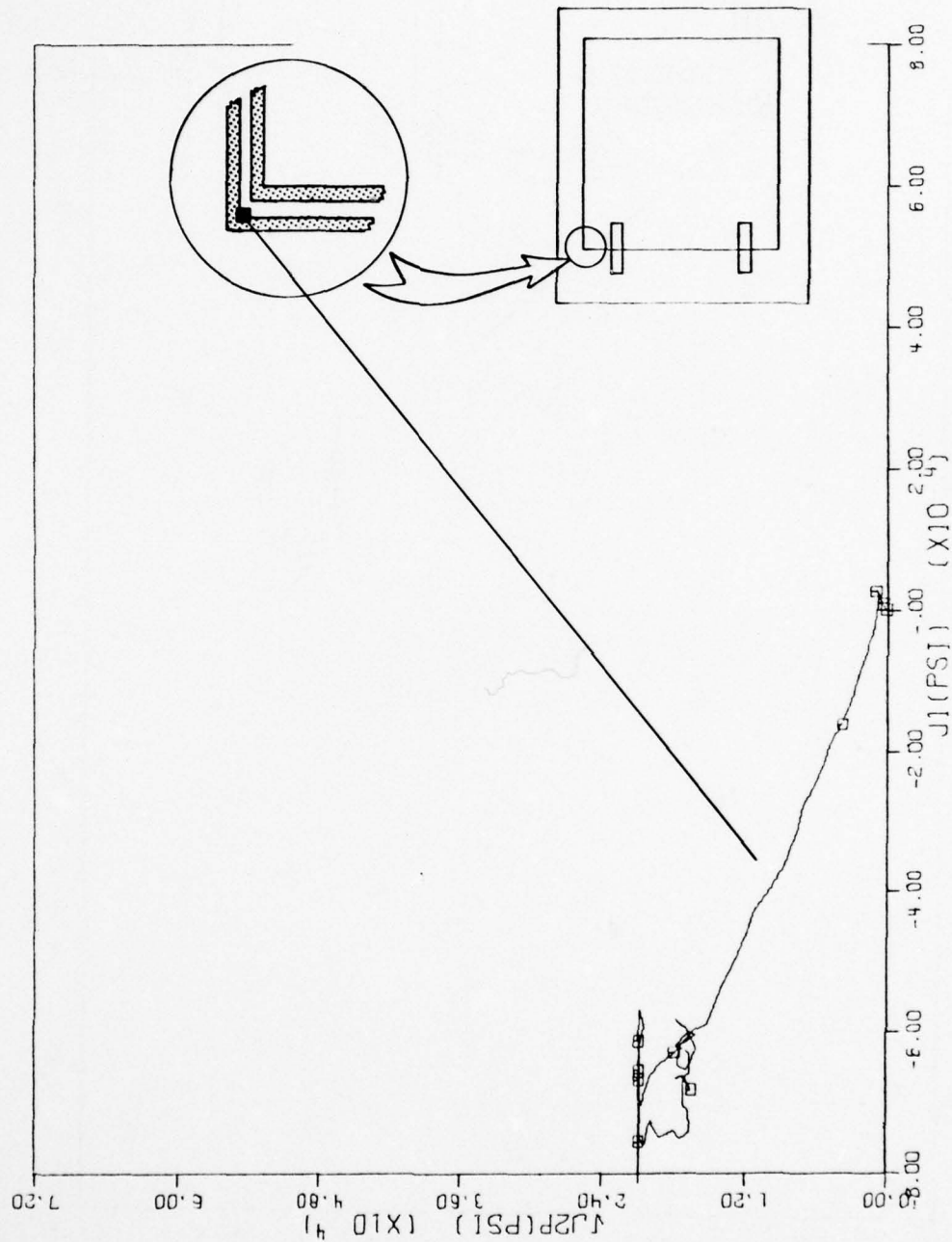
Figure 5-16a. Stress invariant plot for upper frame corner, inner steel lining, Calculation 2A
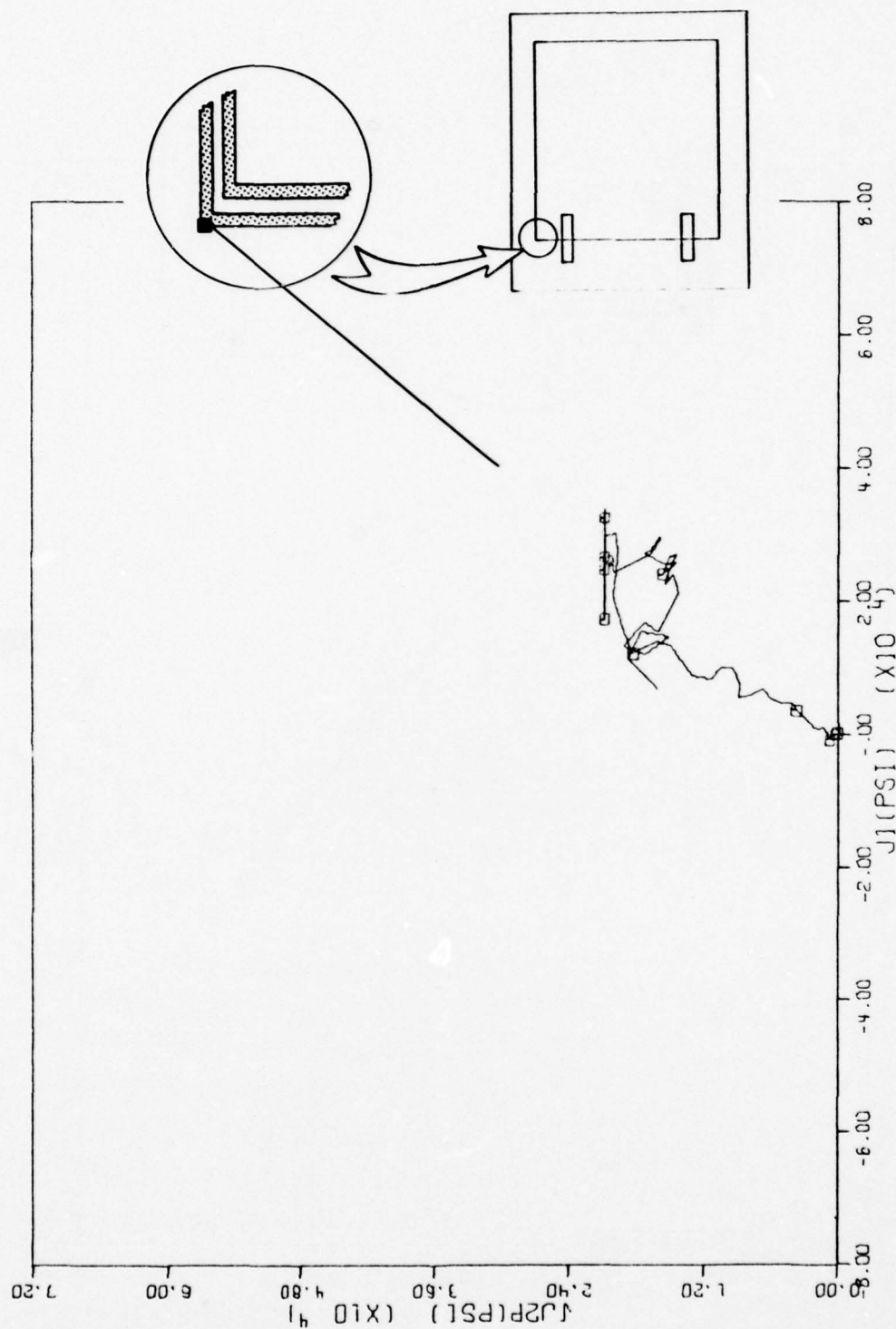
Figure 5-16b. Stress invariant plot for upper frame corner, outer steel lining, Calculation 2A
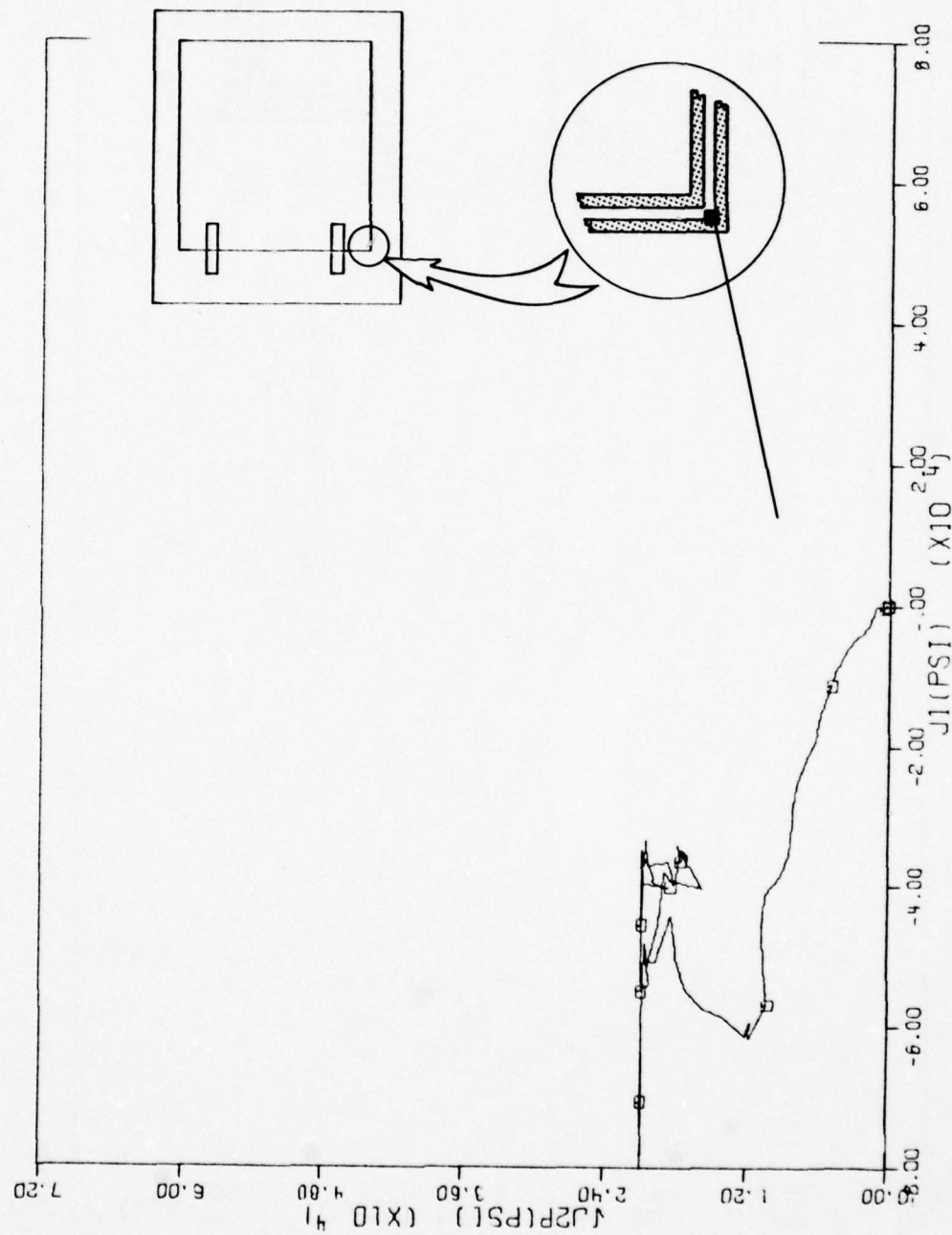
Figure 5-17a. Stress invariant plot for lower frame corner, inner steel lining, Calculation 2A
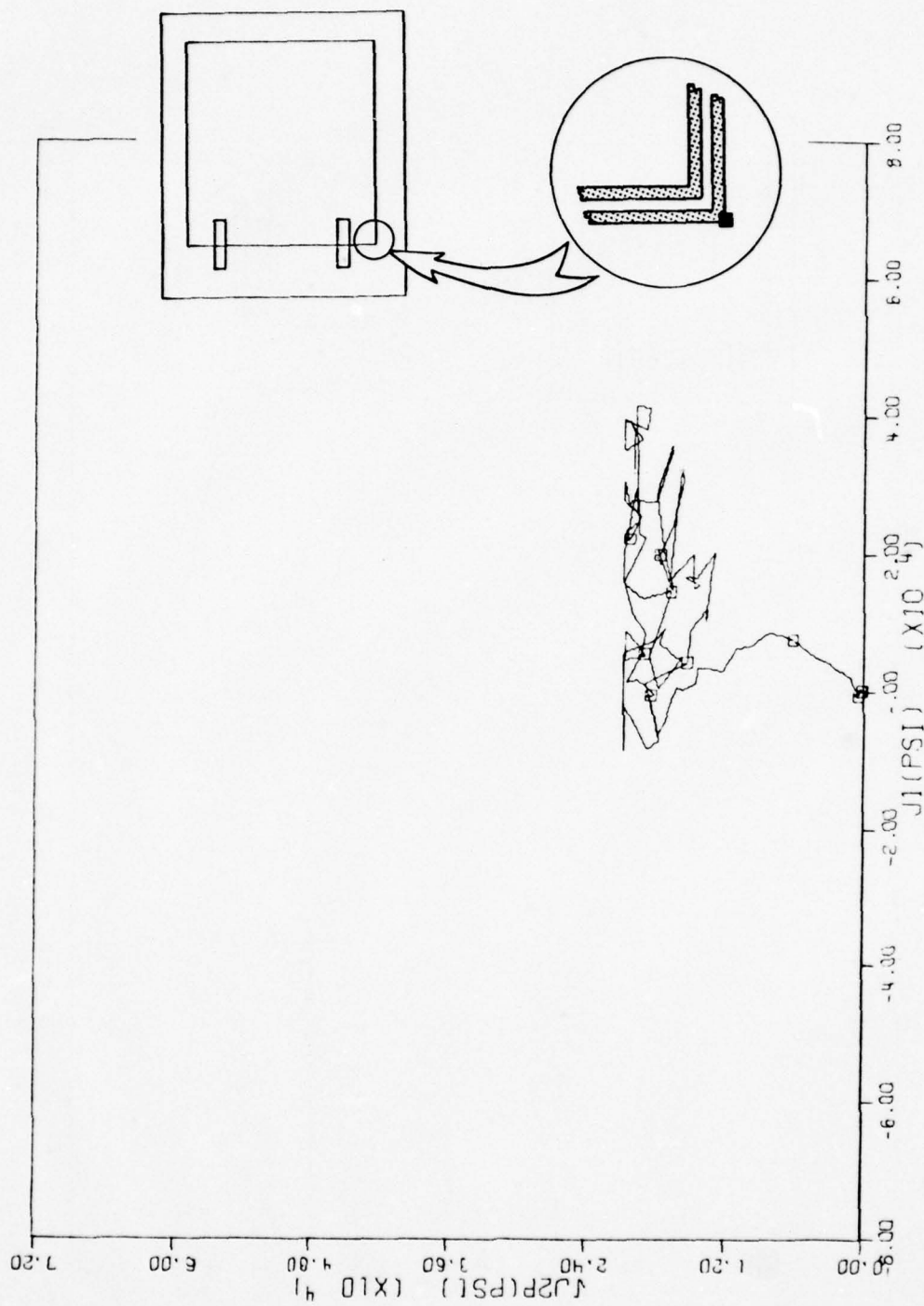
Figure 5-17b. Stress invariant plot for lower frame corner, outer steel lining, Calculation 2A
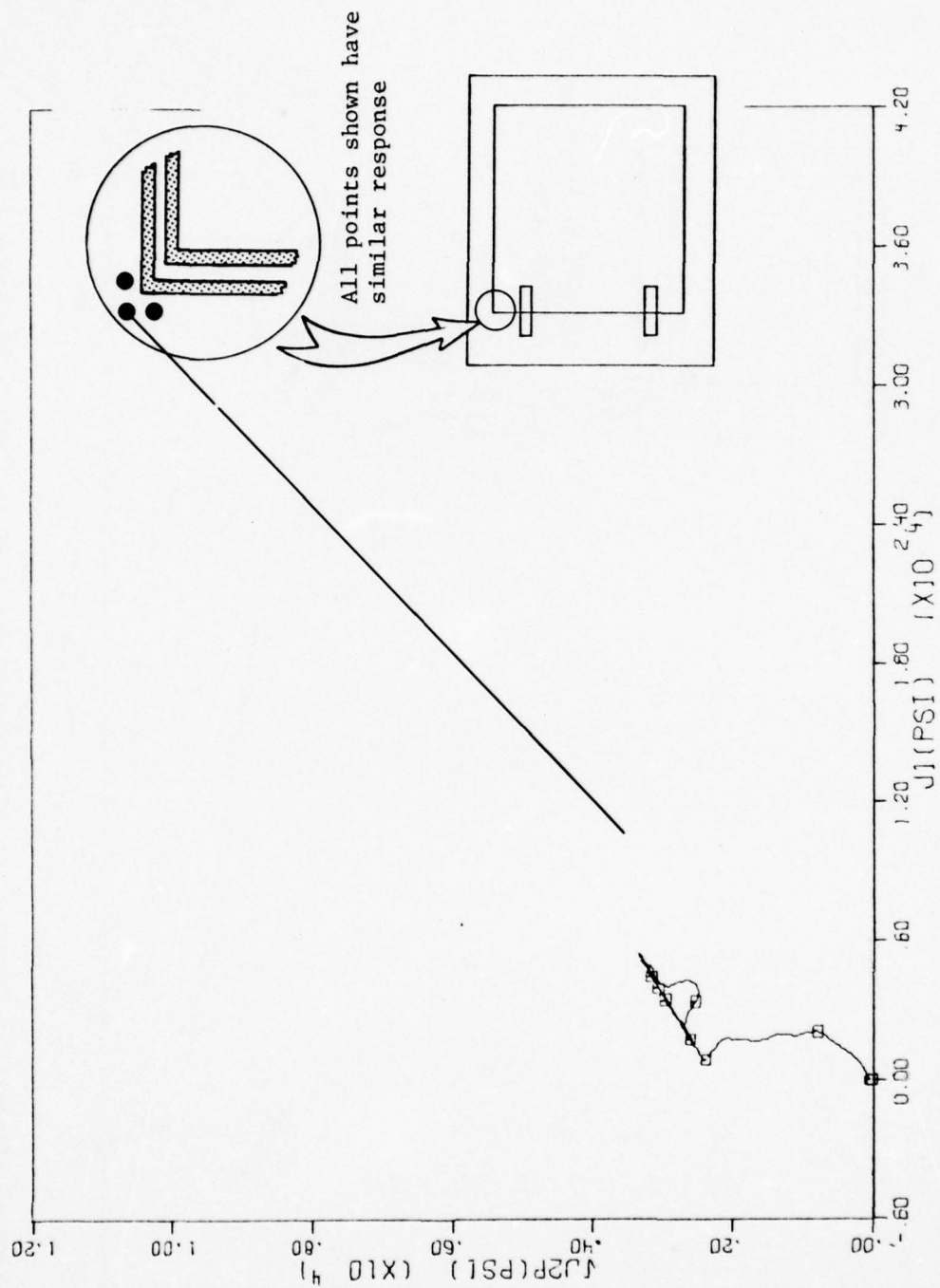
Figure 5-18. Typical stress invariant plot for concrete in upper frame corner, Calculation 2A

All points shown have
similar response
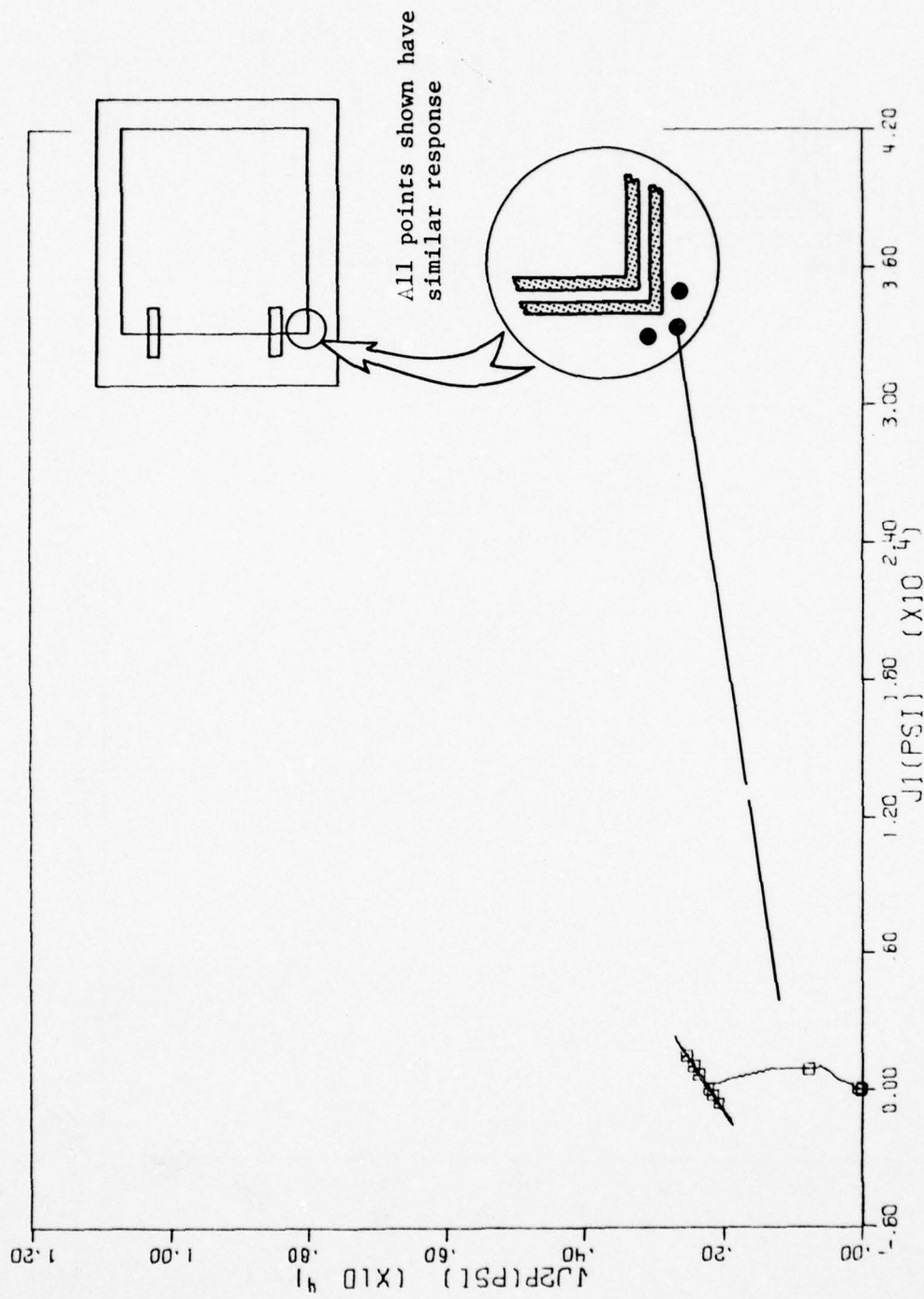
Figure 5-19. Typical stress invariant plot for concrete in lower frame corner, Calculation 2A
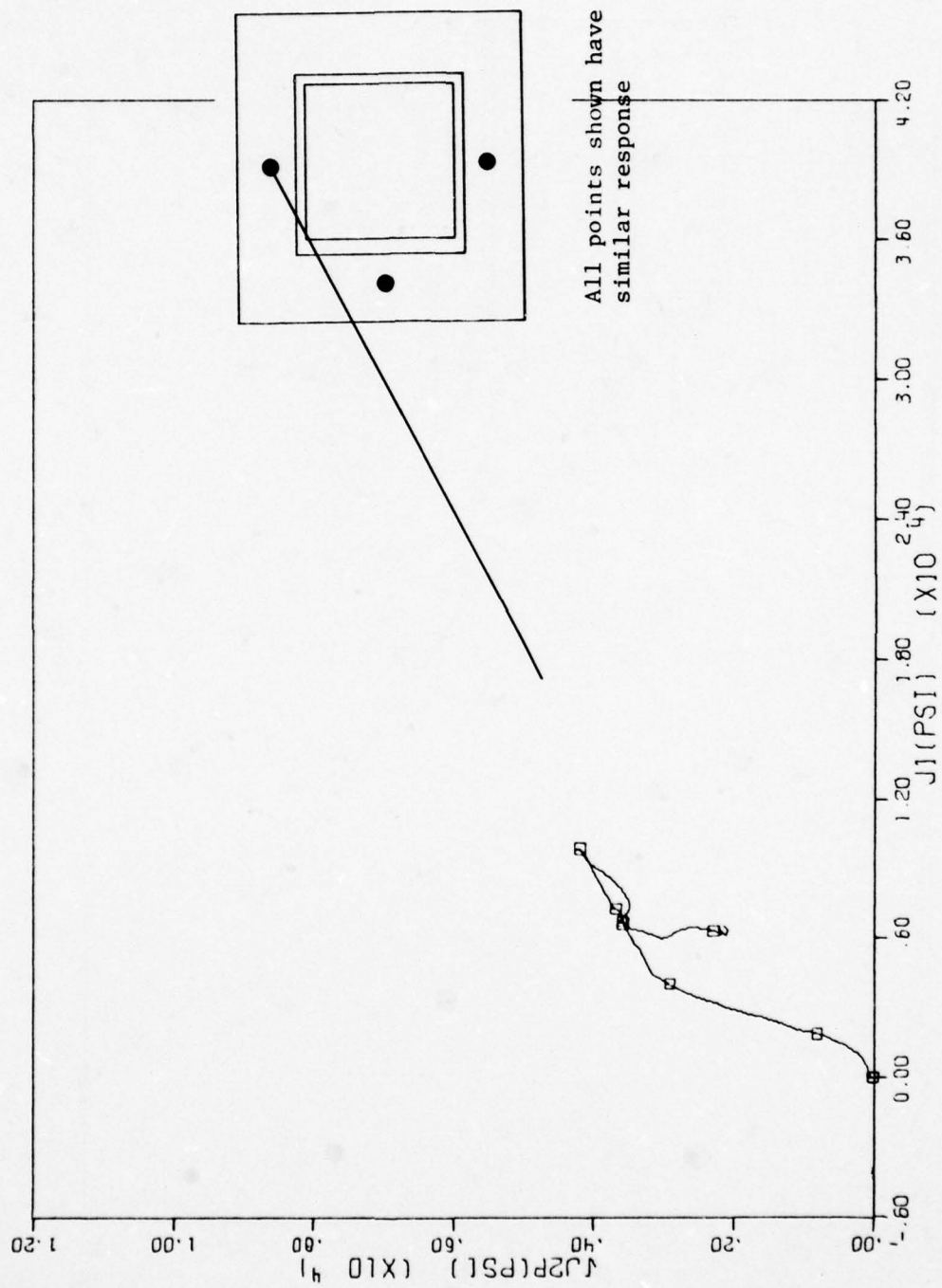
Figure 5-20. Typical stress invariant plot for concrete in frame gussets, Calculation 2A

All points shown have
similar response
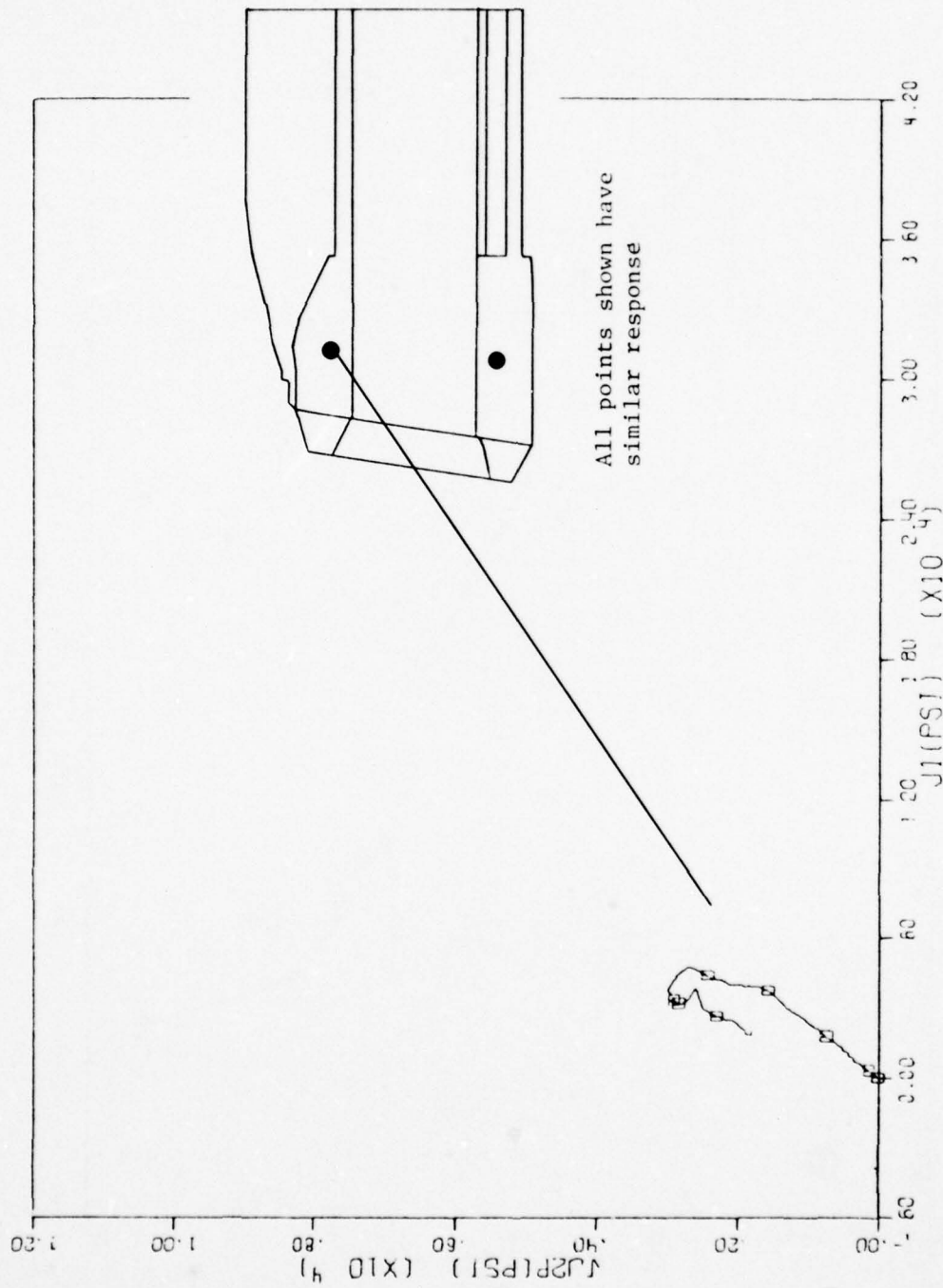
Figure 5-21. Typical stress invariant plot for points in headworks, Calculation 2A
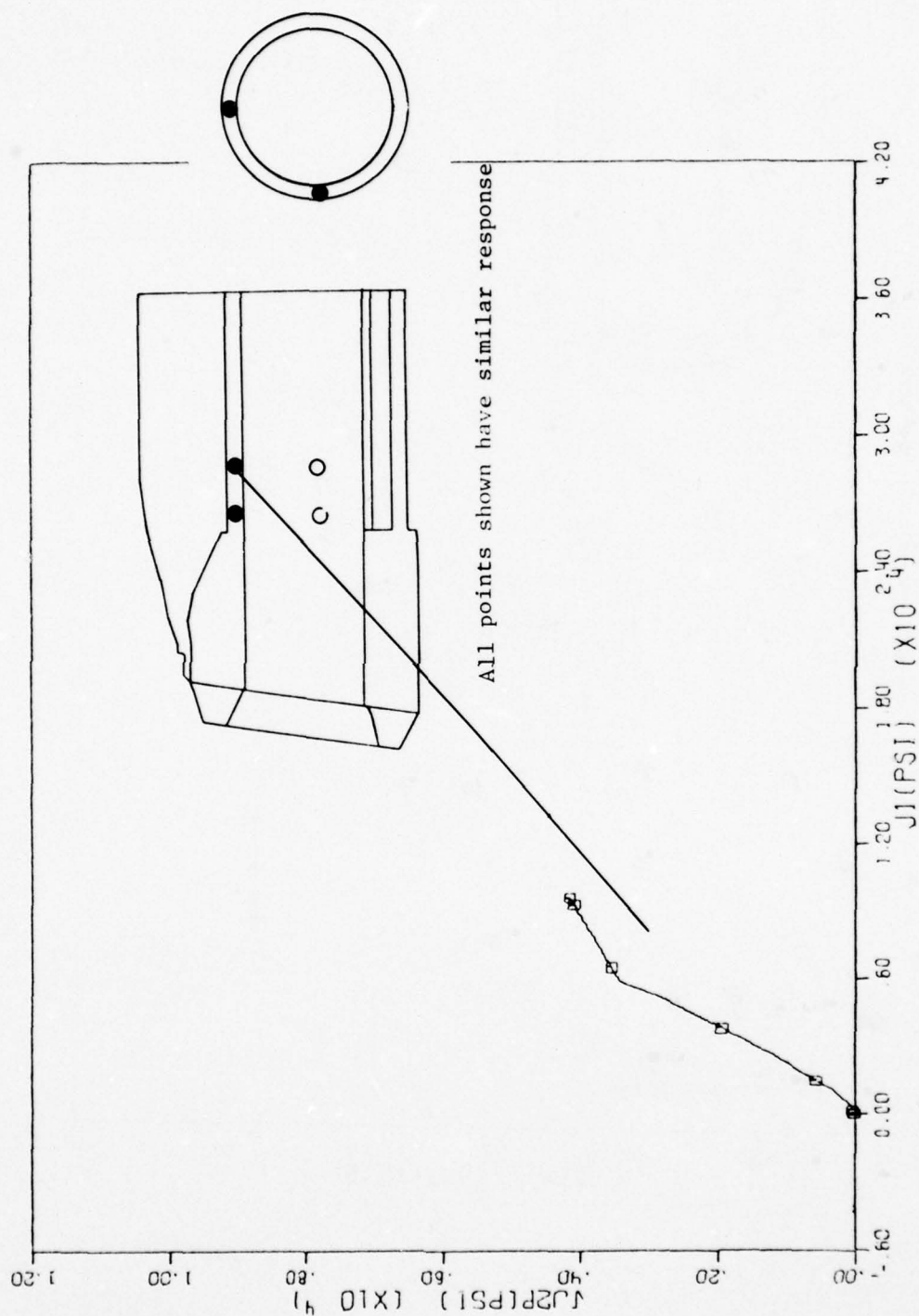
Figure 5-22. Typical stress invariant plot for points in the tubular section near headworks, crown and springline, Calculation 2A
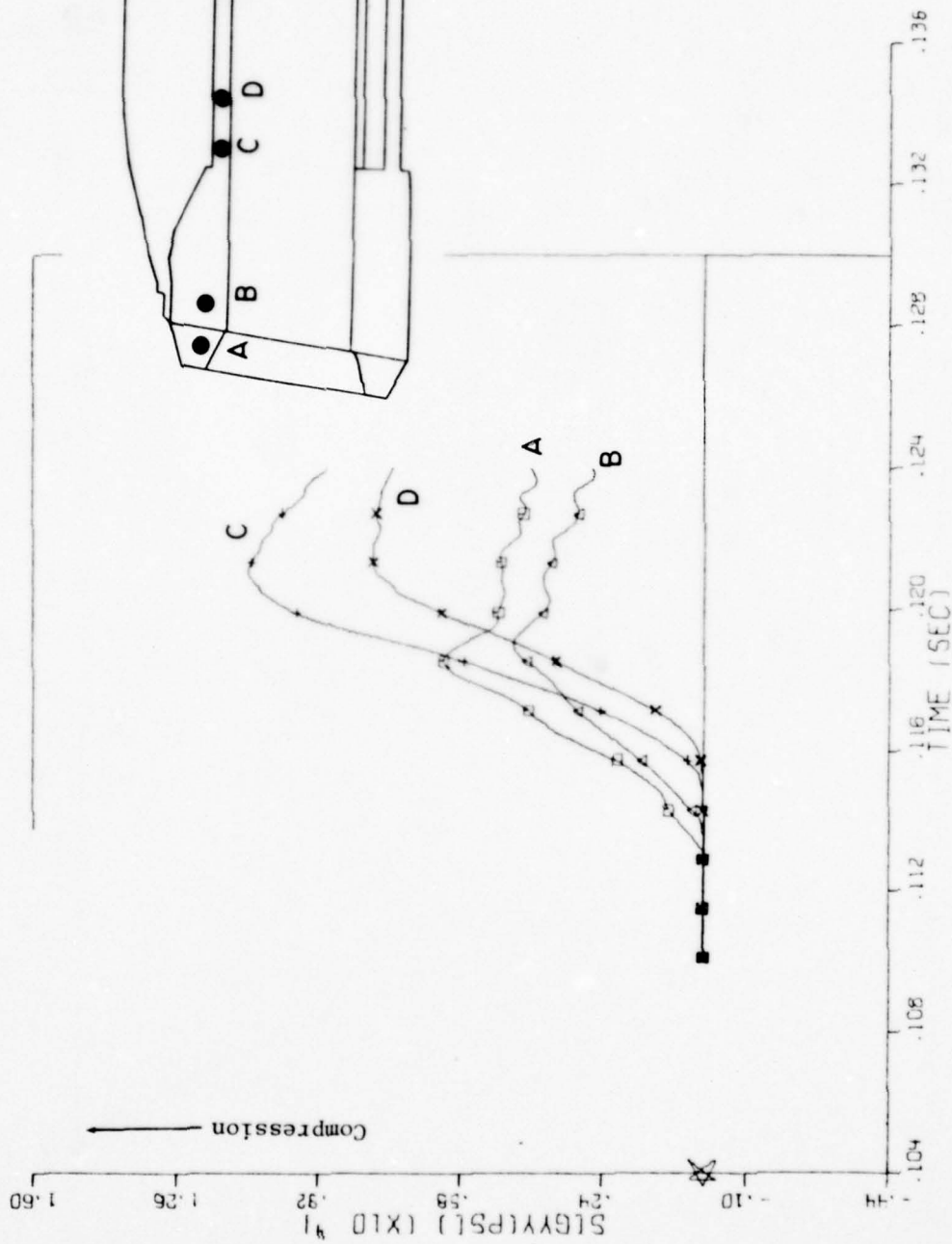
Figure 5-23. Longitudinal stress/time histories for points along upper shelter, Calculation 2A
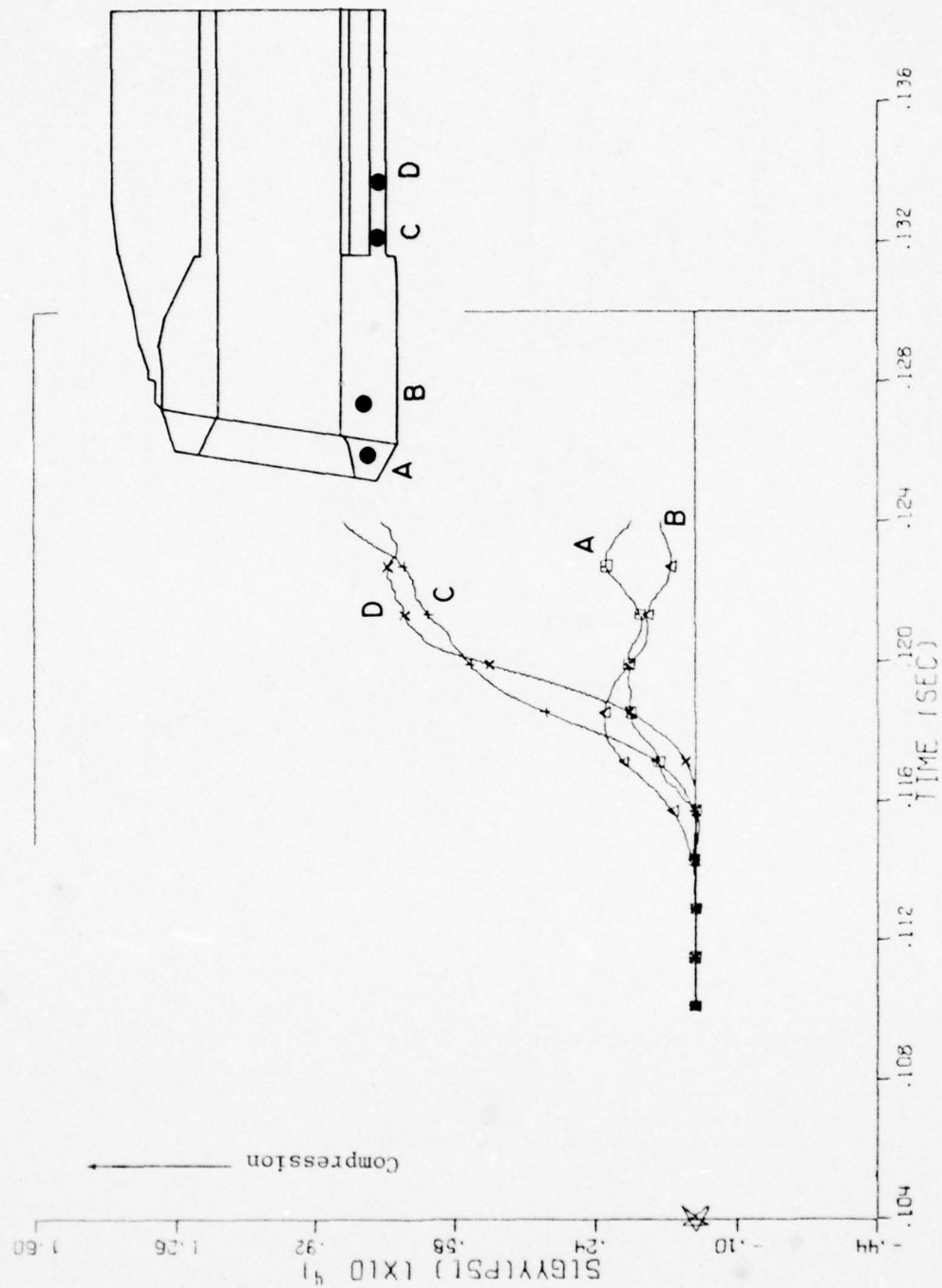
Figure 5-24. Longitudinal stress/time histories for points along lower shelter, Calculation 2A
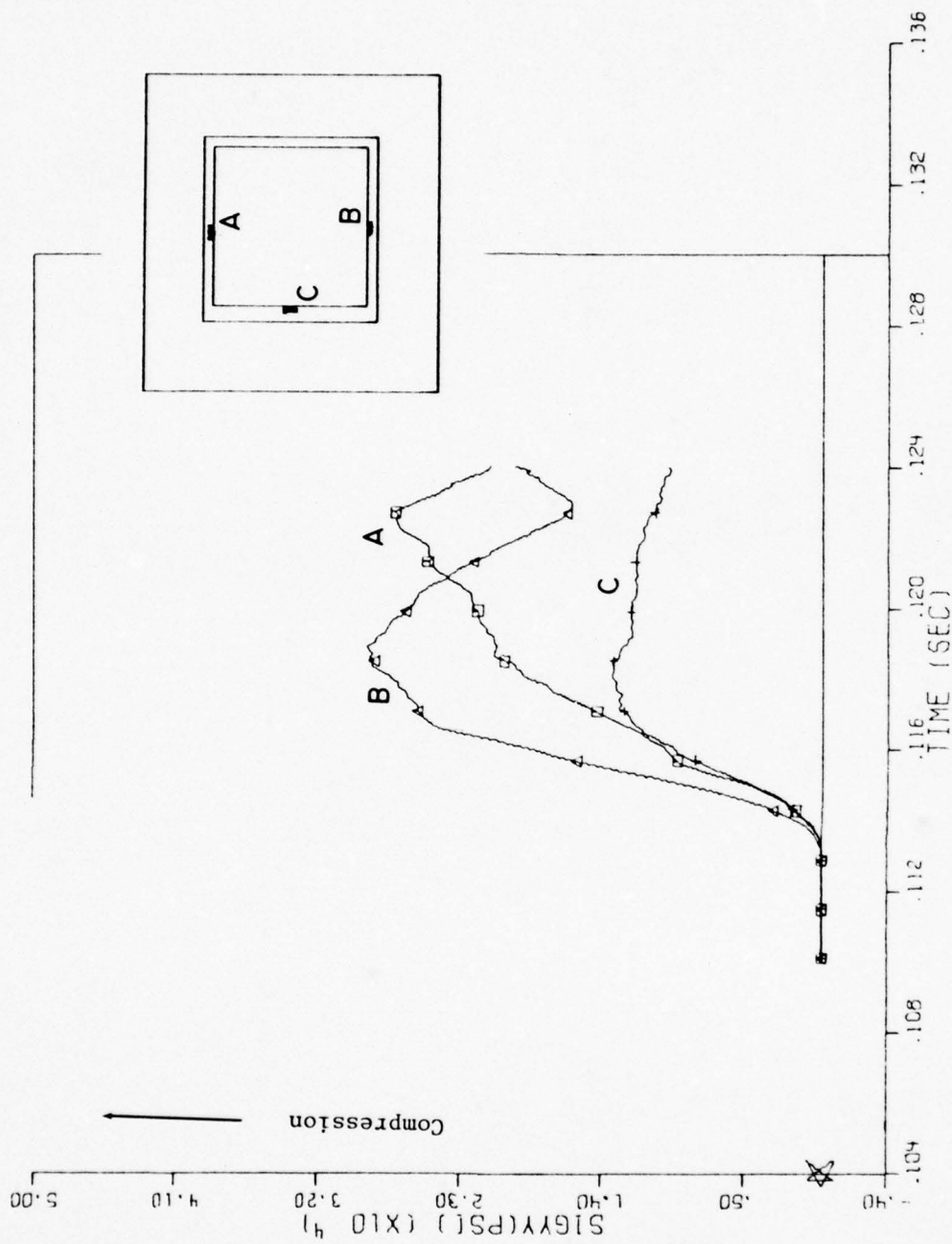
Figure 5-25. Bearing pressure at inner support, Calculation 2A
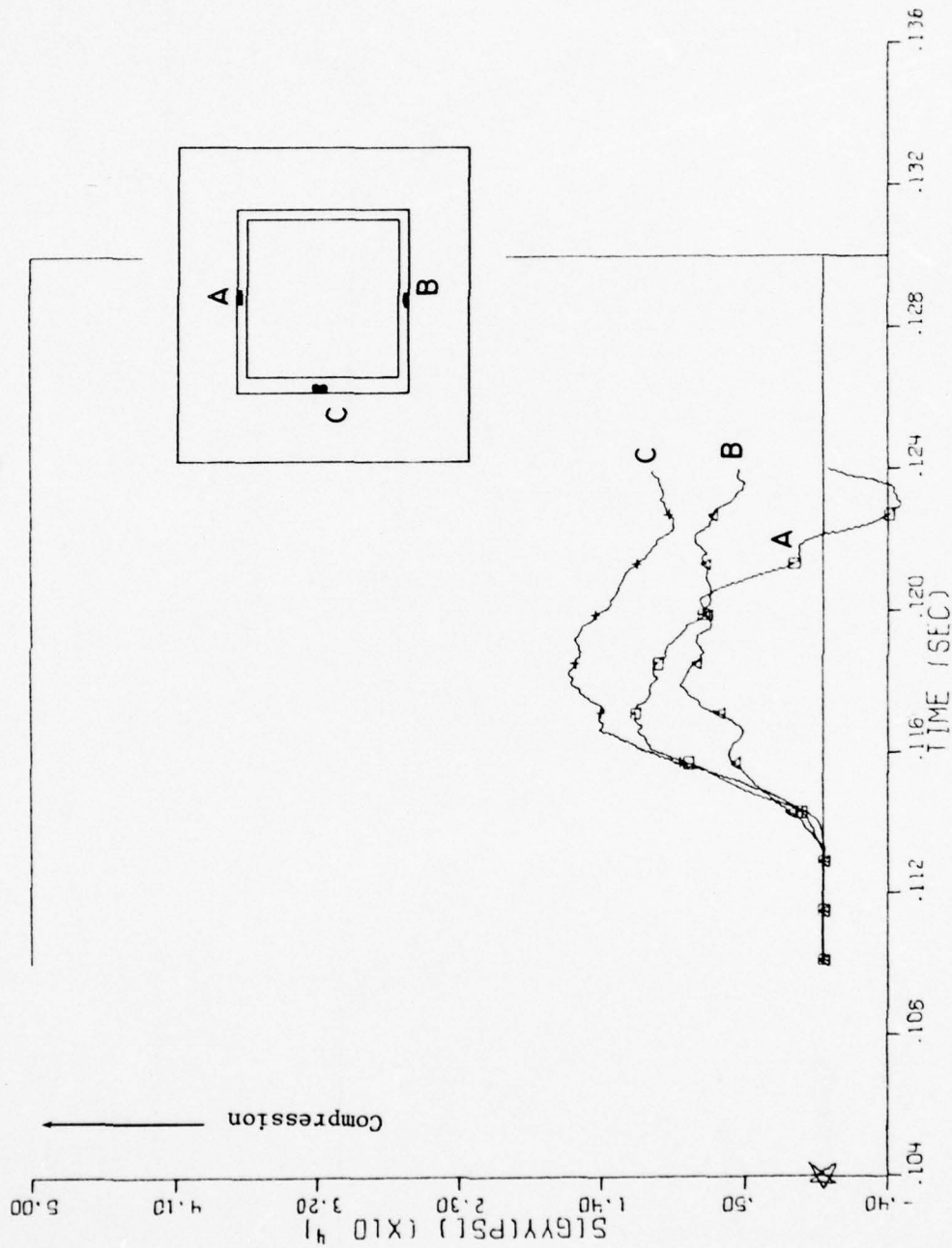
Figure 5-26. Bearing pressure at outer support, Calculation 2A

5-47
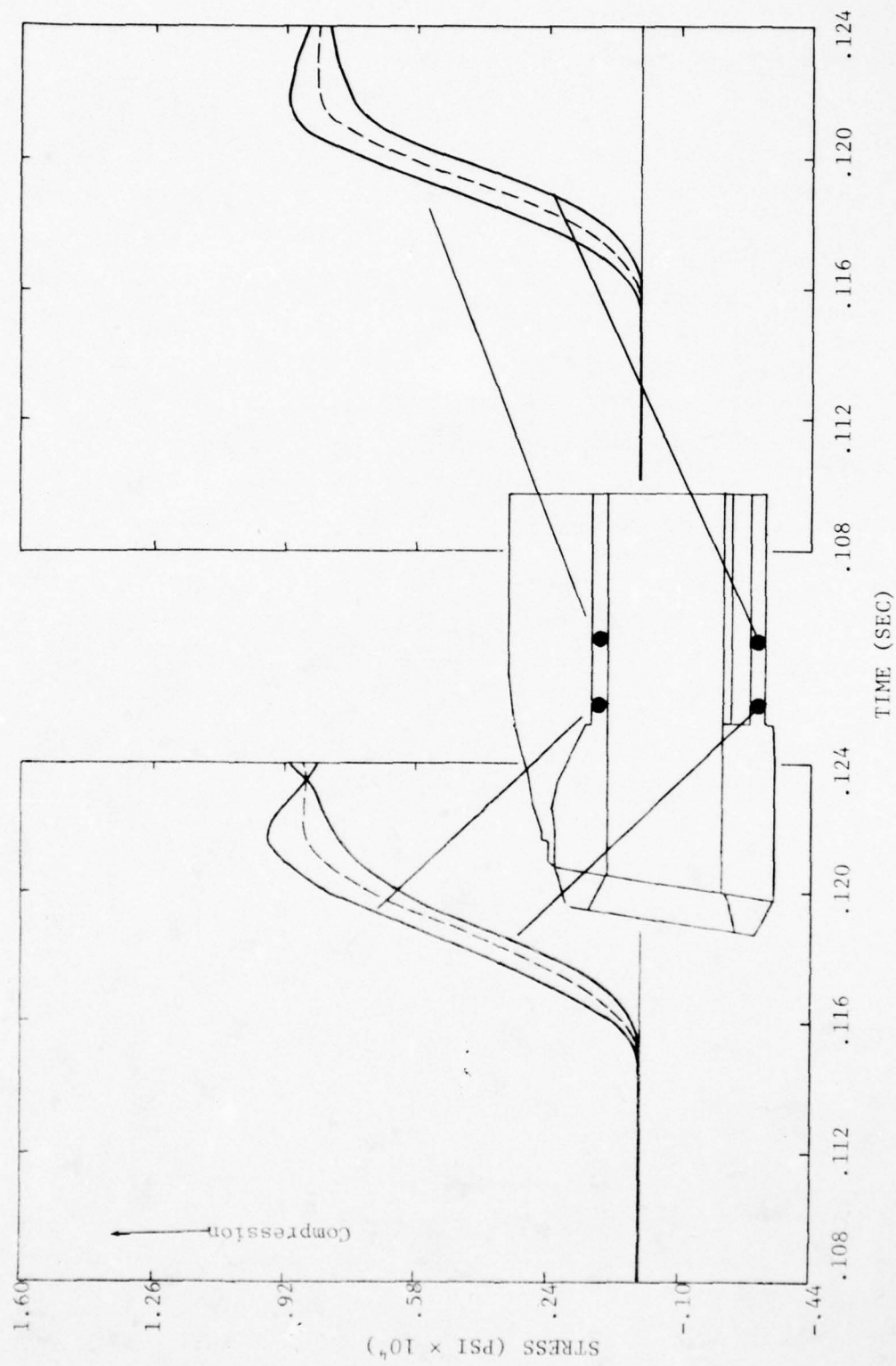
Figure 5-27. Longitudinal stress/time histories, tube sections, behind headworks, Calculation 2A
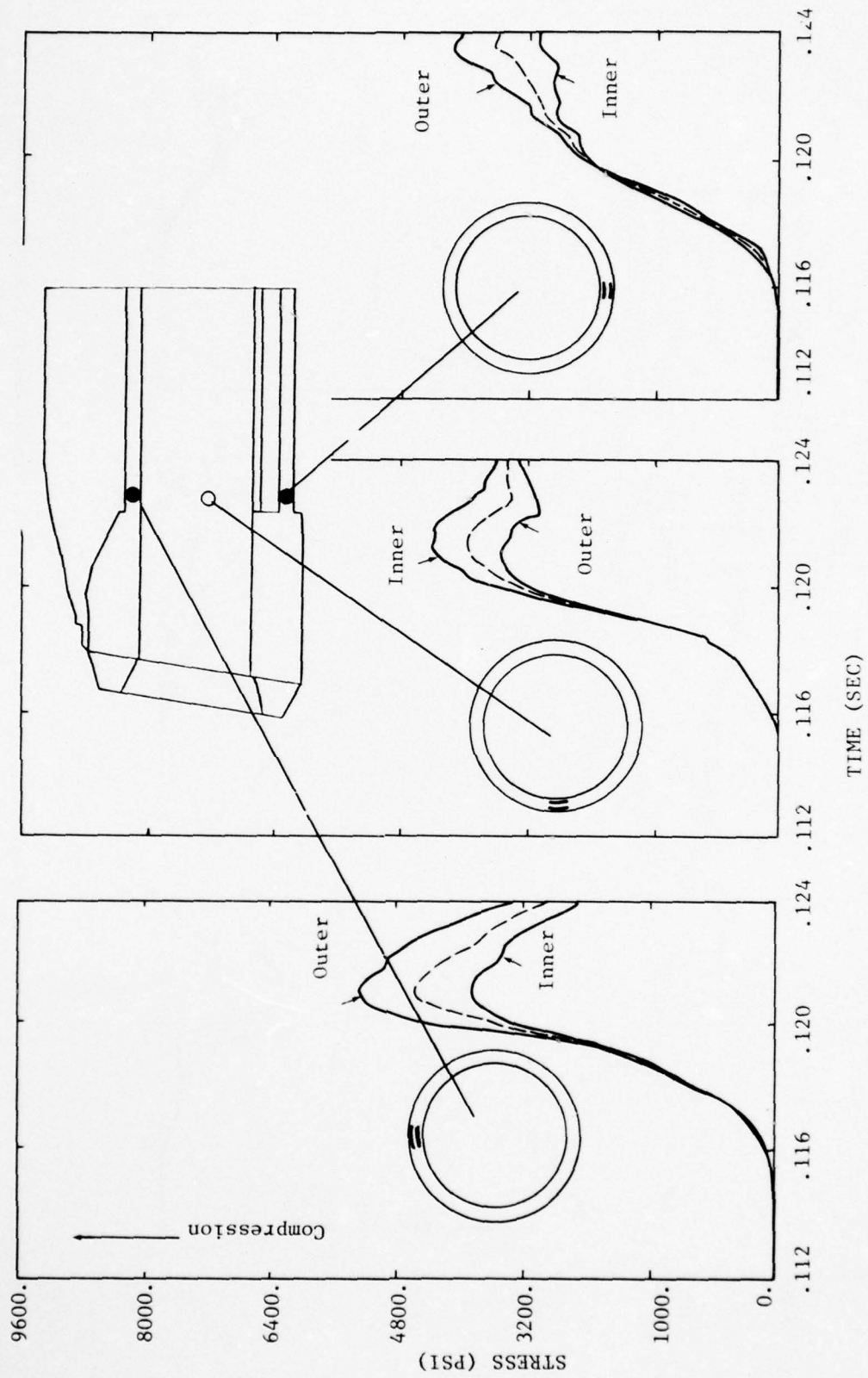
Figure 5-28. Hoop stress/time histories for tube section behind headworks, Calculation 2A
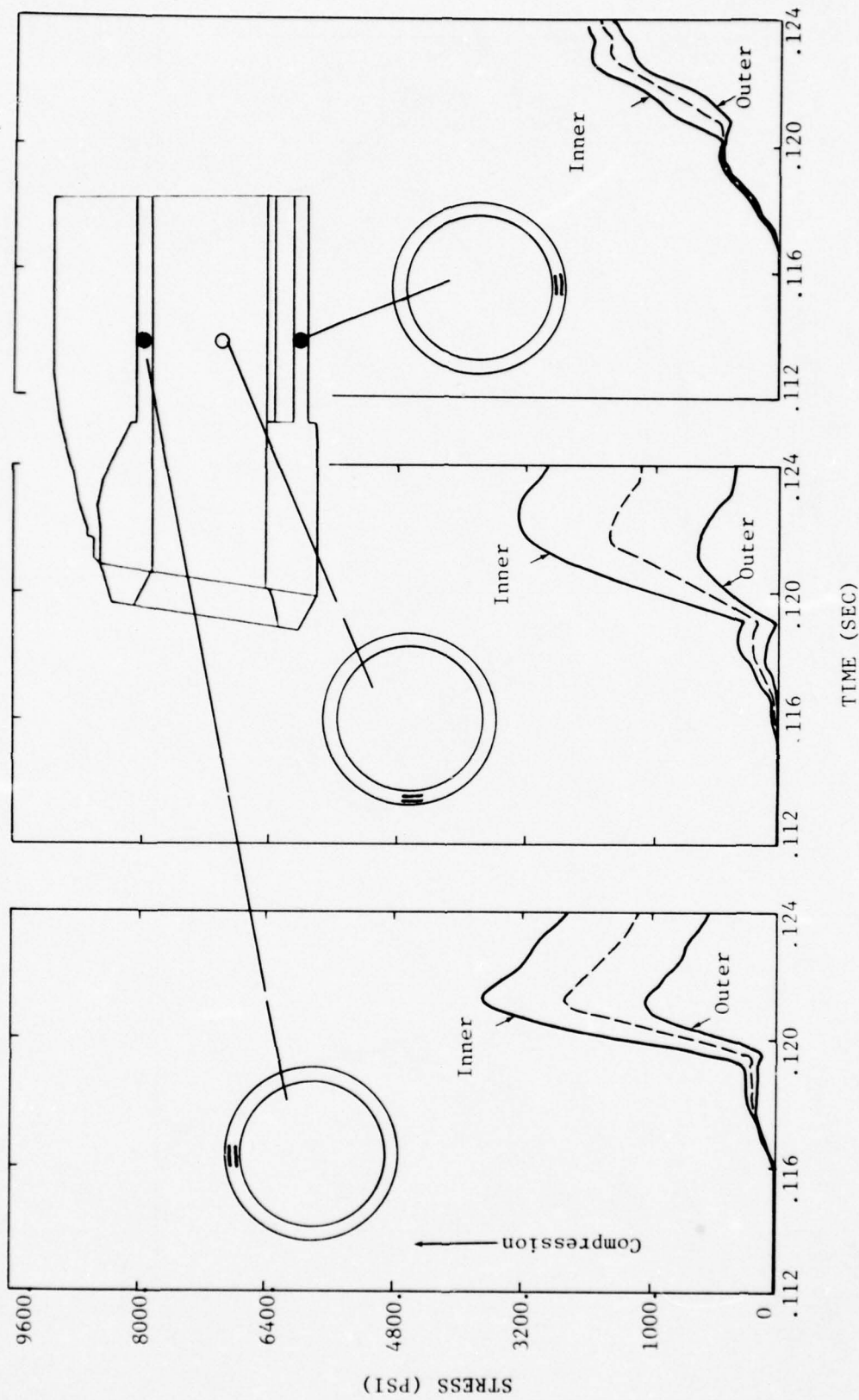
Figure 5-29. Hoop stress/time histories for tube section half tube diameter behind headworks, Calculation 2A
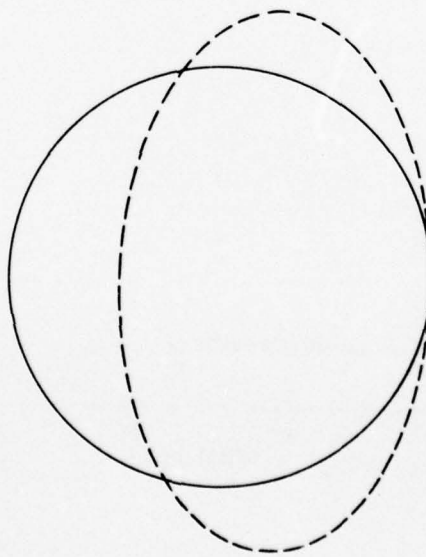
a. Section A
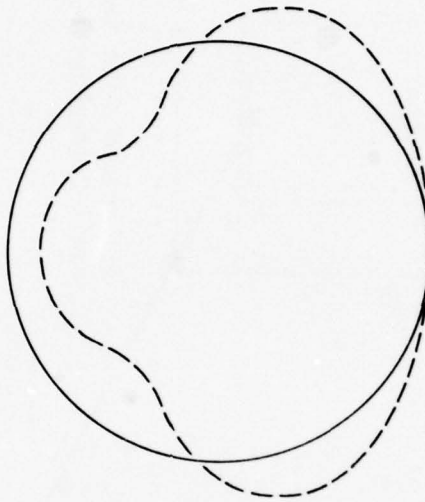
b. Section B

Figure 5-30. Deformation mode of cross-sections of tube (for illustration purpose only). Section A is immediately behind headworks, Section B is half-tube diameter behind headworks.
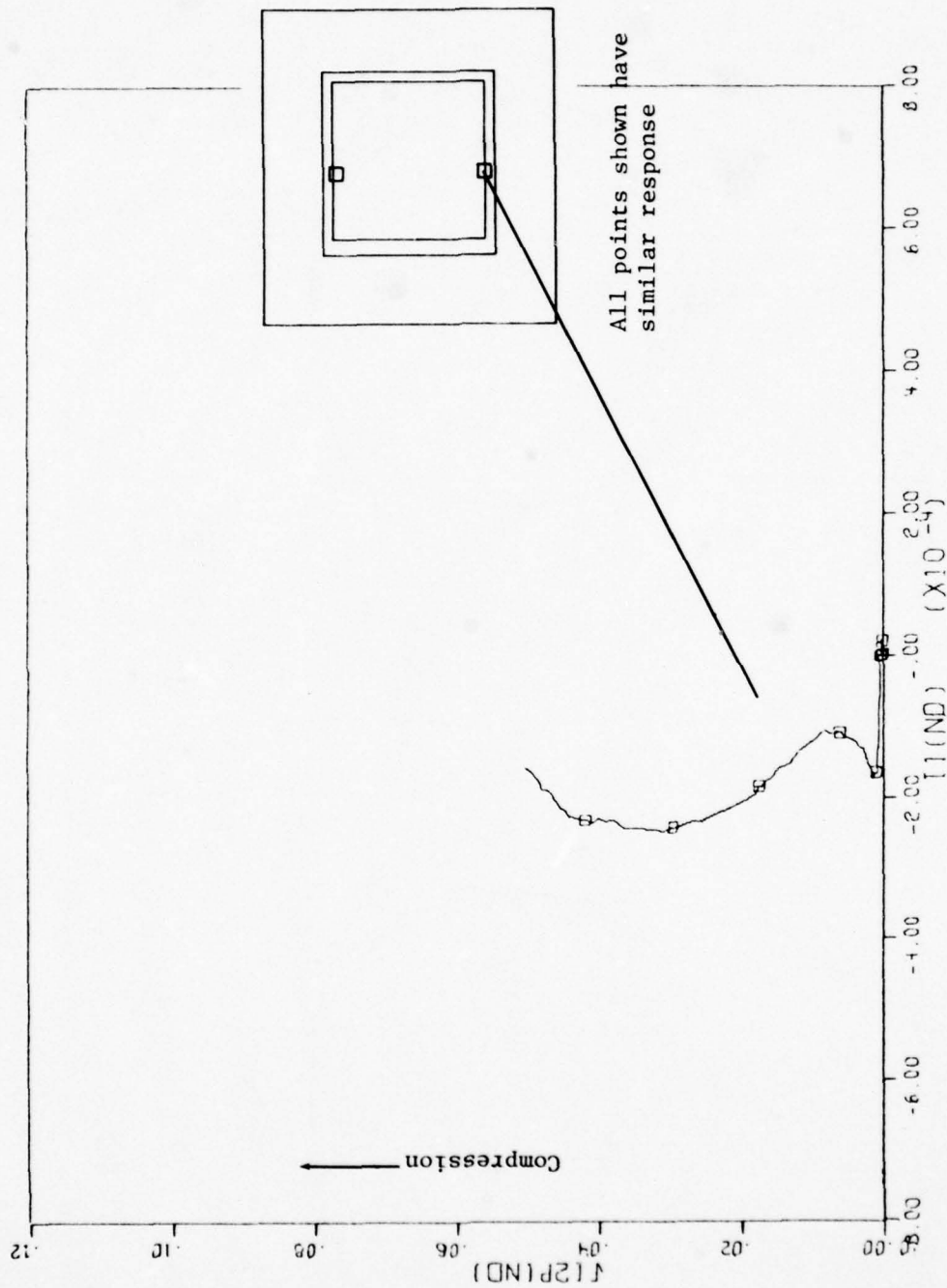
Figure 5-31. Typical strain invariant plot for points in backplate near support, Calculation 2A

All points shown have
similar response

Compression
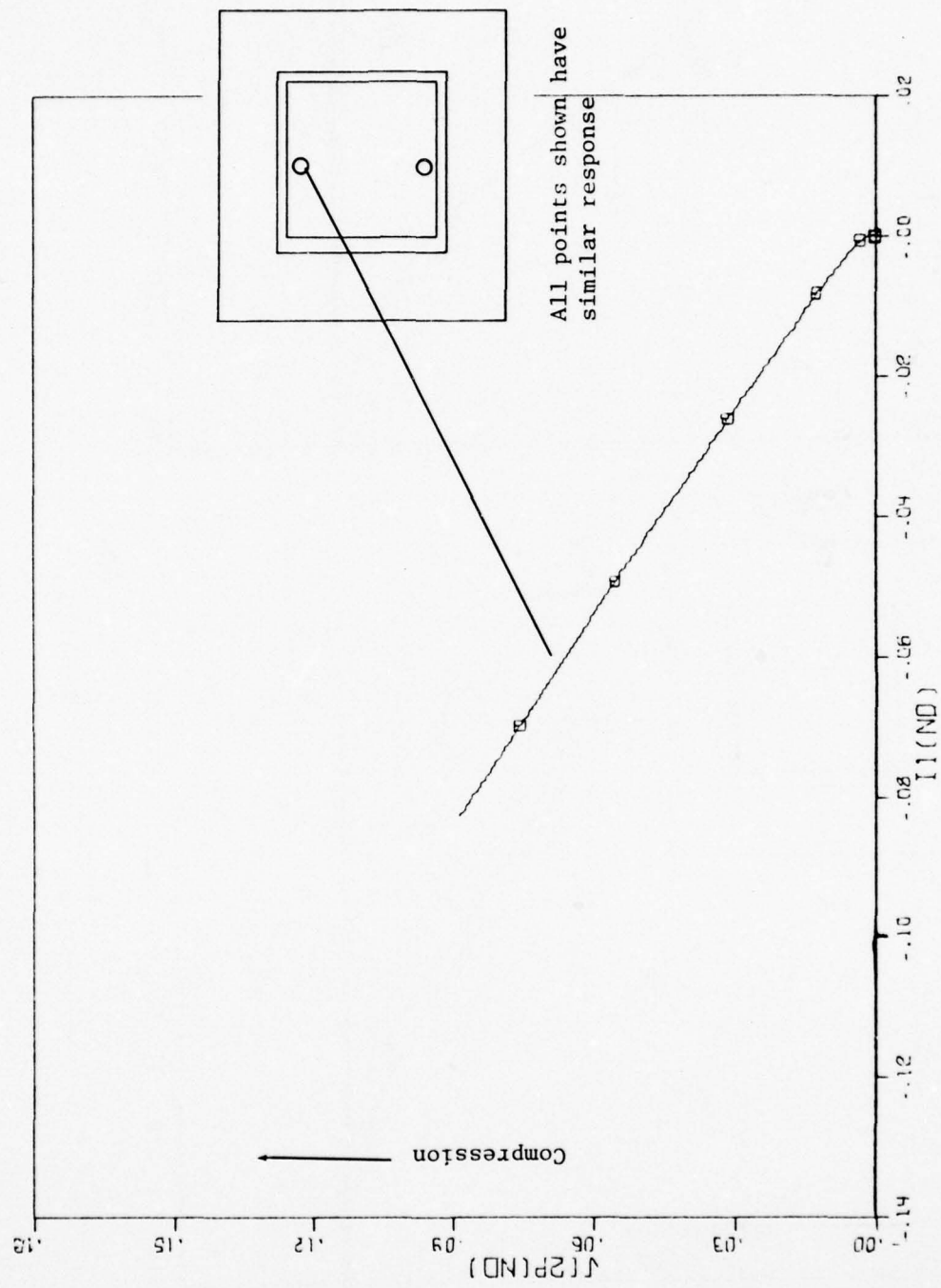
Figure 5-32. Typical strain invariant plot for points in closure concrete near support, Calculation 2A
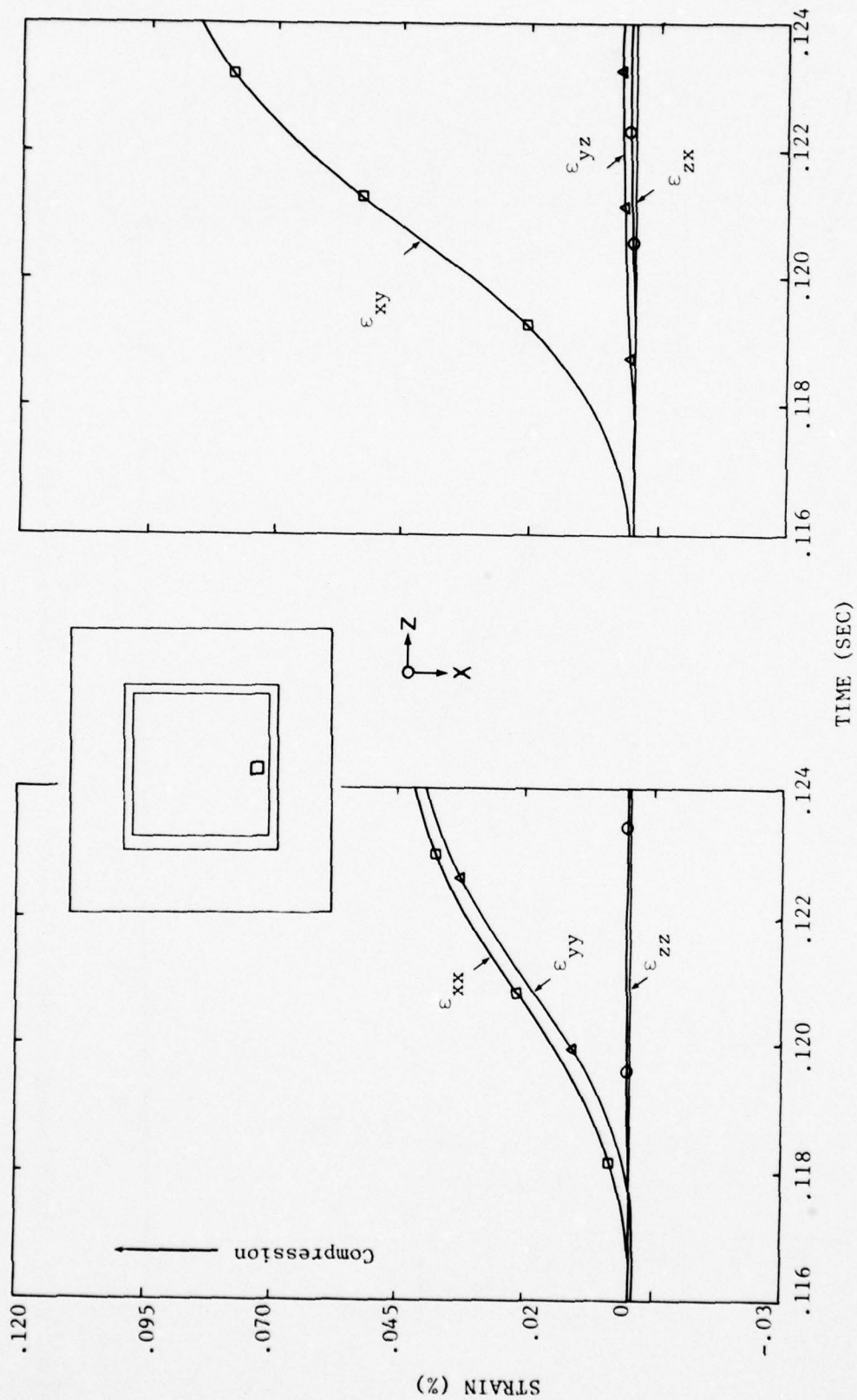
Figure 5-33. Typical strain/time histories for concrete in closure, near support, Calculation 2A
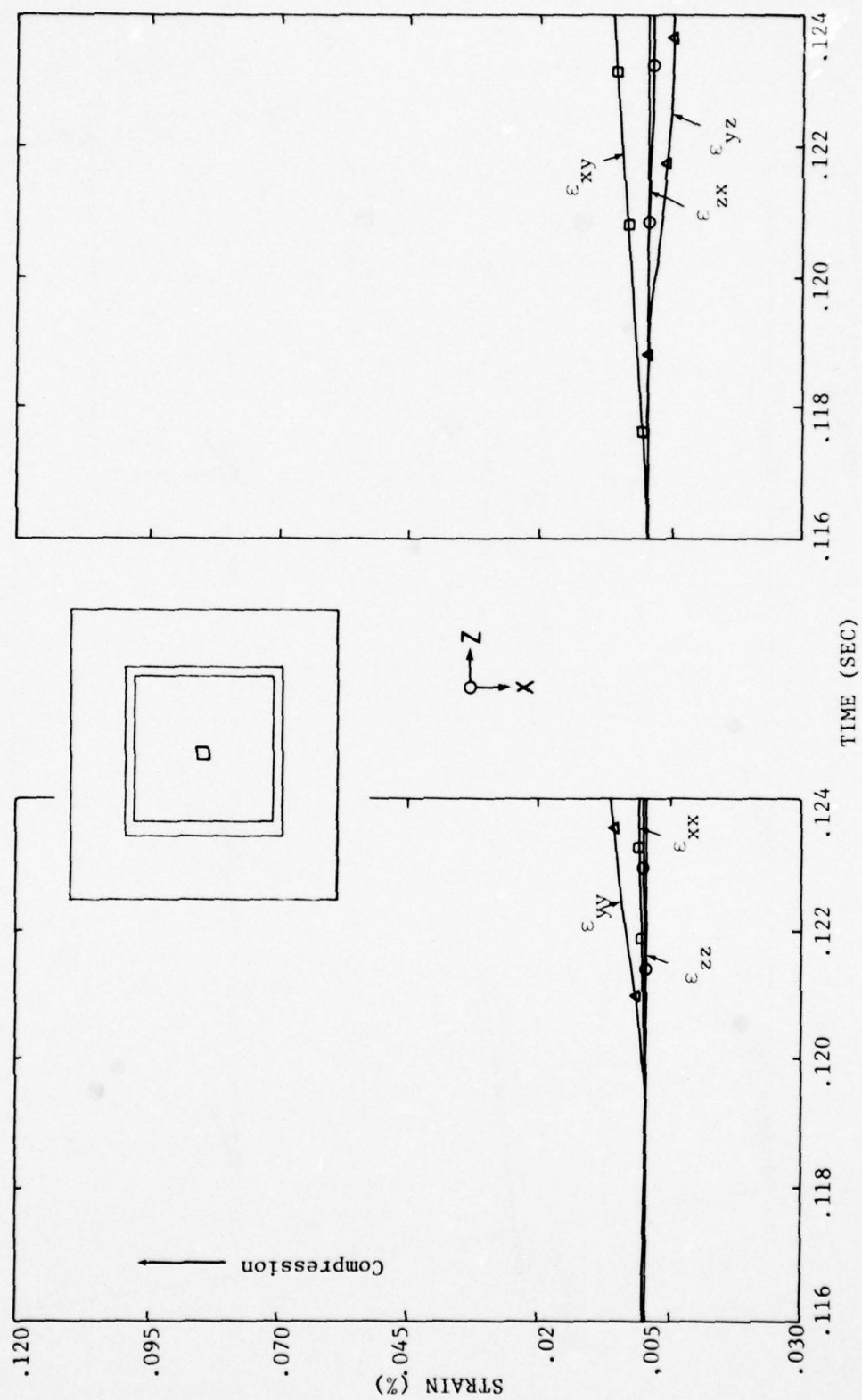
Figure 5-34. Typical strain/time histories for concrete in closure, near center, Calculation 2A

+ at 128 Msec.
o at 130 Msec.

Displacement Scale
(In.)

5

0

Closure
cg
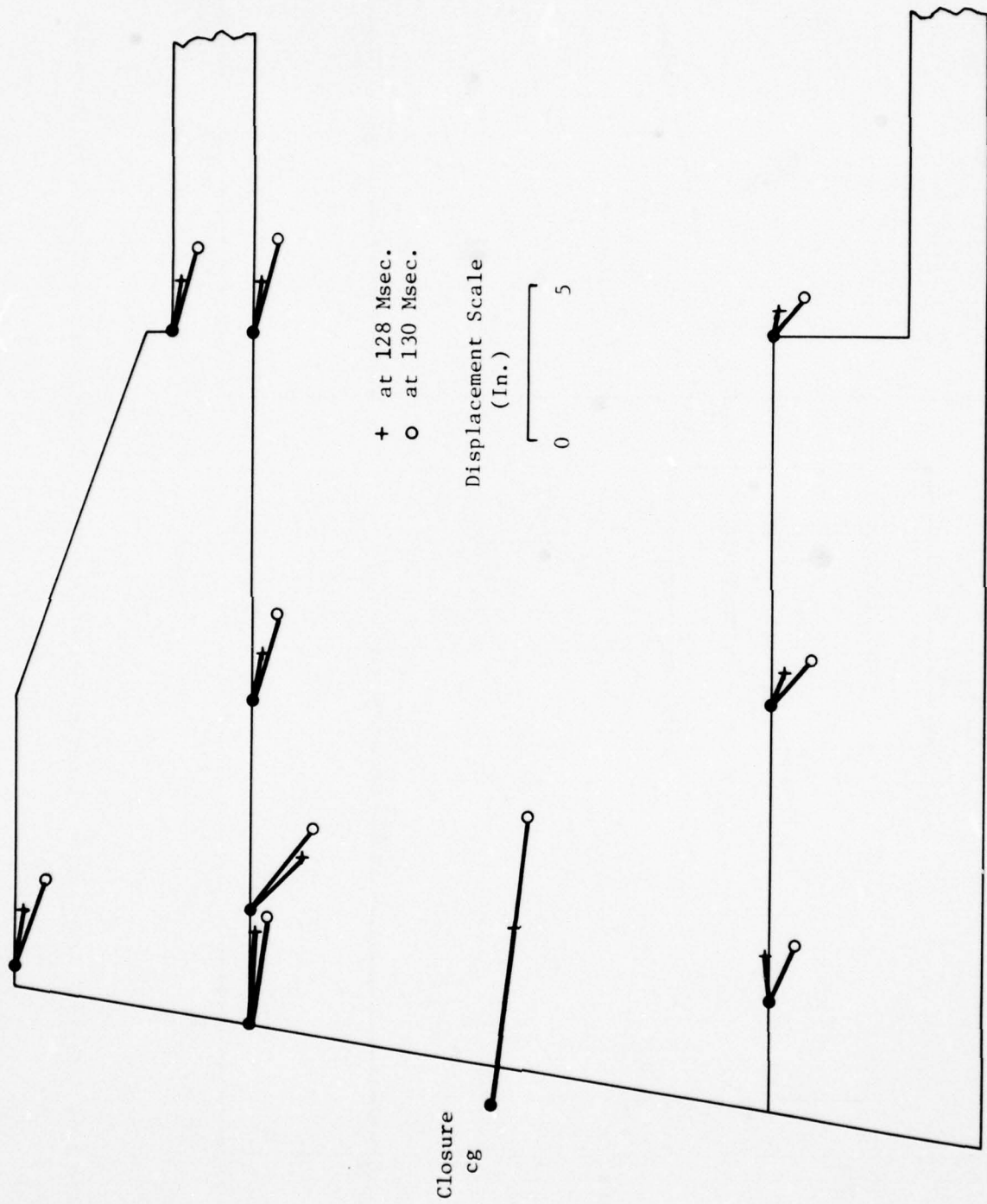
Figure 5-35. Deformation modes of headworks, head-on incidence, Calculation 2B
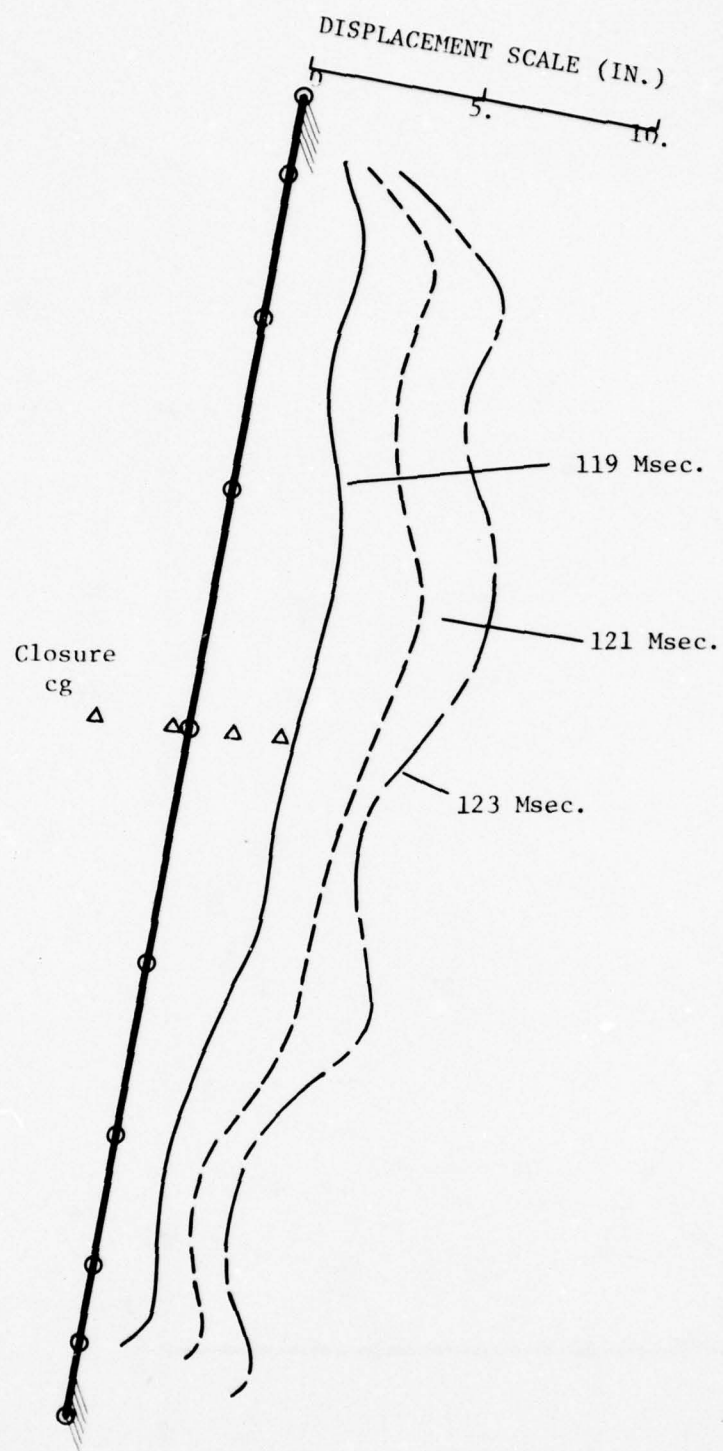
Figure 5-36. Deformation modes of backplate vertical centerline, Calculation 2B

DISPLACEMENT SCALE (IN.)

10.

119 Msec.

5.

121 Msec.

123 Msec.

Closure
cg

℄
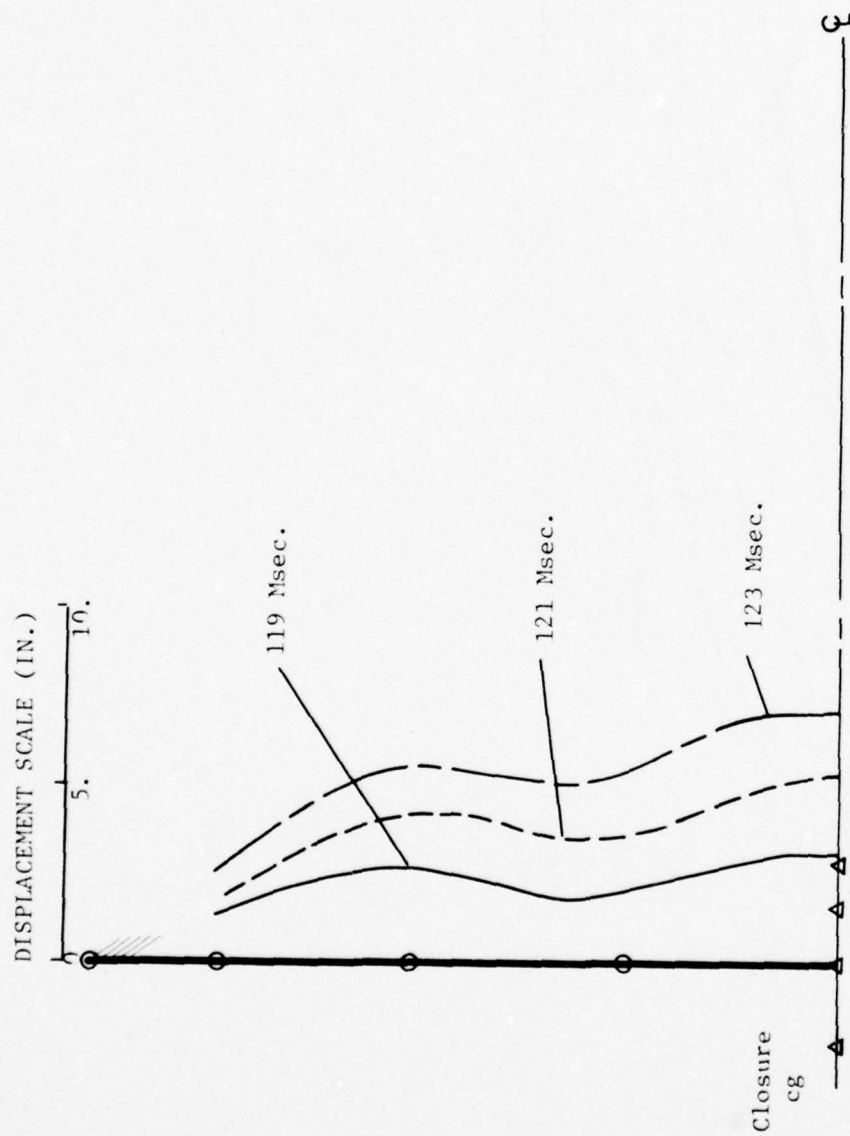
Figure 5-37. Deformation modes of backplate horizontal centerline, Calculation 2B
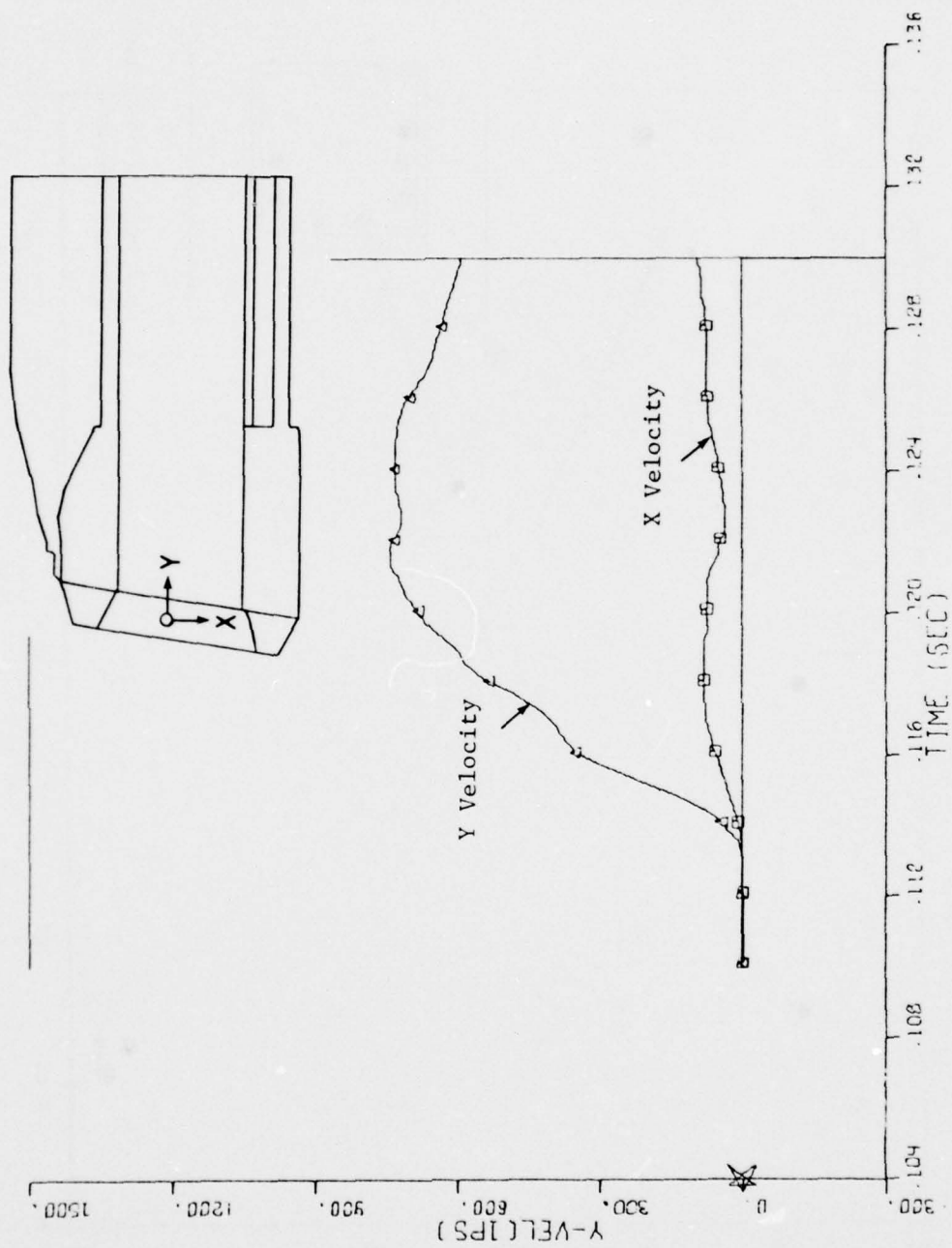
Figure 5-38. Velocity/time histories of closure cg, Calculation 2B

All points shown have similar response
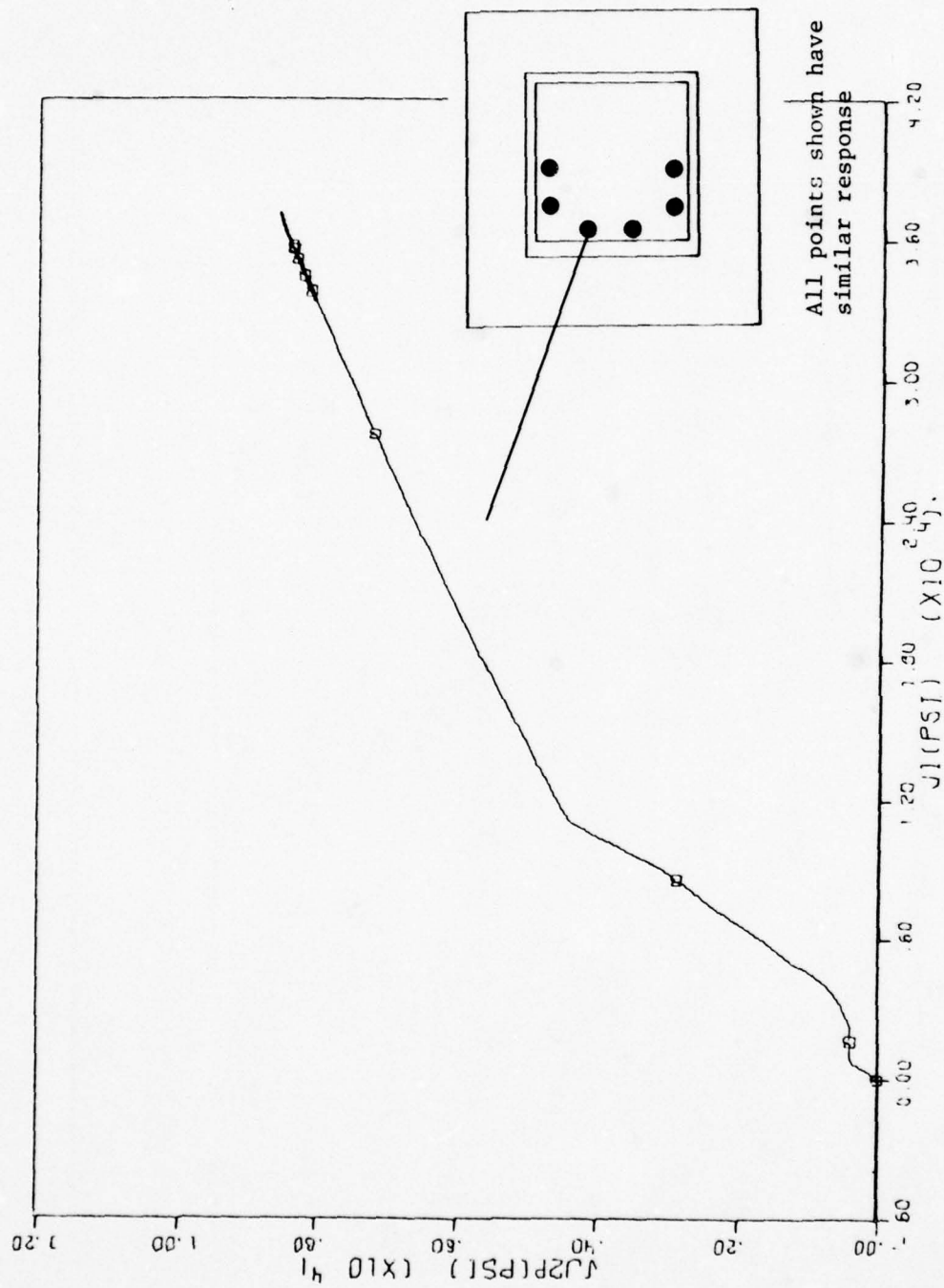
Figure 5-39a. Typical stress invariant plot for points at closure concrete, near support, Calculation 2B
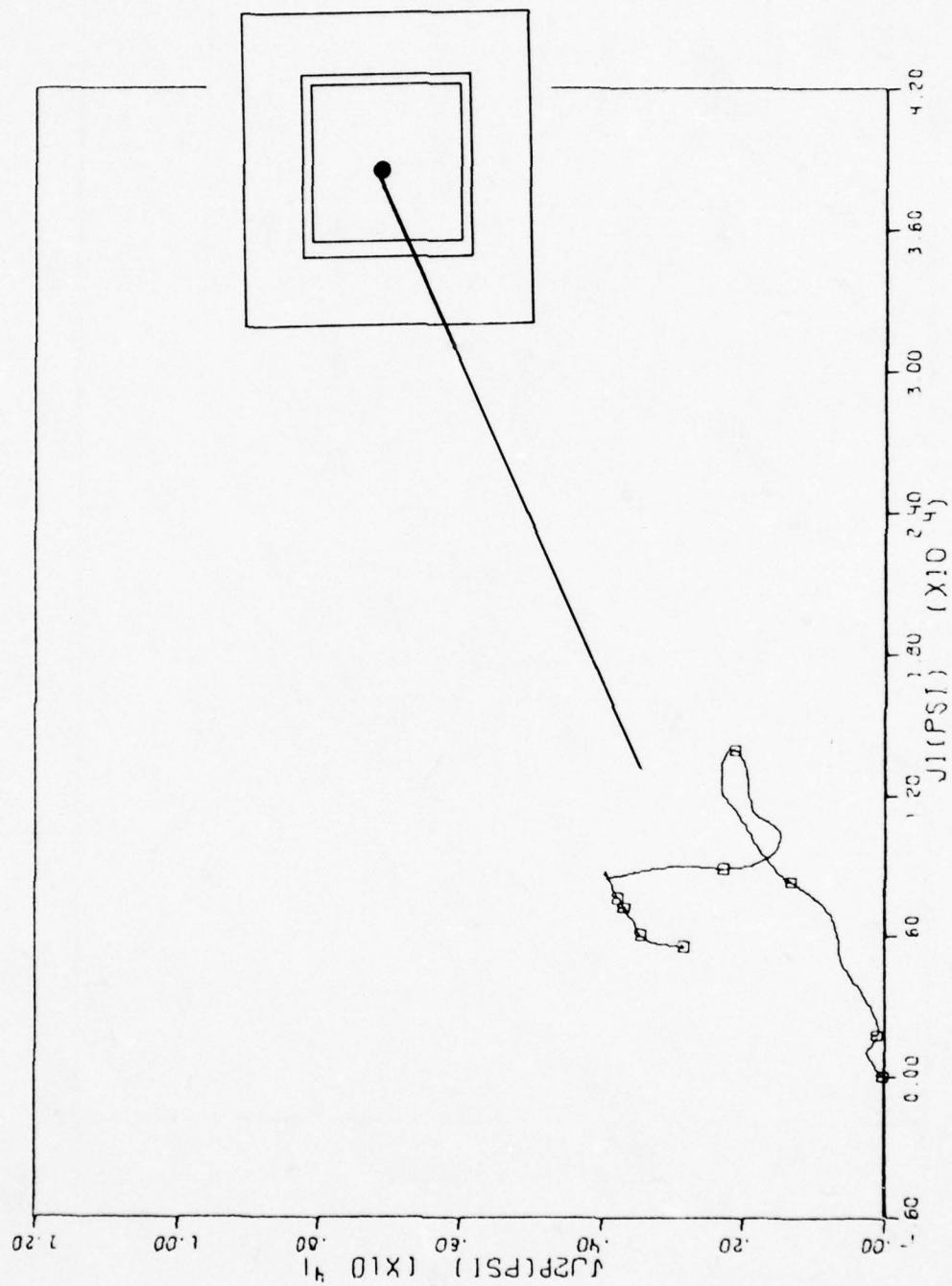
Figure 5-39b. Typical stress invariant plot for points at closure concrete, center, Calculation 2B

All points shown have
similar response

A36 Steel Limit
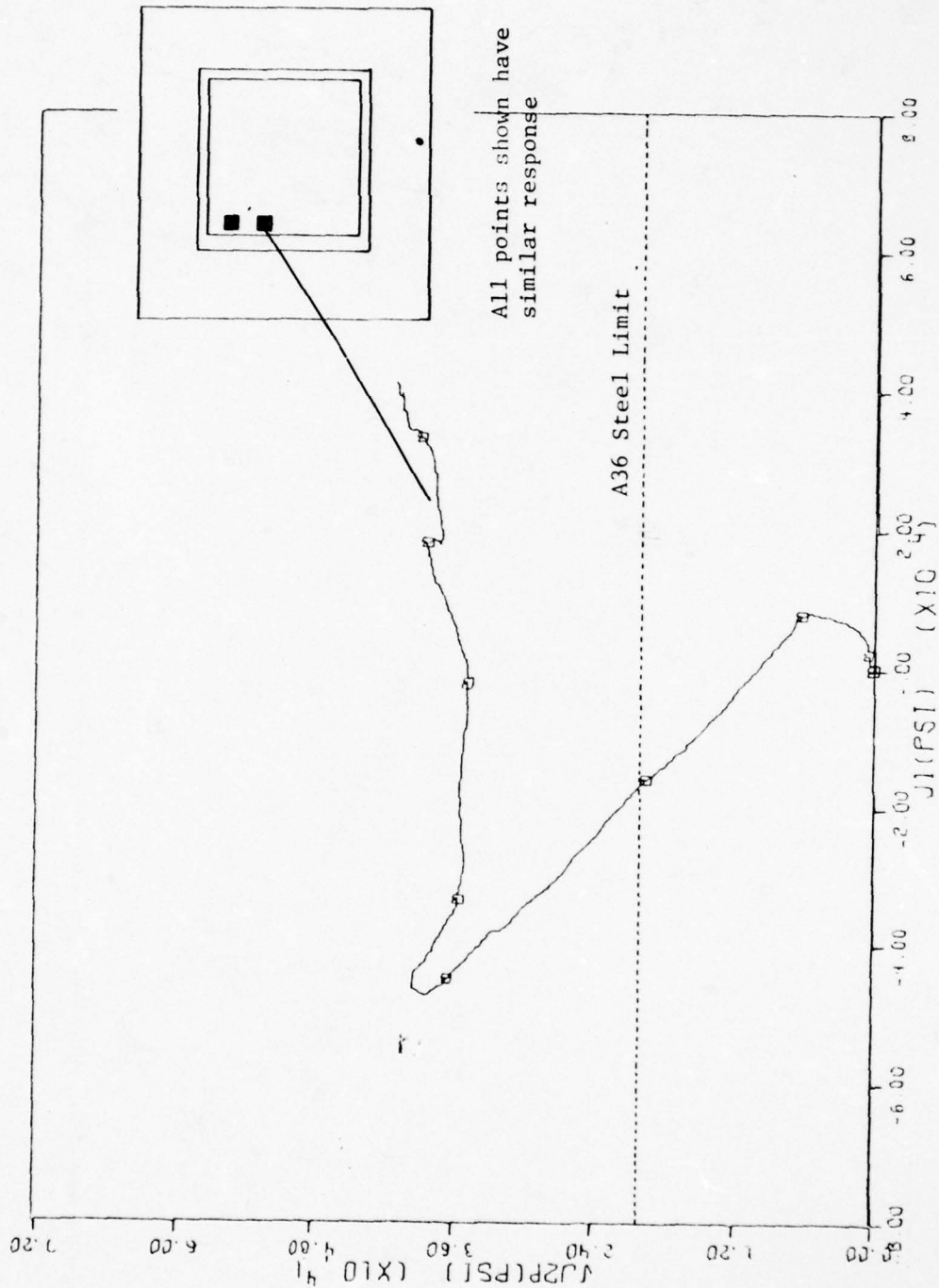
Figure 5-40a. Typical stress invariant plot for points in backplate, near support, Calculation 2B

5-62
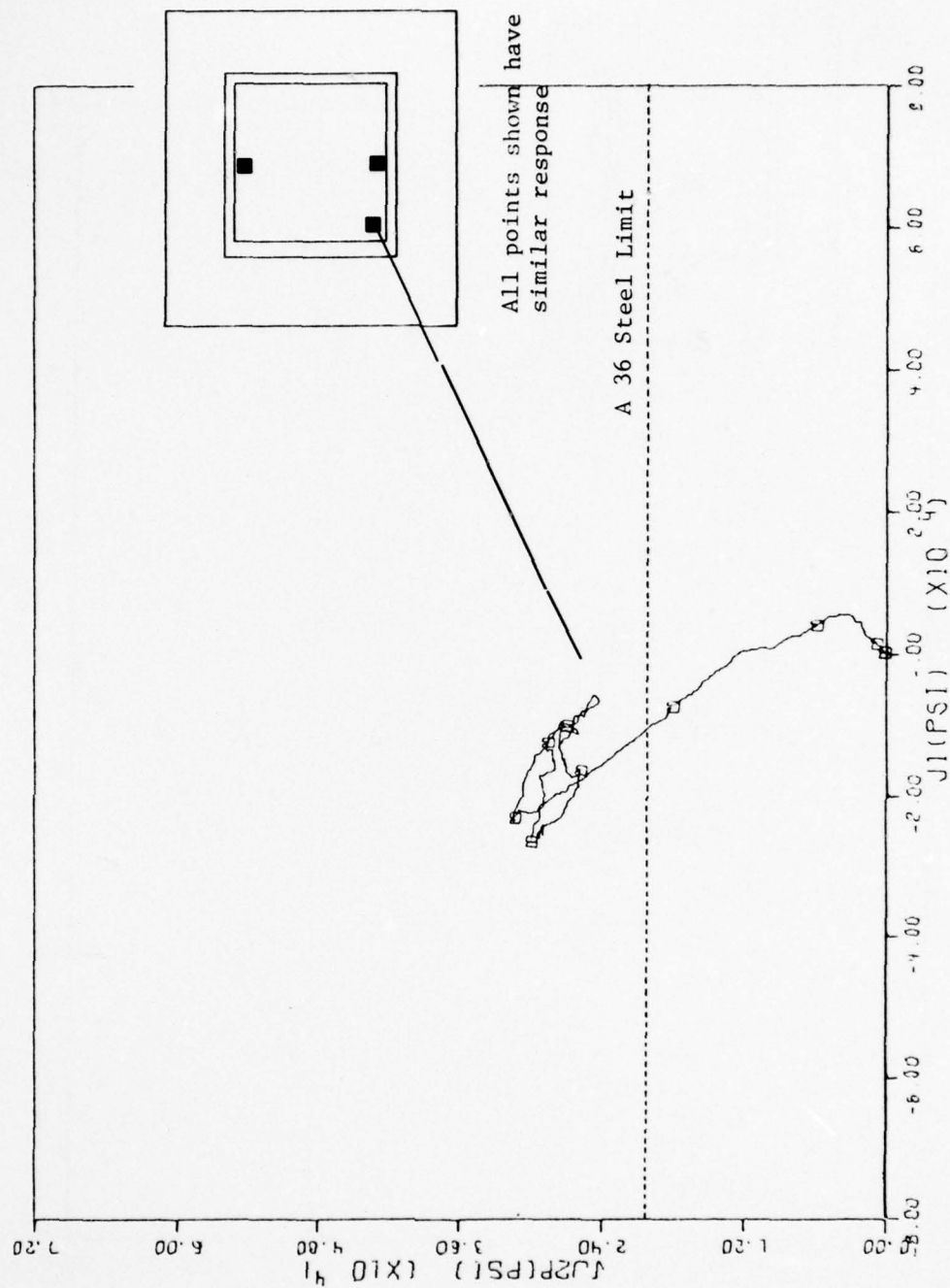
Figure 5-40b. Typical stress invariant plot for points in backplate, near support, Calculation 2B
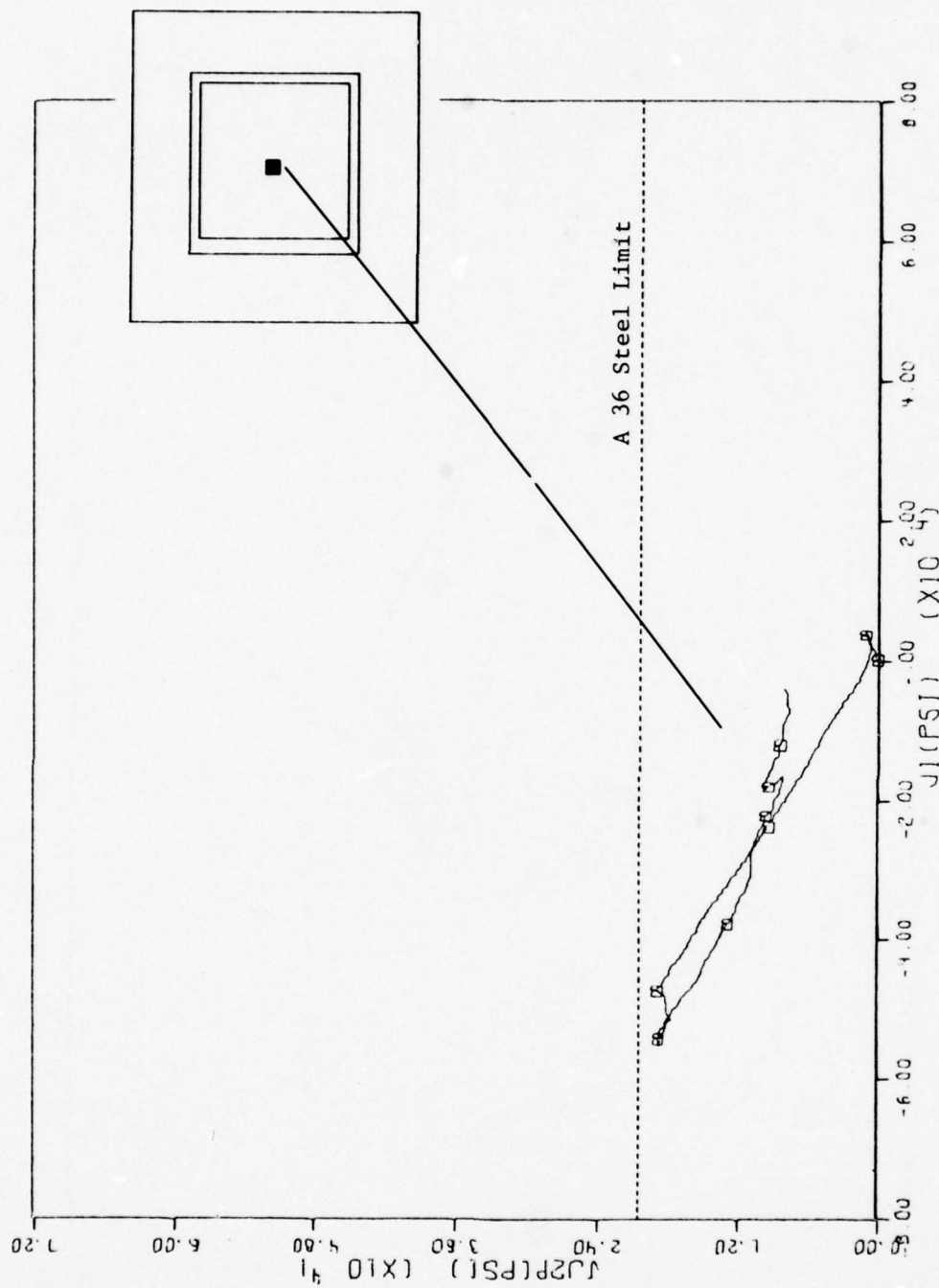
Figure 5-40c. Typical stress invariant plot for points in backplate, center, Calculation 2B
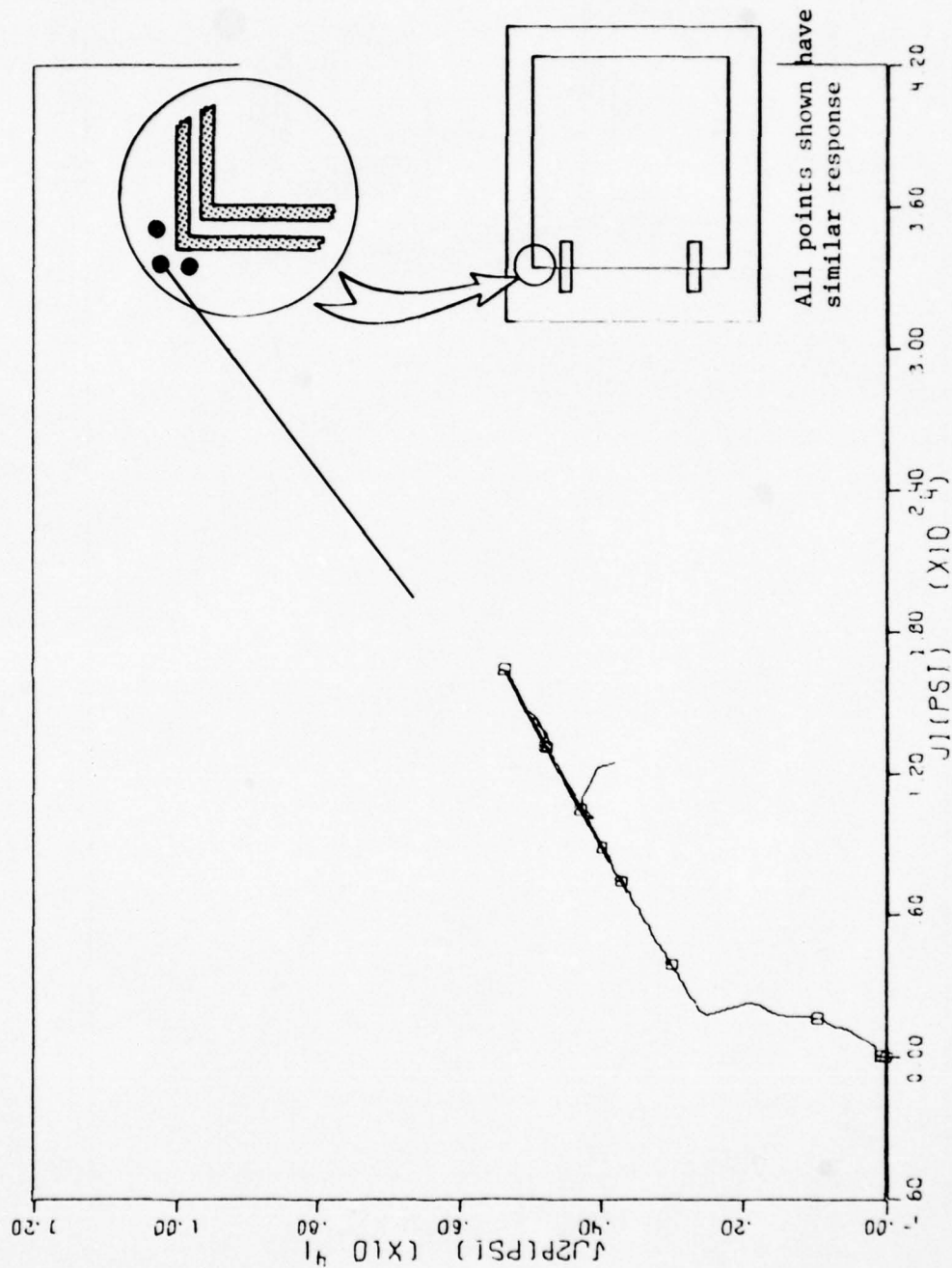
Figure 5-41. Typical stress invariant plot for concrete in upper frame corner, Calculation 2B
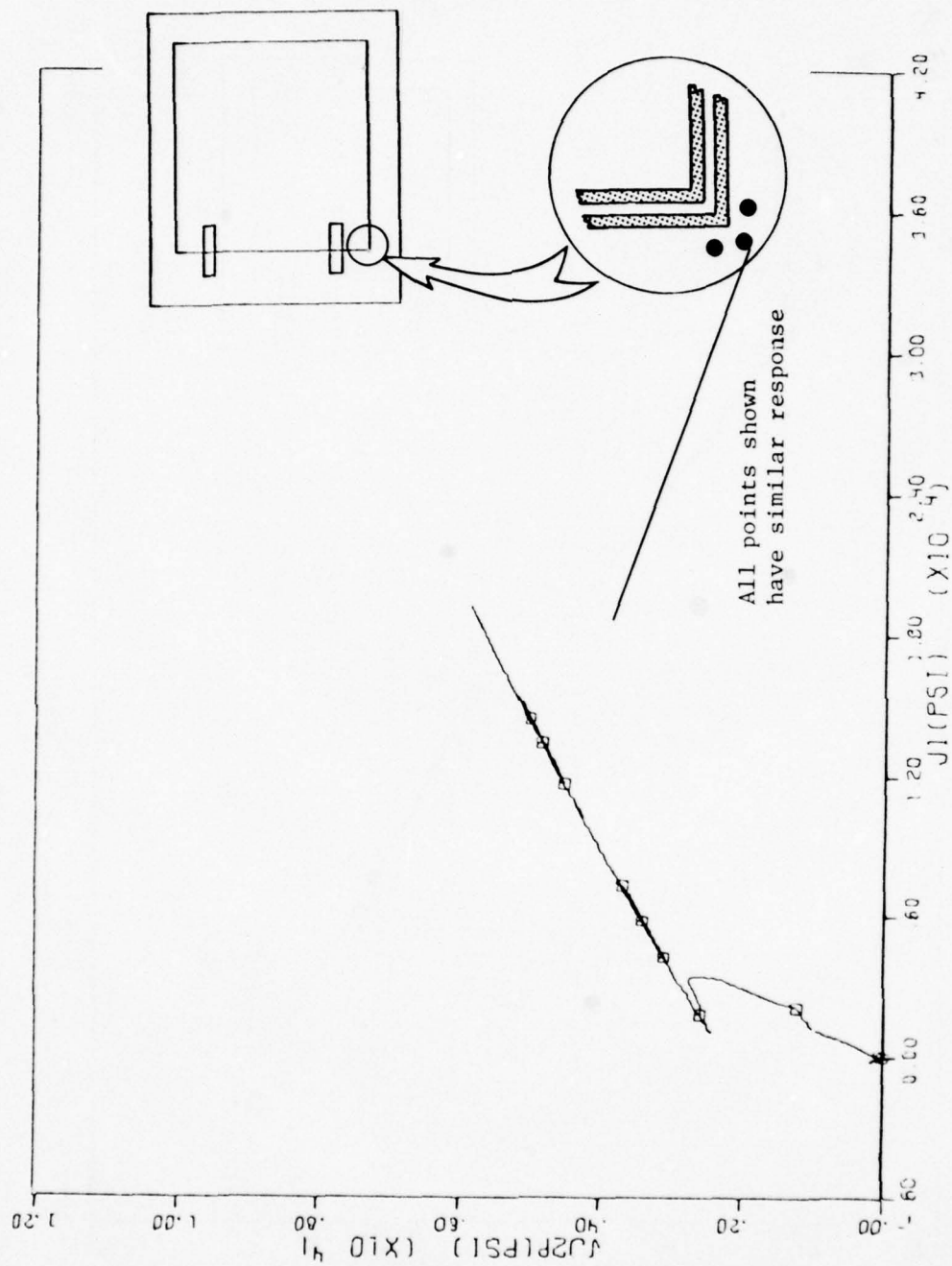
Figure 5-42. Typical stress invariant plot for concrete in lower frame corner, Calculation 2B
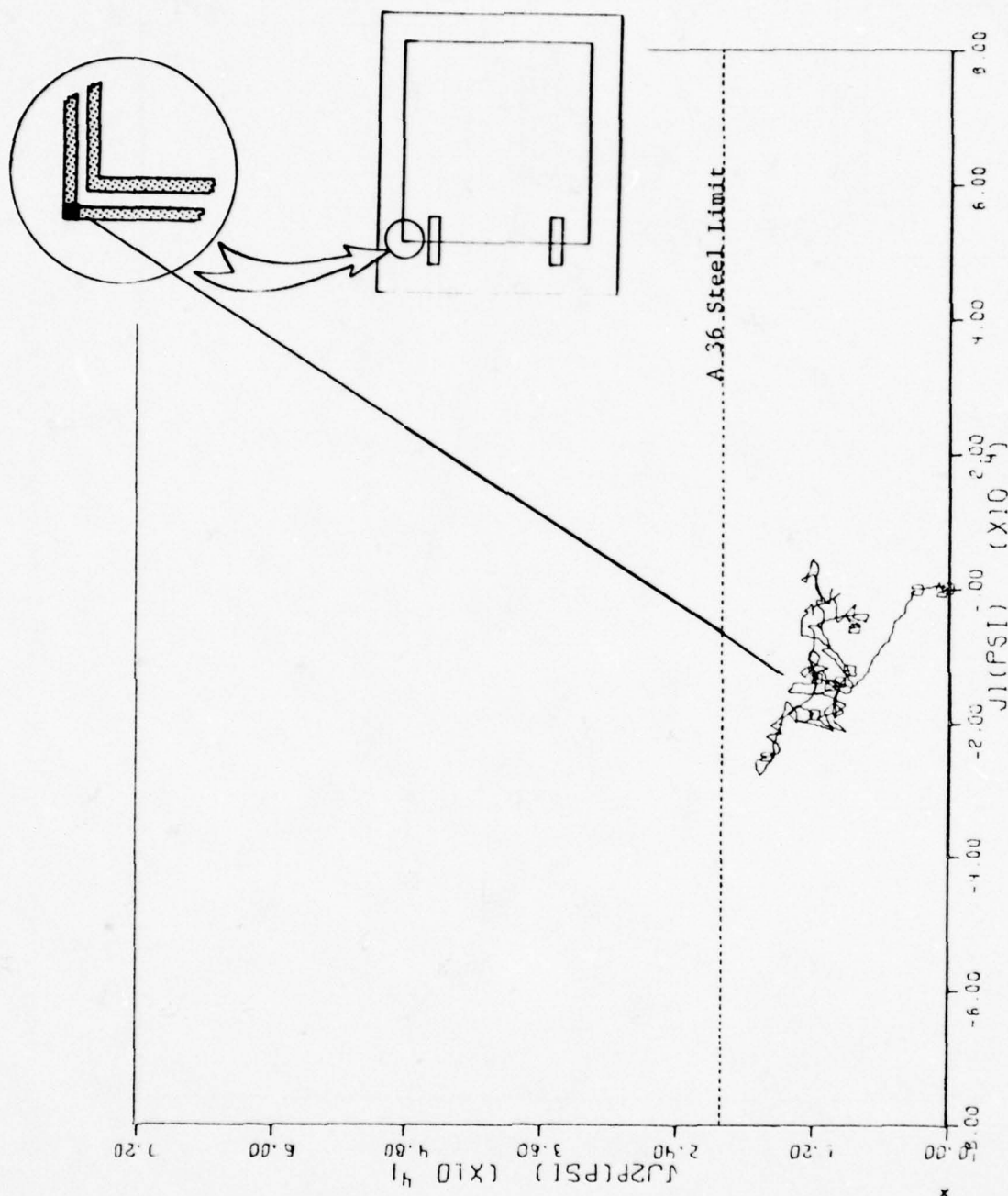
Figure 5-43. Stress invariant plot for steel in upper frame corner, Calculation 2B
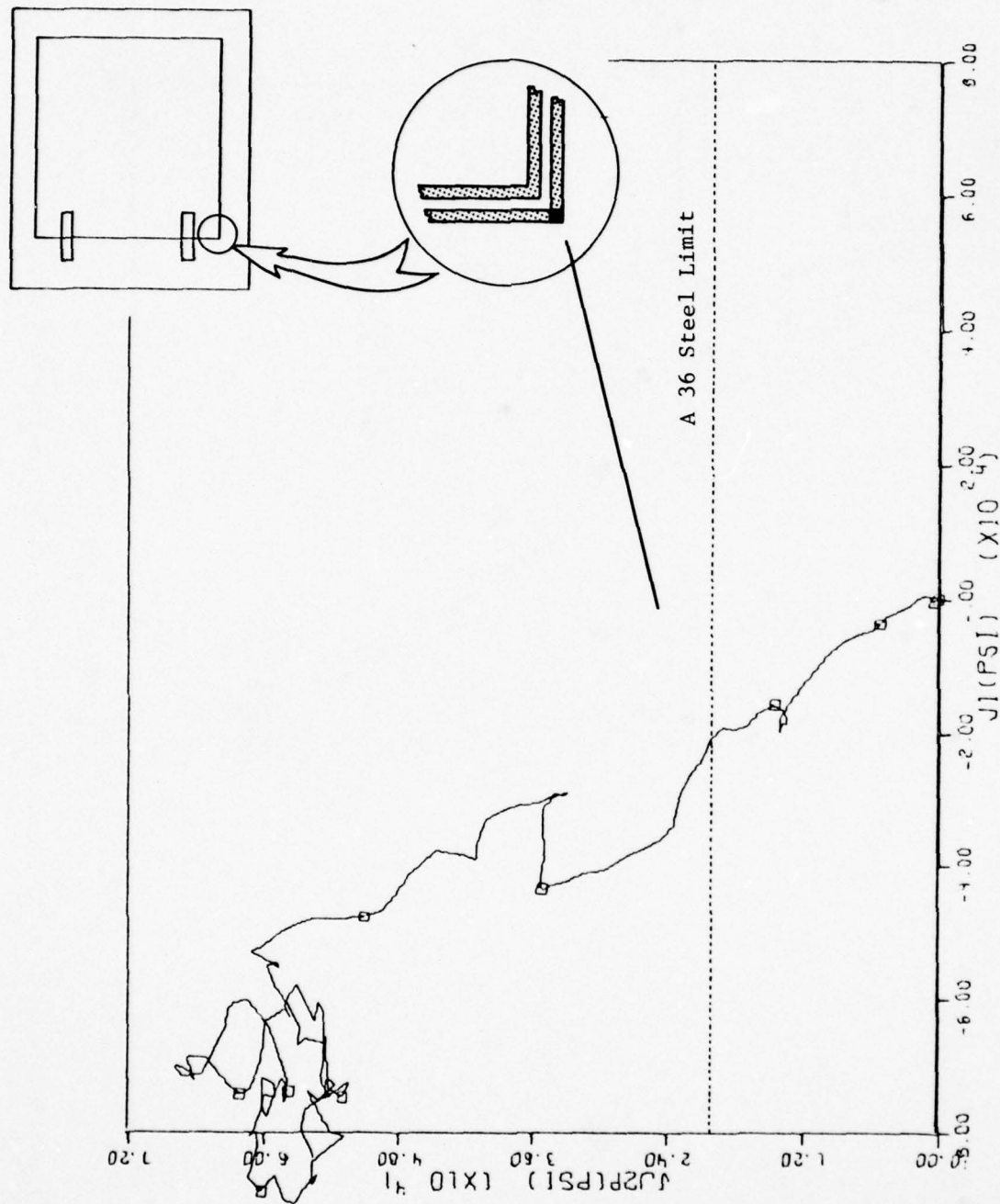
Figure 5-44. Stress invariant plot for steel in lower frame corner, Calculation 2B
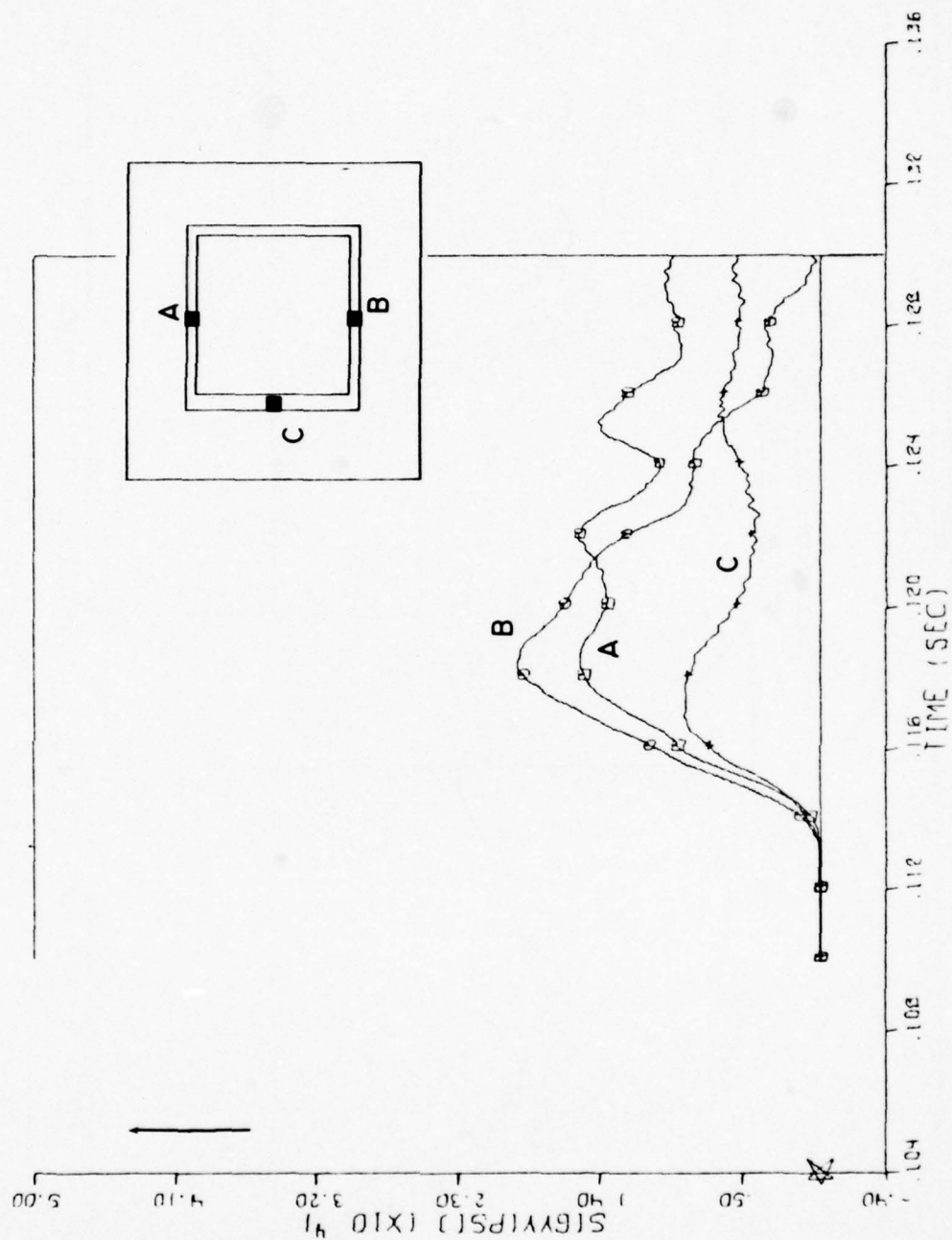
Figure 5-45. Bearing load time histories, Calculation 2B
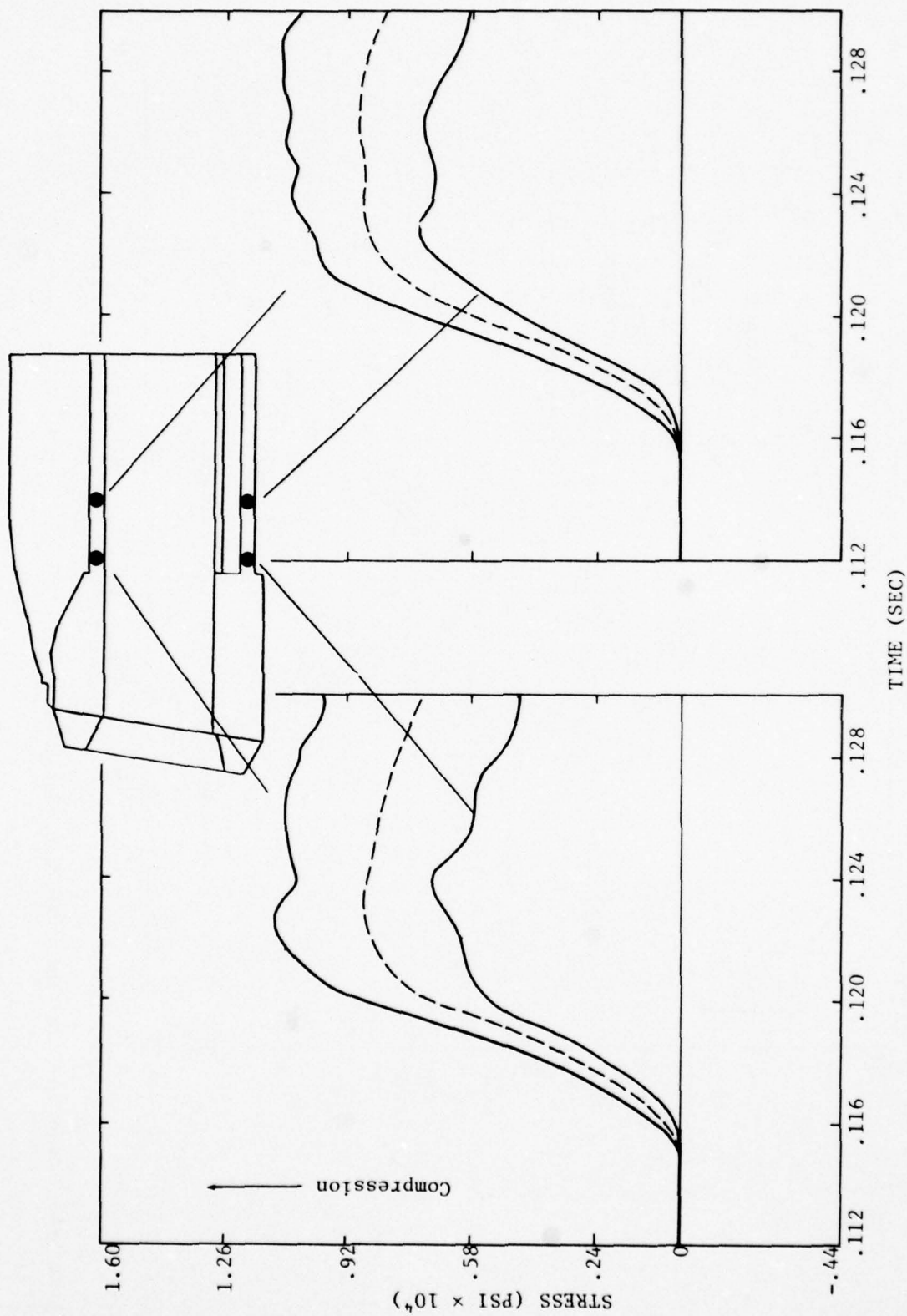
Figure 5-46. Longitudinal stress/time histories, tube sections behind headworks, Calculation 2B
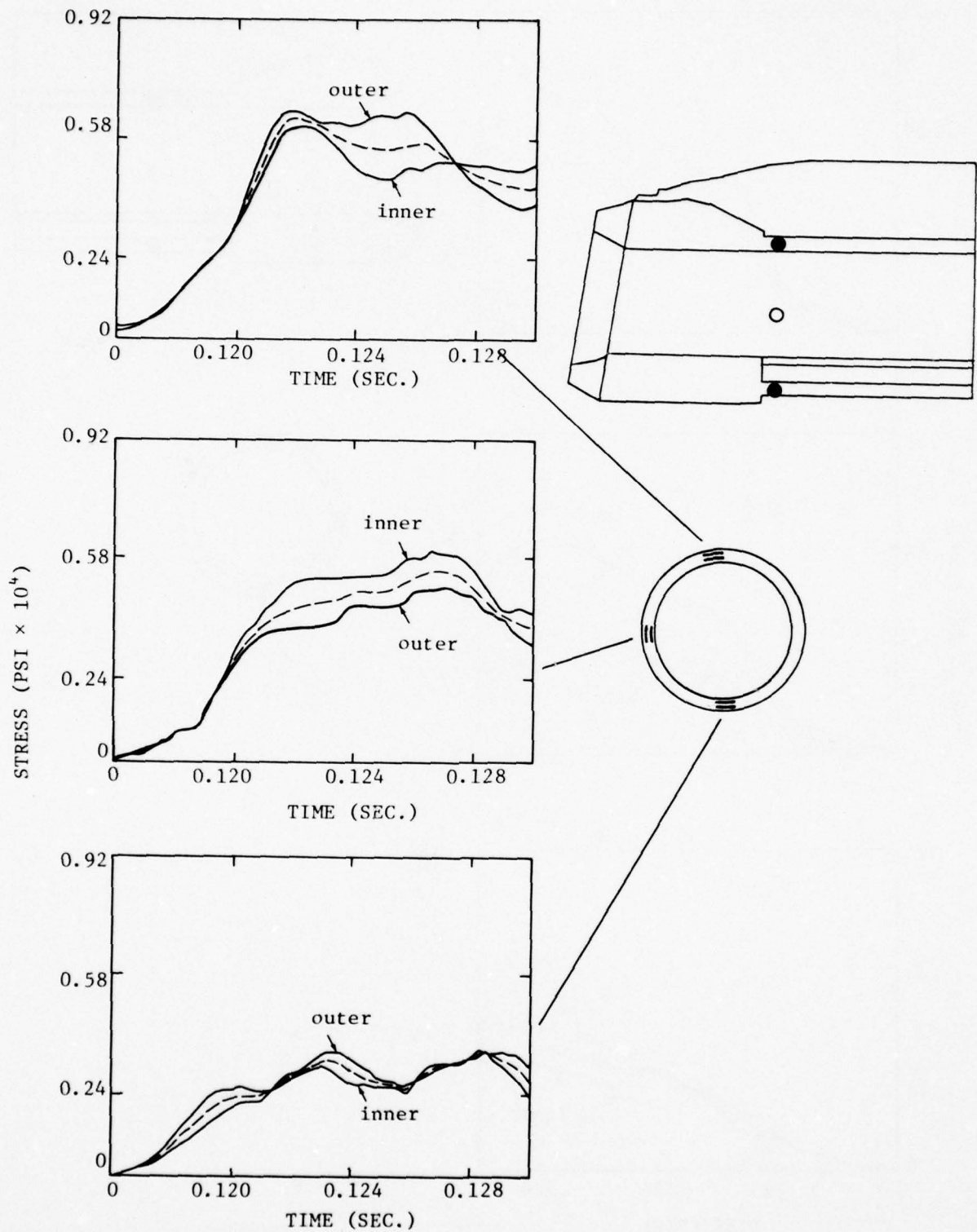
Figure 5-47a. Hoop stress/time histories, tube section immediately behind
headworks, Calculation 2B
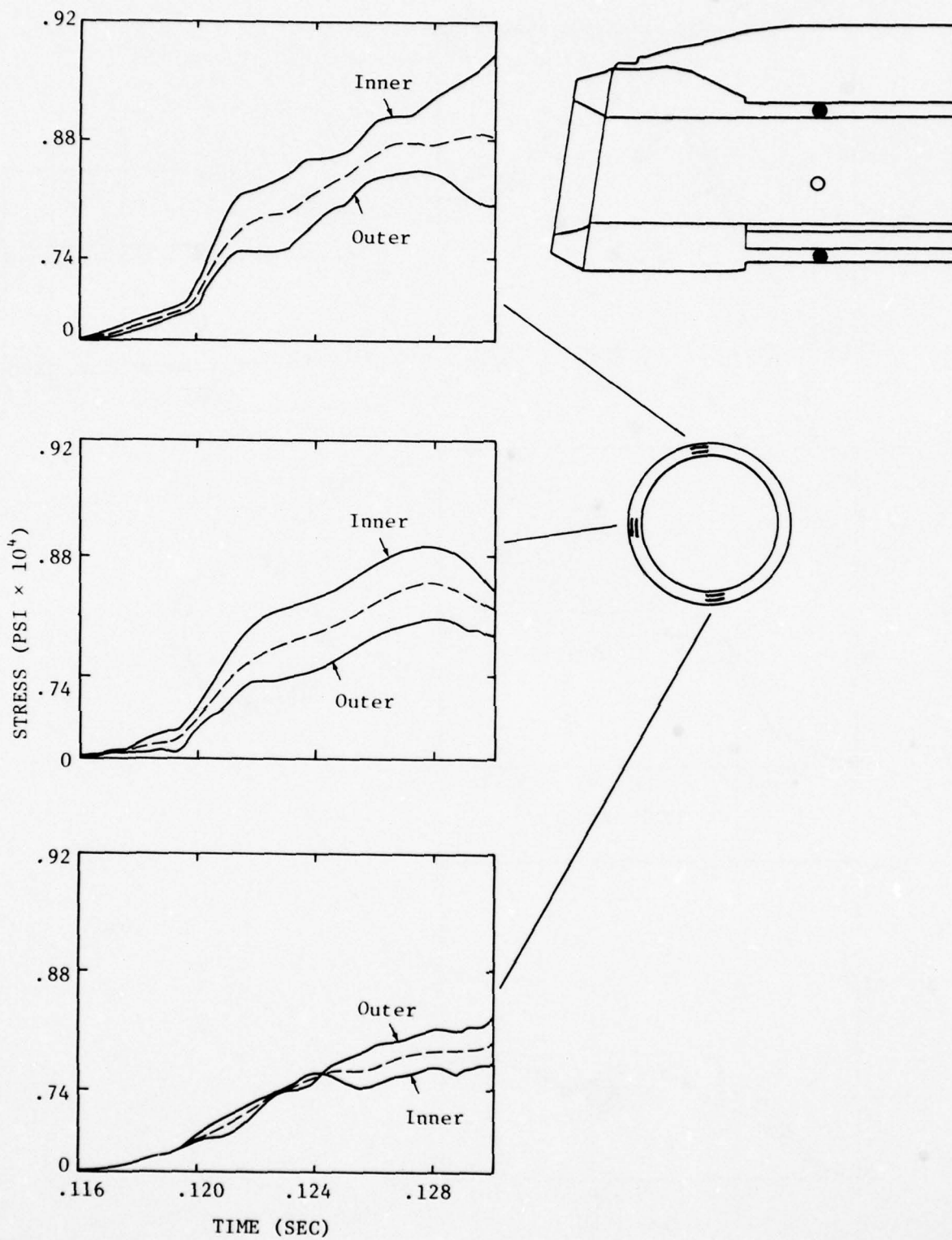
Figure 5-47b. Hoop stress/time histories, tube section half-tube diameter behind headworks, Calculation 2B

+ at 128 Msec.
o at 135 Msec.

Displacement Scale
(In.)

Closure
cg
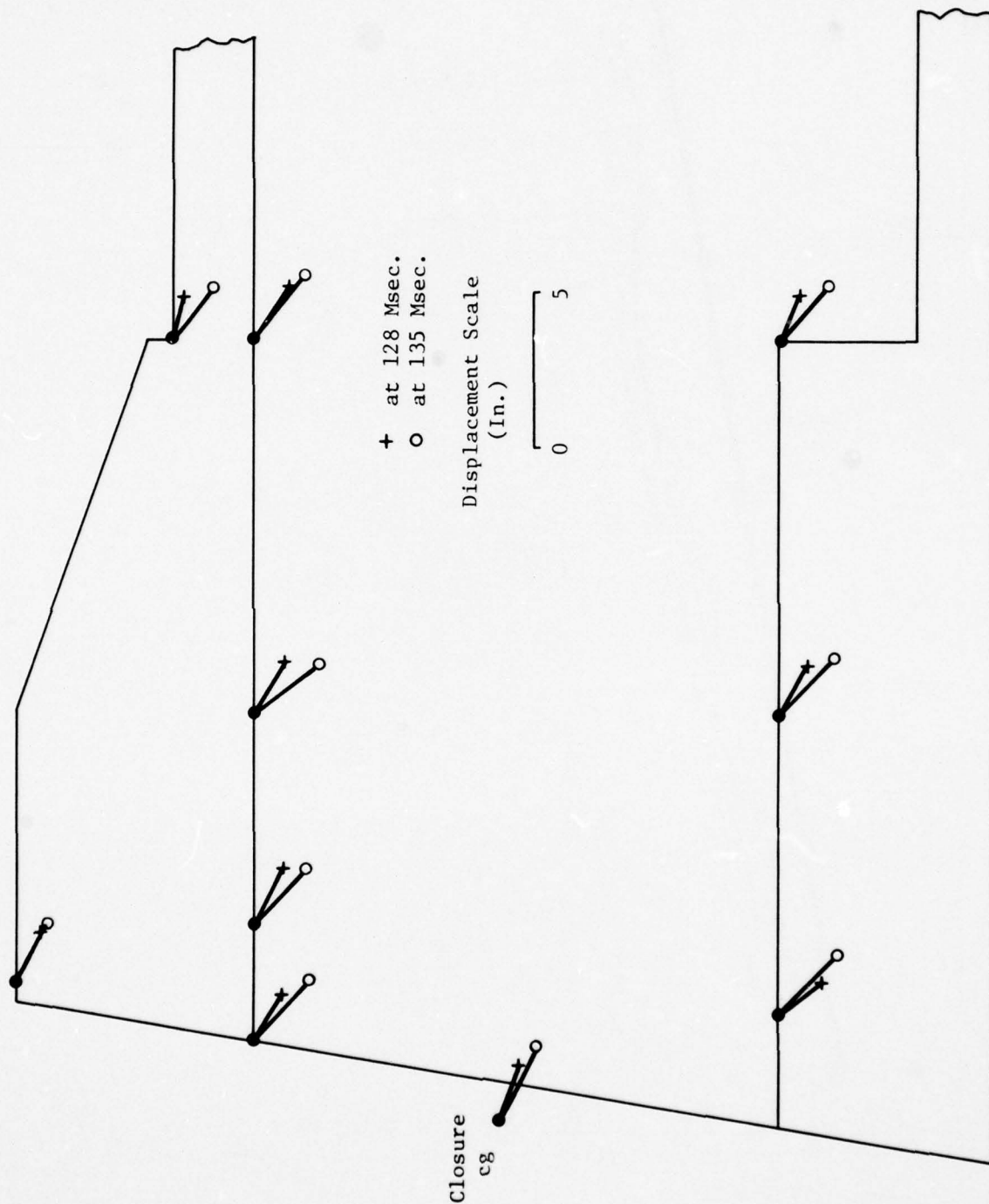
Figure 5-48. Deformation modes of headworks, head-on incidence, Calculation 2C

5-73

DISPLACEMENT SCALE (IN.)

0   5.   10.

119 Msec.

123 Msec.

127 Msec.

133 Msec.
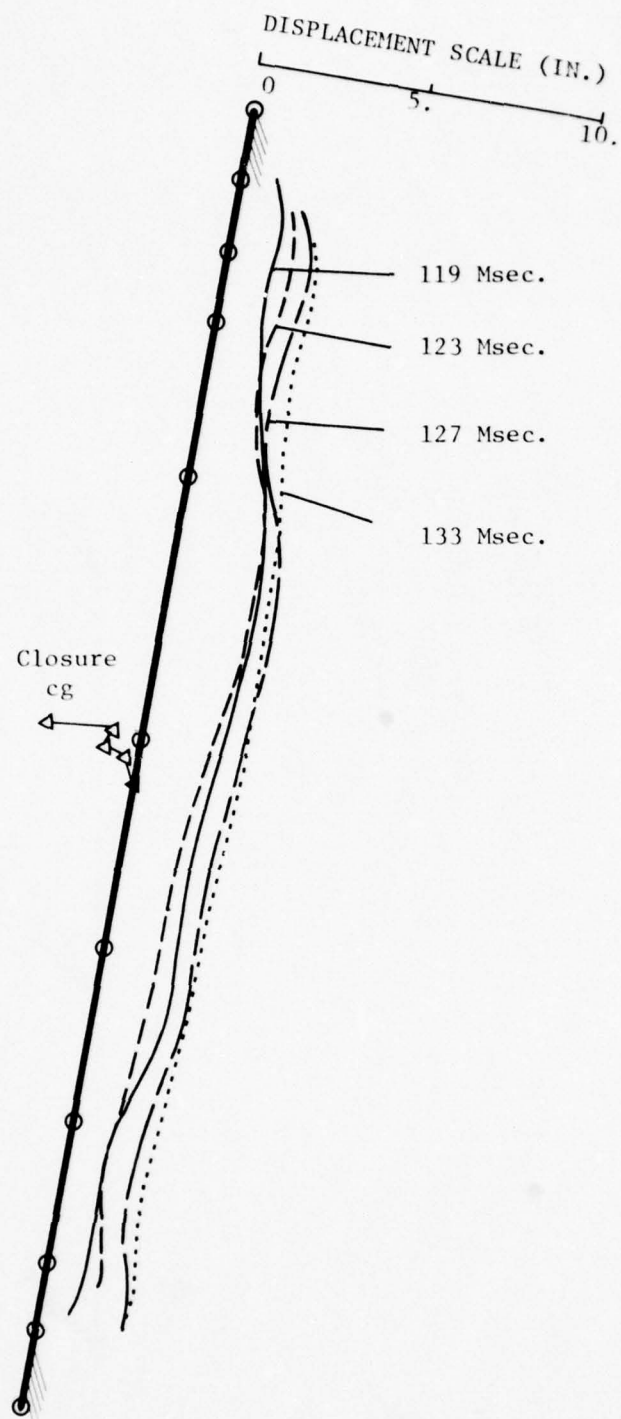
Closure
cg

Figure 5-49. Deformation modes of backplate vertical centerline, Calculation 2C
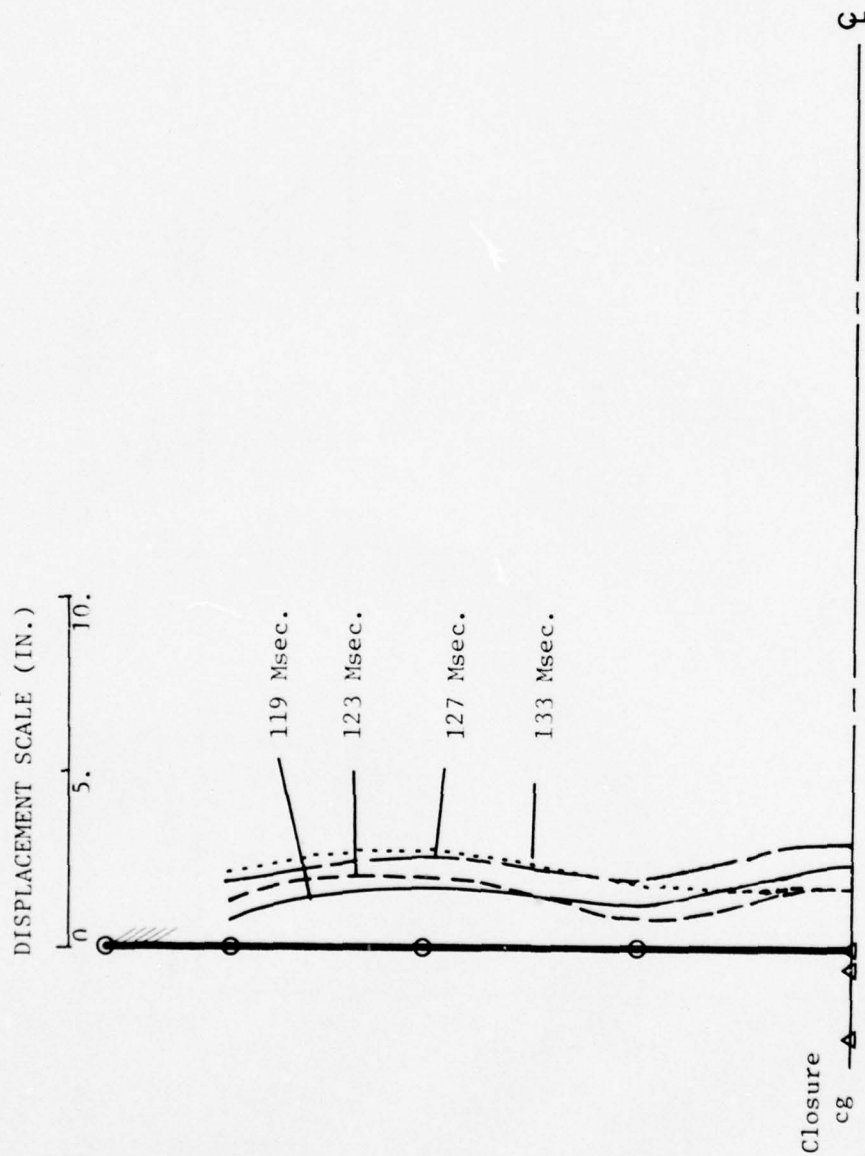
Figure 5-50. Deformation modes of backplate horizontal centerline, Calculation 2C
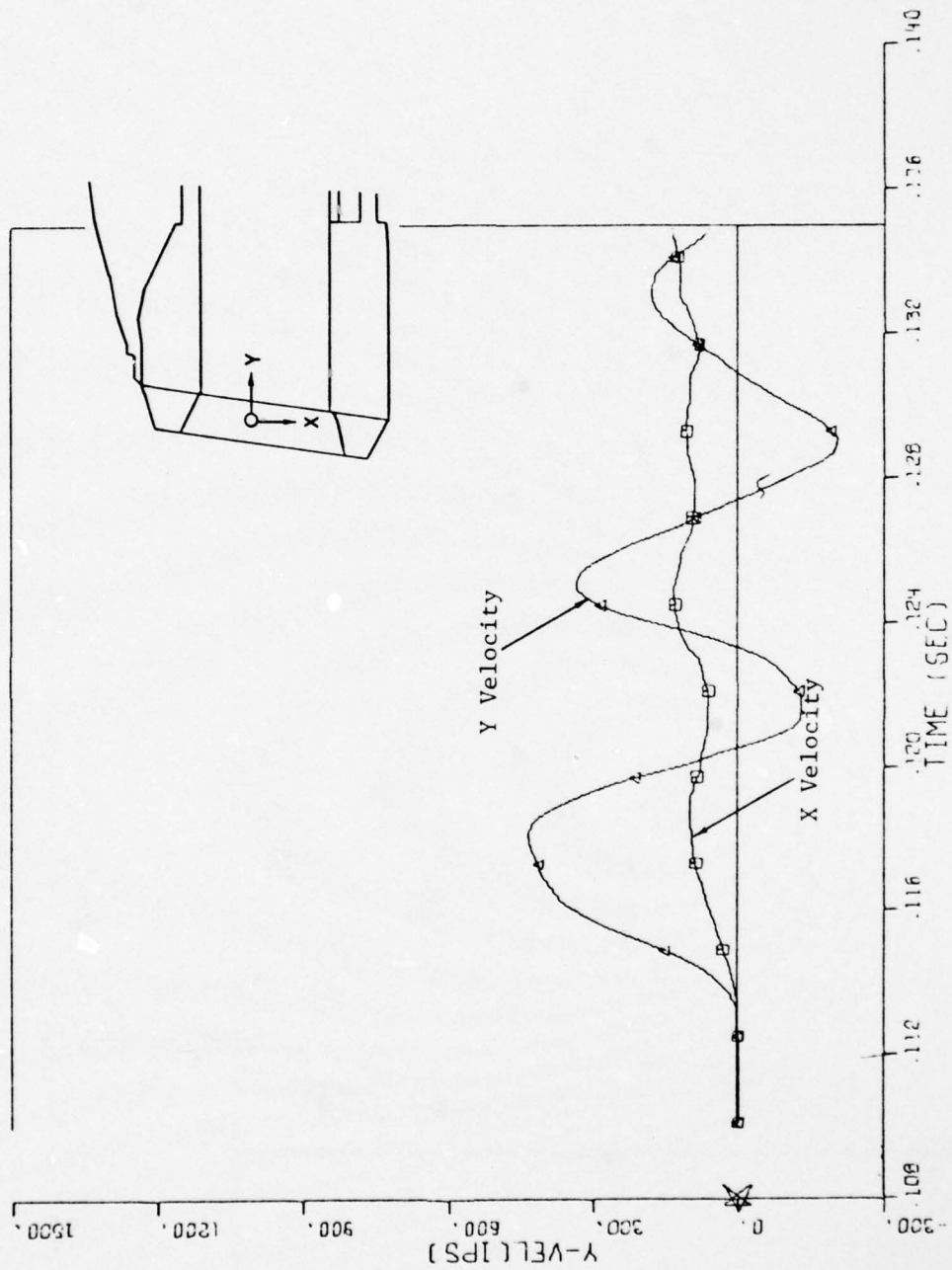
Figure 5-51. Velocity/time histories of closure cg, Calculation 2C
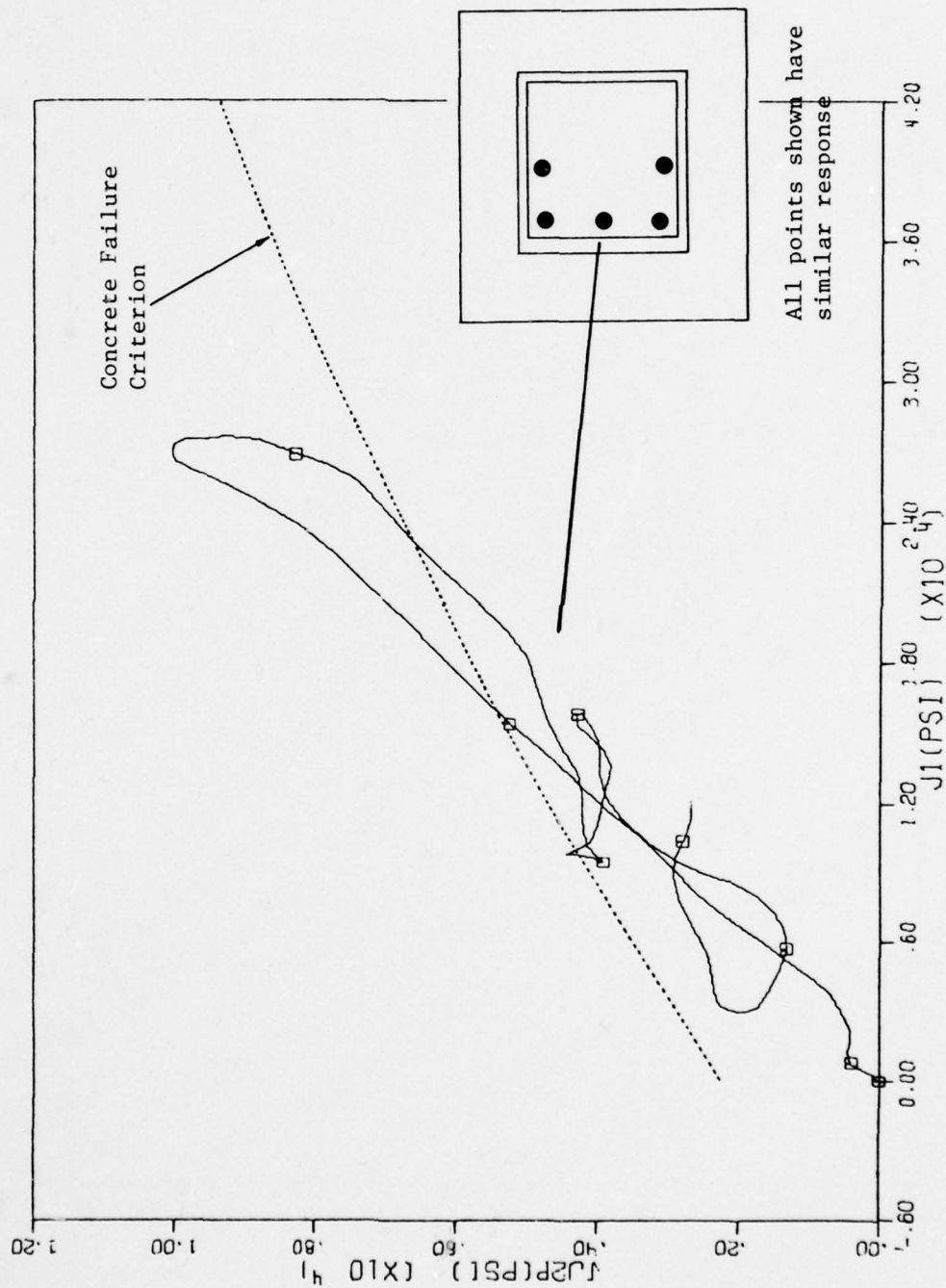
Figure 5-52a. Typical stress invariant-plot for points in closure concrete, near support, Calculation 2C
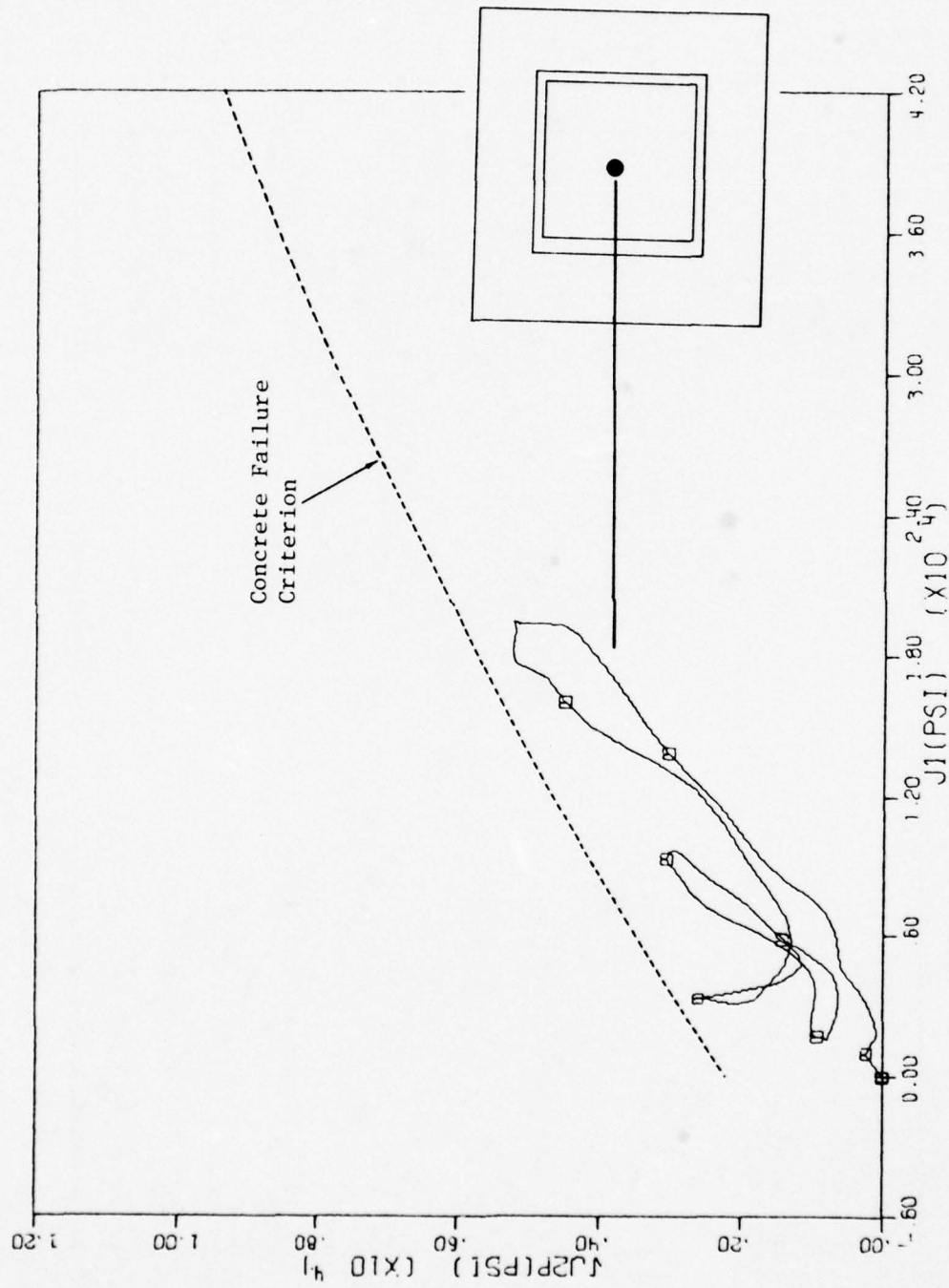
Figure 5-52b. Typical stress invariant plot for points in closure concrete, center, Calculation 2C

All points shown have
similar response
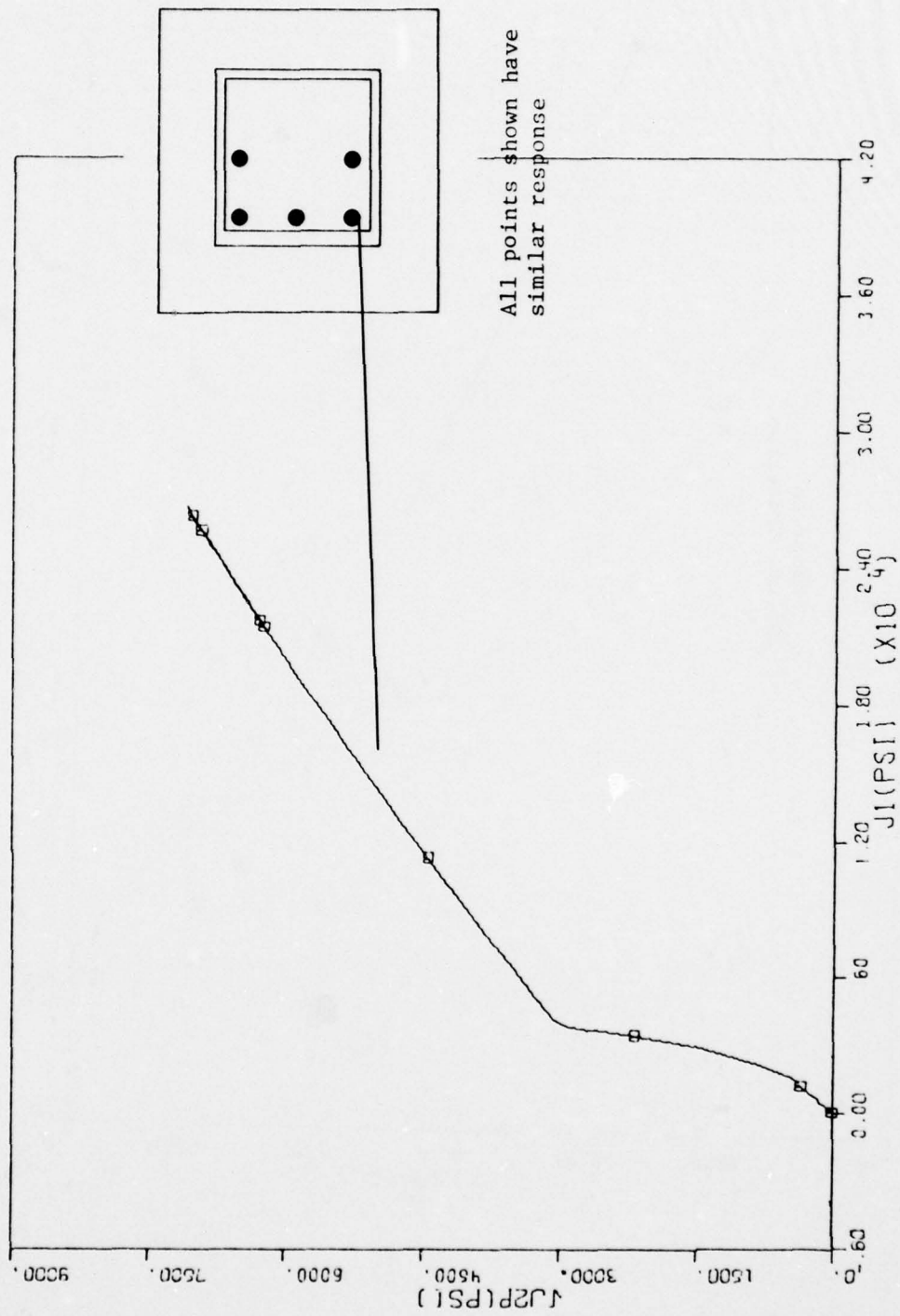
A 36 Steel Limit

J1(PSI) (X10² ⁴)

J.J2P(PSI) (X10 ⁴)
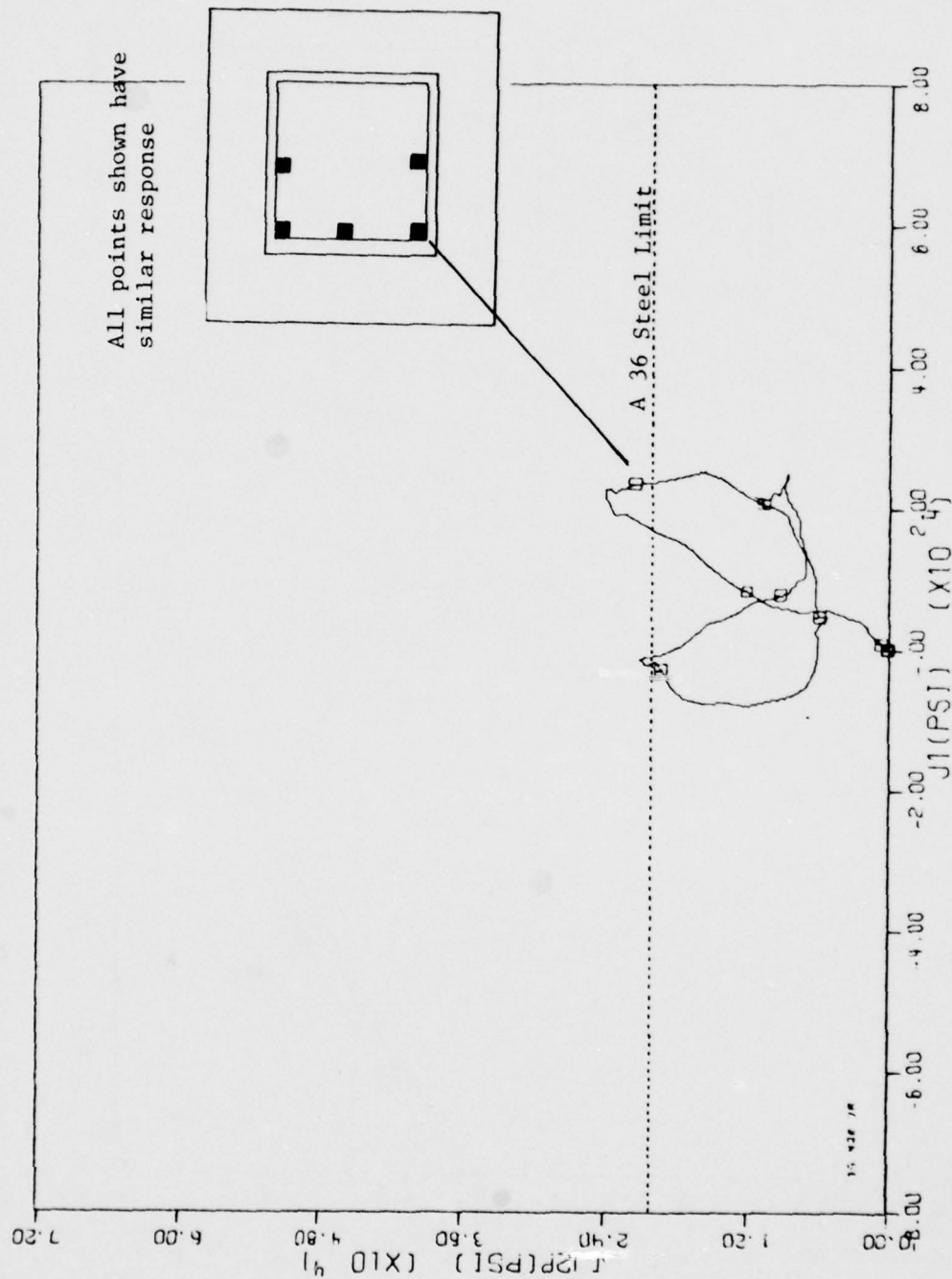
Figure 5-53a. Typical stress invariant plot for points in backplate, near support, Calculation 2C
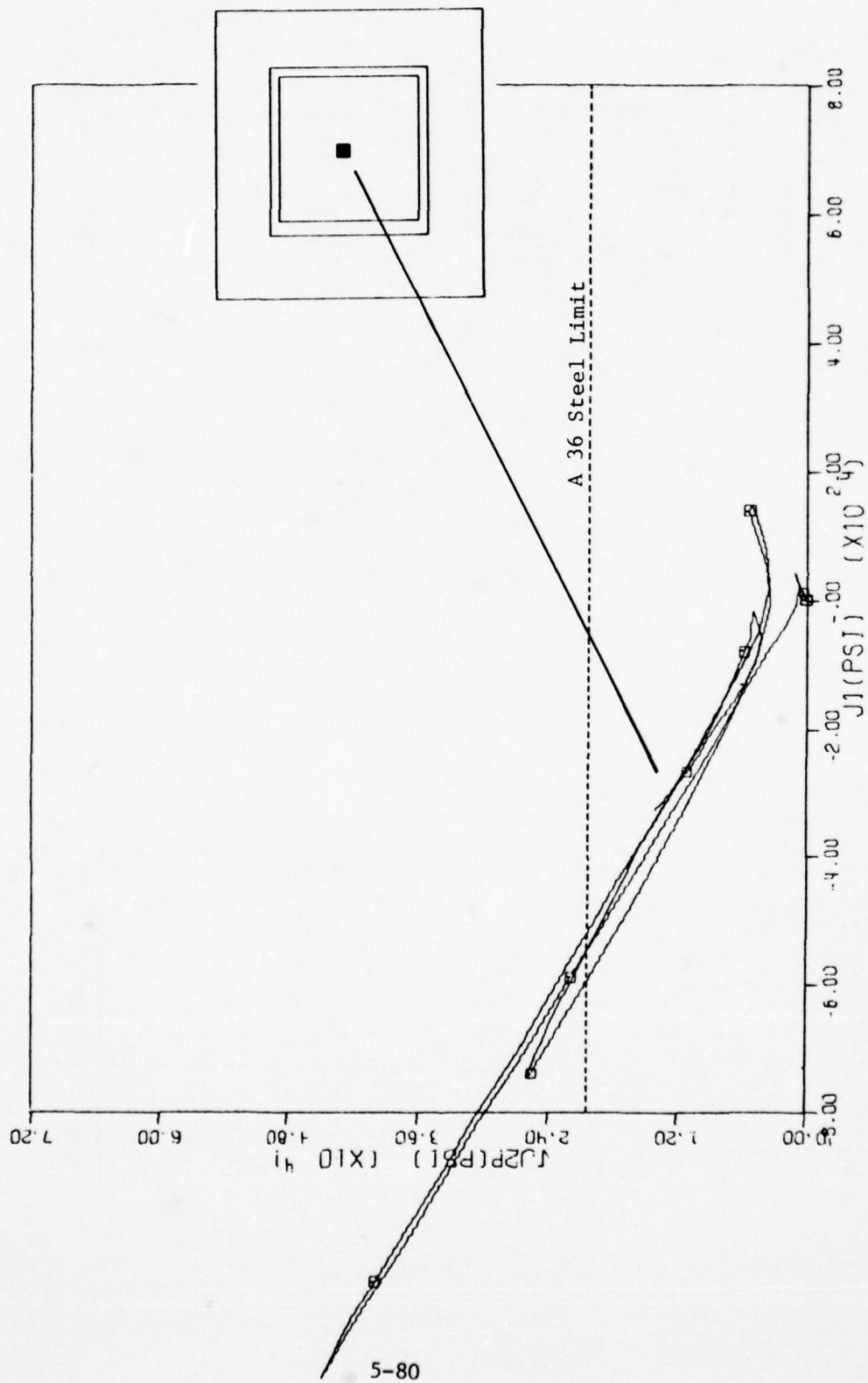
Figure 5-53b. Typical stress invariant plot for points in backplate, near center, Calculation 2C

5-80
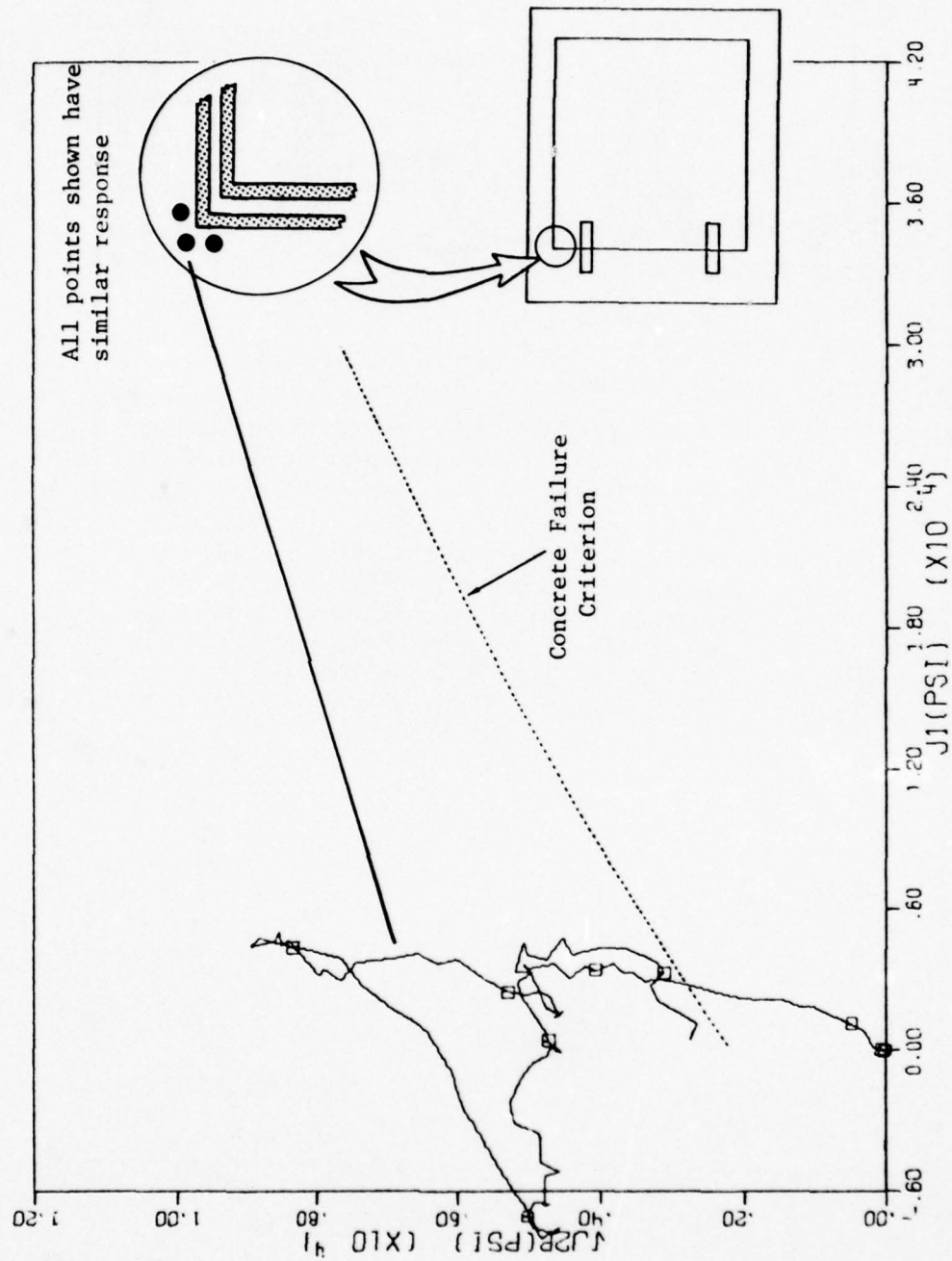
Figure 5-54. Typical stress invariant plot for concrete in upper frame corner, Calculation 2C
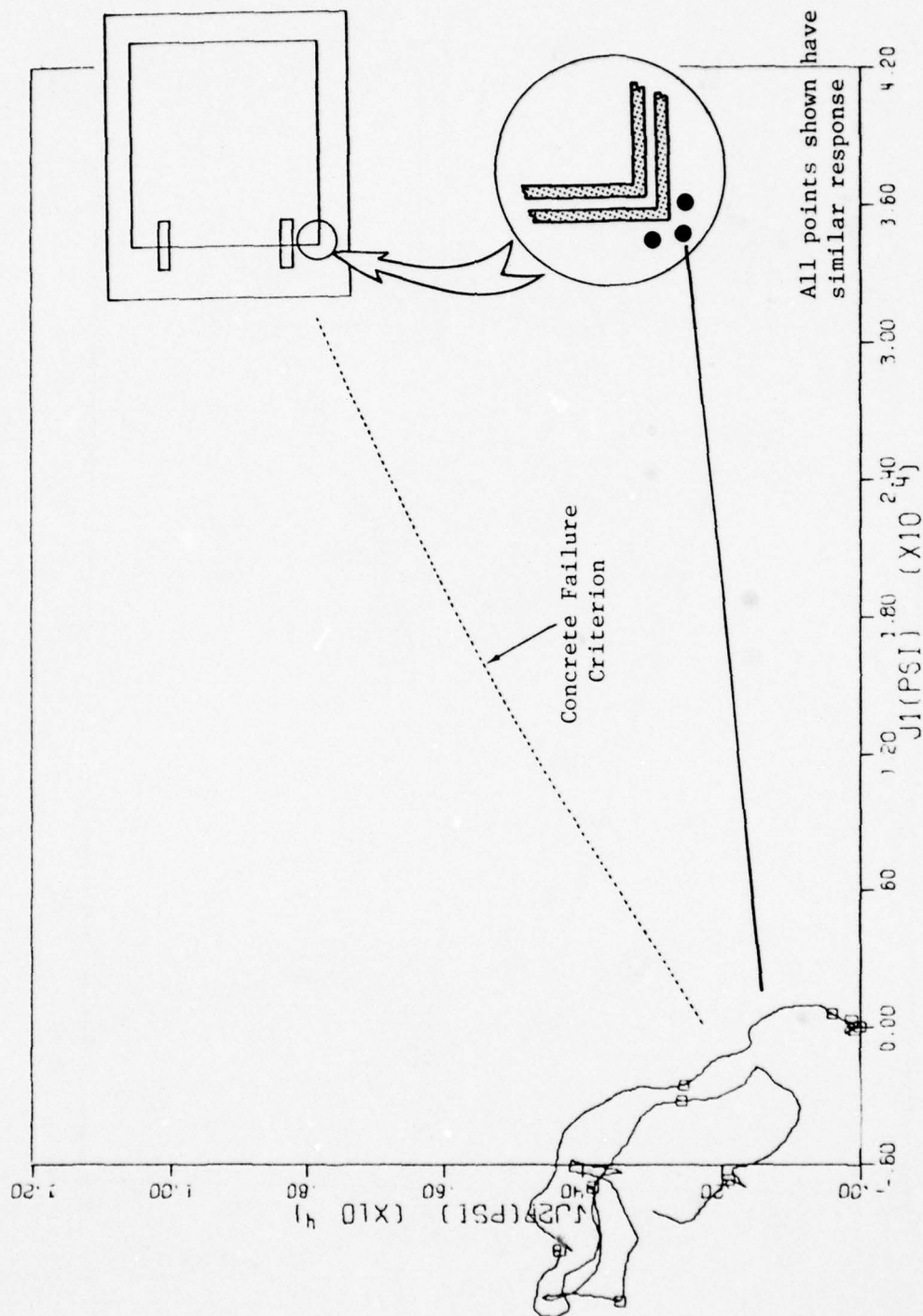
Figure 5-55. Typical stress invariant plot for concrete in lower frame corner, Calculation 2C

5-82
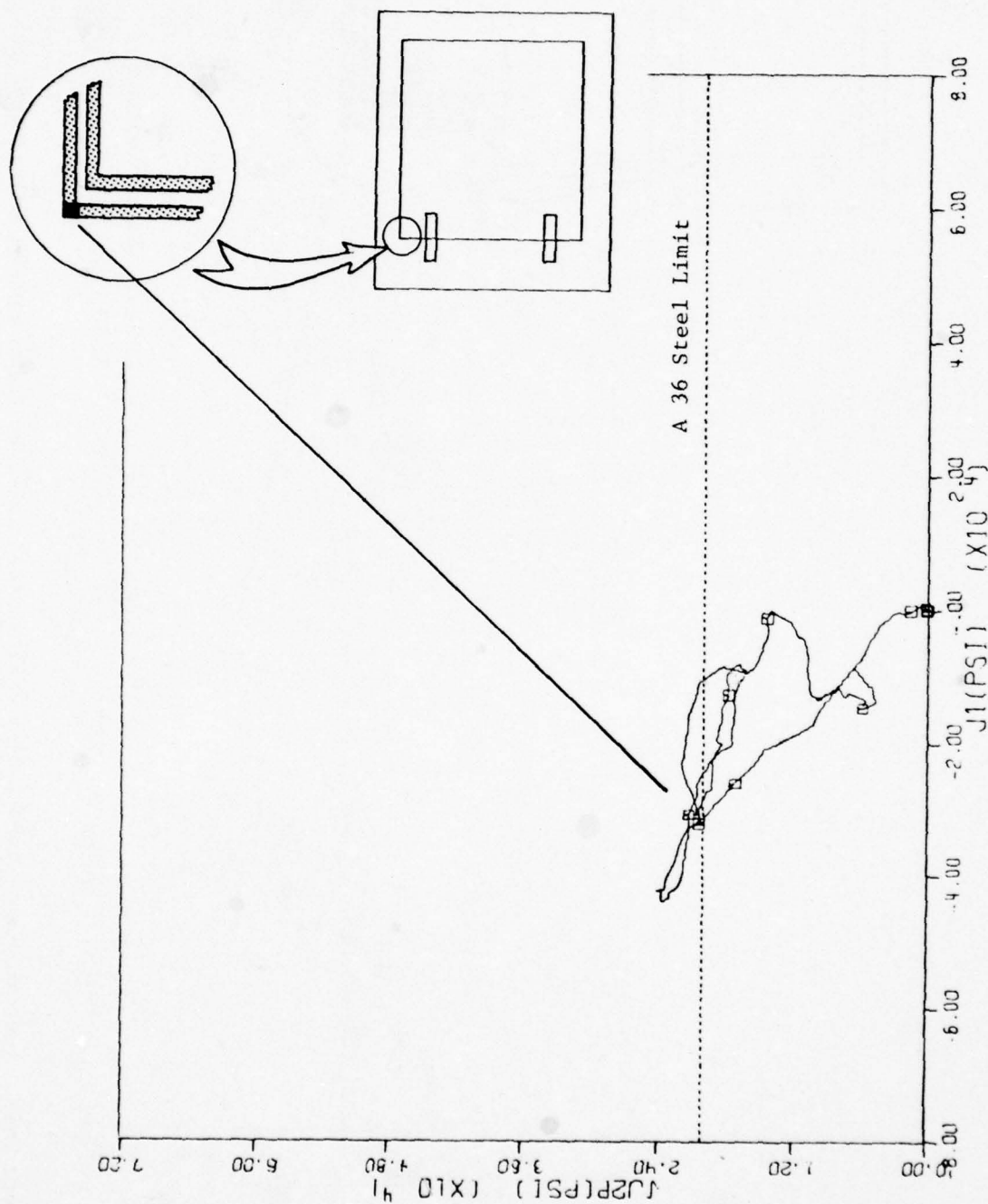
Figure 5-56. Typical stress invariant plot for steel in upper frame corner, Calculation 2C
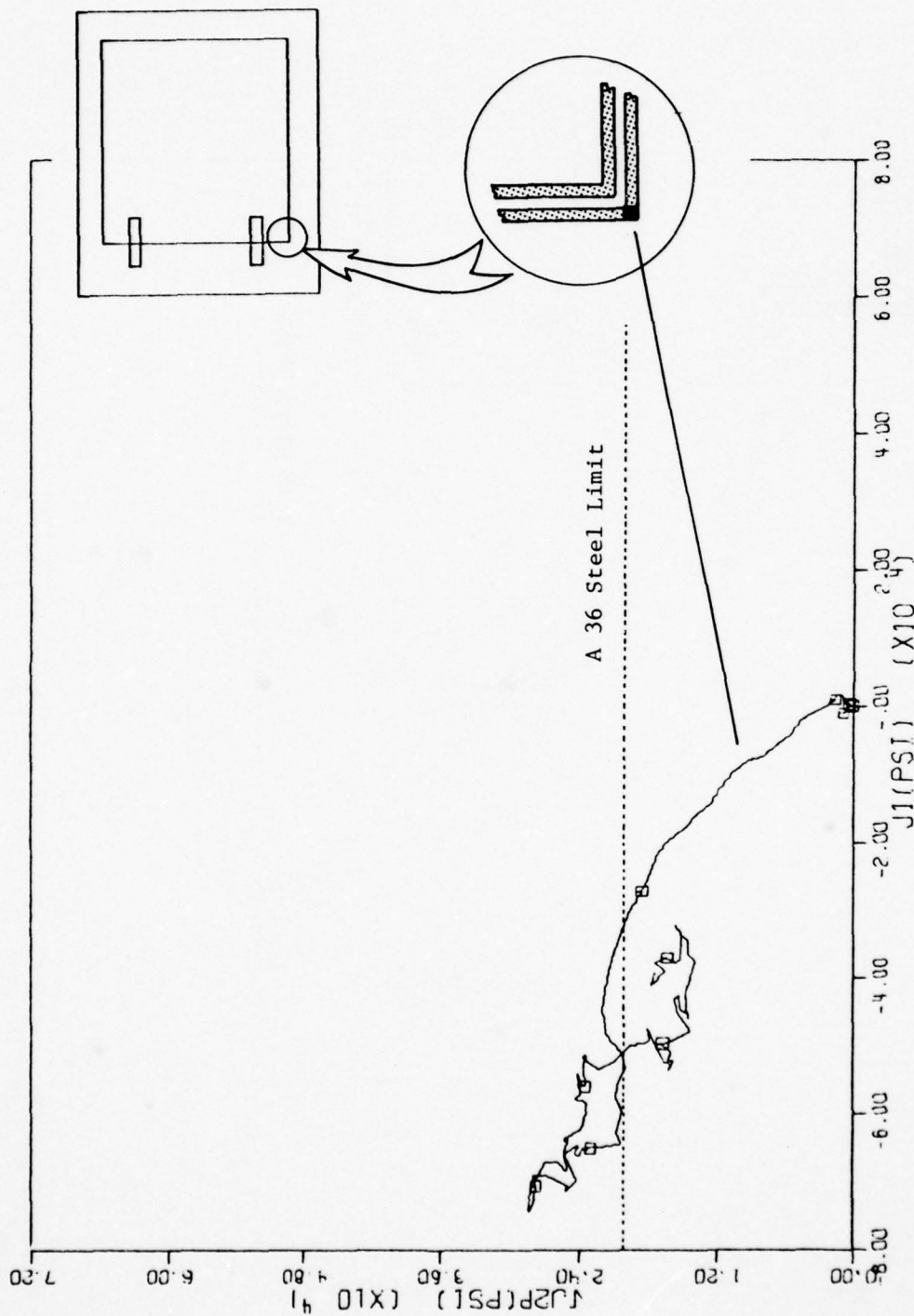
Figure 5-57. Typical stress invariant plot for steel in lower frame corner, Calculation 2C
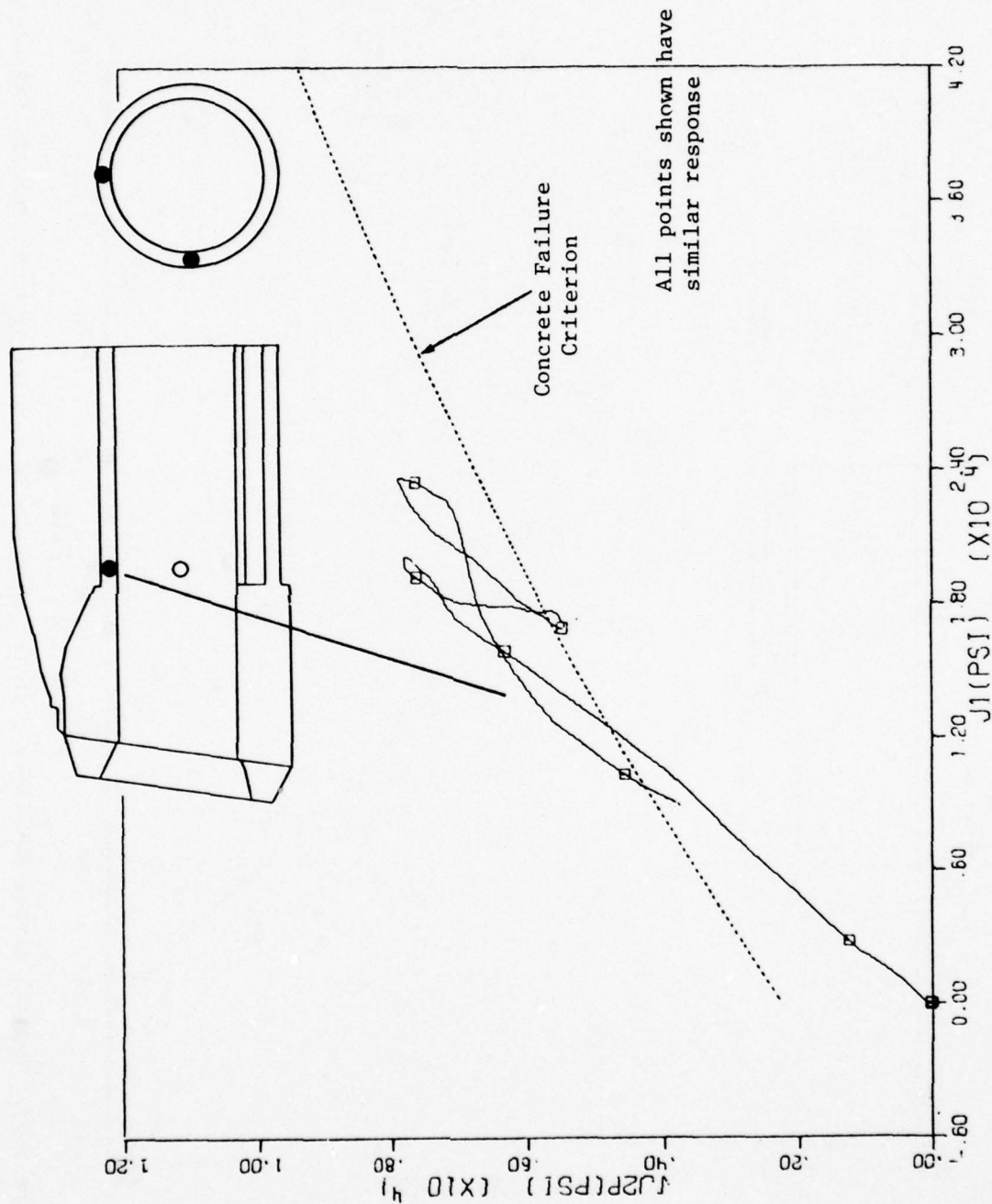
Figure 5-58. Typical stress invariant plot for concrete in tubular section, crown and springline, Calculation 2C
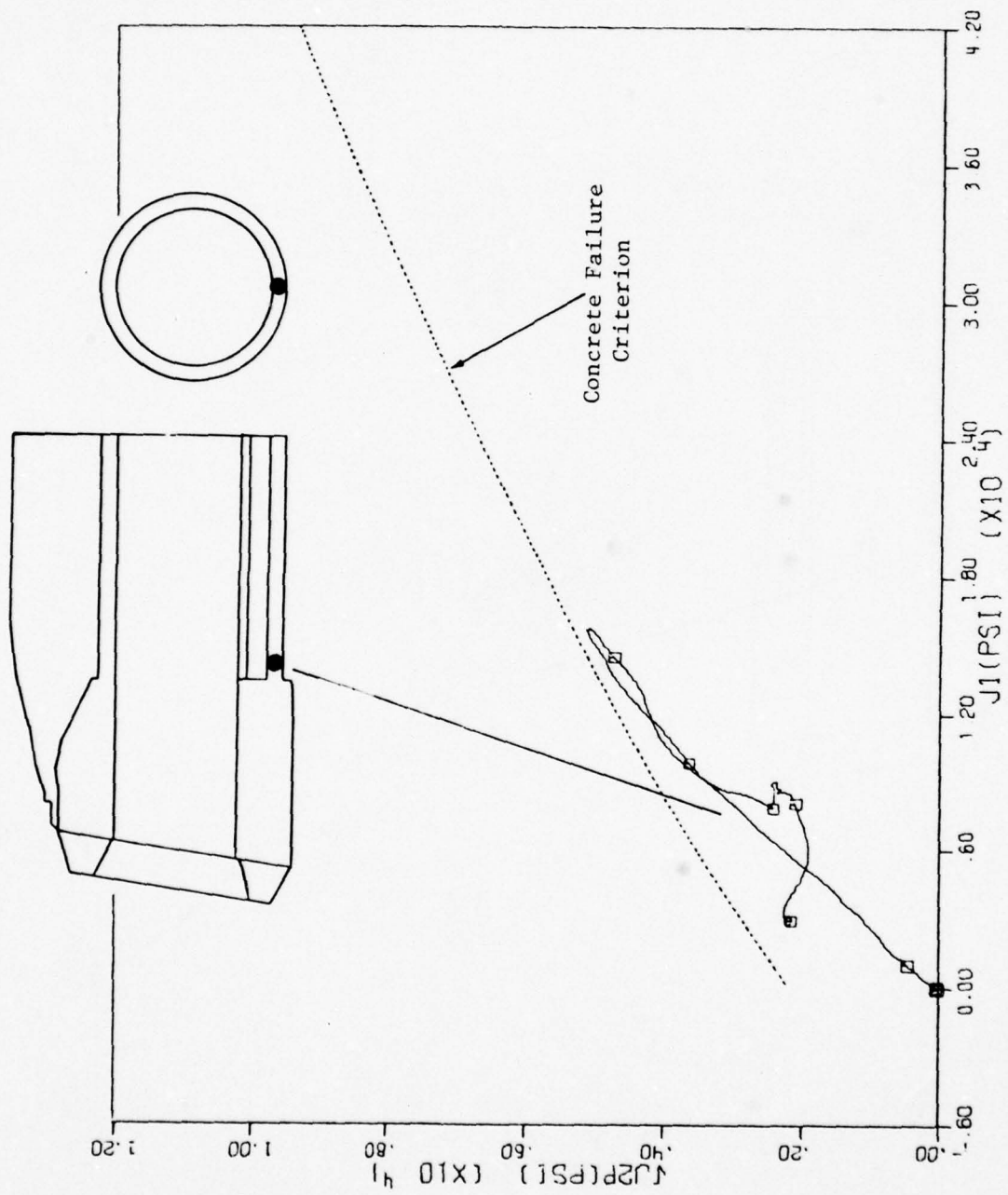
Figure 5-59. Typical stress invariant plot for concrete in tubular section, invert, Calculation 2C
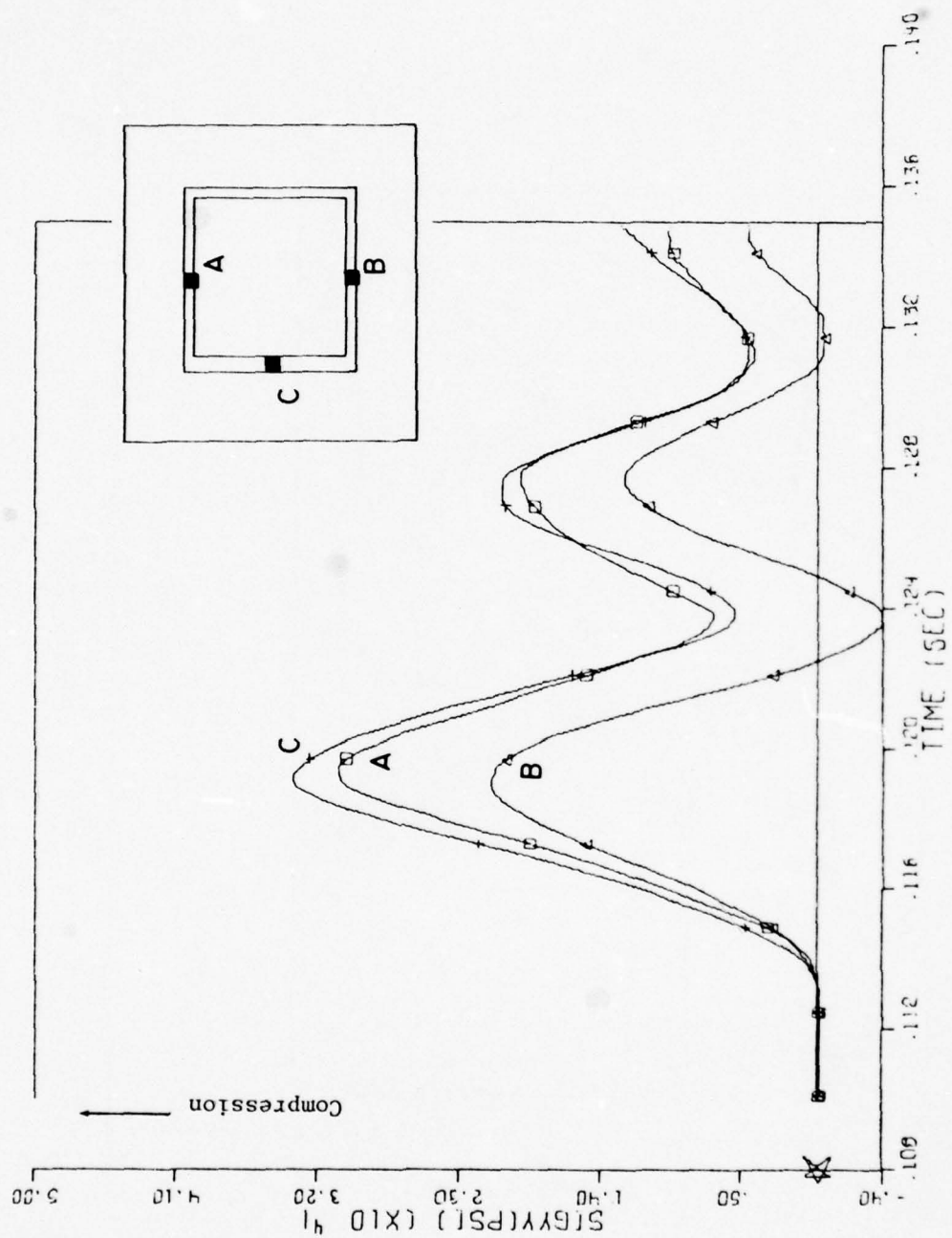
Figure 5-60. Bearing load/time histories, Calculation 2C
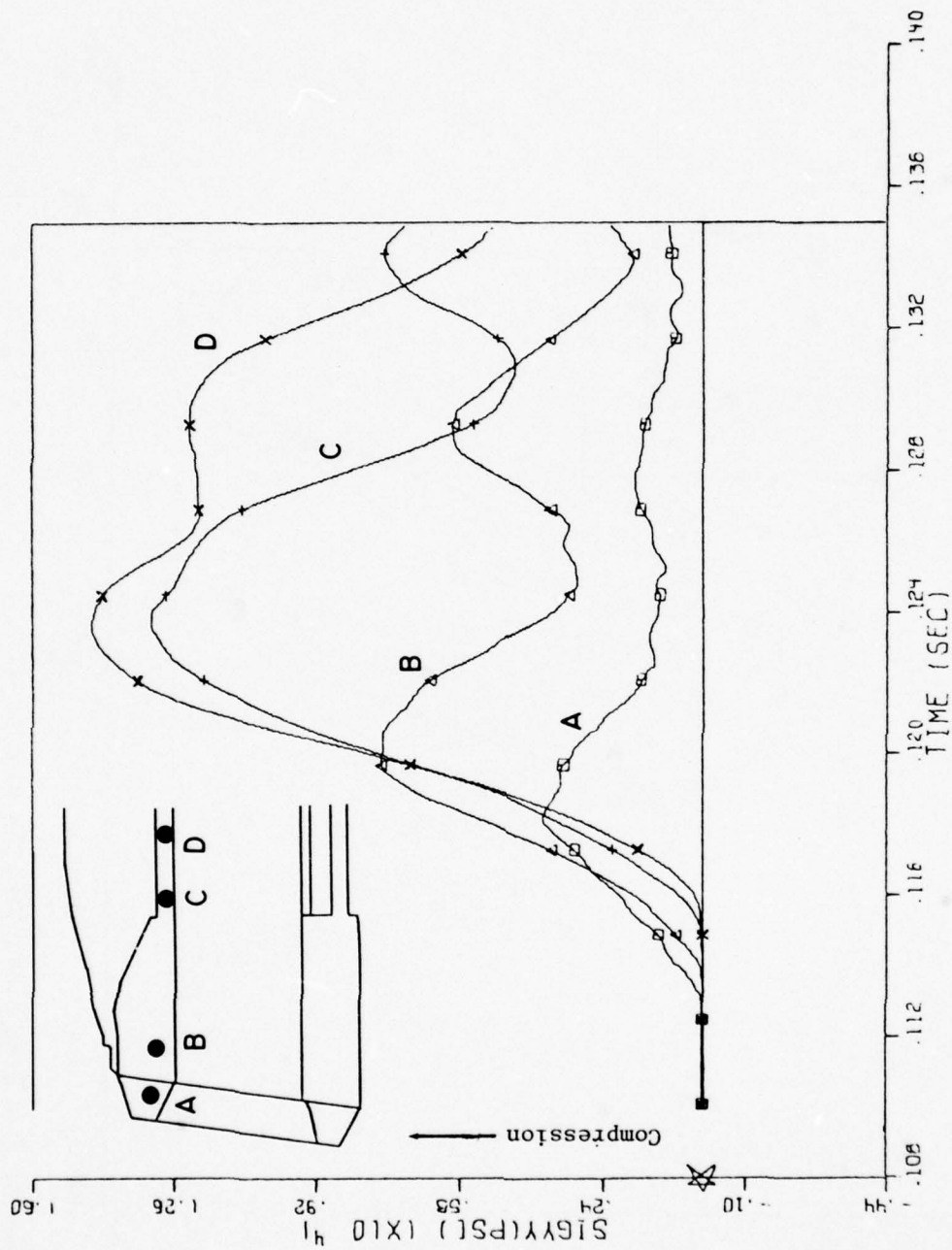
Figure 5-61a. Axial stress/time histories for points in upper shelter, Calculation 2C
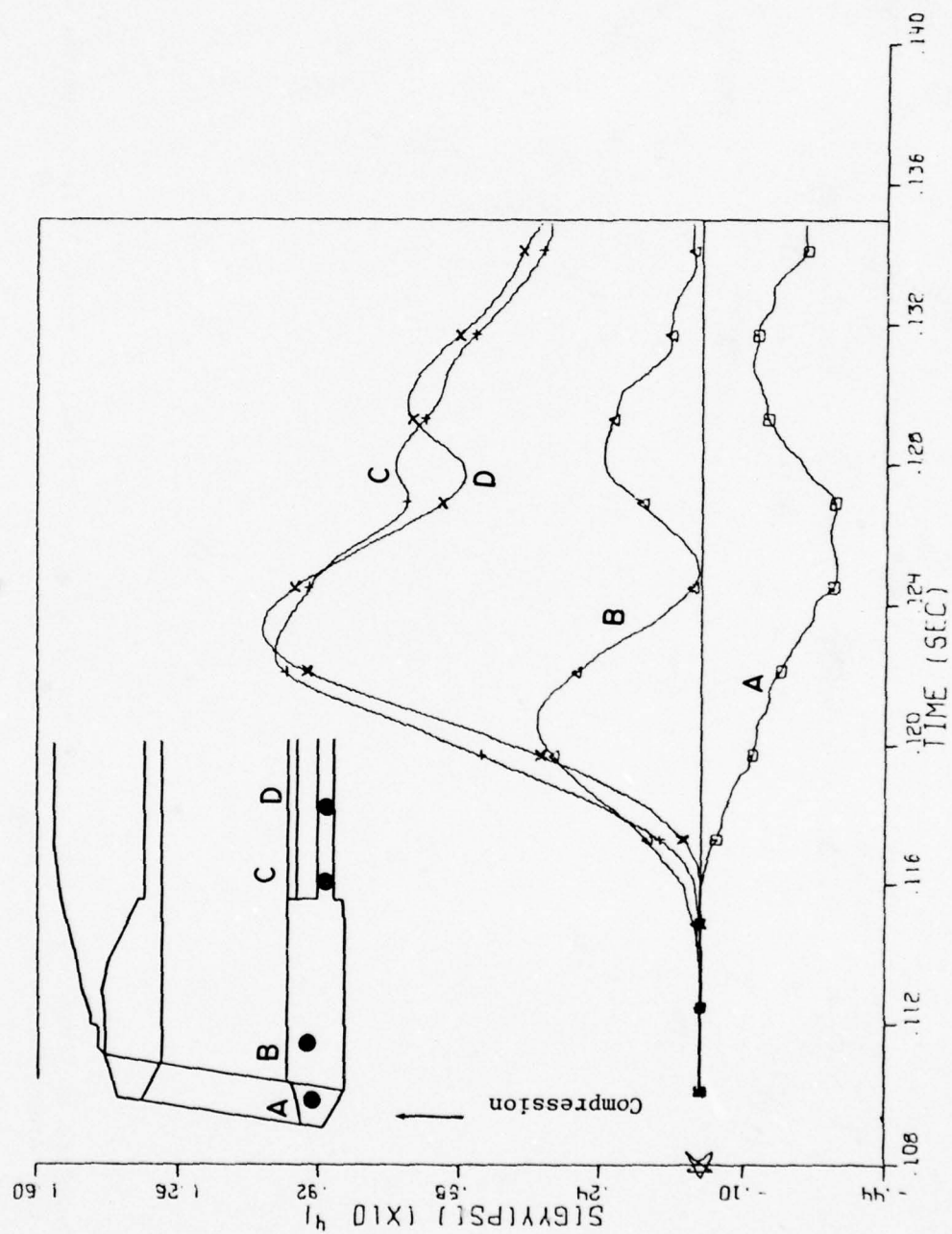
Figure 5-61b. Axial stress/time histories for points in lower shelter, Calculation 2C

TABLE 5-1

MATERIAL PARAMETERS FOR S4 MODEL

Material	Density (pcf)	Bulk Modulus (ksi)	Shear Modulus (ksi)	Yield Surface Parameters			CAP Parameters		
				A (ksi)	B (ksi^{-1})	C (ksi)	D (ksi)	R	W
Concrete*	150.	2333.	1750.	20.	.012	17.8	NO CAP		
Steel**	490.	26850.	11000.	20.8	0.	0.	NO CAP		
Soil	110.	190.	90.	2.1	.1	2.	.06	3.	.15
Backfill	120.	220.	100.	2.1	.13	2.	.18	3.	.15

*Used in conjunction with different tension cutoffs (7.2 ksi to 0.5 ksi) to model various reenforced concrete in the structure, headwall, slab floor and grout.

**For back and side plates in the closure and frame, bearing ring.

SECTION VI

INTERPRETATION OF PHASE 2 RESULTS

Major results of Calculations 2A, 2B and 2C all based on the S4 shelter configuration and head-on incidence are discussed below. Since emphasis of the study is not on structural response per se, the discussion on structural response will be kept to a minimum; details are given only to provide a common data base for subsequent discussions which address the main purpose of the study.

6.1. DEFORMATION MODE

The overall deformation pattern of the shelter is consistent with that observed in Phase 1 which is based on the S1 configuration. The dominant force comes from the direct head-on load acting on the front face. The structure responds like a beam-column supported by the soil medium; the headworks is pushed back in the longitudinal direction by this load with some downward motion due to the inclined front-face and overburden load. The motion of the headworks in turn induces some bending of the tubular section behind the headworks, notably in the longitudinal plane. In-plane bending of the tubular section of the shelter also exists as a result of the longitudinal load at first and later on as a result of the overburden load acting on that section.

An imbalance of the longitudinal stress exists in the upper (top) and lower (bottom) portions of the headworks. The imbalance is due to two factors; (a) the shielding effect of the soil which protects the lower portion of the front face from direct airblast load; and (b) the higher load bearing capability of the medium supporting the lower portion of the shelter. Consequently, the top portion of the headworks and part of the tubular section which follows sustain greater motion than the lower portion.

The downward motion of the headworks on the other hand depends on the overburden load and the timing of this downslap depends on the wave propagation speed of the berm medium. For a soft berm (loose backfill) the overburden load does not reach the structure for the first 10 msec. or so after airblast arrival at the front face; it is effectively screened out for short-time response consideration. Little downward motion of the headworks results. When the berm material has a higher wave speed (dense backfill), the downslap force is immediate and downward motion is almost concurrent with the longitudinal motion.

Since the bulk of the headworks remains elastic it is not surprising that the general deformation pattern as summarized above holds true for Calculations 2A, 2B and 2C. Local inelastic deformations in the frame and closure support areas account for some of the variations in details in this general pattern (see Figures 5-35 and 5-48 for instance).

6-1

The closure is pushed straight back by the incident airblast into the bearing ring and its support area in the headworks. Consequently, the steel bearing ring and in particular the concrete region behind it are severely deformed. The 10° incline of the closure also causes a downward component of the closure motion which is evident at the bottom edge of the closure and lower bearing area.

The deformation of the closure is very much affected by the closure material description. This is because the closure behaves like a thick plate in flexure (which is slight because of the large thickness-to-span ratio) in the elastic range and like a slab in punching deformation in the inelastic range. The two deformation modes are significantly different as can be seen by comparing Figures 5-7 and 5-49 showing the deformed profile of the backplate. Because of its importance in subsequent discussion the extrusion or punching mode will be described in the following paragraphs.

For the closure the airblast load at the front face (lateral surface of the slab) is transformed into shear forces in the slab. High shear stresses first develop in the concrete portion near the support edge as a result of the high frontal load and the equally high reaction forces along the support edge. This shear stress is highest at the bottom concrete which is next to the backplate. Upon yielding of this bottom concrete, i.e., when the shear bearing capability of the concrete is reached, the surplus shear stress is transferred to the concrete immediately in front which in turn yields. This process which continues for sufficiently high applied load until the front-most concrete in the closure is similarly affected, is often referred to as the shear crack propagation phenomenon.

Once the propagation is complete, i.e., it extends through the thickness of the closure concrete any additional load must be carried by the steel backplate. When the additional load is sufficiently high as is the case in Calculations 2A and 2B the backplate undergoes a shear deformation at the support edges. The closure in effect is extruded or punched into the headworks cavity shearing at the edges, but with the overall backplate remaining relatively flat.

This punching deformation of the closure is not sensitive to the backplate details at least as far as the first 10 to 15 msec. of response is concerned. Changing the backplate material from elastic to elasto-plastic and increasing the number of elements across the plate thickness from 1 to 2 do not seem to have significant effect on the deformation pattern of the closure. What is found to have significant influence on the closure response is the shear bearing capability of the closure concrete. Changing the closure concrete material from elastic (infinite shear bearing capability) to elasto-plastic (limited shear bearing capability according to confinement pressure) causes an estimated four-fold increase in the

maximum deflection as measured by the center deflection of the backplate relative to its support.

This sensitivity can also be observed by examining the motion of the closure cg for the two cases, elastic closure and inelastic closure, reproduced in Figures 6-1a and 6-1b. Discounting the 10° incline, the Y-component of the velocity can be viewed as the component perpendicular to the plane of the closure. In the elastic case the cg is seen to exhibit an oscillatory response with a period of about 8 msec. The velocity is similar to that of a single degree-of-freedom _elastic_ system subjected to a triangular pulse with duration several times that of the period of the system. The onset of inelasticity and the formation of shear cracks, however, change all that. The velocity-time history of the inelastic closure cg is not unlike that of a single degree-of-freedom _elasto-plastic_ system.

These conclusions have great ramifications in cost-hardness trade-off of the shelter (closure). High cost and low sensitivity for the steel backplate suggest that it may not merit the amount of attention that it has received. On the other hand, low cost plus great sensitivity for the closure concrete dictates that it be considered as a very important cost-hardness trade-off parameter.

Once the closure is extended into its punching deformation mode the airblast impulse in the main pulse duration governs the response, i.e., how fast or slow the pressure pulse decays from its peak value. Hence, it is expected that higher frequency contents which may be important to the closure response in the elastic realm (for vibration and resonance considerations) are no longer as important since they do not greatly change the load impulse. In other words if the closure is designed to respond in the punching mode the only overpressure wave form parameter of interest (aside from peak magnitude) is the total impulse and how fast this impulse is achieved.

The tubular section of the shelter immediately behind the transition section undergoes an ovaling deformation partly due to the oncrushing headworks (short-term effect) and partly due to the overburden load from the top (longer-term phenomenon). The section about half shelter diameter behind the headworks shows the deformation pattern of a mode higher than ovaling, possibly the n = 3 mode although the results obtained are not comprehensive enough to be conclusive.

6.2. STRESS DISTRIBUTION IN SHELTER

The airblast load acting on the front face (frame/closure) is transmitted through the headworks to the tubular section. The peak magnitude of this longitudinal stress is amplified in going from the headworks to the tubular section because of the abrupt drop in load bearing area available in the latter although the amount of amplification is not as

high as would be expected based on bearing area consideration alone. There are two contribut-
ing factors for this: the load bearing limit in the tubular section which corresponds to
the strength of concrete used (6,000 psi, unconfined), and the load transfer between closure
and bearing plate, which will be discussed presently.

Accompanying the amplification in longitudinal stress is a change in wave form
partly due to geometric dispersion and partly due to inelastic deformation. The change
due to dispersion can be measured by the elastic results of Calculation 2C and the contri-
bution due to inelastic deformation by comparing these with the results of Calculation 2A
or Calculation 2B.

The longitudinal stresses in the upper portion of the shelter are invariably
higher than those in the lower portion as has been mentioned in discussing the deformation
mode. This difference in the tubular section tends to diminish farther away from the head-
works. Although not verified directly it is expected that the longitudinal stress differ-
ential vanishes altogether about several tube diameters down the tube.

The axial stress transmitted to the tubular section is sufficiently high in areas
close to the headworks that inelastic deformation is observed there both at the crown and
springlines and to a lesser extent at the invert.

The stress state in the closure itself has also been covered in connection with
the discussion on the punching deformation of the closure. In the following paragraphs
the stress state at the closure/bearing interface will be described.

Much like a plate under lateral load, the airblast loading acting on the closure
induces reaction forces at the bearing ring. In the static situation the ratio of the re-
action pressure to the uniform applied load is proportional to the ratio of the loaded sur-
face to the supported area. Results of Phase 2 indicate that the dynamic reaction load
induced in the bearing ring is lower than the static equivalent. Furthermore, the reaction
load is concentrated at the innermost edge of the ring which is consistent with the punch-
ing deformation of the closure. The average bearing pressure is found to be insensitive to
the details of the interface model whether the backplate is elastic or inelastic and whether
it has two elements or only one element across the plate thickness. A fine mesh representa-
tion of course should be used to represent the bearing area if the stress concentration
nature of the bearing load is to be reproduced.

The model used in Phase 2 assumes a bonded interface between the closure and bear-
ing ring. The actual physical interface condition is of course complicated and appears
time dependent. The gap pressure wave which precedes the main airblast load at the front
face will tend to slip past the bearing interface into the headworks cavity. This was

observed in the HAVE HOST Sl test (Reference 11) and the so-called blow-by is sometimes so significant that it knocks off equipment and cables inside the headworks. During this period which occurs when the closure is relatively unloaded the interface condition is one of slip. Upon the establishment of the full airblast load on the closure the interface is one of friction or no-slip depending on the normal force and the relative motion of the backplate with respect to the bearing ring. When loaded on its front face the closure will tend to extend sideways. The confinement pressure on the other hand will tend to move it in the opposite direction. What actually takes place is not totally clear and no doubt depends on the relative magnitude of the confinement (gap) pressure and front airblast load. The effect of interface condition on shelter response is expected to be minor. The interface (or edge) condition may be important to the response of the closure, and its effect needs to be assessed.

The aforementioned aspects of stress distribution in the shelter, namely, the bearing pressure, the peak mean longitudinal stress and bending moment in the tubular section, etc., are found to be insensitive to the modeling details of the closure (comparing results of Calculations 2A and 2B). Although the observation is based on short-term response we believe that it applies also to long-term response as well, leading one to conclude that as far as the overall response of the shelter is concerned a crude model of the closure suffices. By the same token for detailed analyses of the closure the headwork and tubular section may be replaced by some equivalent, but much simplified system suitable chosen to maintain the correct impedance and energy transmission properties.

Based on results obtained in Phase 2 and the discussions of Sections 6.1 and 6.2, the following observations on the effect of inelasticity (and elasticity) on shelter response can be made.

A. Effect of Inelasticity

The foremost effect of inelasticity on shelter response is manifested in the deformation and response of the closure. Limiting the shear bearing capability of the closure concrete results in the formation of a shear crack causing the closure to respond in the punching mode wherein it is extruded into the headworks cavity for sufficiently high loadings. Consequently, the steel bearing ring and the concrete region behind it are also severely stressed. This distress is more evident at the bottom edge of the closure and lower bearing area.

An indirect effect of inelasticity in the closure is that, once the closure is in the punching mode, the closure deformation is governed by the loading impulse and is no longer as sensitive to high frequency components of the overpressure wave form as is when it remains elastic.

Inelastic deformations are found in the frame, notably at the upper and lower inner corners. The effect of inelasticity is local in the sense that it does not affect the response of the main headworks and shelter structure.

Incipient plastic deformations are also found in the tubular section immediately behind the headworks where the high axial load at the crown is limited by the concrete strength and is redistributed to the lower portion of the tube causing a more uniform distribution over the tube cross-section.

B. Elastic Versus Inelastic Analysis

By comparing the elastic and inelastic response obtained it is observed that an elastic analysis of the shelter is valuable in identifying both the overall deformation modes of the structure especially those that are uneffected by the onset of inelasticity and possible regions of distress. Some examples from the S4 configuration are the headworks deformation, load transfer from closure to headworks, load transfer from headworks to tubular section, stresses in the frame, stresses in the closure and tubular section, and response of the closure provided that it remains elastic.

The usefulness of an elastic analysis can be further enhanced when its results are interpreted based on sound engineering judgment. For example, by comparing the elastic stresses against the failure criterion of the material, an indication of whether the material may be overstressed can be obtained. Imposing a limit on the load bearing capability of the material an experienced analyst might be able to transfer the surplus load to other parts of the structure as is indeed what actually happens. The transfer between the upper and lower corner of the frame, the transfer between the upper and lower portion of the tubular sections, the transfer from rear closure concrete to the front are some of the lessons learned in the case studies of Phase 2.

Elastic analyses of the shelter can provide useful transient (short term) response data here because the structure under study is semi-buried and subjected to a direct loading which dominates the short-term response. The elastic analyses will be more effective if some allowance is made for energy dissipation inherent in the real material.

For a detailed quantitative analysis of the shelter and particularly the closure, there is no substitute for an inelastic analysis. Whereas the motion of the closure cg can be approximated readily by an equivalent single degree-of-freedom system, the punching deformation mode and the shear crack propagation phenomenon are prevalent only in an inelastic three-dimensional dynamic analysis of the structural component involved.
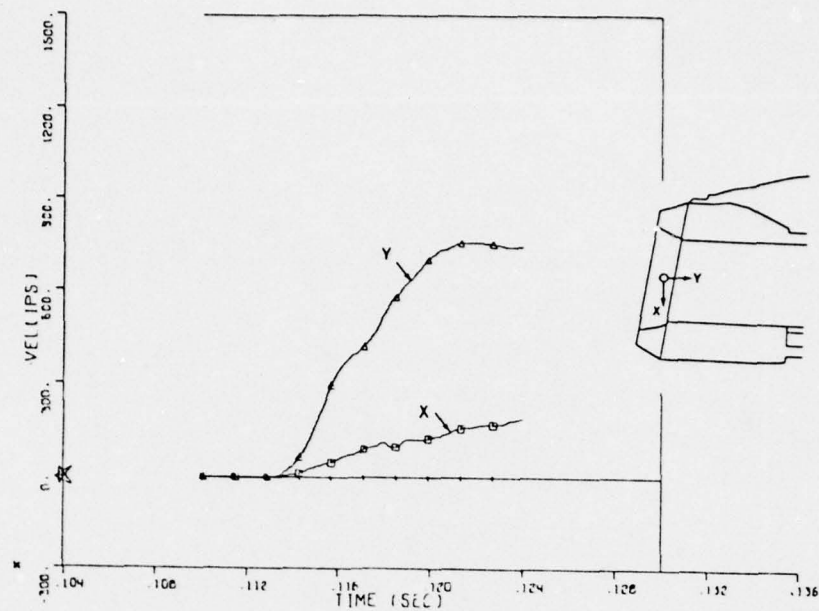
a.   Inelastic Closure, Calculation 2A
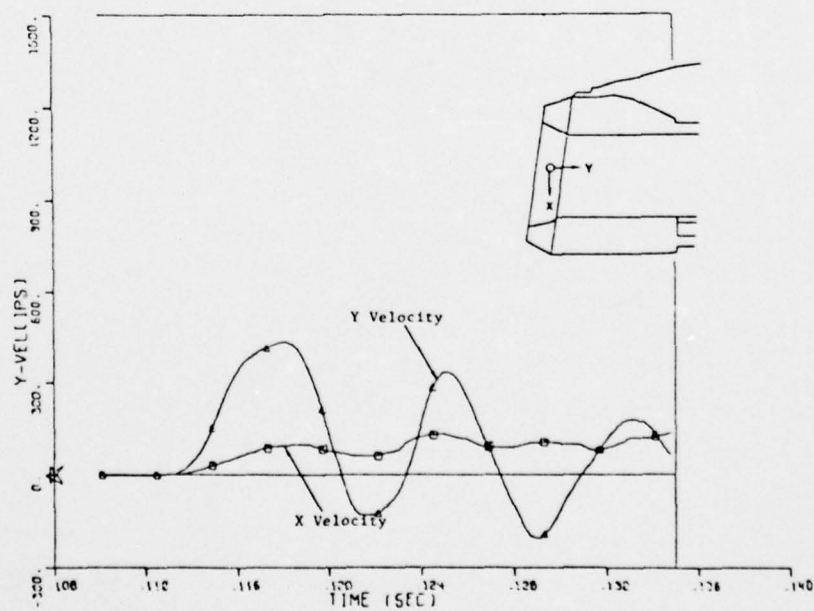
b.   Elastic Closure, Calculation 2C

Figure 6-1.   Comparison of velocity/time histories of closure cg

6-7

SECTION VII

CONCLUSIONS

This section begins with a summary of all modeling considerations found to have significant impact on shelter response. Basic deformation modes of the shelter under different loading conditions are described and their sensitivity to airblast loading characteristics summarized. The effect of inelasticity on modeling, deformation pattern and airblast sensitivity is then delineated. Once the effect of material nonlinearities has been identified the merit and limit of the use of elastic analyses (and hence inelastic analyses) will become apparent.

With knowledge gleaned from these conclusions a viable approach to performing dynamic analyses of the shelter is developed and described. The procedure involves modeling the shelter-like structure and its medium according to the guidelines established, factoring in those characteristics of the air overpressure which have been found significant and separating the analysis into complementary components: short-term analysis and long-term analysis.

7.1. STRUCTURAL MODELING CONSIDERATIONS

Several regions of the structure need to be modeled with attention. These are the closure, the front face, the inside corners in the frame, the gap between the closure and frame and the transition region including the front portion of the tube.

7.1.1. Closure

Details in the closure model do not seem to significantly effect the response of the remainder of the structure. When only the gross response of the structure is desired a crude model may be used for the closure in order to accommodate a large integration time step for an explicit code. This is essential in computing the long time response of the shelter. When accurate response of the closure itself is desired the closure model should be sufficiently refined to preserve its response characteristics (natural vibration in the elastic realm and punching or shear failure in the inelastic range). The remainder of the shelter, however, may be replaced by an equivalent system provided the replacement system retains the same impedance and radiation damping.

Closure response, in addition, is very sensitive to the material description of the closure constituents and in the case of a composite slab, the sensitivity to concrete properties is much higher than that to steel. Hence, an accurate material model for the closure concrete should be used.

The effect of support condition on closure response needs to be assessed but does not appear significant. Hence the closure/bearing interface model may be crude as far as closure response or headworks response is concerned. If it should become desirable to obtain the peak bearing load, however, a fine mesh is necessary since this load is concentrated near the edges and decays quite rapidly with distance away from the edge.

7.1.2. Frame and Gap

The effect of the gap pressure is significant especially when the inner frame is unprotected. The pressure tends to push the frame outward and this action is most severe at the interior corners. Accordingly the gap and the frame corner areas should be included in a detailed model. The effect is, however, local in that the headworks response is unaffected by it.

The degree of refinement in the front face (frame/gap and closure) should be compatible with the overpressure distribution since the latter dominates the shelter response and bending of the headworks in particular.

7.1.3. Headworks

The sensitive region in the headworks appears to be the region behind the bearing ring which is severely stressed as the closure is pushed against the support. Otherwise the bulk of the headworks is relatively unstressed and a nominal model suffices.

7.1.4. Transition and Tube

A large axial stress gradiant exists in the transition region from headworks to tube. This together with the abrupt change in cross-sectional shape (at least in the configurations studied) make the transition region one of the most important segments of the shelter as far as overall shelter response is concerned.

The front tubular section of the shelter, i.e., the portion of the tube immediately behind the transition region, is another sensitive region in the shelter response. In addition to transmission and merging of the axial loads from the headworks it transfers the bending moment exerted by the headworks on the tube. Its deformation is further constrained by the relatively rigid transition region and includes contributions from modes higher than simple ovaling and breathing which are standard for the remainder of the tube.

7.2. DEFORMATION MODE

The deformation mode under head-on loading is studied quite extensively using elastic and inelastic calculations. The studies of side-on and oblique front-on loadings are limited and based exclusively on elastic analyses. The following discussions are

limited to the short-term response for the first 10 to 15 msec. after airblast first arrival.

7.2.1. Head-On Loading

The basic deformation of the structure under head-on loading is one of axial compression with minor variations in the form of headworks rotation, longitudinal bending and downslap motion depending on details of the air overpressure distribution on the exposed surfaces, shelter front-face configuration and berm material.

The response is dominated by the tremendous front load acting at the frame/closure; consequently, is influenced by its distribution at the front face. More will be said about this in the section on airblast characteristics. Suffice it to say at this point that the headworks is pushed back into the tube section causing severe distress in the transition section and the front portion of the tube. In addition there is a downward motion induced by the 10° incline of the front face such as in the S4 configuration and/or the overburden load. There is also a rotation/bending of the headworks, the nature and severity of which depend on several factors: any imbalance in the front loading, offset between center of pressure and center of structure stiffness, magnitude of overburden load and inclination of the front face.

In the environment considered the closure deforms in the punching mode where it is pushed back against the bearing ring and extruded into the headworks cavity. The remainder of the slab remains relatively flat. Large shear deformations occur in the closure both in the concrete and steel backplate, mostly along the support edges. The shear deformation initiates at the back concrete, then propagates toward the front face. Upon completion of the "shear cone," the excess load is transferred to the steel backplate which then yields in the punching mode.

Gap pressure which acts in the opening between the closure and frame tends to push out on the frame and contain the closure. As a consequence the frame sustains high hoop tension especially at the two inner corners where tension failure at the concrete and yielding of the steel lining is observed. The gap is also opened by this internal pressure and the lower lip opens more than the upper lip.

The high axial stress and any longitudinal bending of the headworks are transmitted to the tubular section with the fore portion of the tube bearing much of the load. In-plane deformation of the ring cross-section in this region is mostly ovaling (n = 2) with some n = 3 mode contribution, for the short time considered before arrival of the overburden load from atop.

7.2.2. Oblique Front-On Loading

In the elastic calculation the deformation mode in the yaw plane shows the longitudinal compression accompanied by displacement of the headworks with the blast. Bending of the headworks in the yaw plane is first toward the blast because of the arrival time effect of the load at front face and is then reversed due to the effect of loads acting at the blast side of the headworks which is exposed for this calculation. The yaw bending moment induced in the tubular section is about one-half of the pitch plane moment for the distribution of airblast loads assumed. The shear stress in cross-sections of the headworks perpendicular to the longitudinal axis does not seem to be greatly affected by the additional out-of-plane load.

7.2.3. Side-On Loading

The deformation mode due to side-on loading under the two-dimensional assumption wherein only the tubular section of the shelter is analyzed as a ring consists mainly of ovaling with some breathing mode contribution.

7.3. AIRBLAST CHARACTERISTICS AND DEFORMATION MODES

The conclusions of airblast characteristics are based on limited airblast data and mostly elastic results.

7.3.1. Spatial Characteristics

Because of the direct application of load to the exposed surfaces in the shelter concept the airblast overpressure distribution about the exposed surface has significant effects on the resulting structural response. This is especially true because of the complex geometry involved and the sensitivity of the overpressure characteristics to this geometry.

In the front-on loading case the single most important parameter is of course the reflection coefficient related to the front face. Peak stresses in the headworks and tube are directly governed by the peak front load. The load distribution about the front face is another significant factor which affects the amount of rotation imparted to the headworks. Its significance is diminished for an inclined front face. The main action of the overburden load which is to push the headworks downward is mostly indirect in that the overpressure wave has to transverse the backfill medium to reach the structure and does not exhibit as much sensitivity as the front load. The magnitude of the overburden load is also substantially less than the front load, making it of secondary importance. Loading on the sides of the headworks contributes to the confinement pressure and its effect is probably significant only in the oblique incidence case when it contributes to deformation of the structure in the yaw plane.

Another front-face load parameter which merits consideration is the pressure distribution in the gap. Its magnitude governs shear deformation in the inner upper and lower corners of the frame and in addition provides confinement to the closure concrete. The effect of its distribution in the gap space is not studied here. It appears that the effect of minor deviations from uniform distribution will not be detected in the response. In any case the impact of the gap on the frame and closure is localized to these regions and is not felt in the headworks.

In contrast to the direct load the effect of indirect loads such as those acting on the berm is moderated by passing through the dissipative backfill material. Any variation in its spatial distribution is tempered by material damping by the time the ground shock reaches the structure. This insensitivity is indicated in the two-dimensional calculation where a two-fold increase in the load on the blast side of the berm does not cause any significant increase in the structural response as measured by peak bending moment and hoop stress.

7.3.2. Temporal Characteristics

Among the many characteristics which fall under this category the most important one is probably the impulse associated with the front load for the front-on loading condition. When the closure deforms in the punching mode the impulse-time history becomes the parameter which governs the closure response. The magnitude of the total impulse and the rate at which this impulse is applied have a direct impact on the maximum and permanent deformation of the closure. This is in contrast to the situation when the closure remains elastic where the important closure response considerations are vibration and resonance and the important airblast characteristics the frequency content at the natural frequency of the closure.

In general, the remark made earlier about spatial characteristics can also be made about the temporal characteristics, i.e., when the loading is direct the transfer of the temporal characteristics of the load to structure is most complete, especially the high frequency components. However, when loading is not direct the backfill and soil mass surrounding the structure will act to filter out any high frequency content of the overpressure and only the lower frequency components are expected to be important.

Arrival time or rather the sequencing of arrival times of the overpressure at different points of the structure is also another important characteristic. In the front-on situation phasing of the front load and overburden load determines the amount of rotation imparted to the headworks. Arrival time differential in the fr t loads in the oblique incidence case determines the initial bending moment into the blast. These effects

are transmitted down the shelter to the transition section and tube section where they become really important.

7.4. EFFECT OF INELASTICITY

As far as response of the shelter is concerned the foremost manifestation of the effect of inelasticity is in the closure deformations, i.e., the punching phenomenon discussed in Section 5.1. This response is sensitive to the strength of the concrete assumed.

Other inelasticity effects are observed in the frame notably the inner corners, in the bearing ring and concrete region behind it in the headworks, and in the fore portion of the tubular section near the headworks. These effects are mostly confined locally to the region mentioned and do not influence response in other parts of the shelter. The only exception is the inelastic deformation in the closure bearing region whereby the headworks deformation is uncoupled from the effect of front load acting at the closure.

Limiting the strength of the concrete in the tubular section also limits the amount of axial load the tube section can transmit and thus facilitates the uniform distribution of axial compression in the section. The impact of this effect, if any, has not been identified.

Inelasticity in the medium has the effect of modifying the stress pulse before it reaches the structure and provides material damping. It follows then that its effect is proportional to the expanse of medium separating the structure from the load. Hence it can be surmised that the most significant effect of inelasticity in the medium, aside from its effect on the overburden load described earlier, is to diminish long-term response and affects only the gross response of the shelter.

7.4.1. Elastic Versus Inelastic Analysis

Having identified the effect of inelasticity on the response of the structure, the merits of elastic analyses performed for the same structure can be assessed.

By themselves elastic analyses of the shelter can yield useful (and exaggerated) information on (a) possible deformation modes of the structure under different loading conditions; (b) sensitivity of these deformation modes to variations in overpressure distribution and wave form; (c) possible areas of distress which need further examination; and, of course (d) stress states in parts of the shelter where the material remains elastic.

When used in conjunction with engineering judgment the quantitative data obtained in elastic analyses can be extended to yield qualitative data on inelastic behavior. When used in conjunction with inelastic analyses an elastic analysis serves as an excellent

7-6

baseline to be referenced and compared to in order to assess and identify certain effects of inelasticity and their sensitivity.

An elastic analysis, of course, will not provide data pertaining to deformation and mechanism which are purely inelastic in nature, e.g., closure response. Nor will it provide good estimates for long-term effects due to the lack of damping and it invariably overestimates peak values for short-term response.

The reason an elastic analysis is more useful here than in other situations is that the shelter structure is semi-buried and subjected to direct loading which dominates the short-term response. It would be less effective, for instance, if the response of the tubular section under side-on loading is sought.

In the current application inelastic analysis also has its limitations. Foremost is the uncertainty of material properties (modeling, parameters, etc.), especially in the dynamic realm. Dynamic plain concrete properties are not readily available, not to mention reinforced concrete properties which reflect the complex reinforcing patterns in the shelter configuration. Soil properties have always been a major difficulty in structure-medium interaction analyses, although in the case of the shelter the interaction effect is not critical.

7.5. GROUND MOTION EFFECT

The effect of airblast induced ground motion on shelter response has not been studied and hence, definitive conclusions on this aspect of the dynamic analysis and the role of the soil island approach in shelter-medium interaction calculations cannot be made.

Because direct airblast loading dominates the shelter response, in the short term at least, it is expected that the ground motion effect, if any, will affect only the long-term response and the gross behavior of the shelter structure such as the longitudinal bending and in-plane deformation of the tube but not, say, the closure deformation.

Based on ground motion results obtained in Weidlinger Associates' study, DNA 001-77-C-0036, there is no appreciable outrunning ground shock in the (revised) baseline site at the 600 psi range. In the outrunning region (100 psi to 20 psi), the motions exhibit a sustained low frequency (1.5 Hz) response in both the horizontal and vertical directions. Ground motion effect, therefore, is expected to influence the response of a shelter located at this range, the direct airblast effect no longer as dominant due to the lower overpressure involved.
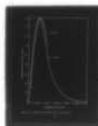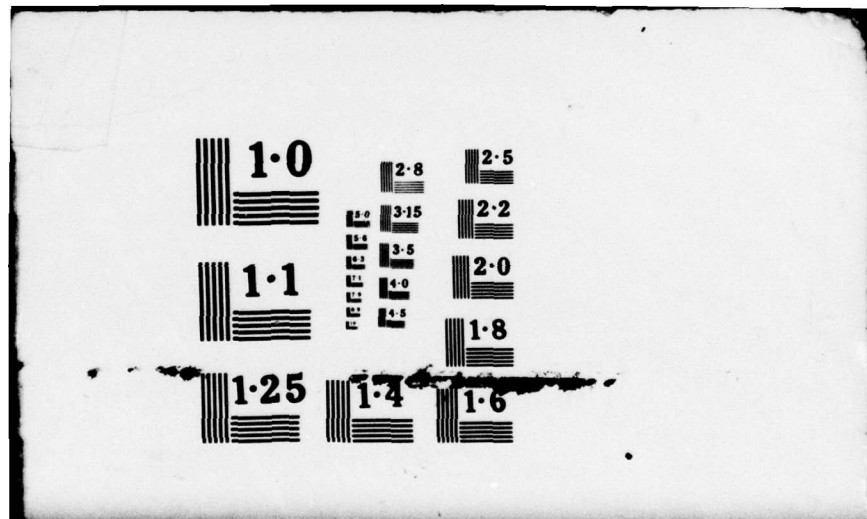
Depth of water table (100 to 300 feet) is found not to have significant effect on the surface ground motion. The effect of water table at depths less than 100 feet has not been studied.

From the above discussions it can be concluded that the direct ground motion effect on shelter response is probably secondary to the airblast effect for the site and environment considered. However, if the site profile is changed, for example by raising the water table, a reassessment of this tentative conclusion will be necessary.

From a numerical analysis viewpoint the use of appropriate ground motion at the soil island boundaries effectively extends the size of the island thereby enabling dynamic calculations to be carried out for a longer period than would be possible otherwise. This is absolutely necessary in large-scale three-dimensional calculations such as those attempted in the present study when long-term structural response of the shelter is analyzed.

7.6.   SHELTER ANALYSIS METHODOLOGY

From the foregoing it appears that a three-dimensional dynamic analysis of the shelter using numerical methods can best be performed in two parts: short-term and long-term. In the short-term analysis, response of the front end of the shelter which is exposed to direct airblast load is examined. Peak stresses in the headworks, frame and closure and peak deformation of the closure are obtained. Long-term analysis includes what happens afterwards and addresses mostly the response of the tube and the gross motion of the shelter. (In the rear-on incidence case the short-term response would include the time from first arrival at the rear-end to arrival at the front.)

This distinction of short and long-term responses follows directly from the shelter concept wherein the structure is subjected both to direct airblast and indirect ground motion loads. Detailed subcomponents of the shelter are located up front (e.g., frame, gap, closure) and their response is dominated by the direct airblast load. Their important response time is both short, about the order of magnitude of the main pressure pulse (up to 30 msec. at the most for the environment considered here), and local. The fundamental period of the closure for instance is about 8 msec., whereas the period for longitudinal bending of the tube is 100 msec., and ovaling of the ring cross-section about 40 msec.

The distinction can also be made from a frequency viewpoint. High frequency effects, if any, are more likely to come from the direct airblast load. Airblast induced ground motion by its nature is more appropriately called low frequency input.

The short and long-term response distinction is also one of (modeling) analysis expediancy. Modeling of the front end is by necessity a detailed task in order to reproduce the response characteristics of the subcomponents, say, the closure. The detailed model usually puts a strain on the capacity of the computer. The core storage of the computer is taxed if the fine mesh used for the front end is continued all through the shelter/berm configuration. Small element sizes for the front end imply small integration time steps for an explicit code (an analysis program which uses an explicit solution procedure). Either of these restraints is undesirable and is to be avoided if possible.

Results obtained in the present study indicate that the two-part analysis methodology is both practicable and correct. The key observation based on Phase 2 studies is that minor details of the closure do not significantly affect response of the main shelter and vice versa. This suggests that analysis of the closure and main shelter can be uncoupled to certain extent, leading to the short-term and long-term methodology proposed here.

An analysis procedure for performing dynamic three-dimensional finite element analyses of a shelter-like structure can be formulated based on this methodology. The procedure is outlined in the following.

As in any finite element analysis, the procedure starts with modeling considerations then moves on to guidelines on performing the dynamic analysis in two parts, short-term and long-term. An attempt has been made to keep the comments and references general enough for the class of shelter-like structure considered; specific examples are made to illustrate a point even though the example may not be valid for a particular shelter configuration.

A. Modeling Consideration

Special attention in modeling should be given to the following shelter subregions:

• Closure--sufficient details should be included to reproduce the basic deformation mode which is punching and shear in the inelastic range and fundamental period in the elastic range. Any steel back and side plates should be so modeled as to reflect its bending capability. Concrete material properties should be as accurate as possible since the closure response (but not the main shelter structure) is sensitive to the material properties used.

• Front Face--the front face model should be as detailed as the air overpressure distribution on it dictates in order to bring out any axial load imbalance which acts to rotate the headworks.

• Frame/Gap--existence of the gap (and gap pressure) must be included in the model. The inner lower and upper corners of the frame, for a square closure, as well as any other steel lining on the frame must be modeled.

• Bearing Ring--a high stress gradient exists in the bearing area supporting the closure. A fine mesh is necessary here to reproduce the stress concentration that is the bearing load. Yielding and deformation of the bearing region will affect the overall response of the closure.

• Transition Section--the high axial stress from the front load is amplified as the load bearing area decreases and a high stress gradient results in this region. A moderately detailed model for the transition section is probably sufficient although any abrupt change in cross-sectional shape (such as those in S1 and S4) should be modeled with care.

• Fore Tube Section--the front portion of the tubular section immediately behind the headworks bears the axial compression and bending moment transferred from the headworks. A fine subdivision of elements should be used in this critical region and at the crown in particular. It should also be sufficiently detailed to accommodate in-plane deformation modes as high as n = 3.

• *Main Tube Section--the model for the main tubular section of the shelter should reflect its dynamic characteristics such as longitudinal flexure and in-plane bending.*

• Soil Medium--careful modeling of the soil medium immediately in front of the shelter is necessary not so much to admit correct transmission of the airblast load as to prevent erroneous distribution of this load to the structure. Modeling of soil medium elsewhere should be consistent with the dynamic characteristics of the tube section.

B. Airblast Characteristics

Special care should be exercised in determining the following airblast characteristics since they have significant influence on structural response. The exact effect, of course, varies with loading conditions. In general the characteristics are more important in the event of a direct loading than otherwise.

• Head-On Condition--airblast parameters of importance are the front-face reflection factor, its spatial distribution about the front-face and impulse and impulse time constant. The reflection coefficient governs the peak pressure and hence the peak stresses in the headworks and closure. Its distribution about the front face is also important in determining the amount of bending of the headworks. Impulse is important to the closure when the latter deforms in the punching mode and the peak inelastic deflection is then determined by the impulse.

• Oblique Front-On and Side-On Condition—reflection coefficient at the blastward and rear sides of the headworks, if exposed, is an important parameter. It governs the amount of bending in the yaw plane and its importance increases as it approaches the front-face reflection coefficient in value.

The effect of pressure distribution on the gap, especially the differential between the blastward side and the rear sides, needs to be assessed.

• Overburden Load—effect of overburden load on the shelter, whether it is head-on, side-on or rear-on, is not expected to be as significant as the direct load parameters. Its action is to push the structure down and with the blast and is usually tempered somewhat by the expanse of backfill surrounding the structure. Its characteristics should be as refined as the backfill properties and tube response characteristics require.

C. Short-Term Analysis

A short-term analysis of the response of the front-end should be based on a fine model of the closure, front face, frame/gap, bearing ring and transition section (see Section 7.1). It may be desirable to begin with an elastic analysis which can serve as a baseline for the subsequent inelastic calculations.

That portion of the shelter after the transition section may be replaced by a simpler model which can reproduce approximately (i) the impedance to axial load; (ii) the energy radiation along the longitudinal axis; and (iii) the resistance to bending of the headworks. Springs and dashpots for instance can be used to replace the aft-half of the tubular section and medium in the longitudinal direction while holding it fixed in the transverse direction. The short-term analysis should be terminated after peak stresses in the headwork and frame/closure and maximum deflection in the closure have been obtained.

An inelastic model of the closure should be used and it should be sufficiently refined to produce the punching deformation mode and the shear crack propagation phenomenon for sufficiently high loading.

D. Long-Term Analysis

Long-term analysis includes also the structure response from wave front arrival; but it is not designed to yield response of detailed substructures (e.g., closure) provided by the short-term analysis. It should therefore be based on a course model of the front face, closure, frame/gap and bearing ring, but using the appropriate models for the transition section, tube section and medium as described in Section 7.1. Care, however, must be used in choosing the approximate front face model so that important overpressure characteristics are not lost. The approximate closure model also must be choosen so that

7-11

it is still capable of transferring the front face load to the headworks. For instance, the composite closure of the S4 configuration may be replaced by an equivalent all reinforced concrete model for analysis purposes so that the steel back and side plates no longer impose constraints on the time step requirement.

To carry the calculation out for a long period (about 200 msec. for the S4 case) the soil island approach must be used to limit the interference due to unwanted signals coming from the boundaries. The extent of error introduced by boundary signals depends on the loading condition, size of the soil island and dissipative properties of the medium. An elastic analysis is probably not appropriate for a long-term analysis mainly because it lacks material damping characteristics. Ground motion input at the soil island boundaries is definitely necessary in this case. In general an elastic analysis tends to overestimate the response and introduce spurious signals.

SECTION VIII

REFERENCES

1. Progress Report No. 1 to Defense Nuclear Agency, Contract No. DNA 001-77-C-0104, Weidlinger Associates, May 1977.

2. Wong, F. S., and Isenberg, J., "Pretest Simulation of HAVE HOST S4 Half Scale MAP Shelter Test," DNA (TBD), Weidlinger Associates, Contract No. DNA 001-C-77-0104, TO BE PUBLISHED.

3. Drawings No. 8-06-2, "Sixth Scale Symmetric Shelter," AFWL, June 14, 1976, Revised November 23, 1976.

4. Stucker, M. D., "1 MT Surface Burst, 600 psi Ideal on MX Shelter, Front Incidence," AFWL/DYN Interim Data Report No. 19.8041 (HULL), April 18, 1977.

5. Stucker, M. D., "1 MT Surface Burst, 600 psi Ideal on MX Shelter, Side Incidence," AFWL/DYM Interim Data Report No. 19.8042 (HULL), March 15, 1977.

6. Drawings Code Ident No. 81205, "MX Shelter, HSEM," Contract No. FO4704-77-C-0005, The Boeing Company, September 29, 1977, Revised October 11, 1977.

7. Shinn, J. D., "HAVE HOST Backfill Model," AFWL/DES-G Memo, March 4, 1977.

8. Elsberry, R., "S4 Full Sized Front-On Numbered Loads," AFWL/DES, Private Communication, December 19, 1977.

9. Progress Report No. 3 to Defense Nuclear Agency, Contract No. DNA 001-77-C-0036, Weidlinger Associates, May 1977.

10. Baylor, J. L., Bieniek, M. P., and Wright, J. P., "TRANAL: A 3-D Finite Element Code for Transient Nonlinear Analysis," DNA 3501F, Weidlinger Associates, June 30, 1974.

11. McNickle, P. J., "HAVE HOST S-1 Quick Look," AFWL/DE, May 26, 1977.

12. Buckey, C. F., "S-4 TWG Meeting Minutes," TRW/NAFB, August 3, 1977.

13. Buckey, C. F., "S-4 TWG Meeting Minutes," TRW/NAFB, May 10, 1978.

APPENDIX A

MODIFICATIONS TO TRANAL

TRANAL is designed to treat three-dimensional soil-structure systems subjected to airblast and induced ground shock loadings. The structure is assumed totally buried and the airblast loading surface a flat ground. The air overpressure is fashioned after Brode and is retained in its analytical form in the family of subroutines BR73.

In preparation for the planned soil-structure investigation and the S4 pretest calculation extensive modifications have been made to the code to facilitate the rather complex geometry and applied load distribution. The airblast loading surface is no longer flat nor a single surface and the overpressure time histories are given in digitized format. In addition, because of the size of the problem involved, other modifications to the code are also necessary in order to fit the maximum size into the computer. These changes will be described briefly in this appendix which, however, is not meant to be a formal documentation of the code. Most of the necessary programming is done by John Baylor of Weidlinger Associates, New York.

A.1. APPLIED PRESSURE LOAD MODIFICATIONS

Pressure load can be applied to the exposed surfaces of the structure and berm in one of two ways depending on the details of the geometry and overpressure involved and of course the users' choice.

A.1.1. Overall Loading

This method of applied load is intended for large surface areas (such as the berm surfaces or any large expanse of exposed surface). Where the geometry is simple (plane) and the pressure load does not change drastically from one location to another. This loading mode constitutes a generalization of the code's original applied pressure (Brode) module. Discretized pressure time histories are given for points on a spatial network covering the surface to be loaded. The required loading at any point on the surface is obtained through spatial interpolation of the data involved.

A.1.2. Detail Loading

This mode of applied load is tailored to complicated surface description (such as those on the front face, headworks and gap in the structure, neighboring soil surfaces and cutouts in the driveway) and irregular pressure distribution. In its most refined form, each discretized structural element can have its own pressure loading description (or pressure cell) consisting of time-pressure pairs, loading direction and time of arrival.

A.1.3. Code Modifications

Changes to the code are made to the input module, element table set up and applied load processing. The modified and new subroutines are described briefly below approximately in their order of execution; names with an asterisk correspond to new subroutines.

READ PROCESSOR

UNT OPT -- expanded to include input data unit option for pressure cell specification

PRT OPT -- expanded to include option to print pressure cell data

CAP 75R -- material property specification is expanded to include pressure cell "property," with zero mass and scale factor and arrival time substituted for elastic bulk and shear moduli

CHK LCL* - pressure time history number is checked for validity

RED LOD* - pressure data are read in

RED TBL* - pressure time history pains are read in

CHK LOD* - pressure data is checked for validity

ELM SET -- new name for old block of codes in SRTOUT

ELM MAT* - pressure cell subroutine

ELM RED* - pressure cell specification data are read in

CHK ELM -- cell specification is checked for validity

CHK MAT* - pressure cell specification is checked for validity

CNG NAM* - utility routine, name of a data block is changed

ELM SRT* - utility routine, elements are rearranged according to processing (zone) order

BLD TBL -- element table set up routine, modified for pressure cell applications

ILZ ZON* - utility routine, sets up zone count parameters

ILZ ELM* - utility routine, sets up element count parameters

SET ELM* - element table entry is updated for pressure cell applications

MAT PTR -- material pointer is inserted in element table

RUB MAT* - utility routine, a data block is erased

COORDINATE PROCESSOR

B MATRIX - slight modification to accommodate pressure cell specification

NOD MAS -- *slight modification to accommodate pressure cell specification*

XEQ PTR -- expanded to set up pressure cell related parameters for execution phase

TIME PROCESSOR

ZP HEX* -- expanded to include new pressure options

CHK LCE* - element to be processed is checked to see if it is a pressure cell

UPL CNF* - nodal forces for a pressure cell are updated

LOD CELP* - pressure in a pressure cell is computed

LOD CELF - forces in a pressure cell is computed

UP LCNV* - nodal velocities for a pressure cell are updated

STRS BD -- modified for generalized overpressure load

MAS CHK* - mass of boundary node is checked for non-zero value

FC CNTR* - utility routine, determines centroid of a surface element

FELIX W* - generalized overpressure load is determined

WONG FX* - generalized overpressure load is determined

CHK IDX* - utility routine, surface index for pressure cell is checked for validity

DMP PAK* - utility routine, a packed-word data block is unpacked and dumped

NORMAL* -- utility routine, unit normal vector to a surface is determined

PAK WRD* - the six surface indices are packed and meshed into the element table entry for each element

UNP WRD* - unpacked the word packed in PAK WRD

A pressure cell is designated by an element with zero mass and has a corresponding material description with material number equal to the pressure-time history number to be applied. As such it is equivalent to specifying the material property of an element and is indeed used for that purpose. Since ordinarily the material description in TRANAL is described in terms of region (a region can have more than one element, but all elements within a region must have the same material property). This affords the user another option in

specifying material makeup of a region and has been found to be quite useful especially when only a few elements of an existing model need to be changed.

Prescribing the pressure load within an element is only part of the pressure cell description; additional information must be given to specify which of the six faces which make up an element are acted upon by this load. This is done by specifying any or all of the surface indices 1, 2, 3, 4, 5 or 6. These data are then packed into one word and stored as an entry to the element table. Before each subsequent use then this word must be unpacked and the required data retrieved. This process enables the original structure of the code, i.e., element table with one word per element, be conserved although a nominal penalty in execution time is incurred.

A.1.4. Sample Check Problem

The elastic axisymmetric problem of a steel-lined cavity in rock is used as a formal check case for the applied pressure load modifications.

Uniform load in the form of a triangular pressure pulse is applied at the surface of the steel liner. Three TRANAL runs are made using the model of the steel and medium as shown in Figure A-1. The same pressure time history is used in all three runs, but a different mechanization is exercised each time corresponding to the original (old) loading module, the overall loading module and the detail loading module (pressure cell method) described previously.

Results obtained from the three runs are identical. The TRANAL code results have also been compared with numerical results obtained by Lockheed Palo Alto Research Laboratory and this comparison is given in Figure A-2 for membrane stress in the steel liner and in Figure A-3 for the radial displacement also in the liner.

Extensive functional checkout of the routines has also been performed, but is not described herein.

A.2. OTHER MODIFICATIONS

A.2.1. Region Coordinate Edge Processing

The region coordinate edge processing is changed from the whole soil island basis to a zone basis; this change is made so that larger soil island (problem) can be accommodated in the machine, at least through the COORDINATE PROCESSOR stage and that the approach is more consistent with the subsequent TIME PROCESSOR, which also processes the elements on a zone by zone basis. Four additional peripheral units need to be declared; one for coordinate and the other three for x-edges, y-edges and z-edges, respectively, if these are not linear edges. The effected subroutines are:

READ PROCESSOR

REG CRD -- modified to accommodate new coordinate edge processing approach

REG EDG -- modified to accommodate new coordinate edge processing approach

COORDINATE PROCESSOR

COR DPP -- modified to accommodate new coordinate edge processing approach

RGN CRD -- modified to accommodate new coordinate edge processing approach

BLD RGN* - region coordinates for a zone are built and saved

BLD RDG* - region edge coordinates are built and saved

A.2.2. Stability and Volume Check

For an explicit code using the finite differencing scheme to step forward in
time the integration time step used must satisfy the Courant's stability criteria, i.e.,
the time step used must be a fraction of the smallest transit time across an element. This
check which prior to this time is the responsibility of the user is mechanized. At the same
time and a negative volume check is also made to detect errors in coordinate data which may
result in a negative volume for the element. The modified and new subroutines involved are:

COORDINATE PROCESSOR

COR DPP -- modified for stability and volume check

STB ILZ* - stability check zone parameters are set up

DST RCP* - utility routine, determines distance between points

STB CHK* - the stability characteristics of an element are checked

STB DMP* - utility routine, the stability table is dumped

STB SET* - parameters for stability check are set up

A.2.3. Region Material Description

Prior to this change the region material data are read in according to zone; this
has the disadvantage that any change to the zone makeup will necessitate a corresponding
change to the region material input data. This modification enables the material data to
be read on the soil island basis, hence independent of zone configuration. The modified
subroutine is ZND CRP. Naturally it is no longer possible to designate a whole zone as
VOID and the necessary VOID regions must be included in the input data.
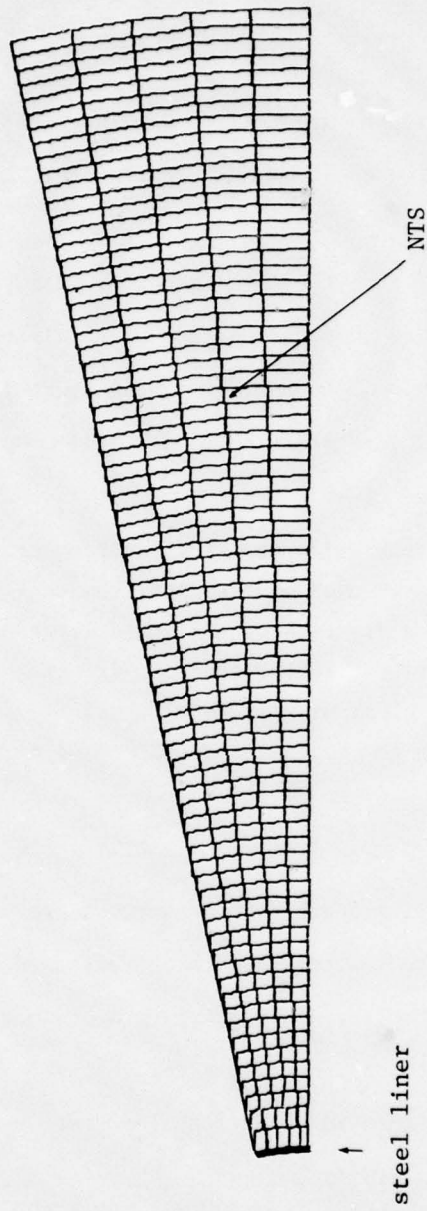
NTS

steel liner

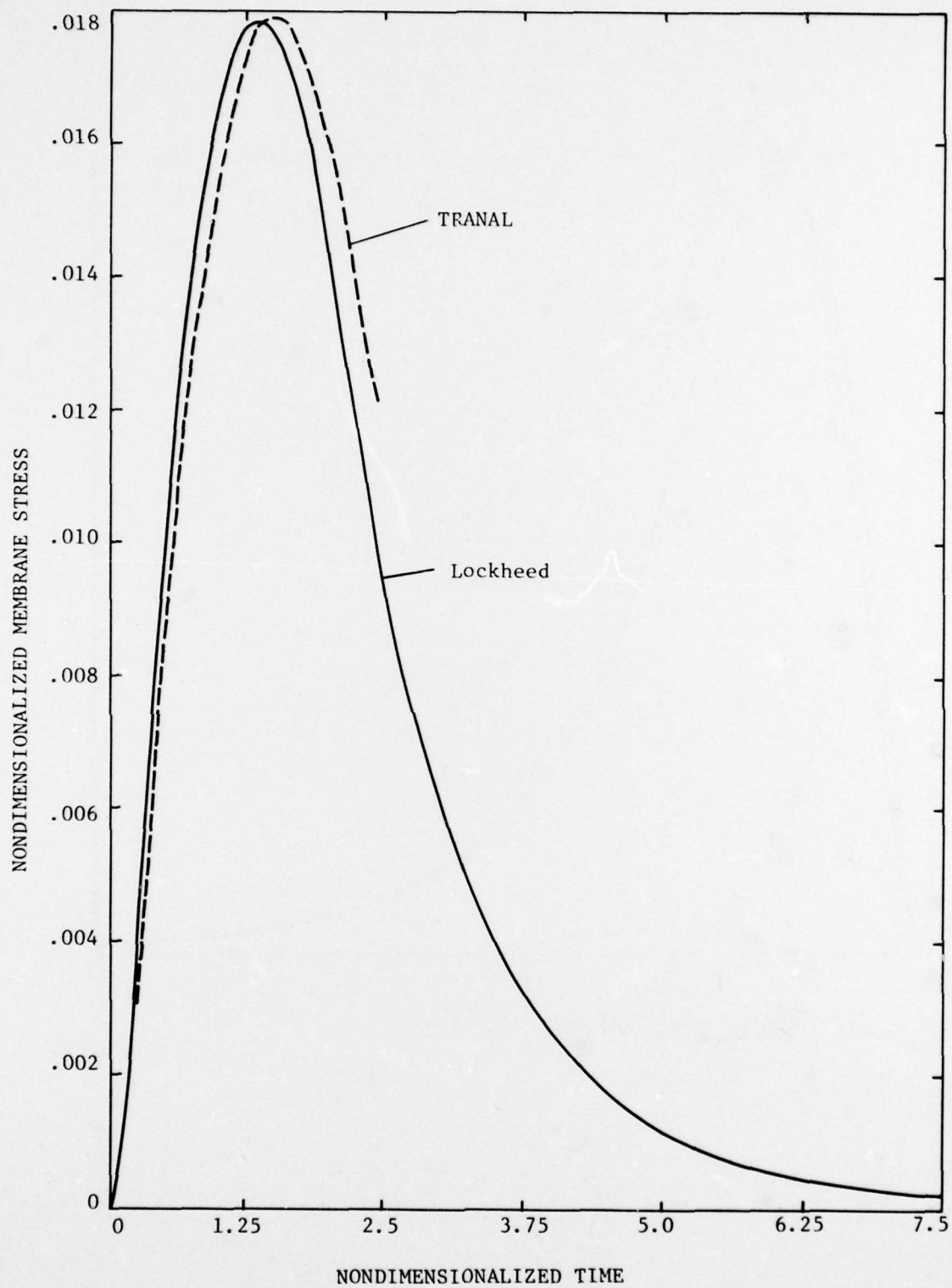Figure A-1. Model for TRANAL check problem

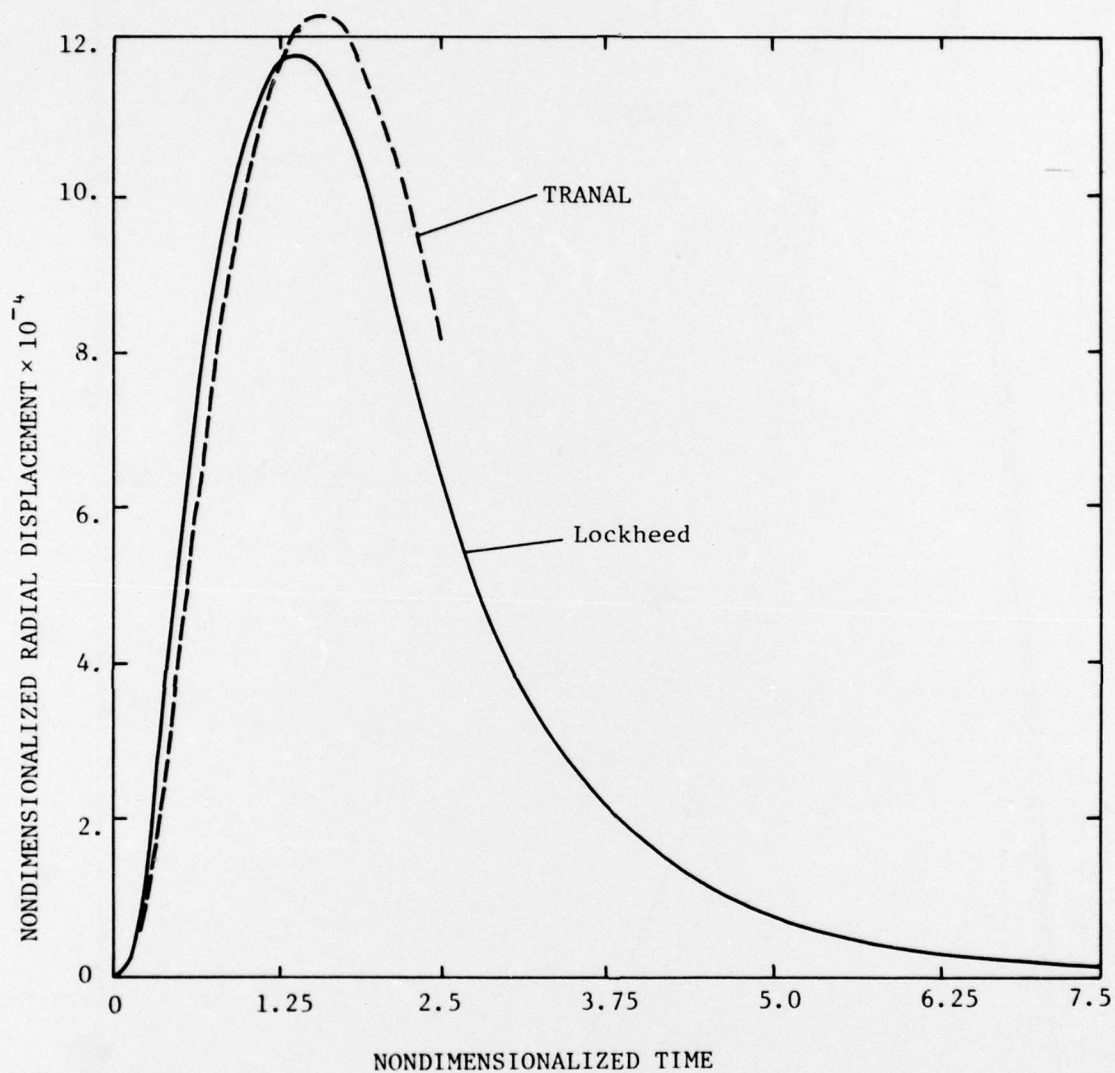Figure A-2. Comparison of membrane stress in steel liner

Figure A-3. Comparison of radial displacements in steel liner

DISTRIBUTION LIST

DEPARTMENT OF DEFENSE

Assistant to the Secretary of Defense
    ATTN: Executive Assistant

Defense Advanced Rsch. Proj. Agency
    ATTN: TIO

Defense Civil Preparedness Agency
Assistant Director for Research
    ATTN: Staff Dir. Rsch., G. Sisson
10 cy ATTN: Admin. Officer

Defense Communications Agency
    ATTN: CCTC C670, R. Lipp
    ATTN: Code 930
    ATTN: CCTC C672, F. Moore

Defense Documentation Center
12 cy ATTN: DD

Defense Intelligence Agency
    ATTN: DB-4C, E. O'Farrell
    ATTN: DT-1C
    ATTN: DT-2
    ATTN: RDS-3A
    ATTN: DB-4E

Defense Nuclear Agency
    ATTN: DDST
 4 cy ATTN: TITL
 2 cy ATTN: SPSS

Field Command
Defense Nuclear Agency
    ATTN: FCT
    ATTN: FCPR
    ATTN: FCTMOF

Joint Strat. Tgt. Planning Staff
    ATTN: NRI-Stinfo Library
    ATTN: DOXT
    ATTN: XPFS
    ATTN: JLTW-2

Livermore Division, Field Command, DNA
Department of Defense
Lawrence Livermore Laboratory
    ATTN: FCPRL

Under Secy of Def. for Rsch. & Engrg.
    ATTN: Strategic & Space Systems (OS)

WWMCCS System Engineering Org.
    ATTN: T. Neighbors

DEPARTMENT OF THE ARMY

BMD Advanced Technology Center
    ATTN: ICRDABH-X
    ATTN: CRDABH-S

Program Manager
BMD Program Office
Department of the Army
    ATTN: DACS-BMT, J. Shea

DEPARTMENT OF THE ARMY (Continued)

BMD Systems Command
Department of the Army
    ATTN: BMDSC-TEN, N. Hurst

Chief of Engineers
Department of the Army
    ATTN: DAEN-RDM
    ATTN: DAEN-MCE-D

Deputy Chief of Staff for Ops. & Plans
Department of the Army
    ATTN: Dep. Dir. for Nuc. Chem. Matters
    ATTN: MOCA-ADL

Harry Diamond Laboratories
Department of the Army
    ATTN: DELHD-N-NP
    ATTN: DELHD-N-TI

U.S. Army Ballistic Research Labs.
    ATTN: DRDAR-BLE, J. Keefer
 2 cy ATTN: Technical Library

U.S. Army Engr. Waterways Exper. Station
 2 cy ATTN: L. Ingram/Library
 2 cy ATTN: G. Jackson/W. Flathau

DEPARTMENT OF THE NAVY

Civil Engineering Laboratory
Naval Construction Battalion Center
    ATTN: S. Takahashi
    ATTN: Code L08A
    ATTN: R. Odello

David W. Taylor Naval Ship R & D Ctr.
    ATTN: Code L42-3

Naval Facilities Engineering Command
    ATTN: Code 09M22C
    ATTN: Code 03A
    ATTN: Code 04B

Naval Research Laboratory
    ATTN: Code 8440, F. Rosenthal
    ATTN: Code 2627

Naval Surface Weapons Center
    ATTN: Code F31

Naval Surface Weapons Center
    ATTN: Tech. Library & Info. Services Branch

Office of Naval Research
    ATTN: Code 474, N. Perrone
    ATTN: Code 715
    ATTN: Code 461, J. Warner

DEPARTMENT OF THE AIR FORCE

Aerospace Defense Command/XPD
    ATTN: XP
    ATTN: XPDQQ

DEPARTMENT OF THE AIR FORCE (Continued)

Air Force Systems Command
    ATTN: DLCAM

Air Force Weapons Laboratory
    ATTN: DE, C. Needham
    ATTN: DE-I
    ATTN: J. Thomas
    ATTN: DE, M. Plamondon
    ATTN: DES-C, R. Henny
    ATTN: SUL
    ATTN: DEX

Deputy Chief of Staff
Research, Development, & Acq.
Department of the Air Force
    ATTN: AFRDPX
    ATTN: AFRDQSM

Space & Missile Systems Organization/DE
Air Force Systems Command
    ATTN: DEB

Space & Missile Systems Organization/DY
Air Force Systems Command
    ATTN: DYS

Space & Missile Systems Organization/MN
Air Force Systems Command
    ATTN: MNNH
    ATTN: MMN

DEPARTMENT OF DEFENSE CONTRACTORS

Aerospace Corp.
    ATTN: Technical Information Services

Agbabian Associates
 2 cy ATTN: M. Agbabian

BDM Corp.
    ATTN: Corporate Library

BDM Corp.
    ATTN: R. Hensley

Boeing Co.
    ATTN: Aerospace Library

Brown Engineering Company, Inc.
    ATTN: M. Patel

Battelle Memorial Institute
    ATTN: Library

California Research & Technology, Inc.
    ATTN: S. Shuster
    ATTN: K. Kreyenhagen
    ATTN: Library

Civil/Nuclear Systems Corp.
    ATTN: J. Bratton

Eric H. Wang
Civil Engineering Rsch. Fac.
    ATTN: N. Baum

General Electric Co.—TEMPO
Center for Advanced Studies
    ATTN: DASIAC

DEPARTMENT OF DEFENSE CONTRACTORS (Continued)

IIT Research Institute
    ATTN: Documents Library
    ATTN: R. Welch

University of Illinois
Consulting Services
    ATTN: N. Newmark

Information Science, Inc.
    ATTN: W. Dudziak

J. H. Wiggins, Co., Inc.
    ATTN: J. Collins

Kaman Sciences Corp
    ATTN: F. Shelton
    ATTN: Library

Lockheed Missiles & Space Co., Inc.
    ATTN: TIC-Library
    ATTN: J. Gears

R & D Associates
    ATTN: C. MacDonald
    ATTN: Technical Information Center
    ATTN: A. Latter
    ATTN: J. Lewis
    ATTN: R. Port

R & D Associates
    ATTN: H. Cooper

Rand Corp.
    ATTN: C. Mow

Science Applications, Inc.
    ATTN: Technical Library

Science Applications, Inc.
    ATTN: D. Maxwell
    ATTN: D. Bernstein

Science Applications, Inc.
    ATTN: B. Chambers, III

SRI International
    ATTN: G. Abrahamson

Systems, Science & Software, Inc.
    ATTN: D. Grine
    ATTN: Library

TRW Defense & Space Sys. Group
    ATTN: P. Bhutta
 2 cy ATTN: P. Dai
    ATTN: Technical Information Center

TRW Defense & Space Sys. Group
    ATTN: E. Wong

Weidlinger Associates, Consulting Engineers
    ATTN: M. Baron

Weidlinger Associates, Consulting Engineers
    ATTN: J. Isenberg
    ATTN: F. Wong